Investigating the cooperation of *APC* and *KRAS* mutations in Colorectal Cancer

David Michael Gay, MBiochem

Supervisor: Prof. Owen Sansom

Thesis submitted to the University of Glasgow for the Degree of Doctor of Philosophy (PhD)

College of Medical, Veterinary and Life Sciences

October, 2017

Cancer Research UK Beatson Institute

Garscube Estate

Switchback Road

Glasgow, G61 1BD

United Kingdom

Abstract

Colorectal Cancer (CRC) progresses in a stepwise manner accumulating mutations in particular signalling pathways. Despite our knowledge of the genetic progression of the disease, the resulting phenotypes of the different mutation combinations remains poorly understood. I used genetically engineered mouse models to investigate the cooperation of two frequent early mutations - loss of the tumour suppressor gene *APC* and activating *KRAS* mutations, to try and identify potential therapeutic targets.

Hyperactivated Wnt signalling is a hallmark of CRC, although efficacious therapies are limited. In **chapter 3** I focussed on targeting this pathway at the level of ß-catenin mediated transcription. I showed that deletion of BLC9 and BCL9l, two proteins involved in ß-catenin mediated transcription, suppresses proliferation and the expression of a subset of Wnt target genes following loss of APC and KRAS activation. I showed that these two proteins are dispensable intestinal homeostasis. I also showed that deletion of BCL9 and BCL9l significantly accelerated tumour initiation.

In **chapter 4** I performed unbiased quantitative proteomics on crypt cultures from *VillinCre*^{ER} *Apc*$^{fl/fl}$ (APC) and *VillinCre*^{ER} *Apc*$^{fl/fl}$ *Kras*$^{G12D/+}$ (APC KRAS) mice to identify deregulated signalling pathways between these two genotypes. I identified a 'nutrient stress' phenotype in APC KRAS crypts. I show that this might be driven by a significant increase in protein synthesis, since APC KRAS cells are trying to regulate their rates of protein synthesis via eIF2α signalling.

In **chapter 5** I investigated changes in the metabolomes between APC and APC KRAS cells. I show that APC KRAS crypt cultures are highly dependent on glutamine for growth and upregulate many genes involved in glycolysis and glutaminolysis. I show that APC KRAS cells are metabolically flexible and also highlight the role the environment plays in metabolic phenotypes.

Overall, I have shown that intestinal epithelial cells with high-Wnt and high-MAPK signalling are sensitive to Wnt inhibition. I have also shown that these two signalling pathways cooperate to drive increased protein synthesis and deregulated metabolism to fuel proliferation.

Contents

List of Tables

List of figures

Acknowledgements

Firstly, I want to thank my supervisor Owen Sansom for giving me the opportunity to undertake this PhD and all the support and guidance he has given me throughout. His tuition and guidance has developed me into the scientist I am today and know that it will serve me well in my future career.

I'd also like to thank all members of the Sansom lab, in particular to Andy Campbell, Rachel Ridgway and Tam Jamieson for all the help they have given me within the lab over the past four years. I'd also like to thank all of the members of my office (Muffin Fridays) past and present: Liam Faller, Patrizia Cammareri, David Huels, John Knight and Michael (The Legend) Hodder – they not only provided practical and theoretical help with experiments, but also stimulating discussions as well as welcomed coffee breaks and created a very happy working environment.

I'd like to thank both Liam Faller and John Knight who took me under their wings and helped me on a daily basis with any practical issues and advice in the lab. Thanks also to Fatih Ceteci and Arafath Najumdeen (Rafa) who helped me greatly in my metabolic studies.

Thank you to my advisor, Sara Zanivan, who helped me with my proteomic experiments, but also acted as a source of support and advice. The Beatson Institute has many fantastic core services, without which much of the work within this thesis would not have been possible. An enormous thank you to Sergio Lilla, David Sumptom, Gillian Mackay, Billy Clark, Ann Hedley, Colin Nixon and his histology team, all members of the Biological Service Unit and Central Services for everything they have helped me with over the last four years. I'd also like to pay special thanks to the agencies that funded my PhD – Cancer Research UK and the European Research Commission (Colon Can grant).

Away from the lab, I'd like to thank Hillhead Hockey Club for welcoming me into the 'HHC Family' as if one of their own. Finally, I'd like to thank my entire family, particularly my parents who have supported me throughout everything that I have done. Without their love and support I know that I would never have achieved what I have done. For this I owe them everything.

Author's declaration

I am the sole author of this thesis and all the work presented is my own unless stated otherwise. No part of this work has been submitted for consideration as part of any other degree or award

Abbreviations

APC – Adenomatous Polyposis Coli

ATF4 – Activating transcription factor 4

ATP – Adenosine Triphosphate

BCL9 – B-cell lymphoma 9

BCL9l –B-cell lymphoma 9-like

BMP – Bone Morphogenic Protein

CRC – Colorectal Cancer

DNA – Deoxyribose nucleic acid

eEF2 – eukaryotic elongation factor 2

EGF – Epidermal Growth Factor

eIF2 – eukaryotic initiation factor 2

ER – Endoplasmic Reticulum

FAP – Familial Adenomatous Polyposis

FZD – Frizzled

GCN2 – General Control Nonderepressible 2

GDP – Guanosine Diphosphate

GEF – Guanine nucleotide Exchange Factor

GPT – Glutamate-pyruvate transaminase

GSK – Glycogen Synthetase Kinase

GTP – Guanosine Triphosphate

HNPCC – Hereditary Non-Polyposis Colon Cancer

ISC – Intestinal Stem Cells

ISRIB - Integrated Stress Response Inhibitor

KRAS – Kirsten Rat Sarcoma Virus

LGR5 - Leucine-rich-repeat-containing G-protein-coupled receptor 5

LOH – Loss of Heterozygosity

LRP - Low-density lipoprotein (LDL)-receptor-related protein

MAPK – Mitogen Activated Protein Kinase

MMR – Mismatch repair

mRNA – messenger Ribonucleic Acid

mTOR – mammalian target of rapamycin

NEAA – non-essential Amino acid

PCR – Polymerase Chain Reaction

PERK - PKR-like endoplasmic reticulum kinase

PI3K - Phosphatidylinisotiol-3-kinase

TA-cell – Transit Amplifying cell

tRNA – transfer Ribonucleic Acid

UPR – Unfolded Protein Response

Wg - wingless

WNT – Wingless-related integration site

Chapter 1: Introduction

Colorectal Cancer (CRC) is the third most common cancer in the world, and it has the second highest mortality rate in Europe (Ferlay et al., 2013). The age-standardised rate of diagnosis of CRC in the UK is 70 [1].

In the UK, and many other countries, screening is routinely carried out to ensure early detection. Screening is usually via colonoscopy, although there have been recent developments in less invasive techniques to replace colonoscopy. These include testing stool samples for certain mutations (Imperiale et al., 2014) or via Faecal Immunochemical Testing – testing samples for haemoglobin (Songster et al., 1980)

Following detection, surgery is the best option for patients – with a 90% survival rate for patients with localised CRC [2]. However, for patients that are detected at a later stage and have distant metastases, the 5-year survival rate drops to 14% [2]. This highlights the importance of early detection and the benefit of screening programmes in order to improve early detection rates.

Advanced stage CRC patients are treated with a number of DNA-damaging agents such as 5-fluorouracil (5-FU) and Oxaliplatin in combination with particular targeted therapies, such as anti-EGFR or anti-VEGF agents (Hurwitz et al., 2004; Van Cutsem et al., 2010). However, with recent developments in DNA sequencing, there is hope that identification of genetic mutations could serve to guide personalised treatment programmes and classify patients into different subtypes. Furthermore, it is important to remember that CRC exists as multiple diseases and therefore a need for a greater understanding of the progression of the genetics of the disease and the inter- and intra-tumour heterogeneity.

These topics, along with the signalling pathways that are deregulated in CRC will be discussed in greater detail throughout this introduction, as well as the approaches that have been developed over the years to better understand the progression of colorectal cancer and identify translatable therapeutic targets.

1.1 Wnt signalling

The canonical Wnt signalling pathway has been shown to play a key role in both cancer and developmental biology, and was first discovered over 30 years ago.

The Int-1 gene was discovered by Nusse and Varmus, who identified it as a gene that is activated following integration of Mouse Mammary Tumour Virus (MMTV) DNA in virally induced murine breast tumours (Nusse & Varmus, 1982). A couple of years prior to this, the *wingless* (*wg*) gene was discovered as a critical regulator of segment polarity during the development of *Drosophila* (Nusslein-Volhard & Wieschaus, 1980). Int-1 was subsequently shown to be the mammalian homolog of *wg* (Rijsewijk et al., 1987). Following this discovery, it was decided to unite the two fields and use a common nomenclature for this family of proteins – Wingless-related integration site 1, Wnt1. The Wnt1 gene encodes a secreted, cysteine-rich protein.

Given that *wg* mutation leads to segmentation defects in *Drosophila* embryos, this paved the way for the discovery of other components of the Wnt signalling pathway. The Wnt receptor was identified as the Frizzled family of proteins in *Drosophila* (Bhanot et al., 1996). Another segment polarity gene, *arrow*, which encodes a single-pass transmembrane protein, was shown to be required for transduction of wingless signals in *Drosophila* (Wehrli et al., 2000). The arrow protein is a low-density lipoprotein (LDL)-receptor-related protein (LRP), which shares a high degree of homology with both human and murine LRP5 and LRP6 (Wehrli et al., 2000). The Frizzled/LRP5/6 co-receptor complex is recognized as the Wnt ligand receptor. Another segment polarity gene, *armadillo*, was identified (Wieschaus & Riggleman, 1987) and was subsequently shown to be regulated post transcriptionally by wingless protein expression (Riggleman et al., 1990). ß-catenin has subsequently been shown to be the mammalian homolog of *armadillo* (Mccrea et al., 1991) Interestingly, the study by Riggleman and colleagues showed that the regulatory effect of wingless upon armadillo levels was dependent upon the genes *porcupine* and *dishevelled*.

The evolutionarily conserved Porcupine protein was subsequently shown to be required for wingless protein processing (Kadowaki et al., 1996); it catalyses the palmitoylation of Wnt proteins – a critical step in Wnt ligand

secretion (R. Takada et al., 2006). Mutations in the *Porcn* gene leads to a defect in Wnt ligand secretion in mouse embryonic stem cells (Biechele et al., 2011). Dishevelled was identified as a critical mediator of wingless protein signals, and acts upstream of *armadillo* (Klingensmith et al., 1994; Noordermeer et al., 1994). Furthermore, dishevelled was shown to function in a cell-autonomous manner, unlike wingless proteins which have a non nonautonomous function (Klingensmith et al., 1994). Dishevelled was shown to physically interact with Frizzled via Nuclear Magnetic Resonance (NMR) spectroscopy (Wong et al., 2003). Hence, there was an emerging model – wg protein secretion is dependent on the *porcupine* protein, these wg proteins then act on the recipient cells and increase the expression of armadillo at the post-transcriptional level in a process that is dependent on the wg receptor complex, frizzled and arrow, as well as the dishevelled protein. However the mechanism by which wg signalling controls levels of armadillo remained unclear.

Another segment polarity gene shown to act in a cell-autonomous manner was *zeste white 3* (*shaggy*), which is the *Drosophila* homolog of mammalian Glycogen Synthase kinase-3 (GSK3), was shown to act as a repressor of wingless signalling (Siegfried et al., 1992). van Leeuwen and colleagues showed that armadillo is rapidly degraded in the absence of wingless proteins in cultured *Drosophila* imaginal discs, and that addition of exogenous wingless leads to a rapid stabilisation and increase of armadillo protein levels, which could be inhibited by using an antibody against wingless (van Leeuwen et al., 1994). At the same time, another study showed that *zeste white 3* mutant *Drosophila* embryos accumulated very high levels of armadillo protein, and that armadillo is located downstream of zeste white 3 (Peifer et al., 1994a). It was subsequently shown that as well as their opposing effects on the levels of armadillo, wingless and zeste white 3 share a similar reciprocal relationship on the phosphorylation of armadillo (Peifer et al., 1994b). It was proposed that zeste white 3 phosphorylates armadillo reducing its' stability within the cytoplasm, but that this is inhibited in the presence of a wingless signal (Peifer et al., 1994b). An additional kinase, Caesin Kinase I (CKI), was shown to transduce Wnt signal in *Xenopus* embryos (Peters et al., 1999). CKI was subsequently shown to phosphorylate armadillo in *Drosophila* and that this is also responsible for the degradation of armadillo (Yanagawa et al., 2002).

Inhibition of the proteasome results in the stabilisation of ß-catenin in a panel of cell lines (Aberle et al., 1997). Subsequently, ß-TrCp (ß-transducin repeat-containing protein) was shown to be a negative regulator of the Wnt pathway (J. Jiang & Struhl, 1998; Marikawa & Elinson, 1998), and was proposed to be required for the ubiquitination and subsequent degradation of ß-catenin/armadillo. Two other negative regulators of the Wnt pathway were discovered; Axin (Zeng et al., 1997) and the product of the Adenomatous Polyposis Coli (APC) gene (Munemitsu et al., 1995). APC had previously been shown to interact with ß-catenin (Rubinfeld et al., 1993; Su et al., 1993), whilst Axin had been shown to interact with Dishevelled, resulting in its recruitment to the membrane (Cliffe et al., 2003). APC and Axin, have been shown to serve as scaffold proteins that form the ‘destruction complex‘ consisting of APC, Axin, GSK3, CKI and ß-TrCp and mediates the destruction of cytoplasmic ß-catenin (Behrens et al., 1998; Hart et al., 1998). This formed the basis of canonical Wnt signalling.

In the absence of a Wnt signal, ß-catenin is sequestered to the destruction complex by APC, and is phosphorylated by GSK3ß and CKI (Peifer et al., 1994b; Peters et al., 1999). Phospho-ß-catenin is subsequently ubiquitinated and then degraded via the proteasome in a ß-TrCp dependent manner (J. Jiang & Struhl, 1998). However, upon binding of Wnt ligands to the Frizzled-LRP5/6 co-receptor complex, Axin is recruited to the membrane via its interaction with Dishevelled (Cliffe et al., 2003). As a result, ß-TrCp can no longer bind to phosphorylated ß-catenin. Consequently, the destruction complex saturates with ß-catenin, until all complexes are fully occupied and unphosphorylated ß-catenin accumulates in the cytoplasm and can then translocate to the nucleus and mediate Wnt target gene expression (Li et al., 2012). This is summarised in Fig 1.1.

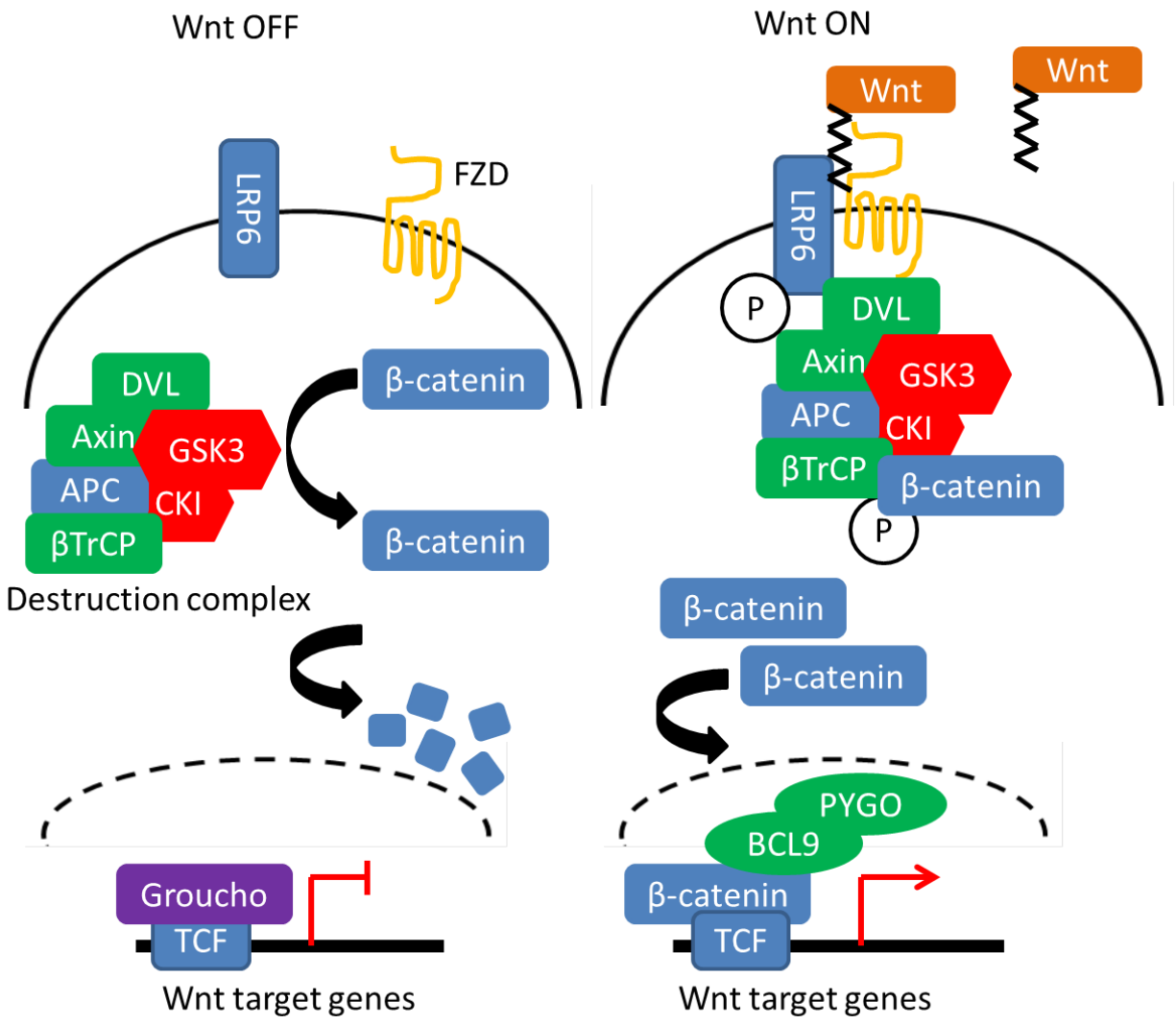

Figure 1.1: Canonical Wnt signalling

In the absence of a Wnt ligand bound to the Frizzled(FZD)/LRP co-receptor (Wnt OFF) ß-catenin is degraded by the destruction complex consisting of APC, DVL, AXIN, GSK3, CKI and ßTrCP. GSK3 and CKI phosphorylate ß-catenin which is then ubiquitinated by ßTrCP marking ß-catenin for proteasomal degradation. Upon binding of Wnt ligands to the Frizzled/LRP co-receptor complex (Wnt ON), the destruction complex is recruited to the receptor complex by dishevelled (DVL). ß-catenin can still be phosphorylated, but not ubiquitinated by ßTrCP, leading to the saturation of the destruction complex with phosphorylated ß-catenin, leading to an accumulation of cytoplasmic ß-catenin. The accumulated ß-catenin then translocates to the nucleus where it binds to TCF/LEF transcription factors, and other transcriptional co-activators such as BCL9 and PYGO, to drive transcription of Wnt target genes.

Early studies revealed that the majority of ß-catenin/armadillo is located and the membrane, bound to E-cadherin (Ozawa et al., 1989), it was also noted that ß-catenin/armadillo accumulates in the nucleus, as outlined in figure 1.1. Nuclear ß-catenin was shown to interact with two transcriptional factors - Lymphoid Enhancer Factor-1 (LEF1) (Behrens et al., 1996), and T-cell factor (TCF) (Molenaar et al., 1996). Upon binding of ß-catenin to these two transcription factors, they are transiently converted to transcriptional

activators, inducing the transcription of Wnt target genes. It is thought that additional transcriptional co-activators of ß-catenin such as B-cell lymphoma 9 (BCL9) (Kramps et al., 2002) and Pygopus (Pygo) (Belenkaya et al., 2002) can mediate ß-catenin dependent transcription. In the absence of a Wnt signal, TCF and LEF-1 transcription factors have been shown to bind to Groucho, which act as transcriptional repressors of Wnt signalling (Cavallo et al., 1998; Roose et al., 1998). Thus, the presence of a Wnt signal determines whether ß-catenin or Groucho proteins are bound to TCF/LEF transcription factors and the subsequent expression of Wnt target genes.

The inclusion of APC within the destruction complex provided a link between Wnt signalling and Colorectal Cancer. Germline mutations in the *APC* gene were identified in patients with Familial Adenomatous Polyposis (FAP), a hereditary form of colorectal cancer (Kinzler et al., 1991). It was subsequently shown that tumours from FAP patients displayed approximately three times higher expression of ß-catenin compared to normal adjacent epithelium, but more importantly that they displayed significantly higher levels of nuclear ß-catenin compared to normal tissue (Inomata et al., 1996). It was also shown that approximately 80% of spontaneous cases of colorectal cancer harboured mutations in *APC* (Munzy et al., 2012). These mutations result in the expression of a truncated form of APC, which often lack the 20 amino acid repeat domains that are required for ß-catenin binding, hence leading to a nuclear accumulation of ß-catenin in these tumours.

1.1.2 Lgr5-RSpondin axis

In addition to Wnt ligands there are a number of other secreted factors that serve to potentiate Wnt signalling. RSpondin proteins are secreted factors that bind to their concomitant receptor Lgr5 (leucine-rich-repeat-containing G-protein-coupled receptor 5). Upon binding of RSpondin ligands, Lgr5 interacts with the E3 ubiquitin ligases Rnf43/Znrf3, mediating the internalisation of these proteins. In the absence of an RSpondin ligand, Rnf43/Znrf3 ubiquinate frizzled receptors, marking them for internalisation and degradation (De Lau et al., 2014). Hence, these ubiquitin ligases, which are also Wnt target genes, serve as part of a negative feedback to loop to limit Wnt signalling (De Lau et al., 2014).

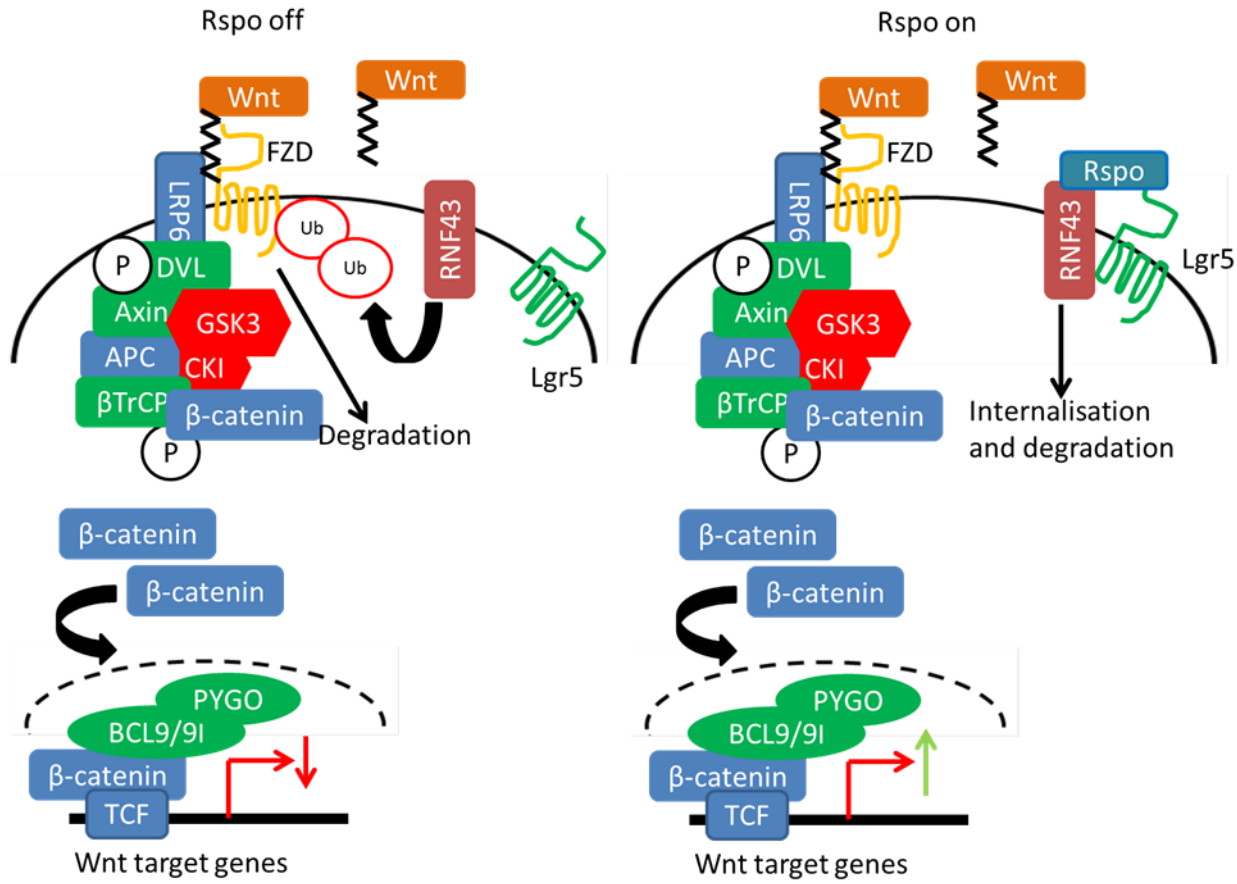

Figure 1.2: Lgr5-RSpondin axis
In response to Wnt signalling, the Wnt target genes *Lgr5*, *Rnf43* and *Znrf3* are upregulated. The protein products of these genes are found at the plasma membrane. In the absence of an RSpondin ligand, RNF43/ZNRF3 ubiquinate Frizzled receptors, marking them for degradation. This in turn releases the destruction complex from the LRP6/FZD co-receptor complex, resulting in the degradation of the ß-catenin and subsequent reduction in the expression of Wnt target genes. Upon binding of RSpondin ligands, Lgr5, Rspondin is able to interact with RNF43/ZNRF3 resulting in its clearance from the membrane. Consequently, the Frizzled receptor is stabilised, ensuring sustained Wnt signalling

1.2 The biology of the intestine

The mammalian intestine is a highly proliferative organ and renews every 3-5 days. The small intestine contains proliferative crypts (crypts of Lieberkuhn) and differentiated villi; an equivalent structural arrangement exists within the colon, although villi are absent.

The crypts contain intestinal stem cells (ISCs) and secretory Paneth cells which are required for the maintenance of the intestinal stem cell niche. There are on average 5-15 Paneth cells per crypt and can be identified by the large number of granules within the cells, which can be stained using periodic Schiff stain (Porter et al., 2002). Paneth cells are one of the longest-lived

differentiated lineages in the intestine, and typically reside in the base of the crypt for approximately 30 days (Troughton & Trier, 1969). Paneth cells are involved in microbial defence secreting peptides and enzymes such as defensins (Ouellette et al., 1999) and lysozyme (Ghoos & Vantrappen, 1971). Additionally, following the development of intestinal organoids culturing techniques (discussed later), Paneth cells were show to secrete a number of growth factors required for stem cell maintenance *in vitro*, including Epidermal Growth Factor (EGF) and Wnt3 ligands (Sato et al., 2011). Deletion of Wnt3 throughout the intestinal epithelium of adult mice is tolerated *in vivo*, due to compensation by mesenchymal-derived Wnt ligands (Farin et al., 2012). EGF has been shown to stimulate proliferation in the intestine (Potten et al., 1995), however a 60-day treatment of mice with an Epidermal Growth Factor Receptor (EGFR) inhibitor was well tolerated (Torrance et al., 2000). These studies suggest that some of the factors secreted by Paneth cells are not essential for intestinal stem cells *in vivo*, but rather support their niche. Indeed, even after ablation of Paneth cells (and other secretory lineages) following deletion of *Atoh1* in the murine intestine, a transcription factor important for determining secretory cell fate, functional ISCs were still present at the base of the crypt (Durand et al., 2012; Kim et al., 2012).

The other differentiated lineages arise in the villi of the intestine; the progeny of ISCs are transit-amplifying (TA) cells which proliferate rapidly and migrate up the crypt-villus axis, terminally differentiate and then are shed off at the top of the villi. TA cells give rise to the majority of differentiated cells within the small intestine. TA cells are thought to divide 4-5 times before terminally differentiating (Marshman et al., 2002). Furthermore, TA cells have been shown to cycle faster than intestinal stem cells and are significantly more abundant than intestinal stem cells. Hence this TA-zone acts as the source of differentiated lineages within the intestinal villi.

The predominant differentiated lineage in the small intestine are enterocytes (approximately 80%), which are required for the absorption of nutrients from the lumen of the small intestine. The mucus secreting goblet cells constitute around 5% of intestinal epithelial cells, however this number increases as you move from the proximal small intestine to the distal small intestine, whilst in the colon, goblet cells are the most abundant epithelial lineage. Goblet

cells secrete mucins, to provide a mucinous layer that acts as a lubricant and protects the underlying intestinal epithelium from bacteria. Another secretory lineage consists of enteroendocrine cells which secrete a large number of hormones, including serotonin and secretin (Hocker & Wiedenmann, 1998). The final differentiated lineage are the DCLK1 (Doublecortin-like kinase 1) positive Tuft cells (Gerbe et al., 2009). These tuft cells were shown to be dependent on the transcription factor ATOH1 and thought to represent a novel short-lived secretory lineage (Gerbe et al., 2011). However, subsequent studies identified a subpopulation of quiescent tuft cells that are long lived and play a role in the epithelial response to injury (Westphalen et al., 2014). The architecture of the small intestine is summarized in figure 1.3.

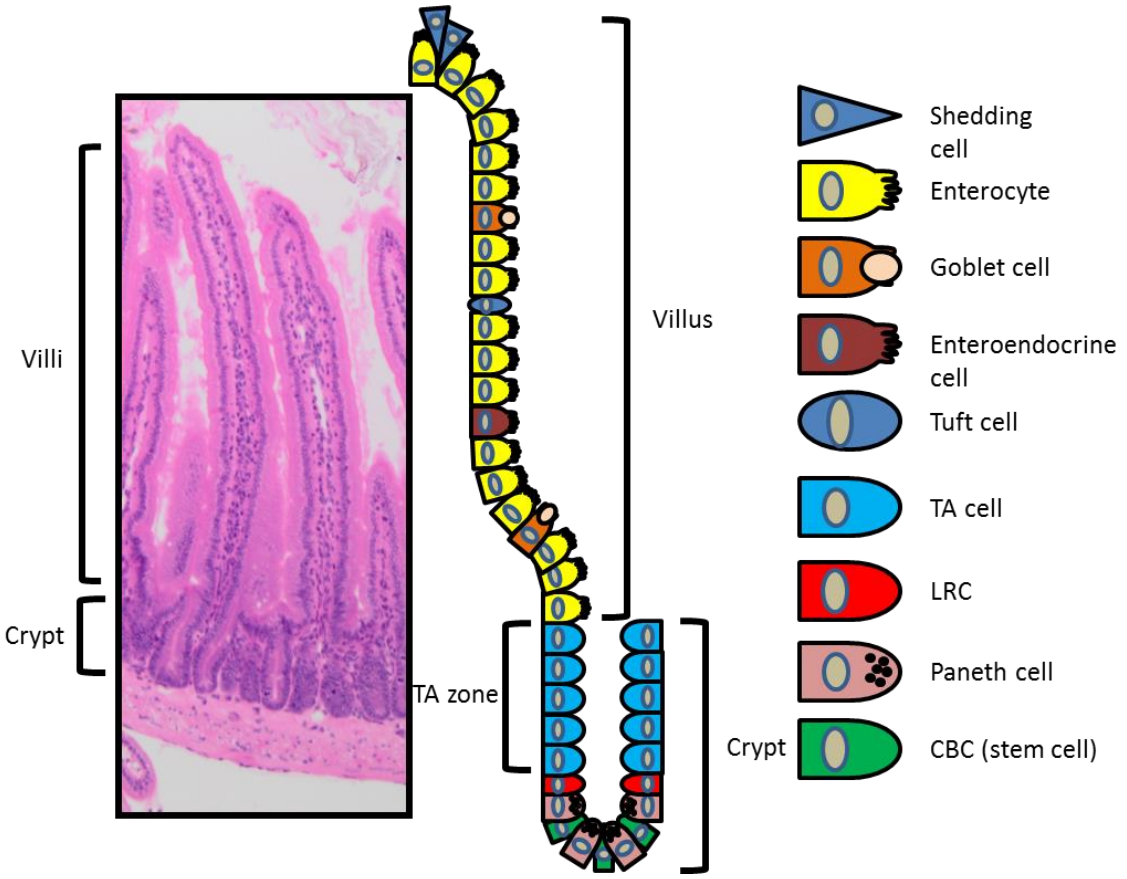

Figure 1.3: Tissue anatomy of the adult small intestine

Intestinal stem cells reside at the base of the crypt, between Paneth cells. The progeny of stem cells, transit-amplifying (TA) cells proliferate for several rounds before migrating up the crypt-villus axis and differentiating into enterocytes, tuft cells, goblet cells or enteroendocrine cells. Once the cells reach the top of the villus they are shed off into the lumen of the intestine, typically after 4-5 days. The label retaining cell (LRC), thought to be a quiescent reserve stem cell resides at the +4 position relative to the base of the crypt. H&E staining of WT small intestine - highlighting the structures of the crypt and the villus.

1.3 Intestinal stem cells

Early studies indicated that there are two different stem cell populations within intestinal crypts. Two studies in 1974 identified these two populations, based on their cycling times. The cycling crypt base columnar (CBC) stem cell was identified at the base of crypts, interspaced between Paneth cells. Tracing injected ^{3}H-thymidine over a time-course *in vivo* revealed that the four differentiated lineages; Paneth cells, goblet cells, enterocytes and enteroendocrine cells (Tuft cells hadn't been discovered yet) are derived from these CBC stem cells (Cheng & Leblond, 1974). Many years later, these stem cells were shown to be positive for *Lgr5*. Lineage tracing using *Lgr5-EGFP-IRES-creERT2* knock in mice crossed with *Rosa26-lacZ* reporter mice confirmed that these Lgr5-positive CBC stem cells generated all intestinal lineages within a 60 day period, suggesting that *Lgr5* expression marks these stem cells (Barker et al., 2007). Furthermore, when *Lgr5*-positive cells are isolated from mice and seeded as single cells, they can grow into self-renewing intestinal organoids that recapitulate the characteristics and lineages of the intestinal epithelium observed *in vivo*, highlighting their stem cell identity (Sato et al., 2009).

The second study in 1974 identified another, slow-cycling cell, which retained its' DNA radio-labelling (Potten et al., 1974) and was thought to represent another stem cell population. These label retaining cells reside at position +4 relative to the base of the crypt and were thought to be marked by the expression of *Bmi1*. Lineage tracing using *Bmi1Cre^{ER} Rosa26-LacZ* mice showed that these cells can give rise to all differentiated lineages within the intestinal epithelium (Sangiorgi & Capecchi, 2008). Interestingly, tamoxifen induction of *Bmi1Cre^{ER} Rosa26$^{DTA/+}$* mice led to the ablation of crypts following expression of diphtheria toxin in the *Bmi1*-positive cells – suggesting a loss of stem cells in these crypts (Sangiorgi & Capecchi, 2008). This could be in part be explained by subsequent studies that show that *Bmi1* is more ubiquitously expressed within the intestinal crypt, for instance *Bmi1* was detected in all *Lgr5*-positive fractions isolated via FACS from *Lgr5-EGFP-IRES-CreERT2* mice (van der Flier et al., 2009), whilst two separate studies revealed that *Bmi1* is expressed throughout the crypt (Itzkovitz et al., 2011; Muñoz et al., 2012).

A number of other markers for this +4 stem cell have been proposed such as *Hopx* (Takeda et al., 2011), *Tert* (Montgomery et al., 2010) and *Lrig1* (Wong et al., 2012). Each study showed that these genes were expressed in +4 stem cells, and that they could populate entire crypts. Interestingly, the *Lrig1* study identified a small number of *Lgr5*-positive *Lrig1* expressing cells in the base of the crypt, although this only constitutes 0.5% of intestinal stem cells (Wong et al., 2012), whilst *Hopx*-positive +4 cells can give rise to CBCs and vice versa (Takeda et al., 2011). A comprehensive transcriptomic and proteomic analysis of FACS (Fluorescent activated cell sorting) sorted *Lgr5*-positive cells revealed, that *Bmi1*, *Lrig1*, *Tert* and *Hopx* were expressed in *Lgr5*-positive cells, and in most cases the expression of these genes was highest at the base of the crypt (Muñoz et al., 2012). It was proposed that the *Lgr5*-positive cell population served as a workhorse population, fuelling the turnover of the intestinal epithelium under normal homeostasis, however a 'reserve' pool of *Lgr5*-negative quiescent stem cells exists above the crypt.

This notion was supported by a study that ablated the *Lgr5*-positive stem cell population via the inducible expression of Diphtheria toxin receptor (DTR) in *Lgr5Cre^{ER}-DTR* mice (Tian et al., 2012). In this study the authors showed that following induction, homeostasis in these *Lgr5Cre^{ER}-DTR* mice was not significantly perturbed and that the stem cells were repopulated by *Bmi1*-positive cells that became *Lgr5*-positive. This suggests that these different stem cell populations may have specific roles during homeostasis compared to an injury response. However a subsequent study showed that crypts depleted of *Lgr5*-positive cells following DTR expression were unable to regenerate following intestinal irradiation. This would suggest that *Lgr5*-negative stem cells are radiosensitive, and that *Lgr5*-positive cells are required to mediate intestinal regeneration (Metcalfe et al., 2014). It has also been proposed that TA cells could revert to stem cells in response to damage (Marshman et al., 2002). This was subsequently investigated using *Dll1-GFP-IRES-CreERT2* knockin mice (van Es et al., 2012). Delta-like 1 (Dll1) is expressed by a subset of immediate stem cell daughter cells, and is required for secretory lineage commitment. Lineage tracing revealed that *Dll1*-high cells can populate a crypt, and revert to *Lgr5*-positive stem cells upon irradiation. Furthermore these cells can form long-lived organoids when grown *in vitro*, hence highlighting the plasticity of these

secretory progenitors (van Es et al., 2012). A recent study also showed that enteroendocrine cells could serve as homeostatic and injury-inducible intestinal stem cells (Yan, Gevaert, et al., 2017). All of these different studies highlight the plasticity of the intestine and the ability of certain lineages to act as reserve stem cells upon damage to the stem cell compartment or during homeostasis.

1.3.1 Neutral drift

Maintenance of the stem cell pool is paramount for intestinal homeostasis. It was postulated that stem cells undergo asymmetric cell division; producing one TA cell and one daughter stem cell. However, other models suggest that stem cell homeostasis can be maintained by daughter cells that do not display divergent fates. For instance, a stem cell could produce two daughter stem cells, a TA cell and a stem cell or two TA cells. However, in this instance there must be mechanisms in place that ensure that on average each stem cell division produces one TA cell and one stem cell.

Two studies in 2010 sought to model the dynamics of intestinal stem cells, and in both cases concluded that intestinal stem cells exhibit neutral drift dynamics (Lopez-Garcia et al., 2010; Snippert et al., 2010). That is to say intestinal stem cells undergo symmetrical divisions and subsequent stochastic replacement of one another in order to maintain intestinal stem cell number. Both studies utilised lineage tracing to show that over time, crypts became monoclonal – that a crypt was repopulated by the progeny of just a single stem cell, and hence other stem cells had been replaced (Lopez-Garcia et al., 2010; Snippert et al., 2010). Snippert and colleagues used the confetti mouse – which upon tamoxifen induction leads to the expression of green fluorescent protein (GFP), yellow fluorescent protein (YFP), red fluorescent protein (RFP) or cyan fluorescent protein (CFP) from the *Rosa26* locus. The expression of these different fluorescent proteins is random; GFP expression is approximately 25% lower than the other three colours, which were present at equal levels. Given that over time crypts became monoclonal, it was concluded that these stem cell replacement events was stochastic (Snippert et al., 2010).

A subsequent study from the Winton lab sought to develop a system that would allow the investigation of intestinal stem cell dynamics and their implications for tumour initiation. The tomato, *tdRFP,* reporter mouse was

crossed to *AhCre*^{ER} mice and upon a very low level induction of tamoxifen, such that recombination would occur on average in only one stem cell per crypt. The recombined stem cells would be tomato positive and over-time you could track the ability of these single stem cells to repopulate a crypt (Vermeulen et al., 2013). The authors went on to show that stem cells carrying oncogenic mutations have a greater probability to replace their neighbouring stem cells, however their modelling also highlighted that there is a probability that mutant stem cells can also be replaced and therefore lost from within the intestinal stem cell niche. For instance, the model predicted that on average 4.3 hits were required in a crypt for an *Apc* deficient crypt to arise, highlighting how the architecture of the intestine suppresses the accumulation of mutations (Vermeulen et al., 2013).

1.4 Signalling pathways in the intestine

1.4.1 Intestine development

Several signalling pathways play a key role in the mammalian intestine both during development and homeostasis. The small intestine is formed from endoderm, and as the mammal develops, crypt-villus structures are formed. Once the gut tube is fully formed, by embryonic day 9.0 (e9.0), it condenses and then lengthens between e9.5-e13.5 as the embryo grows – increasing both its' circumference and lumen (Cervantes et al., 2009). This process was subsequently shown to be dependent on non-canonical Wnt5a signalling, since Wnt5a-null mice showed an 80% reduction in small intestine length and approximately 65% reduction in colon length compared with controls (Cervantes et al., 2009). It is thought that during the early stages of development the primitive gut exists as a stem-cell like pool. *Lgr5* has been shown to be expressed uniformly throughout the intestinal epithelium at e12.5, ahead of villus formation (Shyer et al., 2015). As villi structures begin to form, *Lgr5*-expression is lost from the cells within the villi forming tips, and by e15.5 *Lgr5*-expression is confined to the spaces between the forming villi (Shyer et al., 2015). Whilst these localised *Lgr5*-positive cells have been shown to be the progenitors of post-natal stem cells (Shyer et al., 2015), it is not until after birth that these *Lgr5*-expressing pockets mature into crypts.

The presence of different signalling gradients, with opposing roles, along the crypt-villus axis, namely Bone Morphogen Protein (BMP) and Wnt signalling serve to segregate the differentiated villi from proliferative crypts.

1.4.2 Bone Morphogen Protein (BMP) signalling

The restriction of these *Lgr5*-positive stem cells is driven by mechanical forces and subsequent morphogen signalling. Villi are first formed in mice at e14.5 following the folding of the underlying mesenchyme. This leads to increased Hedgehog (SHH) signalling within the tips of these villi structures, inducing the expression of villi-cluster genes within the mesenchyme, including many bone morphogen proteins (BMP). It is thought that this decreasing BMP gradient serves to restrict *Lgr5*-positive stem cells from the tips of the growing villi, since treatment of *ex vivo* cultured developing mouse guts with the SHH pathway inhibitor, cyclopamine, resulted in an expansion of the proliferative compartment and the expression of stem cell markers, *Cd44*, *Sox9* and *Lgr5* into the forming villi tips (Shyer et al., 2015). BMP signalling is also observed in the adult intestine – BMP-4 is expressed in the intervillus mesenchyme, but absent from the intercryptal mesenchyme (Haramis et al., 2004). Furthermore, nuclear phosphorylated Smad-1,-5 and -8 are observed within the villus epithelium, an indicator of paracrine BMP signalling from the mesenchyme to the villus epithelium (Haramis et al., 2004). Similar to the result observed by Shyer and colleagues using a SHH inhibitor, ectopic expression of the BMP inhibitor *in vivo*, Noggin, results in the formation of numerous ectopic crypts perpendicular to the crypt-villus axis (Haramis et al., 2004), again highlighting the role of BMP signalling in confining the proliferative compartment of the intestinal epithelium to the base of the crypt. Similarly, epithelial expression of another BMP antagonist Gremlin-1, which is usually expressed by pericryptal myofibroblasts, leads to ectopic crypt formation, and intestinal tumours (Davis et al., 2015) Interestingly, germline mutations within the BMP signalling pathway have been found within Juvenile Polyposis Syndrome patients – an autosomal dominant gastrointestinal syndrome (Howe et al., 1998; Howe et al., 2001). Whilst Hereditary Mixed Polyposis Syndrome patients harbour mutations that drive epithelial expression of *GREM1* (Jaeger et al., 2012). This highlights the role of BMP signalling in confining proliferation to the base of the crypt. The distribution of BMP signals along the crypt-villus axis is summarised in figure 1.4.

1.4.3 Wnt signalling

Numerous studies have implicated Wnt signalling in the proliferation of intestinal epithelial progenitor cells. For instance, cells residing at the base of the crypt accumulate nuclear ß-catenin (figure 1.3), whilst deletion of ß-catenin's transcriptional activator, Tcf4 results in the loss of proliferative crypts *in vivo* (Korinek et al., 1998). Furthermore, ectopic expression of Dickkopf1 (Dkk1), a secreted Wnt inhibitor, in the intestine results in a significant reduction in proliferation and a concomitant loss of crypts (Pinto et al., 2003). Dkk1 has been shown to be a Wnt target gene, and constitutes part of a negative feedback loop (Niida et al., 2004). Another Wnt signalling negative feedback loop was shown to be required for confining proliferative cells to the crypt base. Two genes encoding related transmembrane E3 ubiquitin ligases, *Rnf43* and *Znrf3*, are uniquely expressed in *Lgr5*-positive stem cells – they are required for the targeting of Frizzled receptors for degradation (Koo et al., 2012). Deletion of *Rnf43* and *Znrf3* throughout the intestinal epithelium leads to a significant expansion of the proliferative crypt region and an accumulation of nuclear ß-catenin in cells higher up the crypt (Koo et al., 2012).

Ectopic expression of RSpondin drives increased proliferation and *Lgr5* expression in small intestinal crypts – driving an expansion of the crypt (Yan et al., 2017). A recent study has highlighted some key differences between RSpondin and Wnt ligands and that they cannot simply be interchanged. Yan and colleagues reveal that in the absence of Wnt and RSpondin ligands, Lgr5-positive intestinal stem cell is to differentiate, since Wnt ligands are not sufficient to induce intestinal stem cell renewal. Rather, Wnt ligands induce a basal expression of Lgr5, which upon binding of RSpondin potentiates Wnt signalling to induce a transcriptional programme that drives intestinal stem cell progenitors (Yan et al., 2017). In addition to a role in intestinal stem cell renewal, Wnt signalling plays a key role in the regulation of proliferation and cell localisation in intestinal crypts.

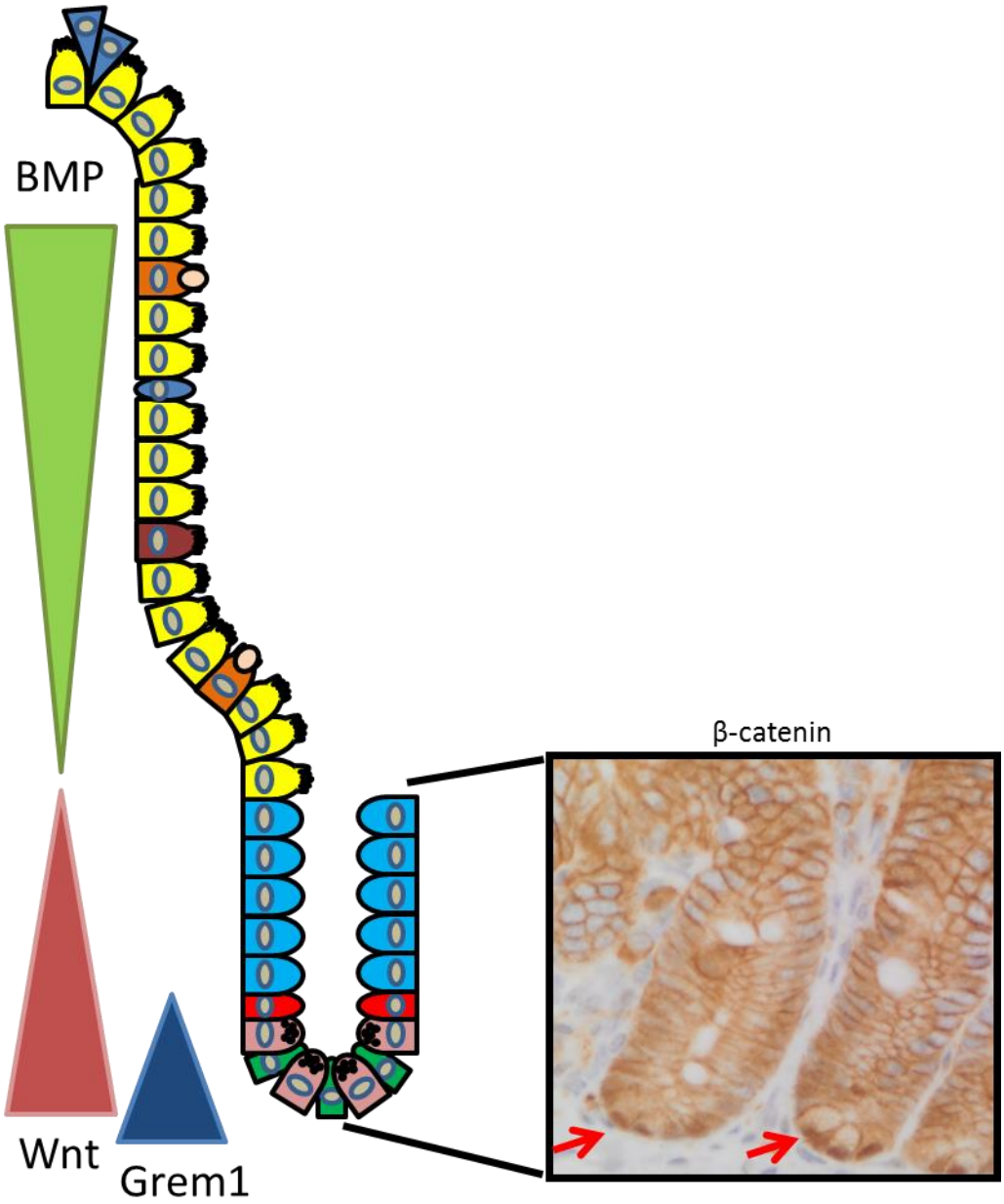

Figure 1.4: Signalling pathways in the mammalian intestine

Wnt and BMP gradients exist in opposing directions within the small intestine. At the bottom of the crypt, BMP signalling is reduced by the secretion of BMP antagonists. Wnt signalling is highest at the base as indicated by the nuclear accumulation of ß-catenin (red arrows) in the cells in the base of the crypt. Gremlin is secreted by pericryptal myofibroblasts, creating a decreasing gradient along the crypt axis.

Wnt signalling plays a key role in the switch between proliferation and differentiation within the intestine. TCF4 knockout mice (*Tcf7l2*$^{-/-}$) die shortly after birth (Korinek et al., 1998), however the role of TCF4 was studied in the embryonic development of intestinal crypts, referred to as 'prospective crypts'. These prospective crypts express TCF4, CD44 and c-MYC, whilst p21, which is repressed by c-MYC, is expressed in the intestinal villi of these embryos. Upon

TCF4 deletion CD44 and c-MYC expression is lost from these prospective crypts whilst p21 is now expressed in these crypts (van de Wetering et al., 2002). The authors made a similar observation using human colorectal cancer cells; overexpression of a dominant-negative TCF that lacks ß-catenin binding activity leads to a significant reduction in proliferation in these cells lines and the induction of an intestinal differentiation programme (van de Wetering et al., 2002). Wnt signalling was also shown to control the exact positioning of cells within the intestinal epithelium via the ß-catenin/TCF dependent expression of EphB and EphrinB (Batlle et al., 2002).

1.4.4 Notch signalling

Notch signalling has been shown to play a key role in the differentiation of secretory lineages in the adult intestine. Both Notch receptors and ligands are bound to the membrane; hence this pathway is only active between adjacent cells. Upon binding of Notch ligands to their receptor, the receptor is cleaved, leading to the translocation of the Notch intracellular domain (NICD) to the nucleus and expression of Notch target genes (Bray, 2006). The notch ligand, *Dll1*, has been shown to be expressed by early TA cells, and that these *Dll1*-positive cells have been shown to give rise to secretory lineages in the intestine (van Es et al., 2012). Indeed, genetic and pharmacologic inhibition of Notch signalling leads to a significant increase in goblet cell production (van Es et al., 2005).

1.5 Colorectal Cancer

1.5.1 Hereditary forms of Colorectal Cancer

A number of hereditary genetic predispositions to colorectal cancer have been defined, the most commonly studied being Hereditary Non-Polyposis Colorectal Cancer (HNPCC) and Familial Adenomatous Polyposis (FAP).

HNPCC was one of the first hereditary cancer syndromes to be described and is an autosomal dominant syndrome. Patients with this disease present with proximal colonic tumours which are characterised by various distinct histological features, including mucinous differentiation, increased lymphocytic infiltration and Chron's disease-like lymphocytic differentiation. HNPCC patients have a microsatellite instability (MSI) phenotype, due to mutations in DNA mismatch

repair (MMR) genes, such as *MLH1* and *MSH2*, which account for 70% mutations in HNPCC patients (Vilar & Gruber, 2012).

FAP is also an autosomal dominant syndrome which accounts for approximately 0.5% of colorectal cancers. Patients develop hundreds to thousands of colonic polyps by the age of 30, with a handful progressing to carcinoma; hence the patient's colon is often removed to manage the disease. The underlying genetic event of FAP is germline mutations in the Adenomatous Polyposis Coli (*APC*) gene. Approximately 95% of these mutations are either frameshift or nonsense mutations resulting in the expression of a truncated version of the *APC* protein (Galiatsatos & Foulkes, 2006). There is a clustering of these mutations towards the 5' end of the APC gene, with two hotspots at codons 1061 and 1309 (Segditsas & Tomlinson, 2006). The second copy of *APC* is mutated – approximately 30% of patients show a Loss of Heterozygosity (LOH) event, with the remaining two-thirds exhibiting truncating mutations in the second copy of *APC* (Lamlum et al., 1999).

1.5.2 Genetic progression of Colorectal Cancer

The identification of *APC* as a causal event for FAP, and the fact that it is mutated in approximately 80% of spontaneous colorectal cancer, lead to the notion that mutation in *APC* is a critical event in the early stages of colorectal cancer. The observations that larger adenomas contained more mutations lead to the suggestion that colorectal cancer progressed in a step-wise manner, with the accumulation of additional mutations. Fearon and Vogelstein investigated the frequency of some of the most common mutations in colorectal cancer at different stages of the disease, such as adenoma and carcinoma and proposed the step-wise accumulation of mutations as outline in Figure 1.6 (Fearon & Vogelstein, 1990). Whilst they found that nearly all tumours, regardless of stage had mutations in the FAP locus, approximately only 50% had mutations in *KRAS*, interestingly the tumours harbouring *KRAS* mutation were predominantly classed as 'intermediate adenomas' or at a later stage. Similarly, Chromosome 17p loss was associated with larger adenomas or carcinomas, therefore suggesting that these mutations accumulate in a step-wise manner over time (Fearon & Vogelstein, 1990).

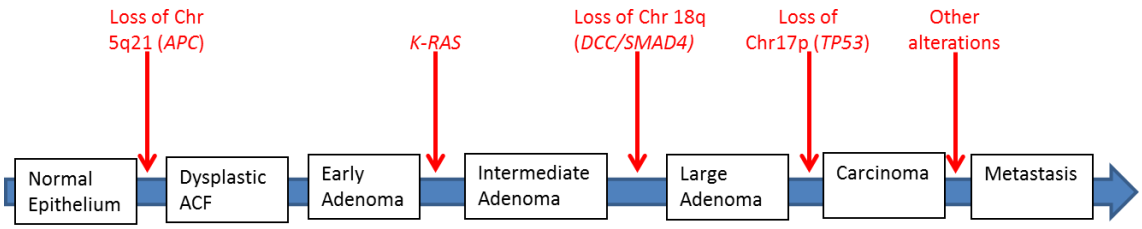

Figure 1.6: Genetic progression of Colorectal Cancer
Simplified model of colorectal cancer progression, adapted from (Fearon & Vogelstein, 1990). Abbreviations, ACF = aberrant crypt foci and Chr= chromosome.

The locus of FAP has been mapped to chromosome 5q (Leppert et al., 1987), which has subsequently been shown to *APC* (Groden et al., 1991; Kinzler et al., 1991), whilst the region within chromosome 17p that is lost contains the tumour suppressor gene *TP53* (Baker et al., 1989). Hence, in their model Vogelstein and Fearon showed that the progression of CRC is driven by a combination of the loss of tumour suppressor genes and activation of oncogenes, but that it is the loss of the tumour suppressor genes, such as *APC*, is the dominating factor.

More recently, advances in DNA sequencing has allowed the large scale sequencing of human tumours. It was discovered that colorectal cancer tumours contain on average 80 mutations (Wood et al., 2007), and that these mutations result in a broad range of inter-tumour heterogeneity (Munzy et al., 2012; Sjöblom et al., 2006). It is important to remember that not all of these somatic mutations will have a causal effect, that is to say some mutations will be 'driver' mutations and others 'passenger' mutations (Greenman et al., 2007). Of the 80 mutations within colorectal cancers, it was shown that only 15 were considered real 'driver' mutations required for the initiation, progression and maintenance of the tumour (Wood et al., 2007). Furthermore, rather than these driver mutations affecting a particular gene, they are found within recurrent pathways – such as WNT-, MAPK-, TGFß-, p53- and PI3K-signalling. For instance, it was shown that over 94% of colorectal cancer tumours had a mutation in one or more components of the WNT pathway (Munzy et al., 2012), whilst it has been shown that *KRAS* and *BRAF* mutations are mutually exclusive in colorectal cancer (Di Nicolantonio et al., 2017).

1.5.3 Classification of Colorectal Cancer

Originally, Colorectal Cancer tumours were broadly classed into three groups:

1. **Chromosome Instability (CIN) phenotype** – karyotyping analysis revealed that these tumours display numerous chromosomal alterations, such as loss of chromosome 17p, but are microsatellite stable.
2. **Microsatellite Instability (MSI) phenotype** - these are characterized by alterations of microsatellite sequences at many loci across the genome. MSI is observed in approximately 15% of sporadic colorectal cancers (Thibodeau et al., 1993). These tumours often have defects in MMR genes.
3. **CpG island methylation phenotype (CIMP)** can be subdivided into two groups, CIMP-LOW and CIMP-HIGH. The CIMP-LOW group is often associated with *KRAS* mutation, whilst CIMNP-HIGH tumours often display hypomethylation of *MLH1* and *BRAF* mutations (Hinoue et al., 2012).

Whilst these broad classifications were used to describe inter-tumour heterogeneity, many tumours display characteristics of more than one group, for instance Weisenberger and colleagues showed that many *BRAF* mutant tumours display both CIMP and MSI phenotypes (Weisenberger et al., 2006).

More recently, a large consortium has further classified colorectal cancer into four consensus molecular subtypes (CMS) using expression data from a central repository (Guinney et al., 2015). The key molecular features of the four different sub-types is summarised in table 1.1.

Table 1.1: Consensus Molecular Subtypes of Colorectal Cancer

CMS1 – MSI immune	CMS2 - canonical	CMS3 - metabolic	CMS4 – mesenchymal
14%	37%	13%	23%
MSI, CIMP high, hypermutation	SCNA high	Mixed MSI status, SCNA low, CIMP low	SCNA high
BRAF mutations	WNT and MYC activation	*KRAS* mutations	Stromal infiltration, TGF-Ɓ activation, angiogenesis

Molecular features of the four consensus molecular subtypes of colorectal cancer. Abbreviations, MSI, microsatellite instability, CIMP, CpG island methylation phenotype and SCNA, somatic copy number alteration. Adapted from (Guinney et al., 2015)

Given my interest in the cooperation of *APC* loss and *KRAS* mutation, the CMS2 and CMS3 subtypes are of greatest interest for this thesis. It is hoped that this sub-typing approach and a greater understanding of these expression profiles will pave the way for stratified medicine.

1.5.4 Mutations in *APC* and other components of the WNT pathway in Colorectal Cancer

In addition to APC's role in FAP development, it also plays a key role in sporadic colorectal cancer. Whilst 94% of colorectal cancer tumours contain mutations in the WNT pathway, highlighting the importance of this pathway in the disease, approximately 80% of all colorectal cancer patients harbour bi-allelic *APC* loss (Munzy et al., 2012). There were also mutations in *AXIN2* and *FAM123B*, both negative regulators of the WNT pathway (Major et al., 2007), whilst *FZD10*, the WNT ligand receptor was overexpressed in approximately 17% of tumours (Munzy et al., 2012). Interestingly, many of these mutations were not mutually exclusive with *APC* mutation. Hence, the cooperation of these mutations and *APC* mutations may confer some selective advantage by further modifying the WNT pathway.

There are two types of somatic *APC* mutations – loss of heterozygosity (LOH) and protein-truncating mutations. The latter, as in FAP patients, have been shown to cluster to a specific region within the 5' end of the gene, referred to as the Mutation Cluster Region (MCR) (Crabtree et al., 2003). The MCR corresponds to codons 1286-1513; this only represents 8% of the gene (Nagase and Nakamura, 1993). This region of the *APC* gene encodes the 20 amino-acid repeats (20AARs) that are required for ß-catenin binding and degradation (Rubinfeld et al., 1997). Hence these truncating mutations will lead to a stabilisation of ß-catenin, activating the WNT signalling pathway, confirming the important role of WNT signalling in Colorectal Cancer.

To further corroborate this, it has been shown using genetically engineered mouse models that activating the WNT pathway independently of *APC* loss can lead to intestinal tumourigenesis. For instance, expression of a stabilised form of ß-catenin throughout the murine intestine leads to a dysplastic transformation throughout the proximal small intestine (Leedham et al., 2011). Whilst deletion of both isoforms of GSK3, the kinase responsible for the

phosphorylation of ß-catenin, leads to the transformation of the mouse small intestine with similar kinetics to homozygous *Apc* deletion (Huels et al., 2015). Despite this, mutations in *CTNNB1*, *GSK3A* and *GSKB* are very rare in colorectal cancer, and as with other mutations within the WNT pathway, are not mutually exclusive with *APC* mutations.

1.5.4.1 'Just-right' levels of Wnt signalling in colorectal tumours

Even though APC is often cited as a classic tumour suppressor gene in colorectal cancer, the frequency of LOH in colorectal cancer is lower than many other tumour suppressor genes in other cancers. A possible explanation for this was provided from a study on tumours from FAP patients. Lamlum and colleagues observed the following patterns of *APC* mutations in FAP patients:

1. LOH is associated with germline mutations between the first and second 20AAR (codons 1285-1379).
2. Germline mutations before codon 1280 are associated with somatic mutations between the second and third 20AAR (codons 1400-1495).
3. Germline mutations after codon 1400 are associated with somatic mutations before 1280.

Consequently, most FAP tumours have *APC* alleles that contain a total of two 20AARs – a similar observation was made in sporadic colorectal cancer (Lamlum et al., 1999). These mutations have been proposed to result an optimal level of Wnt signalling within these tumours (Albuquerque et al., 2002; Lamlum et al., 1999). This is supported by a study that showed that a reduction in APC levels using RNA interference reduced the proliferation of a colon cancer cell line that expresses a truncated APC protein (Schneikert & Fodde, 2006). Whilst truncated APC proteins have been shown to be able to regulate ß-catenin levels, a SW480 colon cancer cell line containing an APC protein with only 2 20AARs had the highest levels of ß-catenin expression (Rubinfeld et al., 1997). Altogether these studies highlight that colorectal tumours select for a combination of *APC* mutations that provide a superior growth advantage for tumour cells, such that a 'just right' level of WNT signalling, which may be sub-maximal, is required for dysplasia.

Genetic mouse models may also give a clue towards this proposed 'just-right' theory. Two spontaneous mouse models of intestinal tumourigenesis, both harbouring germline truncating *Apc* mutations, the $Apc^{Min/+}$ mouse and the $Apc^{1322T/+}$ mouse, display some interesting phenotypic differences. $Apc^{1322T/+}$ mice develop a heavy tumour burden predominantly within the proximal small intestine, whilst $Apc^{Min/+}$ mice develop tumours mainly within the distal small intestine (Pollard et al., 2009). The Apc^{1322T} allele contains 1 20AAR, and the Apc^{Min} allele gives rise to a truncate Apc protein lacking all 20AARs – this has been shown to lead to sub-maximal Wnt signalling within $Apc^{1322T/+}$ tumours, despite a more severe phenotype compared with $Apc^{Min/+}$ tumours (Lewis et al., 2010; Pollard et al., 2009). A subsequent study investigating Wnt signalling levels throughout the murine intestine and colon provided an explanation to the differences in the intestinal tumour locations of $Apc^{Min/+}$ and $Apc^{1322T/+}$ mice. Leedham and colleagues showed that there is a decreasing Wnt and stem cell gradient from the proximal small intestine longitudinally to the colon in mice, and that the basal levels of Wnt signalling affect the distribution of intestinal tumours. The authors proposed that maximal Wnt signalling in $Apc^{Min/+}$ tumours is excessive and suboptimal for tumour formation in the proximal small intestine due to high underlying basal Wnt signalling. Whilst sub-maximal Wnt signalling within $Apc^{1322T/+}$ tumours combined with high basal Wnt signalling is sufficient for tumour formation in the proximal small intestine (Leedham et al., 2011).

Importantly, complete deletion of APC, using the $Apc^{+/\Delta e1\text{-}15}$ allele, reduces tumour latency compared with $Apc^{Min/+}$ mice, although there was no difference in tumour distribution between the two cohorts (Cheung et al., 2009). Surprisingly, despite complete loss of APC, tumours from $Apc^{+/\Delta e1\text{-}15}$ mice had lower levels of ß-catenin activity compared with tumours from $Apc^{Min/+}$ mice (Cheung et al., 2009). It is difficult to speculate as to why complete loss of the APC protein reduces Wnt signalling compared to a truncated protein, aside from potential feedback loops impinging on the pathway. Nonetheless, this $Apc^{+/\Delta e1\text{-}15}$ model, like the $Apc^{1322T/+}$ mouse, reveals that sub-maximal Wnt signalling can yield a more severe phenotype.

1.5.5 RAS signalling

The RAS proteins are small GTPases that serve as binary switches, cycling from an active guanosine triphosphate (GTP)-bound state and an inactive guanosine diphosphate (GDP)-bound state. The switching between these two activity states is mediated by auxiliary proteins: guanine nucleotide exchange factors (GEFs) are responsible for the exchange of GDP to GTP, activating the RAS protein; conversion back to the inactive GDP state is carried out by GTPase activating proteins (GAPs) (reviewed in Wittinghofer et al., 1997), this is summarised in figure 1.5. Many RAS GEFs are activated following upstream activation of receptor tyrosine kinases (RTKs), such as EGFR, which is activated upon binding of its ligand EGF. Following RTK activation, these receptors dimerise and autophosphorylate tyrosine residues within their intracellular domains. These phospho-tyrosine domains in turn recruit SH2-domain containing proteins, such as Growth factor receptor-bound protein 2 (GRB2) (Batzer et al., 1994). GRB2 also contains two SH3 domains which recruits proline-rich domains of other proteins, such as Son of sevenless (SOS) (Flogg et al., 1991). Following translocation of RAS to the membrane, SOS mediates exchange of RAS-bound GDP for GTP, thereby activating RAS (Chardin et al., 1993). The dependency of RAS proteins on their GEFs and GAPs ensures that their activity is tightly regulated. Once activated, RAS proteins activate their effectors following recruitment to the plasma membrane.

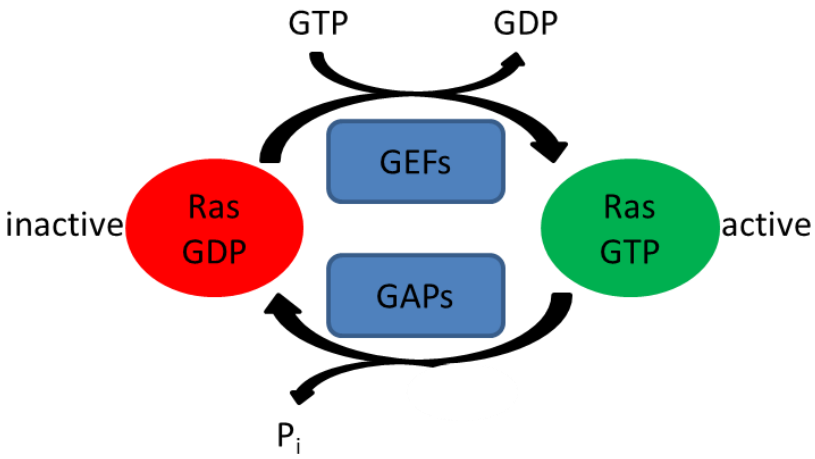

Figure 1.5: RAS proteins act as a binary switch
RAS proteins are activated following binding of GTP, which is mediated by Guanine nucleotide exchange factors (GEFs). Ras proteins are inactivated following hydrolysis of GTP to GDP, which is accelerated by GTPAse activating proteins (GAPs).

There are numerous RAS downstream effector proteins. In normal mammalian cells the major RAS effectors are the RAF kinases (A-RAF, B-RAF and C-RAF). RAF proteins are serine/threonine kinases and function within the Mitogen Activated Protein Kinase (MAPK)-pathway, they are activated by RAS following their recruitment to the plasma membrane (Leevers et al., 1994). The MAPK-pathway is evolutionarily conserved and transduces extracellular signals to the nucleus via a kinase cascade, to control processes such as growth, proliferation and differentiation. There are numerous MAPK cascades; however the most studied pathway is the MEK-ERK pathway. Active RAF mediates phosphorylation of Mitogen-activated protein/extracellular signal-regulated kinase (MEK), which in turn phosphorylates Extracellular signal-regulated kinase (ERK). Once phosphorylated, ERK translocates to the nucleus and phosphorylates nuclear targets to induce a transcriptional programme in response to extracellular stimuli.

RAS proteins have been shown to directly interact with the catalytic subunit of phosphatidylinisotiol-3-kinase (PI3K) in a GTP dependent manner and activate PI3K (Rodriguez-Viciana et al., 1994). PI3K phosphorylates the lipid phosphatidylinositol-4,5-biphosphate (PtdIns(4,5)P_2) to produce phosphatidylinositol-3,4,5-triphosphate (PtdIns(3,4,5)P_3) – which activates 3-phosphoinositide-dependent protein kinase-1 (PDK1), which in turn activates AKT (Protein kinase B) (Khwaja et al., 1997). PI3K/AKT signalling plays a key role in cell survival, but also protein synthesis in response to extracellular stimuli. PI3K activation can also stimulate RAC (Ras-Related C3 Botulinum Toxin Substrate 1), which is involved in the regulation cytoskeleton remodelling and transcription factors, however RAS has been shown to mediate RAC activation independently of PI3K activity via TIAM1 (T-cell Lymphoma Invasion and Metastasis) - a RAC GEF (Lambert et al., 2002). Another number of downstream effectors have been identified – RAS has been shown to interact with Ral GDP dissociation stimulator (RalGDS) (Hofer et al., 1994), which is a GEF for the Ral GTPase protein – thereby linking RAS activation to Ral (Ras-related protein) signalling (Kishida et al., 1997). The Ral proteins have been shown to interact with a wide spectrum of signalling pathways including exocytosis, endocytosis, lipid metabolism and proliferation (reviewed in Neel et al., 2011).

These downstream effectors of RAS proteins play a key role in the regulation proliferation, survival and protein synthesis; therefore aberrant RAS activity could have profound effects upon cell growth and proliferation. Consequently, it is no surprise that it has an oncogenic role in many cancers.

It is important to note that RAS proteins come in a number of different flavours, such as NRAS, KRAS and HRAS, the latter two were originally identified from transforming retroviruses that produced tumours in mice (Harvey, 1964; Kirsten et al., 1970), whilst NRAS was isolated from human neuroblastoma cells. Analysis of a number of other human cancers revealed that these RAS proteins were able to transform mammalian cells, and that the RAS mutant alleles in these cancer contained point mutations which inactivated the protein's GTPase activity, and were therefore constitutively active (Reddy et al., 1982). This was also found to be the case in colorectal cancer, with both *KRAS* and *NRAS* being mutated in colorectal tumours.

1.5.6 Mutations in the MAPK-signalling pathway in Colorectal Cancer

The two small GTPase-encoding genes *KRAS* and *NRAS* are mutated in approximately 40% and 10% of colorectal cancers respectively and in a mutually exclusive fashion, with most frequent mutations in codons 12, 13 and 61 (Munzy et al., 2012). It has previously been shown that mutations in codon 12 are more abundant than codon 13 mutations in colorectal carcinoma, and the most frequent variant being the G>A transition, leading to a glycine to aspartic acid substitution (Rosty et al., 2013). This amino acid substitution results in a constitutively active form of KRAS, since it is unable to hydrolyse guanosine triphosphate (GTP). The RAS proteins functions downstream of different Receptor Tyrosine Kinases, such as EGFR, and despite the frequency of *KRAS* mutation, mutations or amplifications of the EGFR gene are rare in colorectal cancer (Leary et al., 2008).

Kras and *Nras* mutations have been shown to have differential affects in the mouse colon. Oncogenic KRAS drives a hyperproliferative phenotype and alters differentiation in a MEK-dependent manner (Feng et al., 2011; Haigis et al., 2008). *Nras* mutation on the other hand did not induce a hyperproliferative phenotype, but conferred resistance to apoptosis (Haigis et al., 2008). These studies highlight that mutations in different RAS genes in the intestinal

epithelium can give rise to different phenotypes via preferential activation of downstream effectors.

Downstream of KRAS is BRAF, which is a serine/threonine kinase, and mediates the phosphorylation and subsequent activation of MEK. *BRAF* is mutated in approximately 10% of colorectal cancers, with the most frequent mutation being at codon 600 – a T>A substitution, resulting in a valine to glutamic acid substitution – which in turn results in constitutive kinase activity (Davies et al., 2002). Mutations of *KRAS* and *BRAF* are mutually exclusive in colorectal cancer, and as previously mentioned above, tumours harbouring either mutations have different phenotypes – *KRAS* mutant tumours are associated with a CIMP-LOW phenotype and fall within the CMS3-metabolic sub-type, whilst *BRAF* mutant tumours display a MSI and CIMP-HIGH phenotype, and are grouped in the CMS1 – MSI immune subtype (Guinney et al., 2015; Hinoue et al., 2012). Hence, despite *KRAS* and *BRAF* mutations both activating MAPK-signalling (KRAS can activate other parallel pathways); the arising phenotypes of the tumours are very different.

The CMS3 subtype, hallmarked by *KRAS* mutation, has been shown to be enriched for multiple metabolism signatures, including glycolysis and glutamine metabolism (Guinney et al., 2015). This is in agreement with other studies showing that activating *KRAS* mutations induces metabolic adaptation involving glucose (Ying et al., 2010) and glutamine metabolism (Son et al., 2013), as well as scavenging for macromolecules (Bar-Sagi & Feramisco, 1986; Kamphorst et al., 2013). These metabolic adaptations allow for the growth of transformed cells via nutrient scavenging or anabolic processes, and therefore are likely to be required during stressed conditions, such as low nutrient supply or hypoxia. Recall that Vogelstein and colleagues observed that *KRAS* mutations was only observed in approximately 10% of adenomas less than 1cm, whilst approximately 60% of adenomas larger than 1cm and nearly 50% of carcinomas harboured *KRAS* mutation (Vogelstein et al., 1988). Therefore, it is possible that *KRAS* mutations are required for the progression of colorectal cancers as the tumours develop and outgrow their existing nutrient supplies.

1.5.7 Potential therapeutic targets identified from CMS subtypes

In this thesis I will be focussing on the cooperation of APC and KRAS mutations. These two mutations are particularly enriched in the CMS2 and CMS3 subtypes (Guinney et al., 2015). As previously mentioned above KRAS mutation are known to affect metabolism, hence looking at changes in metabolism following KRAS mutation could uncover metabolic vulnerabilities. Similarly, APC is mutated in approximately 80% of CRC patients, resulting in Wnt pathway activation (Munzy et al., 2012). However, at present there are no successful therapies targeting this pathway, but a proof of principle study that re-expressed APC regressed murine colonic carcinomas, highlighting the dependency of CRC tumours on Wnt signalling for their progression (Dow et al., 2015). Hence, identification of successful Wnt inhibitors could yield a significant therapeutic window in CRC. Finally, the CMS2 subtype had a ribosomal/translation signature – we have previously shown that inhibition of translation elongation suppresses growth of APC-deficient intestinal epithelial cells (discussed further in 1.6.1). However, it is also know that KRAS mutation can affect the translation machinery (Bhat et al., 2015). Hence, translation, which is frequently deregulated in cancer, might provide another therapeutic window in *KRAS* driven CRC. Moreover oxaliplatin, the current standard of care for CRC, has recently been identified to induce ribosomal biogenesis stress in human colon cancer cell lines (Bruno et al., 2017). These hypotheses will form the basis of this thesis and discussed further below.

1.6 Models to study Colorectal Cancer

In addition to multiple human derived colorectal cancer cell lines, a number of Genetically Engineered Mouse Models (GEMMs) have been developed over the years to study colorectal cancer.

1.6.1 Mouse models of Colorectal Cancer

One of the most routinely used mouse models for studying colorectal cancer was developed in 1990. A pedigree was derived from a mouse that had been treated with the mutagen *N*-ethyl-*N*-nitrosourea (ENU), which was predisposed to spontaneous intestinal cancer (Moser et al., 1990). The mutant gene termed multiple intestinal neoplasia (Min), was subsequently mapped to

the murine *Apc* gene (Su et al., 1992), and these mice are now referred to $Apc^{Min/+}$ mice. The mutation in $Apc^{Min/+}$ mice converts codon 850 from a leucine residue (TTG) to a stop codon (TAG), resulting in the expression of a truncated form of the APC protein (Su et al., 1992). This nonsense mutation is similar to that observed in FAP patients, however unlike FAP patients who develop a large number of colonic adenomas, $Apc^{Min/+}$ mice develop a large number of small intestinal adenomas with only a few colonic lesions (Moser et al., 1990). The development of these intestinal adenomas is dependent on the loss of the second copy of *Apc* via sporadic LOH in the adult mouse – this differs to the human FAP patients, where LOH is only seen in approximately one-third of patients (Lamlum et al., 1999). Another key difference between the $Apc^{Min/+}$ model and human FAP patients, is that in humans, if not treated, tumours can progress to carcinoma, however this is rarely seen in $Apc^{Min/+}$ mice. This is presumably due to the large tumour burden within these mice, such that they are sampled before the tumours can progress to this stage.

Additional spontaneous mouse models of colorectal cancer have been developed. Similar to $Apc^{Min/+}$ mice, these models also carry germline mutations in the *Apc* gene, but at different locations. For instance, the $Apc^{1322T/+}$ mouse has a mutation that very closely mimics the human mutation at codon 1309 in FAP patients. The $Apc^{1322T/+}$ mice develop a greater number of total tumours, as well as larger tumour, at an earlier onset compared with $Apc^{Min/+}$ mice, but with no invasive lesions (Pollard et al., 2009). Surprisingly, the authors showed that despite this more severe phenotype, the tumours that arose in $Apc^{1322T/+}$ mice displayed reduced levels of nuclear ß-catenin compared with tumours from $Apc^{Min/+}$mice, and this was associated with submaximal Wnt signalling (Lewis et al., 2010; Pollard et al., 2009). Another spontaneous mouse model for colorectal cancer is the $Apc^{1638N/+}$ mouse, which develops far fewer tumours with a much longer latency than the $Apc^{Min/+}$ mouse (Fodde et al., 1994).

As genetics progressed, conditional knockout mice were generated as tools for investigating the role of genes in a tissue-dependent context. Shibata and colleagues generated an *Apc*-flox allele, that contained lox-P sites either side of exon 14; which was used to generate truncated APC proteins (at codon 580) specifically within the colonic epithelium, following local infection of the colon with an adenovirus encoding Cre-recombinase (Shibata et al., 1997). Mice

homozygous for this floxed *Apc*-allele developed colonic adenomas within four weeks of infection, and those aged for longer developed adenocarcinomas (Shibata et al., 1997). This model has an advantage over the $Apc^{Min/+}$ mouse by virtue that one can initiate tumourigenesis in the colon, rather than the small intestine, however going forward, this approach was not so routinely used as the $Apc^{Min/+}$mouse.

The development of tissue specific Cre-recombinases allows for the inducible recombination of target alleles in tissues of interest. The floxed *Apc* allele developed by Shibata and colleagues was combined with the inducible AhCre system, driven by the *Cyp1a1* promoter, which upon administration of ß-napthoflavone induces recombination throughout the small intestine, but not Paneth cells and to a lesser extent the colon (Ireland et al., 2004). Deletion of both copies of APC had a severe impact upon intestinal homeostasis; there was an increase in proliferation, abrogation of migration and altered differentiation; this is referred to as the 'crypt-progenitor phenotype' (Sansom et al., 2004). This phenotype was subsequently shown to be mediated by the Wnt target gene c-*Myc* (He et al., 1998), since deletion of both copies of c-*Myc* reversed this crypt progenitor phenotype (Sansom et al., 2007). This observation is in agreement with the CMS2 subtype which showed strong upregulation of both WNT and MYC downstream targets (Guinney et al., 2015).

This acute deletion of both copies of APC provides a great tool for investigating the mechanism of early tumourigenesis, and is routinely used in the Sansom lab. However, a different Cre-driver is used, due to the poor recombination of *AhCre* in the colon, and promiscuous recombination in other organs - including the liver (Ireland et al., 2004). El Marjou and colleagues generated a Cre system under the control of the *Villin* promoter to drive expression throughout the murine small intestine and colon (El Marjou et al., 2004). They generated two systems, one that is switched on during development from embryonic day 9 (E9) - *VillinCre*, and the other an inducible Cre-recombinase -$VillinCre^{ER}$ – which can be switched on following administration of tamoxifen (El Marjou et al., 2004). As markers of particular lineages have been discovered, this has allowed the development of Cre-recombinase systems within a specific cell lineage. In 2007, the $Lgr5Cre^{ER}$ (*Lgr5-EGFP-IRES-creERT2*) mouse was generated, allowing the recombination specifically within intestinal stem

cells, which reside at the bottom of the crypt (Barker et al., 2007). Importantly, this transgene contains an enhanced green fluorescent protein (EGFP) – thereby allowing the visualisation and tracking of intestinal stem cells.

Deletion of both copies of APC using *Lgr5Cre^{ER}* following tamoxifen administration leads to adenoma formation after 3-5 weeks (Barker et al., 2009). In this study, the authors showed that intestinal stem cells act as an efficient cell of origin of intestinal tumourigenesis, when compared with deletion of both copies of APC within the villi and the transit-amplifying zone using an oral dose of ß-napthoflavone in a *AhCre Apc$^{fl/fl}$* mice which gave rose to very few adenomas even after 250 days post-induction (Barker et al., 2009). This data was strongly in agreement with the 'bottom-up' model of intestinal tumour formation that had previously been proposed – stating that adenomas in both FAP patients and sporadic colorectal cancer initiate as unicryptal adenomas, which grow in a bottom-up fashion via crypt fission (Preston et al., 2003). Despite this observation in human familial tumour samples, as well as genetic evidence provided by Barker and colleagues, an alternative model has been proposed following the observation that some human tumours exhibit a 'top-down' morphology (Shih et al., 2001). Indeed, it was recently shown that cells within the villi can dedifferentiate, acquire stem cell-like properties and have tumourigenic potential – providing genetic evidence for the 'top-down' model (Schwitalla et al., 2013). The authors showed that following APC loss and *Kras* mutation (*VillinCre^{ER} Apc$^{fl/fl}$ Kras$^{G12D/+}$*), the villi can dedifferentiate, be propagated *in vitro* and can grow subcutaneously in an allograft model, however when only APC is deleted (*VillinCre^{ER} Apc$^{fl/fl}$*), this was not observed (Schwitalla et al., 2013).

This increased dedifferentiation is one of the key differences between *VillinCre^{ER} Apc$^{fl/fl}$* (APC) and *VillinCre^{ER} Apc$^{fl/fl}$ Kras$^{G12D/+}$* (APC KRAS) mice. There is also a profound increase in proliferation within the crypt of the small intestine (Cammareri et al., 2017) and the colon (Fig1.7a). We also observe differing sensitivities to certain drugs, for example whilst the APC model is sensitive to rapamycin, an mTORC1 (mammalian target of rapamycin complex 1) inhibitor, treatment (Faller et al., 2015), the APC KRAS model is resistant to rapamycin treatment (John Knight – personal communication). Rapamycin treatment had no impact upon proliferation in the small intestines of APC KRAS mice compared

with vehicle controls, but also there was no change in the phosphorylation status of one of mTORC1's downstream targets – ribosomal protein S6. This observation suggests that expression of oncogenic KRAS leads to a significant rewiring of signalling pathways following APC loss in the mouse intestine.

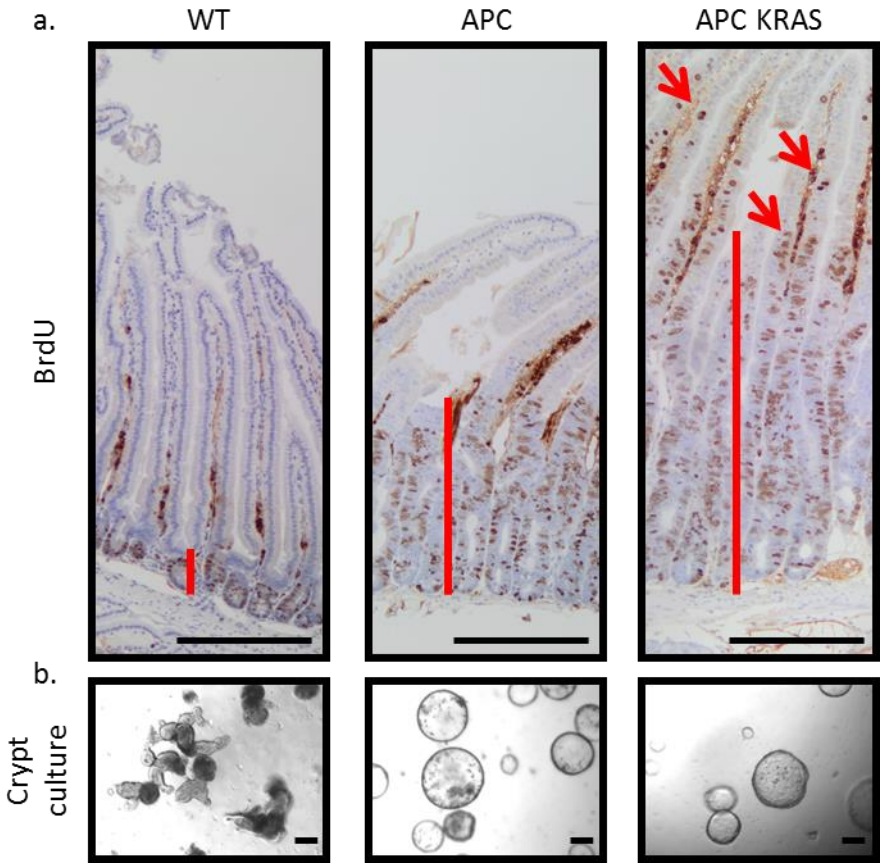

Figure 1.7: Acute models of APC deletion and KRAS activation
a. BrdU staining of small intestine from tamoxifen-induced WT, *VillinCre*^{ER} *Apc*$^{fl/fl}$ (APC), *VillinCre*^{ER} *Apc*$^{fl/fl}$ *Kras*$^{G12D/+}$ (APC KRAS) sampled 4- and 3-days post induction respectively. Red bars indicate the approximate size of the proliferative zone – marking the extent of the 'crypt-progenitor phenotype'. Red arrows in APC KRAS panel indicate dedifferentiating cells in the small intestinal villi of APC KRAS mice b. Representative images of small intestinal crypt cultures from WT, APC and APC KRAS mice. WT crypt cultures grow as budding organoid structure, whilst cultures lacking APC grow as spheroids. Scale bars =200μm

In addition to the acute, *VillinCre*^{ER} *Apc*$^{fl/fl}$ model, the lab also has an inducible mouse model to study intestinal tumourigenesis. *VillinCre*^{ER} *Apc*$^{fl/+}$ mice are induced with tamoxifen and then aged until they develop a few large intestinal adenomas, following loss of the second copy of APC, usually between 200-300 days (Myant et al., 2017). These tumours typically exhibit the 'bottom-up' morphology previously described. When an oncogenic *Kras* allele is added to

this model, *VillinCre^{ER} Apc$^{fl/+}$ Kras$^{G12D/+}$*, there is a significant reduction in survival, as well as an increase in total tumour number (Fig1.8a and Fig1.8b). Interestingly, there is a profound switch to colonic tumours in these mice compared with those that are WT for *Kras* (Fig1.8b). Furthermore in agreement with the observed increased dedifferentiation, addition of *Kras* mutation resulted in a shift towards top-down tumours in the small intestines of these mice (Cammareri et al., 2017).

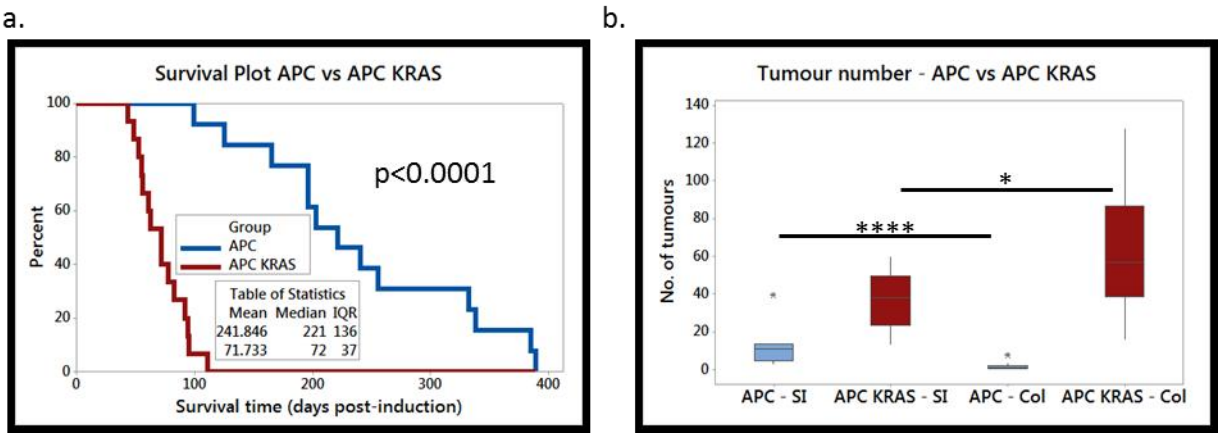

Figure 1.8: Oncogenic KRAS significantly reduces tumour latency
a. Survival curve of tamoxifen-induced VillinCre^{ER} Apc$^{fl/+}$ (APC) and *VillinCre^{ER} Apc$^{fl/+}$ Kras$^{G12D/+}$* (APC KRAS) mice aged until clinical end-point. Log-Rank test, p<0.0001, n=13 for APC, n=15 for APC KRAS. b. Tumour scores from the small intestine (SI) and colon (Col) from APC and APC KRAS mice at end-point. APC mice develop predominantly SI tumours, whilst APC KRAS mice predominantly colonic tumours. p=0.00005 (****) and p=0.015 (*), One-way Mann-Whitney *U* test, n=13 for all groups.

1.6.2 Intestinal organoids

Cell lines derived from human colorectal tumours have served as the workhorse for *in vitro* studies of colorectal cancer for many years. However, given the extensive widespread use of cell lines, there is growing evidence that many cell lines are actually cross-contaminated or not correctly identified, reviewed in (ATCC Standards Development Organization Workgroup ASN-0002, Nature Reviews Cancer 2010). Furthermore, it was recently shown that there is a large genetic and epigenetic diversity across 27 human colorectal cancer cell lines (Ahmed et al., 2013). Whilst this study provides useful information to better aid selection of cell lines for *in vitro* work, interpreting functional results using these cell lines should be taken with caution, given that another colon cancer cell line is very different.

Following a pioneering study by Sato and colleagues, intestinal organoids have now become the gold-standard for *in vitro* investigations into colon cancer. The authors set out to develop an *in vitro* culture system that would meet the growth requirements of the intestinal epithelium (Sato et al., 2009). Firstly, Wnt signalling is required for normal intestinal homeostasis, so the Wnt agonist R-spondin1 (Kim et al., 2005) was added to the media. Secondly, EGF signalling has been shown to be associated with proliferation of an intestinal crypt-derived cell line (Kuorokowa et al., 1987), so exogenous EGF was added. Thirdly, the suppression of BMPs is required for the inhibition of differentiation in the intestine – overexpression of the natural BMP antagonist, Noggin, leads to crypt expansion *in vivo* (Haramis et al., 2004). Finally, the crypt base has been shown to been enriched with laminins (Sasaki et al., 2002). Sato and colleagues isolated small intestinal crypts from WT mice and grew them in a laminin rich matrix, Matrigel, with a cocktail of exogenous R-spondin1, EGF and Noggin. The resulting organoid structures grew with a central lumen and protruding budding structures that housed intestinal stem cells and Paneth cells, whilst the villus domain contained goblet cells, enteroendocrine cells and differentiated enterocytes (Sato et al., 2009). The authors also showed that a single *Lgr5*-positive cell could give rise to an entire organoid, highlighting their role as intestinal stem cells.

This protocol was subsequently used to isolate and grow WT murine colonic and human intestinal organoids with addition of extra growth factors, including Wnt3a (Sato et al., 2011). In the same study, the authors were able to isolate human colonic tumours and intestinal adenomas from $LgrCre^{ER}$ $Apc^{fl/fl}$ mice and propagate them in culture. These transformed epithelial cells formed spheroid structures and grew independently of R-spondin1 and Wnt3a, since the tumour cells had lost both copies of APC; hyperactivating the Wnt signalling pathway. It is thought that the spheroid morphology is due to the absence of a Wnt gradient, following APC deletion, therefore ablating the normal budding organoid morphology.

There have been recent advances in gene editing technology, using the CRISPR-Cas9 system, allowing for the high-throughput targeted genetic modification of cell lines. Two studies in 2015 utilised CRISPR-Cas9 technology to genetically modify four of the most commonly mutated colorectal cancer gene; deletion of *APC*, *TP53* and *SMAD4* and expression of oncogenic *KRAS* in organoids

derived from normal human intestinal epithelium (Drost et al., 2015; Matano et al., 2015). Sequential addition of these mutations resulted in the independent growth from the previously established niche factors. Furthermore, these mutant organoids grew as adenocarcinomas when transplanted in mice. This approach is now being extensively used and laboratories are developing new techniques to transplant these organoids into the colons of mice to try and recapitulate a more physiological setting to study the growth of these genetically modified organoids (Fumagalli et al., 2017).

Intestinal organoids are used extensively within the Sansom lab, most often working with cultures derived from *VillinCre^{ER} Apc$^{fl/fl}$* (APC) and *VillinCre^{ER} Apc$^{fl/fl}$ Kras$^{G12D/+}$* (APC KRAS) mice. Morphologically these crypt cultures are indistinguishable, growing as spheroids (Fig1.6b), however APC KRAS derived crypt cultures grow significantly faster than APC crypt cultures, and also in the absence of exogenous EGF. Furthermore, it has been shown that when seeded as single cells in a colony formation assay, APC KRAS derived cells display a greater clonogenic potential compared with APC derived intestinal epithelial cells. Finally, when transplanted subcutaneously into CD1 athymic mice, APC KRAS derived crypt cultures grow significantly better than APC crypt cultures (Schwitalla et al., 2013). These observations highlight some of the key phenotypic differences between APC and APC KRAS mice and these intestinal organoids culture will prove a valuable tool for trying to dissect the cooperation of *Apc* and *Kras* mutations.

1.7 Protein synthesis

Eukaryotic protein synthesis involves three stages; initiation, elongation and termination. Eukaryotic mRNAs typically consist of a coding sequence that directs protein synthesis, flanked by 5' and 3' untranslated regions (UTRs). Protein synthesis is driven by the ribosome and its' associated translation factors. I will give a brief overview of the regulation of translation initiation and elongation.

1.7.1 Translation initiation

Once transcribed, mRNAs are modified at their 5' end following the addition of the 7-mehtyl guanosine (m^7G) cap catalysed by a series of capping

enzymes (Rottman et al., 1974). This 5' cap subsequently recruits the eukaryotic initiation factor 4F (eIF4F) complex to the mRNA. The eIF4F complex consists of the cap binding protein eIF4E, the adenosine triphosphate (ATP) dependent RNA helicase eIF4A, eIF4G – a scaffold protein that binds eIF4E and eIF4A, as well as the poly(A) binding protein (PABP), finally eIF4B is recruited and is required for efficient eIF4A activity (reviewed in Spriggs et al., 2010). The interaction of PABP with eIF4G and eIF4B circularises the mRNA and stabilises the complex (Bushell et al., 2001). The 40S (small) ribosomal subunit is subsequently recruited to the AUG start codon. The active, GTP-bound eIF2 complex, consisting of eIF2α, eIF2β and eIF2γ, recruits the initiator methionine tRNA ($tRNA_i^{Met}$) forming the ternary complex (Safer et al., 1975). The ternary complex along with the 40S subunit along with eIF1, eIF1A, eIF3 and eIF5 forms the 43S preinitiation complex (PIC) (Sokabe et al., 2012), which is recruited to the 5' end of the mRNA by the eIF4F complex. The PIC then scans along the mRNA until it finds the AUG start codon which is complimentary to the anticodon of the $tRNA_i^{Met}$, causing the PIC to arrest. With the $tRNA_i^{Met}$ positioned within the P-site (peptidyl site) of the ribosome, GTP in the ternary complex is irreversibly hydrolysed to GDP. eIF2-GDP is released, along with other translation initiation factors, and the 60S (large) ribosomal subunit is recruited to form the 80S initiation complex which drives translation elongation.

The eIF2 complex provides a critical control point for protein synthesis. The loading of eIF2 with GTP is mediated by the GEF eIF2B. Phosphorylation of eIF2α at serine 51 inhibits eIF2B activity; since eIF2 is significantly more abundant than eIF2B, a low level of eIF2α phosphorylation is required for the eIF2B to be inhibited (Krishnamoorthy et al., 2001) . This phosphorylation reduces ternary complex availability, and consequently leads to a global reduction in protein synthesis (Farrell et al., 1977), although some mRNAs are selectively translated due to upstream open reading frames (uORFs) within their promoters. eIF2α can be phosphorylated by four different kinases that are activated by a number of different stimuli:

1. General control nonderepressible 2 (GCN2) is activated by amino acid starvation and uncharged tRNAs.
2. Protein kinase RNA-activated (PKR) is activated by double stranded RNA (dsRNA) following viral infection

3. PKR-like endoplasmic reticulum kinase (PERK) is activated by ER stress due to misfolded proteins
4. Haem-regulated eIF2α kinase (HRI) is activated in response to haem deprivation.

Hence, one can see that numerous cellular stresses impinge on eIF2α phosphorylation to reduce global protein synthesis, this is summarized in Fig1.9.

Additionally the availability of the cap binding protein eIF4E is regulated by its binding to eIF4E-bindin protein 1 (4EBP1) (Feigenblum & Schneider, 1996). When not phosphorylated 4EBP1 is able to bind to and inhibit eIF4E (Haghighat et al., 1995), however upon phosphorylation by mammalian target of rapamycin complex 1 (mTORC1) 4EBP1 is inhibited (Brunn et al., 1997; Hara et al., 1997). mTORC1 is the master regulator of cellular growth coupling energy and nutrient status to cellular growth (reviewed in Zoncu et al., 2010), hence cellular energy status can regulate translation initiation via the mTORC1-4EBP1-eIF4E axis.

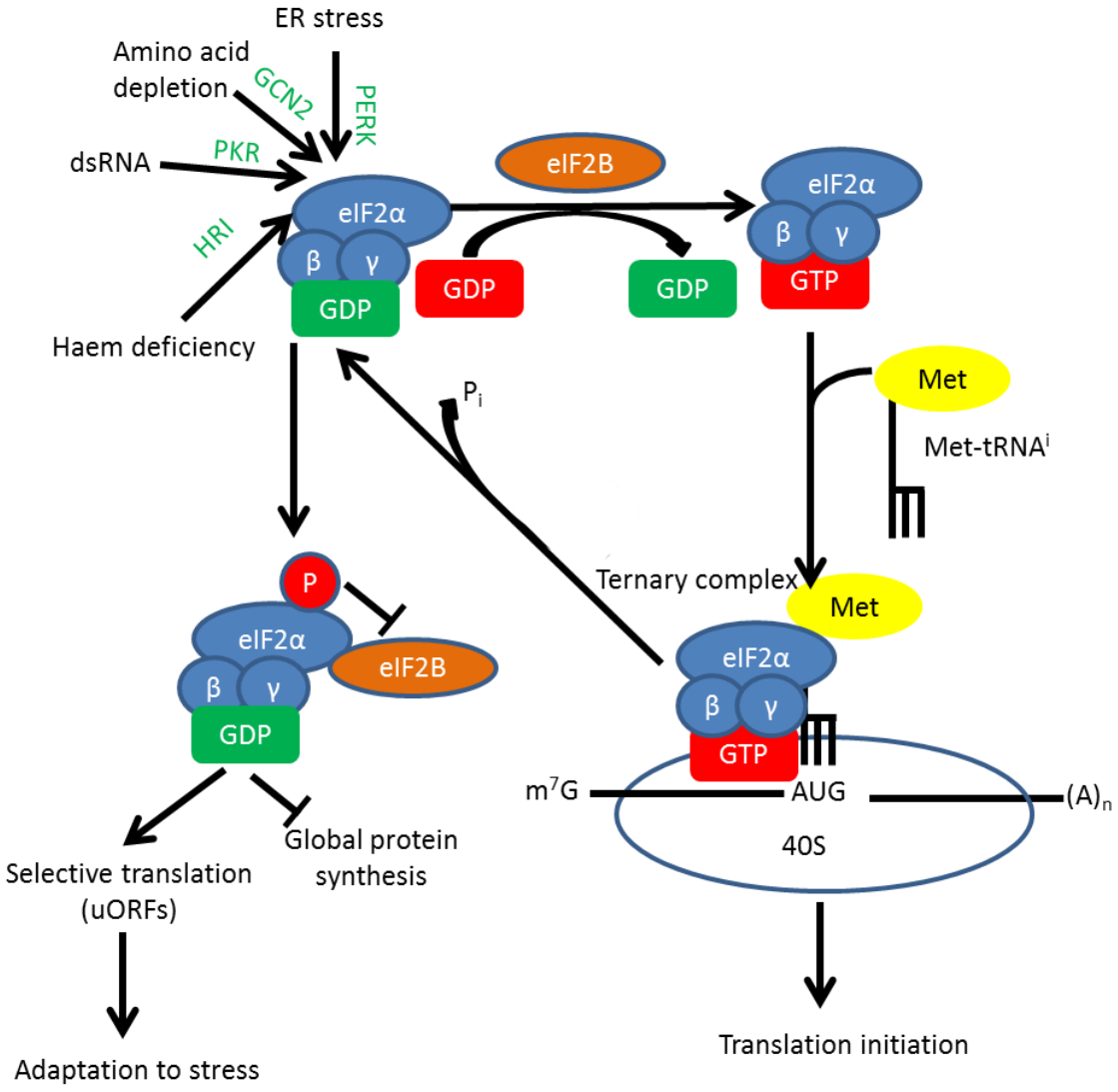

Figure 1.9: Regulation of eIF2 signalling

During translation initiation the eIF2 (α/ß/γ subunits) complex is activated by its' GEF, eIF2B, exchanging GDP for GTP. eIF2-GTP binds to the initiator methionine tRNA (Met-tRNA^i) forming the ternary complex. The ternary complex is recruited to the 40S ribosomal subunit, delivering the Met-tRNA^i to the start codon, initiating translation. eIF2 hydrolyses GTP to GDP, returning to its' inactive GDP-bound state. eIF2α can be phosphorylated at serine 51 by four upstream kinases in response to different stress stimuli: PERK (ER stress), GCN2 (amino acid depletion), PKR (dsRNA) and HRI (Haem deficiency).Following phosphorylation at eIF2α-Ser51, eIF2 binds to and inhibits eIF2B. This reduces the level of ternary complexes available for translation initiation, resulting in a global reduction in protein synthesis; however, some mRNAs are selectively translated to alleviate the cellular stresses.

1.7.2 Translation elongation

Following translation initiation, the initiating methionine tRNA occupies the P-site within the ribosome. Adjacent to the P-site is the acceptor site (A-site) of the ribosome, awaiting the cognate aminoacyl-tRNA that is complimentary to the mRNA codon in the A-site. Eukaryotic elongation factor 1A (eEF1A) mediates the GTP dependent recruitment of aminoacyl-tRNAs to the A-site. Correct codon recognition of the tRNA within the A-site triggers eEF1A-mediated GTP hydrolysis, releasing eEF1A-GDP which can be recycled to its GTP-bound state by the GEF eEF1B. The amino acid attached to the aminoacyl tRNA peptide is attached to the initiator methionine in the P-site, catalysed by ribosomal RNA (rRNA). The A-site must now be vacated to allow the next codon of the mRNA codon to be translated, reviewed in (Dever & Green, 2012)

A ratchet-like mechanism is required for the translocation of the ribosome along the mRNA, such that the A-site is now empty, whilst the tRNA with the growing peptide chain is in the P-site. Finally the now uncharged tRNA occupies the exit site (E-site) and leaves the ribosome. This step in elongation is dependent on eukaryotic elongation factor 2 (eEF2), which is active in its' GTP bound state. eEF2 is negatively regulated by phosphorylation at Thr56 by eukaryotic elongation factor 2 kinase (eEF2K) (Ryazanov et al., 1988). eEF2K is negatively regulated by a number of upstream kinases, including ribosomal S6 kinase (S6K) (Wang et al., 2001). S6K in turn is regulated by mammalian mTORC1 (Isotani et al., 1999). Thus, in addition to regulation of translation initiation via 4EBP1, mTORC1 can regulate translation elongation via the S6K-eEF2K-eEF2 axis, Figure 1.9.

It is important for cells to regulate protein synthesis, since as outlined above, this process consumes large quantities of both ATP and GTP, whilst tRNA charging also consumes ATP; making translation the most energetically cellular process (Buttgereit & Brandt, 1995). Failure to regulate protein synthesis can lead to a cellular energy imbalance and endoplasmic reticulum (ER) stress.

1.7.3 Translation in cancer

eIF4E is the limiting component of the eIF4F complex, and is required for cap-dependent translation of all nuclear-encoded mRNAs. Interestingly, the mRNAs of a number of genes deregulated in cancer, such as cyclin D1 (Rosenwald et al., 1995) and MYC (Li et al., 1997), have been shown to be dependent on eIF4E for their efficient translation. However, changes in eIF4E levels have limited effects on the translation of mRNAs of certain housekeeping genes, such as ß-actin (De Benedetti & Graff, 2004). It is thought that the differential effect of eIF4E levels on the translation of these mRNAs is due to differences within their 5' Untranslated Regions (UTRs). Interestingly, many of these eIF4E sensitive mRNAs have been shown to contain complex secondary structures within their 5' UTRs, such as RNA G-quadruplexes, and that eIF4A is required to unwind these complex structures for translation (Wolfe et al., 2014). eIF4A helicase activity is significantly enhanced when part of the eIF4F complex as opposed to when free (Pause et al., 1994).

Since, eIF4E is the limiting factor for eIF4F complex formation, its overexpression increases eIF4F complex assembly and eIF4A helicase activity. Interestingly, eIF4E has been shown to be upregulated at both early (Rosenwald et al., 1999) and late stages (Berkel et al., 2001) of colorectal cancer. Treatment of *VillinCre^{ER} Apc$^{fl/fl}$* mice with the eIF4A inhibitor, Silvestrol, significantly reduces proliferation as well as MYC expression compared with vehicle controls (Wiegering et al., 2015).

There has also been an interest in targeting translation using rapamycin, which inhibits mTORC1 (Brown et al., 1994). mTORC1 can regulate both translation elongation via S6K or translation initiation via 4E-BP (Fig1.10), however rapamycin predominantly inhibits the S6K arm of mTORC1 signalling (Jiang et al., 2001). APC-driven models of tumourigenesis, *Apc$^{Min/+}$* mice and *Lgr5Cre^{ER} Apc$^{fl/fl}$* mice have been shown to be sensitive to rapamycin treatment (Faller et al., 2015; Hasty et al., 2014). It was shown that following APC loss, mTORC1 drives an increase in translation elongation via the S6K-eEF2K-eEF2 signalling axis, which was inhibited by rapamycin treatment blocking the proliferation of tumour cells and inducing their differentiation (Faller et al., 2015). Indeed, rapamycin has been shown to benefit FAP patients in the clinic

(Yuksekkaya et al., 2016), although it has failed in late stage clinical trials, when tumours display a more complex mutation spectrum.

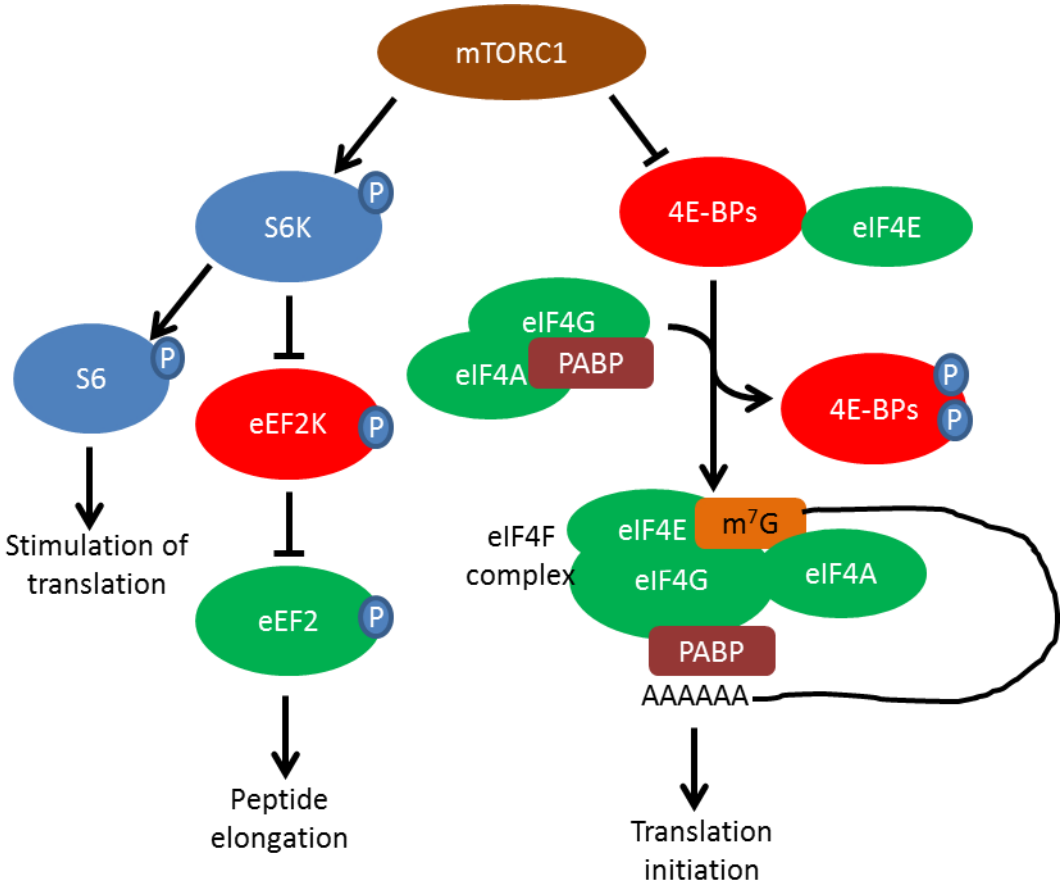

Figure 1.10: Regulation of translation by mTORC1

mTORC1 has two downstream targets that are involved in the control of translation. Ribosomal protein S6 Kinase (S6K) is phosphorylated activated by mTORC1. S6K can in turn phosphorylate ribosomal protein S6 – stimulating translation. S6K also phosphorylates and inhibits eukaryotic elongating factor 2 kinase (eEF2K). eEF2K is a negative regulator of eukaryotic elongation factor 2, a key translation elongation factor; hence activation of mTORC1 promotes eEF2 activity. mTORC1 also phosphorylates and inhibits eIF4E-Binding Proteins (4E-BPs). 4E-BPs bind to eIF4E inhibiting formation of the eIF4F complex, preventing translation initiation. Phospo-4E-BP releases eIF4E, which can now bind to the 7-methyl guanosine (m^7G) cap at the 5' end of mRNA, recruiting eIF4G, eIF4A and poly(A) binding protein (PABP). PABP binds to poly (A) tails at the 3' end of mRNA, circularising the mRNA and stabilising it ahead of translation initiation.

1.8 ER stress

The ER plays a key role in maintaining cellular homeostasis. Novel proteins are synthesised and folded in the ER, with the aid of chaperone proteins such as 78kDa glucose-regulated protein GRP78 – which binds to proteins with hydrophobic residues in unfolded regions (Flynn et al., 1991). GRP78 serves as the master regulator of ER stress, under homeostasis, it resides at the ER

membrane and interacts with and suppresses the activity of the three sensors of ER stress – Activating Transcription Factor 6 (ATF6) (Shen et al., 2002), Inositol-requiring enzyme 1 (IRE1) and PERK (Bertolotti et al., 2000), which when activated initiate the unfolded protein response (UPR). If there is an accumulation of misfolded proteins within the ER, for example in response to a large increase in protein synthesis, GRP78 is titrated away from the membrane, allowing the activation and transduction of ATF6, IRE1 and PERK-mediated signals across the ER membrane and induction of the UPR.

ATF6 translocates from the ER to the Golgi and is cleaved via proteolysis; cleaved ATF6 translocates to the nucleus and induces transcription of GRP78 (Haze et al., 1999). Upon GRP78 release, both IRE1 and PERK have been shown to oligomerise. Activated IRE1 splices the mRNA of the transcription factor *XBP1*, to produce a transcriptionally active protein, XBP1s, XBP1s translocates to the nucleus to induce a transcriptional programme to increase the protein folding capacity of the ER (Calfon et al., 2002; Lee et al., 2003). Homodimerised PERK autophosphorylates to promote its activation, it subsequently phosphorylates eIF2α at Ser51, this reduces global rates of protein synthesis (Harding et al., 1999), however certain mRNAs are selectively translated following eIF2α phosphorylation. For instance the transcription factor ATF4 is selectively translated following eIF2α phosphorylation due to the upstream open reading frames (uORFs) within its promoter (Harding et al., 2000, Harding et al., 2003). ATF4 has been shown to upregulate genes involved in amino acid metabolism and oxidative stress to protect cells from the metabolic consequences of ER stress (Harding et al., 2003). More recently a link between eIF2α signalling and autophagy has been uncovered (B'chir et al., 2013; Bretin et al., 2016). Autophagy is a highly conserved catabolic process of lysosomal degradation of proteins and organelles which can provide nutrients during cellular stress or starvation. The release of amino acids from autophagy can provide a survival mechanism under nutrient stress or ER stress for cells. Furthermore autophagy has been implicated to have a role in ER-associated degradation (ERAD) and the degradation of misfolded proteins in response to ER stress (Houck et al., 2015).

If ER stress is not resolved it can lead to apoptosis. For instance, the proapoptotic proteins BAX and BAK have been shown to deplete ER Ca^{2+} concentrations in response to ER stress; leading to caspase 12 cleavage, inducing

apoptosis (Zong et al., 2000). Whilst CHOP, which is expressed following eIF2α phosphorylation has been shown to downregulate the expression of the antiapoptoic protein BCL2 (Cullough et al., 2001). Therefore restoration of ER homeostasis is paramount for cell survival and function.

1.9 Methods to study Protein synthesis

1.9.1 ^{35}S-methionine incorporation

The incorporation of radiolabelled methionine into protein is often used as a technique to quantify rates of global protein synthesis. Methionine and cysteine are the two amino acids that contain sulphur atoms and since methionine is the first amino acid incorporated into a nascent peptide chain, ^{35}S-radiolabeled methionine is used. Cells are pulsed with ^{35}S-methionine, lysed and the protein precipitated so as to quantify incorporated ^{35}S-methionine, and hence measure the levels of *de novo* protein synthesis. The incorporated ^{35}S-methionine can be quantified via scintillation counting or via an autoradiogram and subsequently normalised to cellular protein concentration. This assay gives a quantitative measurement of global rates of protein synthesis, it does not infer as to whether translation initiation or elongation is rate limiting

1.9.2 Polysome profiling

This is another technique that can be used to look at both the global rates of protein synthesis, but also determine the rate of translation of particular mRNAs. Cells or tissue samples are treated with cycloheximide, which inhibits translation elongation (Schneider-Poetsch et al., 2010), thereby stalling ribosomes on mRNA messages. The samples are subsequently lysed and loaded onto a sucrose gradient of continuously-variable density (10-50%) and then spun in an ultracentrifuge resolving the ribosomal fractions according to their molecular weight. The sucrose gradient is then separated into fractions, the quantity of RNA is measured using a 254nm spectrophotometer, and the absorbance indicates the distribution of ribosomes along mRNA. From the UV spectra, one can detect sub-polysomes; 40S, 60S and 80S and also polysomes – multiple ribosomes bound to mRNA. The ratio of polysomes to sub-polysomes indicates the level of global translation within the sample – typically, increased polysome: sub-polysome ratio suggests increased translation, although that is

not always the case, this is summarised in Figure 1.11. The translation of particular mRNA can be determined following qRT-PCRs on the different sub-polysome and polysome fractions, comparing the ratio of the target message within these fractions.

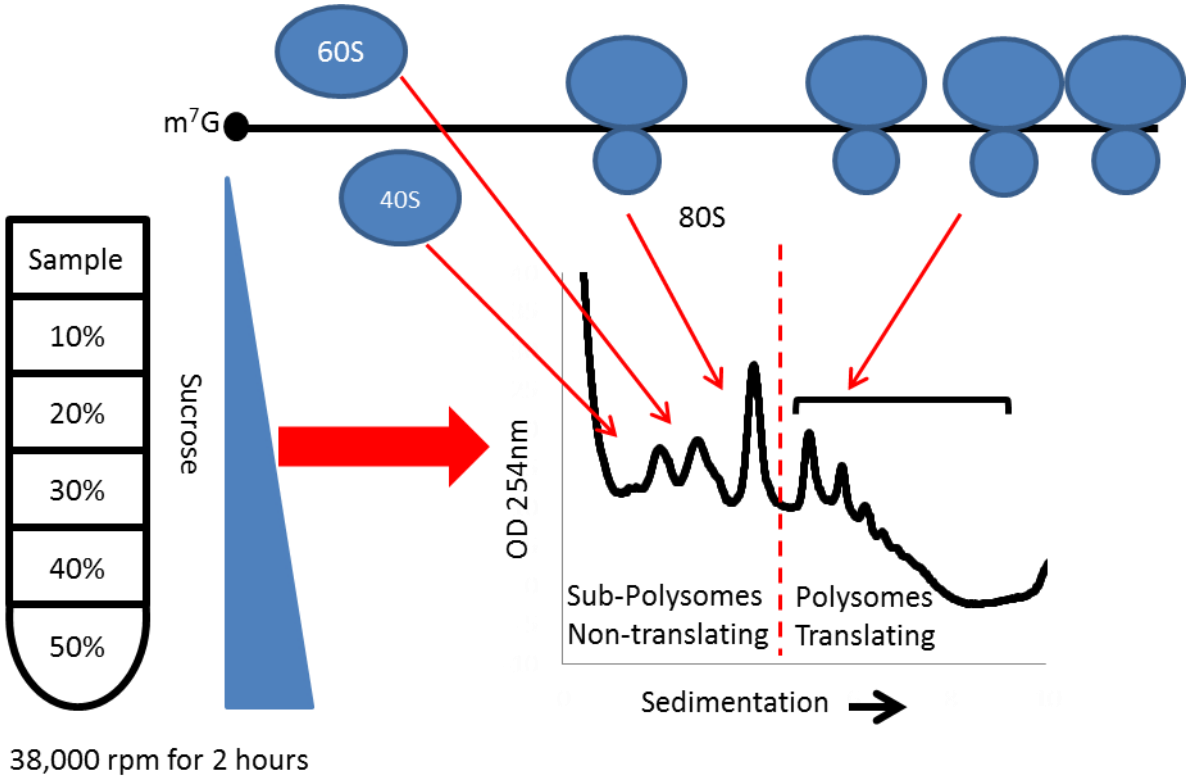

Figure 1.11: Schematic representation of polysome profiling

Tissue or cell lysates are layers on 10-50% sucrose gradient spun at 38000 rpm for 2 hours in an ultracentrifuge. The gradient is then separated through an OD_{254nm} ultraviolet spectrometer. Representative trace assigning peaks to the 'non-translating' 40S, 60S and 80S fractions (sub-polysomes) and the 'translating' polysome fractions. Typically, an increase in the polysome: sub-polysome ratio indicates an increase in global rates of protein synthesis, but not always the case

1.10 Aims

Colorectal Cancer is a highly prevalent disease - it is the third most common cancer in the world and it has the second highest mortality rate in Europe. The genetic progression of the disease has been well characterised; *APC* and *KRAS* are mutated in approximately 80% and 40% of patients respectively. Whilst these two mutational events are thought to occur relatively early during the progression of the disease, there is limited understanding as to how these two genetic events cooperate to drive tumourigenesis.

In this thesis I will discuss the various approaches I used to try and gain an understanding of the cooperation of these two mutations as well as trying to target them. There has been much interest in targeting the Wnt signalling pathway in CRC, given the high frequency of *APC* mutations in CRC, but with limited success. In **chapter 3** I investigate whether targeting downstream of the ß-catenin destruction complex can provide a therapeutic opportunity in mouse models of CRC, but also whether *KRAS* mutation synergises with Wnt pathway activation.

In **chapter 4** and **chapter 5** I take a more unbiased approach by looking at the proteomes and metabolomes of small intestinal crypt cultures isolated from APC and APC KRAS mice. This is to identify changes in protein expression and metabolism between these two genotypes, so as to better understand the cooperation of *APC* and *KRAS* mutations, but also to identify and target novel targets *in vivo*.

[1] http://www.cancerresearchuk.org/health-professional/cancer-statistics/statistics-by-cancer-type/bowel-cancer/incidence#heading-Zero

[2] http://www.cancer.net/cancer-types/colorectal-cancer/statistics

Chapter 2 Materials and Methods

2.1 Mouse colonies:

All experiments were performed according with UK Home Office regulations, male and female mice were used from ages 6-12 weeks for induction. The majority of work was performed on C57BL/6 mice. All mice were maintained under non-barrier conditions and given a standard diet and water *ad libitum*, unless stated otherwise.

2.1.1 Cre recombinase systems

2.1.1.1 *VillinCre^{ER}*

VillinCre^{ER} (El Marjou et al., 2004) mice were induced by intra-peritoneal injection with 2mg tamoxifen. Mice were either induced with two injections over two days for short term experiments (less than 5 days) or with a single injection for longer experiments or if they had the genotype *VillinCre^{ER} Apc$^{fl/fl}$ Kras$^{G12D/+}$*

Tamoxifen stock – 1g tamoxifen powder (Sigma, catalogue no. T5648) was resuspended in 10ml of 100% ethanol and then diluted with corn oil (Sigma, catalogue number C8267) to a final concentration of 10mg/ml

2.1.1.2 *Lgr5Cre^{ER}*

Lgr5Cre^{ER} (Barker et al. 2007) transgene expression was induced by a single IP injection of 0.15mg tamoxifen.

Tamoxifen was prepared as above, however it was diluted in sunflower instead of corn oil to a final concentration of 1mg/ml

2.1.2 LoxP flanked alleles

The following alleles were crossed to the Cre recombinase mice. *Apc^{fl}* (Shibata et al., 1997), Lox-Stop-Lox *Kras$^{G12D/+}$* (Jackson et al., 2001), *tdTom^{fl}* (Madisen et al., 2010), *Bcl9^{fl}* and *Bc9l^{fl}* (Deka et al., 2010), *Atg7^{fl}* (Komatsu et al., 2005) and *Slc7a5^{fl}* (Sinclair et al., 2013). *Gpt^{fl}* – was generated in-house by CRUK Beatson Institute's transgenic team.

2.1.3 Knockout alleles

The following knockout alleles were used – *Apc*$^{Min/+}$ (Moser et al., 1990), *Nupr1*$^{-/-}$ (Vasseur et al., 2002) and *Eif2b5*$^{+/-}$ - generated by CRUK Beatson Institute's transgenic team.

2.1.4 Amino acid deficient diets

The following amino acid deficient diet were used, all purchased from TestDiet:

Diet	**Amino acids missing**
9GBX or 20AA (control diet)	None
9GBZ or -1AA diet	Alanine
9GBY or -4AA diet	Aspartic acid, Asparagine, Proline and Glutamate
9GBW or -5AA diet	Alanine, Aspartic acid, Asparagine, Proline and Glutamate
5BQT or -7AA	Alanine, Aspartic acid, Asparagine, Proline, Glutamate, Serine and Glycine

2.1.5 ISRIB treatment

A stock solution of 1mg/ml ISRIB (Sigma, catalogue no. SML043) was prepared in dimethyl sulphoxide (DMSO), then diluted 1:20 in 50% Poly (ethylene glycol) 400 (Sigma, catalogue no. 202398) and 45% 0.9% saline. Mice were injected once daily, between 9-10am intraperitoneally, with 100µl for a 20g mouse, equating to 0.25mg/kg

2.2 Tissue isolation:

Mice were culled via a schedule 1 procedure ahead of dissection. Routinely, small intestines and colon were removed and flushed with water or PBS; other tissues were sampled when necessary. Several different fixations were used to preserve tissues

2.2.1 Fixation:

2.2.1.1 Quick fixation

Samples were fixed in 10% neutral buffered formalin at 4˚C for no longer than 24 hours before processing and embedding.

2.2.1.2 Long fixation:

Samples were fixed in 10% neutral buffered formalin at room temperature for more than 24 hours before processing and embedding.

2.2.1.3 Methacarn fixation:

Samples were fixed in a fresh methacarn solution, containing methanol (Sigma, catalogue No. 32213), chloroform (Fisher Scientific, catalogue No. C4960/PB17) and acetic acid (Sigma, catalogue No. 695092) in a ratio of 4:2:1, for no longer than 24 hours before being transferred to 10% buffered formalin ahead of processing and embedding.

2.2.2 Snap frozen tissue:

Intestine/colon were flushed with water, opened longitudinally then rolled using forceps and pinned with a needle. Samples snap frozen in liquid nitrogen for approximately 30 seconds, and then stored at -80˚C for long term storage ahead of sectioning or lysis.

2.3 Immunohistochemistry

The tissue was processed and embedded by the CRUK Beatson Institute's histology facility, using standard immunohistochemistry techniques. The following stains were performed by the facility also: BrdU (1:200, BD Biosciences #347580), Sox9 (1:500, Chemicon #AB5535), Lysozyme (1:200, DAKO #A0099) and γH2AX (1:50 Cell Signalling Technologies, catalogue number 9718). Haematoxylin and Eosin, as well as Alcian Blue staining were also performed by the histology facility also.

2.3.1 Immunohistochemistry stains that I performed.

Deparaffinisation

De-wax slides as follows: 3x 2 minute washes in xylene, 2x2 minute washes in 100% ethanol, 1x2 minutes in 70% ethanol, and 1x 2 minutes wash in distilled water.

Antigen retrieval

Antigen retrieval was performed according to the table below; slides were boiled in a boiling water bath for 30 minutes. Supplier information – Citrate Buffer (Thermo Scientific, catalogue no. AP-9003).

Antibody	Antigen retrieval	Primary antibody dilution/incubation	Secondary/Detection
peIF2α (Ser51) CST#9722	Citrate buffer	1:50 in Signal Stain, 4˚C overnight	Anti-rabbit, ABC kit
GRP78 CST#3177	Citrate buffer	1:200 in Signal Stain, 4˚C overnight	Anti-rabbit, ABC kit
GRP94 CST#20292	Citrate buffer	1:800 in Signal Stain, 4˚C overnight	Anti-rabbit, ABC kit
pS6 (Ser235/236) CST#4858	Citrate buffer	1:800 in 5% NGS-TBS-T, 4˚C overnight	Anti-rabbit, ABC kit
pAMPKα(Thr172) CST#2535	Citrate buffer	1:100 in 5% NGS-TBS-T, 4˚C overnight	Anti-rabbit, ABC kit
CD44, BD pharmingen 550538	Citrate buffer	1:50 in 20% NRS-TBS-T, 1 hour RT	Anti-rat, ABC kit
BCL9, Abnova H00000607-M01	Citrate buffer	1:500 in 5% NGS-TBS-T, 4˚C overnight	Anti-mouse, ABC kit
eIF2B5 Santa-Cruz sc-55558	Citrate buffer	1:200 in 5% NGS-TBS-T, 4˚C overnight	Anti-mouse, ABC kit

*Signal Stain solution (Cell Signalling Technologies catalogue no. 8112),

Prevention of endogenous staining

Following antigen retrieval slides were washed in distilled water and incubated in 3% hydrogen peroxidase solution (Fluka, catalogue no. 95321) and then blocking solutions ahead of incubation with the primary antibody as described in table above.

Secondary antibody:

VECTASTAIN Elite ABC kit (Vector labs):

Slides were washed 3x 5 minutes in 1xTBS-T then incubated with a biotinylated secondary antibody from Vectasheild ABC kit (Vector Laboratories, catalogue nos. Rabbit PK-6101, Goat PK-4005, Mouse PK-6102 and Rat PK-6104) – 1/200 in 5% Normal Goat Serum, NGS (DAKO, catalogue no. X0907) or Normal Rabbit Serum, NRS (DAKO, catalogue no. X0902). - TBS-T for 30 minutes at room temperature. Slides then washed 3x 5 minutes with 1xTBS-T and then incubated with the ABC complex – for 30 minutes at room temperature. Slides were then washed 3x 5 minutes in 1xTBS-T ahead of visualisation.

Detection and visualisation

Two different detection kits were used. For slides incubated with Vectashield secondary (see table above) Thermo Scientific kit was used: 1 drop of DAB (3, 3' – Diaminobenzidine) chromogen in 2ml of diluent. Incubate slides with DAB reagent for 5-10 minutes at room temperature in the dark. Wash slides in distilled water to quench the reaction. Keep slides in water until mounting.

Counterstaining and mounting

An automated mounting machine within the core Beatson Histology service was used. Briefly: counterstain slides in haematoxylin for up to 60 seconds, rinse slides in distilled water, 1x 5 minute wash in 70% ethanol, 1x 5 minute wash in 95% ethanol, 2x 5 minutes washes in 100% ethanol, 2x 10 minute washes in xylene. Spot mountant onto coverslip and cover slide, leave to set.

2.3.2 ß-catenin staining

Only Quick Fix samples were used for this stain. Slides dewaxed and rehydrated as described above.

Peroxidase block was carried out by adding hydrogen peroxide (Fluka) to 0.416% Citric Acid, 1.076% DiSodium Hydrogen Phosphate 2 hydrate in water, to a final concentration of 1.5%. Incubate slides are room temperature for 30 minutes.

Antigen retrieval was performed using 4.84% Tris and 3.72% EDTA in distilled water, adjusted to pH8.0. Slides boiled for 50 minutes in boiling water bath, and then left to cool in solution for 1 hour.

Slides were blocked in 1%BSA (Bovine Serum Albumin)-PBS at room temperature for 30 minutes. Washed 3x 5minutes in PBS and then incubated for 2 hours at room temperature with ß-catenin antibody (BD Biosciences, catalogue no. 610154) in 1%BSA-PBS. Wash slides 3x 5minutes in PBS. Slides incubated with anti-mouse HRP-labelled secondary antibody (Dako, catalogue number K4000) for 1 hour at room temperature. Wash slides 3x 5 minutes in PBS.

Detection performed using DAB (Dako, catalogue number K3468), 1 drop of DAB chromogen in 1 ml diluent slides incubated with working solution for 5-10minutes and then transferred to water ahead of counterstaining and mounting as described above.

2.4 RNA in situ (RNAscope)

This was performed by the Beatson's Institute histology facility according to the manufacturer's protocol (RNAscope 2.0 High Definition – Brown, Advanced Cell Diagnostics).

Only quick fix samples were used for RNAscope. The slides were dewaxed and rehydrated as previously described. Incubate slides with Pretreat 1 for 10 minutes at RT. After washing in distilled water, slides were boiled in Pretreat 2 for 30 minutes in a boiling water bath. Wash in distilled water and then 100% ethanol, air dry slides. Slides were then incubated with Pretreat 3 for 30 minutes at 40˚C in the HybEZ oven.

The signal was then detected following probe incubation and amplification. The probe (*Lgr5* 1:5 dilution, *Olfm4* 1:20 dilution, *Nupr*1 1:5 dilution, *Gpt2*, *Slc1a5*, *Got1* and *Got2* were all used neat) was incubated on the slides for 2 hours at 40˚C in the HybEZ oven. Amplification was performed by adding AMP1-AMP6 to the slides and incubated at 40˚C for 15-30 minutes in the HybEZ oven. Between each steps, the slides were washed twice for 2 minutes in 1x Wash Buffer (Advanced Cell Diagnostics).

Signal detection was done by applying a mixture of equal volumes BROWN-A and BROWN-B (DAB) to the slides and incubated at RT for 10 minutes. Slides were counterstained and dehydrated as previously described.

2.5 Proximity Ligation Assay (PLA)

PLA was performed on tissue samples fixed at 4˚C for <24 hours in 10% formalin prior to processing, using the Duolink Detection kit (Sigma). Briefly, slides were dewaxed and rehydrated in 3x 2 minute washes in Xylene, 2x 2 minute washes in 100% Ethanol, 1x 2 minute wash in 70% Ethanol and then kept in distilled water. Slides were boiled in Citrate antigen retrieval buffer (Thermo Scientific, catalogue no. AP-9003) for 30 minutes. Slides were incubated with goat anti-mouse E-cadherin (1:200, AF748 R&D systems) and mouse anti-ß-catenin (1:2000, #610154 BD Biosciences) at 4˚C overnight. Detection was performed with anti-goat and anti-mouse PLA probes conjugated to oligonucleotides. After ligation, amplification the slides were counterstained with Vectashield DAPI mounting medium (Vector Laboratories, catalogue number H-100) before being imaged on a Zeiss 710 confocal microscope. Z-stacks with 40x objectives were taken and processed as maximum intensity projections. PLA dots in crypts were analysed with ImageJ and calculated as fraction area.

2.6 Clonal counting

Lgr5-EGFP-Cre^{ER} R26-Lox-STOP-Lox-*tdTomato* mice were induced with a single intraperitoneal injection of 0.15mg tamoxifen. Mice were culled via a schedule 1 procedure and the 1st 5cm of the small intestine was flushed with PBS, opened longitudinally, removing as much mesenteric tissue as possible and pinned out in 4% paraformaldehyde for 3 hours at room temperature. Intestinal tissue was then transferred to PBS and stored at 4˚C. Prior to imaging, tissue was incubated

with 10µg/ml DAPI (4', 6-diamidino-2-phenylindole) in 0.1% PBS-Tween 20. Tissue was mounted, luminal side down, with Vectashield DAPI mounting medium. Tissue imaged on a Zeiss 710 Upright confocal microscope at 10x magnification. At least 200 crypts per mouse were analyzed.

2.7 Crypt culture

2.7.1 Crypt and villi isolation

Mouse small intestine and colon were isolated and flushed with PBS. Villi scraped from the intestine with a glass cover slip and transferred to ice cold PBS. The small intestine and colon were cut into small pieces and washed in ice cold PBS until no visible debris was present. The villi were pelleted at 800rpm for 3 minutes and then seeded in 20µl Matrigel (Corning, Growth Factor Reduced Matrigel, catalogue no. 356231) spots. Small intestine and colon were incubated in Ethylenediaminetetraacetic acid (EDTA) in ice-cold PBS (2mM for small intestine and 25mM for colon) on rollers for 30 minutes at 4˚C. Pieces washed in PBS to remove EDTA, then pipetted up and down to release crypts – supernatant was kept (fraction 1), this was repeated up to four times. Fractions were pooled, typically fractions 2 and 3 for small intestine and fraction 2 for colon, then spun down for 5 minutes at 1200rpm. Pellets resuspended in 10ml ADF media and passed thought a 70µm strainer, the strainer was washed with an additional 5ml ADF. Suspension was spun down at 800rpm for 3 minutes. Crypts were resuspended in Matrigel and seeded in 24-well plates - 20µl/well. 500ul crypt culture media was added/well. Cultures were kept at 37˚C and 5% CO_2.

Media:

Base ADF -

500ml Advanced DMEM/F12 (Gibco, catalogue no. 12634-028) + 2mM L-glutamine (Gibco, catalogue no. 25030-024), 100U Penicillin/Streptomycin (Gibco, catalogue no. 15140-122) and 10mM HEPES (Gibco, catalog no. 15630-080)

Crypt culture media –

48ml base ADF, plus 1ml B27 supplement (Invitrogen, catalogue no. 12587-010), 500µl N2 supplement (Invitrogen, catalogue no. 17502-048) and 400µl 12.5% BSA (Mycoplasma Free – US Biologicals, catalogue no. A1312)

To this 100ng/ml Noggin (Peprotech, catalogue no. AF-250-38) and 50ng/ml EGF (Peprotech, catalogue no. AF-100-15) was added.

For WT organoids, the above media was used, however (w/v) 25% RSpondin1-conditioned media was added.

2.7.2 Passaging

Upon confluency, media was aspirated and the Matrigel and organoids were mechanically disrupted and collected using a pipette and PBS. Crypts were spun down at 800rpm for 3 minutes. PBS aspirated and the pellets resuspended in 150µl with harsh pipetting (20-30 times), topped up to 5ml PBS and spun down at 800rpm for 3 minutes. PBS was aspirated and crypts resuspended in Matrigel and seeded in 20µl spots in a 24-well plate (Corning).

2.7.3 Adenoma culture

Mouse intestine and colon isolated and flushed with PBS. Adenomas removed from small intestine and colon and cut into small pieces. Tissue washed 3 times with PBS, then incubated with 5mM EDTA for 10 minutes. Tissue washed twice with PBS to removed EDTA then incubated in 5ml 10x Trypsin (Gibco) supplemented with 100-200U DNase (Roche) for 30 minutes at 37˚C. Following trypsinisation, add 5ml of ADF and shake flacon tube vigorously, 5-6 times. Spin down at 1200rpm for 5 minutes, remove supernatant, resuspend pellet in 10ml ADF and pass through 70µm strainer. Wash strainer with another 5ml ADF and spin down suspension at 1200rpm for 5 minutes. Aspirate supernatant, count cells – seed around 10000-50000 cells/well in 20µl Matrigel. Add crypt culture media and maintain as described above.

2.7.4 Amino acid depletion

Crypt cultures were grown as previously described, ahead of assay; crypts were collected in ADF and pelleted at 800rpm for 3 minutes. Media was aspirated, and resuspended in TrpLE express (Gibco, Catalog No.21604-013), with DNase1 (Roche), and incubated for 1 hour at 37˚C, with frequent pipetting. Pass suspension through 40µm strainer and count viable single cells. Wash cells in ADF media and pellet at 1200rpm for 5 minutes. Resuspend cells in 1:1 mixture of Matrigel and PBS and seed 50µl/well of 96-well plate, seeding 10,000cells/well.

Once plate has set, add reconstituted media (see below). 72 hours after seeding, count number of colonies/well. 96 hours post-seeding add 20µl Cell Titre Blue (Promega) to each well and incubate at 37˚C for 4 hours and measure fluorescence (Ex 560nm, Em 590nm).

Prepare Amino acid depleted media:

- Amino acid free advanced DMEM/F12 (Thermo Scientific)
- Prepare stocks of individual amino acids (Sigma) and glucose (Sigma) in PBS and filter sterilise).
- Reconstitute media with desired amino acids
- Add HEPES, Penicillin/Streptomycin, N2, B27, BSA, EGF and Noggin as described in 2.7.1
- Add 100µl of media/well

2.8 Stable Isotope Labelling by Amino Acids in Cell Culture (SILAC)

Intestinal crypt cultures were isolated as previously described 2.7.1, once established the crypt cultures were grown in SILAC DMEM (Gibco, catalogue no. A14431-01) formulated as below. SILAC media was replenished every two days. Crypt cultures were grown and expanded until sufficient labelling was achieved. Heavy- and Light-labelled crypt cultures were generated for each genotype. Crypt cultures were collected as follows, aspirate media, and collect crypt cultures and Matrigel in ice-cold PBS. Wash crypt cultures twice in ice-cold PBS, centrifuge at 800rpm for 3 minutes. Aspirate PBS and incubate pellets in Cell Recovery Solution (BD Biosciences, catalogue no. 354253) on ice for 1 hour. Wash pellets twice more in ice-cold PBS and transfer to eppendorf tubes. Lyse cells in Urea lysis buffer (see below) on ice for 15 minutes. Sonicate samples in sonicating water bath for 1 minute to disrupt DNA, repeat if necessary. Centrifuge at 5000g for 10 minutes at 4˚C, collect supernatant and quantify protein concentration using BCA assay. Prepare 1:1 mixtures of Heavy: Light-labelled samples and store at -80˚C prior to analysis.

Analysis was performed by CRUK Beatson Institute core Proteomics facility. Briefly, SILAC-labelled peptides were reduced with 10mM DTT, diluted 1:1 with Triethylammonium bicarbonate, and then alkylated with 55mM Iodoacetamide. Proteins were then digested with Lys-C protease for 1 hour at 30˚C. Samples

then diluted further (1:3) to reduce urea concentration to 1M, and digested with Trypsin overnight at 35˚C. Peptide mixture then fractionated using a reverse phase column operating at basic pH. All fractions dried, and resuspended in 40µl 2% acetonitrile with 0.1% formic acid. 7µl of each resuspended fraction was injected into the Orbitrap Velos. Raw data was processed using MaxQuant and results were searched against the SwissProt database restricted to *Mus musculus* taxonomy. Additionally, a database containing common proteomic contaminants was searched. Qualitative and quantitative data were analysed using the Perseus software platform. Up/downregulated proteins ratio >1.4 or <0.7 across both forward and reverse-labelled samples. Differentially expressed proteins were analyzed using Ingenuity Pathway Analysis Software (QIAGEN).

Base SILAC media:

To 500ml SILAC DMEM, add HEPES, L-glutamine and Penicillin/Streptomycin as described in 2.7.1

Working media:

To 48ml Base SILAC media add N2, B27, BSA, Noggin and EGF as described in 2.7.1

Then add back Arg-0 and Lys-0 (Sigma) or Arg-10 and Lys-8 (Eurisotope) to a concentration of 0.321mM Arginine and 0.8mM Lysine.

Urea Lysis buffer in MilliQ water: 6M urea, 2M thiourea and 10mM HEPES, adjusted to pH 8.0

2.9 Metabolomics

Organoid cultures were grown in 24-well plates in Matrigel and crypt culture media. 24 hours prior to sampling, change media (no HEPES), including any labelled metabolites (1mM for ^{15}N-alanine, 2mM for^{15}N-α-glutamine, 2mM for ^{13}C-U-glutmaine and 10mM for ^{13}C-U-glucose, all form Cambridge Isotopes). 24 hours later, media from cells was diluted 1:50 in ice-cold extraction buffer and spun for 10 minutes at 4˚C at 13000rpm. Supernatant was collected and transferred to HPLC vials and stored at -80˚C prior to analysis. Aspirate any remaining media, wash cells with 500µl ice cold PBS, then add 200µl extraction buffer to cells. Place plates on a shaker at 70rpm for 10 minutes at 4˚C. Collect

extraction buffer, spin for 10 minutes at 4˚C at 13000rpm - transfer supernatant to HPLC vials and store at -80˚C prior to analysis. Collect cells and Matrigel in 250µl RIPA buffer and transferred to Precellys tubes (Cat No. 03961-1-003) and homogenised. Lysates transferred to eppendorfs and stored at -80˚C prior to quantification.

Sera samples were prepared from mice. Briefly, mice were culled and then blood isolated via cardiac puncture. Whole blood centrifuged for 5 minutes at 10000 rpm at RT, the supernatant (sera) was collected and snap frozen in a fresh eppendorf. Sera samples were diluted 1:50 in extraction buffer, centrifuged for 10 minutes at 4˚C at 13000rpm to pellet proteins. Supernatant transferred to HPLC vials and stored at -80˚C prior to analysis

Samples were run by the CRUK Beatson Institute's Core metabolomics facility. Briefly, samples were run using a pHLIC column, with a total run time of 24.5 minutes per sample, with full MS scanning and polarity switching. The raw data was analysed by LCquant (Thermo Scientific) and Tracefinder (Thermo Scientific) for metabolite identification and quantification). Metabolites were normalized to protein concentration determined via BCA assay (Thermo Scientific).

Extraction buffer recipe (100ml):

Solution	**Quantity (ml)**
Methanol (HPLC grade)	50
Acetonitrile (HPLC grade)	30
Water (MilliQ)	20

2.10 BCA assay for protein concentration determination

BCA assay performed using BCA Protein Assay Kit (Thermo Scientific, catalog number 23225) according to manufacturer's instructions. Briefly, protein standards were prepared in RIPA buffer from a 2mg/ml stock solution of Bovine Serum Albumin (BSA). 25µl of standards plated in duplicate in a 96-well plate, whilst 25µl of sample was plated in triplicate. Working BCA reagent was prepared as follows 50 parts reagent A: 1 part reagent B, from this 200µl was

added to each well of standard/sample and then incubated at 37˚C for 30 minutes. Plate was read on a spectrophotometer at 562nm. A standard curve was produced and then sample protein concentration determined.

2.11 mRNA isolation

mRNA was extracted from whole tissue using QIAGEN RNAeasy kit (Cat no. 74104) according to manufacturer's instructions. Briefly, whole tissue was lysed in 600µl RLT buffer in Precellys tubes (Cat No. 03961-1-003) with Precellys homogeniser. Lysate was mixed with 1 volume of 70% ethanol and 700µl of sample transferred to RNeasy Mini spin column within a 2ml collection tube, centrifuged for 15 seconds at 8000g. Discard flow through, at this stage samples for RNASeq preparation were prepped using on-column DNase digestion kit (see RNASeq protocol) and then prepared according to these next steps. For cDNA synthesis, samples were treated as follows – add 700µl RW1 buffer to RNeasy columns, spin at 8000g for 15 seconds and discard flow-through. Wash the RNeasy columns twice with 500µl RPE buffer, spin first for 15 seconds and then two minutes at 8000g, discard flow through both times. Transfer RNeasy columns to fresh 2ml collection tubes, centrifuge at full speed for 1 minute to dry the membrane. Transfer RNeasy spin columns to 1.5ml collection tubes, add 50µl RNase-free water to the membrane, centrifuge for 1 minute at 8000g. Wash the membrane with the eluate and spin as before.

See cDNA synthesis (2.12) and quantitative Reverse Transcription-Polymerase Chain Reaction (qRT-PCR, 2.13) protocol, or RNASequencing (2.14) protocol for further information

2.12 cDNA synthesis

Following RNA isolation, RNA was quantified using NanoDrop 2000c spectrophotometer (Thermo). Prepare 10µg RNA for each sample prior to DNase digestion (DNA-free kit from Thermo Scientific – catalogue no. AM1906), add 0.1 volumes of 10x DNase 1 buffer and 1µl rDNase 1 to the RNA, make final reaction volume up to 40µl with Nuclease-free water, mix gently. Incubate at 37˚C for 20-30 minutes. Add 0.1 volume of resuspended DNase Inactivation Reagent; incubate at room temperature for 2 minutes. Centrifuge at 10000g for 1.5

minutes and transfer the supernatant to a fresh tube. Determine RNA concentration using NanoDrop 2000c spectrophotometer.

cDNA synthesis was performed using DyNAmo cDNA Synthesis Kit (Thermo Scientific, catalogue no. F-470L) according to the manufacturer's instructions. Reaction mixture was prepared as below:

Components	20µl reaction	Comments
RT buffer	10µl	Includes dNTPs and $MgCl_2$
Random hexamer primers	1µl	
Template RNA	Xµl	Max 1µg
RT enzyme	2µl	
RNase-free water	Xµl	Add water to fill up to the final volume
Total Volume	20µl	

*minus RT reactions were carried out in parallel

cDNA synthesis was performed using the following cycling conditions:

Step	Purpose	Temp	Time
1	Primer extension	25	10 minutes
2	cDNA synthesis	37	30 minutes
3	Reaction termination	85	5 minutes
4	Cooling	4	Hold

cDNA was subsequently diluted 1:10 in Nuclease-Free water and stored at -20˚C ahead of qRT-PCR

2.13 Quantitative Reverse Transcription-Polymerase Chain Reaction (qRT-PCR)

qRT-PCR was performed using DyNAmo HS SYBR Green qPCR Kit (Thermo Scientific, catalogue no. F-410L) according to the manufacturer's instructions.

Reaction set-up:

Components	20µl reaction	Final Concentration	Comments
2x master mix	10µl	1x	Mix thoroughly
Primer mix	Xµl	0.5uM FOR 0.5uM REV	
Template DNA	Xµl		Do not exceed 10ng/µl
Water	To 20µl		

Samples were prepared in duplicate and plated in a 96-well Hard-Shell PCR plates (Bio-Rad, catalogue number HSP9645), sealed and spun-down and the plate loaded onto Bio-Rad CFX96 qPCR instrument.

Cycling conditions:

Stage	Temperature (˚C)	Time (minutes)
1. Initial denaturation	95	3:00
2. Denaturation	95	0:10
3. Annealing	60	0:30
4. Extension	72	0:30
5. Read plate, repeat	Back to step 2	Repeat 39 times
6. Melt curve	65-95, 0.5 increments	0:05
7. Hold	4	Forever

Quantification was performed using Ct values and ΔCt values determined using *Gapdh*.

List of primers:

Xbp1s	Fwd	GAG TCC GCA GCA GGT G
	Rev	CTG GGA GTT CCT CCA GAC TA
Ctnnb1	Fwd	ATC TTA AGC CCT CGC TCG GT
	Rev	CTT CAG GTA CCC TCAG GCC C
Cdh1	Fwd	ACT GTG AAG GGA CGG TCA AC
	Rev	GGA GCA GCA GGA TCA GAA TC
Axin2	Fwd	GCG ACG CAC TGA CCG ACG AT
	Rev	GCA GGC GGT GGG TTC TCG GA
Cd44	Fwd	CAC ATA TTG CTT CAA TGC CTC AG
	Rev	CCA TCA CGG TTG ACA ATA GTT ATG
Lgr5	Fwd	GAC AAT GCT CTC ACA GAC
	Rev	GGA GTG GAT TCT ATT ATT ATG G
Gpt2	Fwd	AAC CAT TCA CTG AGG TAA TCC
	Rev	GGG CTG TTT AGT AGG TTT GGG
Gapdh	Fwd	GAA GGC CGG GGC CCA CTT GA
	Rev	CTG GGT GGC AGT GAT GGC ATG G
Bcl9	Fwd	AGT GCT CTC TCC AGG ATA TGA TG
	Rev	GGG CAA AGA TGT TGA AAT GTT G
Bcl9l	Fwd	AGC AGC ACC TAA TGG GCA AAG
	Rev	GGA TAA GTC GAA CTC AGG AAT GC
cMyc	Fwd	CCC AAA TCC TGT ACC TCG TC
	Rev	TTG CCT CTT CTC CAC AGA CA
Olfm4	Fwd	GCC ACT TTC CAA TTT CAC
	Rev	GAG CCT CTT CTC ATA CAC
Lrig1	Fwd	Primerdesign
	Rev	

2.14 RNAsequencing

Following lysis of tissue with RLT buffer as described in mRNA isolation protocol (2.11), add 350µl RW1 buffer to RNeasy columns, centrifuge at 8000g for 15 seconds, and discard flow-through. Prepare DNase working solution (RNase-Free DNase Set – QIAGEN Cat no. 79524) – add 10µl DNase 1 stock solution to 70µl RDD buffer for each column, mix gently. Add 80µl DNase 1 incubation mixture directly to each RNeasy column membrane and leave at room temperature for 15 minutes. Add 350µl RW1 buffer to each RNeasy column and centrifuge for 15 seconds at 8000g. Discard flow-through. Continue with RNA purification with RPE buffer washes as described in mRNA isolation protocol (2.11).

After RNA has been isolated, quantify RNA concentration using NanoDrop 2000c Spectrophotometer (ThermoScientific). Prepare a 55µl solution with 2µg RNA for analysis. Analysis was carried out by CRUK Beatson Institute's Core RNASequencing facility, by William Clark, briefly:

Quality of the purified RNA was tested on an Agilent 2200 Tapestation using RNA screentape. Libraries for cluster generation and DNA sequencing were prepared following an adapted method from Fisher et al., 2011 using Illumina TruSeq RNA LT Kit v2 , (Quality and quantity of the DNA libraries was assessed on a Agilent 2200 Tapestation and Qubit (Thermo Fisher Scientific) respectively. The libraries were run on the Illumina Next Seq 500 using the High Output 75 cycles kit (2x36cycles, paired end reads, single index).

Analysis of the RNASeq data was carried out by Ann Hedley, as previously described in (Sakamaki et al., 2017):

Quality checks on the raw RNASeq data files were done using fastqc (v0.10.1) [1] and fastq_screen (v0.4.2) [2]. RNASeq reads were aligned to the GRCm38 (Church et al., 2011) version of the mouse genome using tophat(v2.0.13) (D. Kim et al., 2013) with Bowtie (v2.2.4.0) (Langmead & Salzberg, 2012). Relative expression levels were determined and statistically analysed using a combination of HTSeq-count (version 0.6.1p1) [3], the R statistical analysis environment (version 3.2.2), utilizing packages from the Bioconductor data analysis suite. Data normalisation and differential gene expression analysis are based on a generalized linear model using the DESeq2 package (Love et al., 2014).

2.15 Polysome profiling:

2.15.1 Preparation of cell pellets:

Crypt cultures were grown in 6-well plates, once cells had reached confluency, 0.2mg/ml cycloheximide (Sigma, catalogue no. C7968) was added to each well and the cells incubated at 37˚C for 3 minutes. Aspirate media, leave cell in ice-cold PBS with 0.2mg/ml cycloheximide – scrape cells and Matrigel on ice and collect in 15ml falcon tube. Spin samples at 1300rpm at 4˚C for 3 minutes. Aspirate supernatant; resuspend cells in ice-cold PBS-cycloheximide, transfer to an eppendorf and pellet at 1300rpm at 4˚C for 5 minutes. Aspirate supernatant and snap freeze pellets.

2.15.2 Preparation of intestinal epithelium:

For the generation of intestinal tissue for polysome analysis, the first 10cm of the mouse small intestine was isolated and flushed with PBS. The section was opened longitudinally and incubated in RMPI (Gibco, catalogue no. 31870-25) with 10mM EDTA and 0.2mg/ml cycloheximide for 7 minutes at 37˚C, with vigorous shaking. Sections were then transferred to ice-cold PBS with 10mM EDTA and 0.2mg/ml cycloheximide for a further 7 minutes, along with vigorous shaking. This fraction contained isolated crypts, which were then pelleted at 1500rpm for 5 minutes at 4˚C. Pellets were resuspended in ice-cold PBS with 0.2mg/ml cycloheximide and transferred to eppendorfs, spun down at max speed; supernatant aspirated and pellets snap frozen in liquid nitrogen.

2.15.3 Gradient loading:

Cell/tissue pellets were lysed in ice-cold 300mM NaCl, 15mM $MgCl_2$, 15mM Tris (pH 7.5) containing 20 units/µl SUPERase In (Thermo catalogue no. AM2694), 0.2 mg/ml cycloheximide and 1mM DTT supplemented with 0.1% Triton X-100. Nuclei were pelleted following a 5 minute spin at 13000rpm at 4˚C. Lysates were layered on 10ml 10-50% (w/v) sucrose gradients of the same buffer, omitting Triton X-100, DTT and SUPERase In. Gradients were centrifuged at 38000rpm for 2 hours at 4˚C in a SW40Ti rotor (Beckman Coulter) and separated through a live OD_{254nm} ultraviolet spectrometer.

RNA fractions were collected in 7.7M Guanidine (Sigma, catalogue no. 50950) supplemented with GlycoBlue (Thermo, catalogue no. AM915) and 100% Ethanol. Sub- and Polysomal fractions were pooled and stored at -20˚C.

2.16 ^{35}S-methionine labelling of intracellular proteins

Seed organoids in 40µl Matrigel/well of a 12-well plate in 1ml media - in technical triplicate, grow to confluency. Prior to labelling, change media with complete growth factors, plus any drugs/vehicle. After 5-6 hours, add 0.555MBq ^{35}S-labelled methionine (PerkinElmer) per well and incubate at 37˚C for 30 minutes. Aspirate media, wash cells with 1ml ice-cold PBS and store plates at -20˚C ahead of analysis.

Thaw plates to room temperature, collect cells and Matrigel in 400µl lysis buffer (table) and vortex thoroughly in eppendorfs. After lysis, collect 50µl lysate for protein quantification, then add 1 volume of 25% Trichloroacetic Acid and incubate at 4˚C for at least 30 minutes to precipitate protein. Add precipitates to glass microfiber filter (GE Healthcare – Cat No. 1827-024), and collect via vacuum filtration. Wash filters with 70% ethanol and then 100% Acetone. Transfer filters to scintillation tubes and add 3ml Ecoscint A (National Diagnostics, Catalogue number LS-273) and read on scintillation reader.

Determine total protein content of samples using BCA assay (ThermoScientific, Product Number 23225) and normalize as Counts per Minute/µg protein.

Lysis Buffer:

10mM Tris pH7.5
50mM NaCl
0.5% NP40
0.5% SDS

*Before use, add 3µl Benzonase (Sigma – E1014-25KU) to 10ml Lysis buffer

2.17 Western blotting

Pelleted tissue samples or cells were resuspended in RIPA buffer containing NaF, apropotinin, Sodium vanadate and PMSF (see below), vortexed briefly and then left on ice for 30 minutes.

RIPA lysis buffer: 150mM sodium chloride, 1.0% NP-40, 0.5% sodium deoxycholate, 0.1% sodium dodecyl sulphate (SDS) and 50mMTris adjusted to pH 8.0.

Protease and phosphate inhibitors added to 1ml RIPA buffer before use: 12.5µl 100mM PMSF (Sigma, catalogue no. 93482), 1µl apropotinin (Sigma, catalogue no. A6279), 1µl 0.5M NaF (Sigma, catalogue no. 201154) and 1µl Na_3VO_4 (Sigma, catalogue no. S6508)

Lysates were centrifuged at 13000rpm for 5 minutes at 4˚C; the supernatant was transferred to a fresh Eppendorf. Protein lysates were quantified using a BCA assay. 20µg of protein lysate was prepared for each sample as below:

Component	Volume µl
Sample	To 20µg
Reducing buffer (4x)	7.5
SDS reducing agent (10x)	3
RIPA buffer	To 30µl

Samples were boiled for 5 minutes at 95˚C, and then chilled on ice ahead of loading onto a 4-12% gradient pre-cast gel (Novex). Samples were run at 200V for 50 minutes in MOPs (Novex) buffer. Samples were transferred to an MVDF membrane (Millipore) in a semi-dry apparatus, run at 30V for 1 hour 20 minutes with transfer buffer 1400ml water, 400ml methanol and 200ml SDS blotting buffer.

Membranes washed in Ponceau stain to confirm transfer. Membrane was briefly washed in TBS-T and then blocked using 5% BSA in TBS-T at RT for 1 hour. Primary antibodies were incubated in 5% BSA TBS-T overnight at 4˚C or for 1 hour at RT. Primary antibodies used: phospho-eIF2α^{Ser51} (Cell Signalling 3398, 1:1000), eIF2α (Cell Signalling 9722, 1:1000), GRP78 (Cell Signalling 3177, 1:1000), ATF4 (Cell Signalling 11815, 1:500), phospho-eEF2^{Thr56} (Novus Biologicals NB100-92518, 1:1000), eEF2 (Cell Signalling 2332, 1:1000), PERK (Cell Signalling

3192, 1:1000), eIF2B5 (Santa Cruz, SC-55558, 1:1000), ASNS (Atlas Antibodies HPA029318, 1:1000), Hexokinase I (Cell Signalling 2024, 1:1000), Hexokinase II (Cell Signalling 2867, 1:1000), γ-tubulin (Abcam Ab11316, 1:5000) and ß-actin (Sigma A2228, 1:10000). Membranes washed in TBS-T 3x10 minutes at RT, then incubated with HRP-conjugated secondary antibodies (Dako) diluted 1:10000 in 5% BSA TBS-T for 1 hour at RT. Membranes were washed in TBS-T 3x10minutes at RT and then incubated with ECL^{+} working reagent (Thermo Scientific catalogue no. 32132) for 5 minutes, before being developed using X-ray film (Thermo Scientific). Membranes were stripped using Reblot plus (Millipore), at RT for 10 minutes, then rinsed in distilled water 3x2minute washes.

2.18 Statistical analysis

All were analyzed using Minitab stats programme. Graphs were produced using either Minitab or Microsoft excel or PRISM. All bar charts displayed +/- standard error of the mean (SEM). Boxes of box plots represent the interquartile range and the median value, whilst tails represent the range.

[1] http://www.bioinformatics.bbsrc.ac.uk/projects/fastqc
[2] http://www.bioinformatics.babraham.ac.uk/projects/fastq_screen/
[3] http://www-huber.embl.de/users/anders/HTSeq/doc/overview.html

Chapter 3: Investigating the role of BCL9 and BCL9l in intestinal homeostasis and tumourigenesis

3.1 Introduction

It is well established that the loss of the tumour suppressor gene Adenomatous Polyposis Coli (*APC*) is a critical step in the initiation of Colorectal Cancer, and is mutated in approximately 70% **of** human patients. Interestingly though, there are limited mutations in other components of the Wnt pathway, such as *CNNTB1* and *GSK3B*. Since APC loss leads to aberrant Wnt signalling, there has been much interest in targeting this pathway for therapeutic benefit in patients. In this chapter I shall discuss the implications for targeting Wnt-signalling downstream of the ß-catenin destruction complex, to determine whether this can impact the growth of transformed intestinal epithelial cells with high Wnt- and MAPK-pathway activity.

3.1.1 Targeting the Wnt signalling pathway

There have been several approaches to targeting the extracellular components of Wnt signalling both at the receptor-ligand complex level and Wnt ligand secretion level. Ettenberg and colleagues identified two antagonistic anti-LRP6 antibodies that specifically blocked either the binding of Wnt1 or Wnt3a to the LRP6 receptor (Ettenberg et al., 2010). Additionally, these two antibodies were able to block MMTV-Wnt1 or MMTV-Wnt3a xenografts *in vivo*, highlighting their therapeutic potential (Ettenberg et al., 2010).

The development of Porcupine inhibitors, such as LGK974, allows the blocking of Wnt ligand secretion (Jun Liu et al., 2013). Porcupine, *PORCN*, is an O-acyltransferase localised to the ER membrane and catalyses the palmitoylation of Wnt ligands, a critical step for their secretion (Takada et al., 2006). LGK974 treatment shrunk MMTV-Wnt1 allografts in Nude mice, and was well tolerated in rats at an efficacious dose, revealing a therapeutic window for this drug (Jun Liu et al., 2013) . Importantly, these two studies were performed in models where the destruction complex, the negative regulator of Wnt signalling, is active. It has been shown that LGK974 treatment has no impact on proliferation in the intestines of *VillinCre^{ER} Apc$^{fl/fl}$* mice (David Huels – personal communication), since the recycling of the destruction complex has been blocked; hence these epithelial cells are no longer responsive to upstream inhibition of the Wnt

pathway. There have also been recent attempts to target intracellular Wnt signalling in Colorectal Cancer.

A chemical screen for inhibitors of Wnt signalling identified a small molecule, IWR-1, that stabilises AXIN, a key component of the destruction complex (Chen et al., 2009). A similar screen identified another small molecule, XAV939, which also stabilised AXIN levels (Huang et al., 2009). The authors went on to show that both XAV939 and IWR-1 inhibit Tankyrase, which catalyses the addition of several ADP-ribose units (ADP-ribosylation) to Axin, marking it for degradation (Huang et al., 2009). Interestingly, unlike LGK974, XAV939 has been shown to inhibit Wnt signalling in APC-deficient colorectal cancer cells (Huang et al., 2009). Furthermore, a novel Tankyrase inhibitor was shown to reduce the number of intestinal tumours in *Lgr5Cre^{ER} Apc$^{fl/fl}$* mice compared with vehicle controls after three weeks of treatment in a chemopreventative study (Waaler et al., 2012). However, the therapeutic benefit of Tankyrase inhibitors may be limited, since severe intestinal toxicity has been reported with another Tankyrase inhibitor (T. Lau et al., 2013). Also, another study has shown that colorectal cancer cells are resistant to Tankyrase inhibitors due to the upregulation of two Wnt target genes, LEF1 (Lymphoid Enhancer Binding Factor 1) and BCL9l (B-cell CLL/Lymphoma 9-like) (de la Roche et al., 2014). The authors showed that these two transcription factors, are able to sequester *de novo* ß-catenin to the nucleus, thereby protecting it from binding to AXIN and subsequent degradation (de la Roche et al., 2014). This study highlighted the importance of targeting transcriptionally active ß-catenin either directly or via its' binding to other transcription factors.

3.1.2 BCL9 and BCL9l

One of the transcription factors highlighted by de la Roche and colleagues, along with its' paralog BCL9 (B-cell CLL/Lymphoma 9) have been shown to be upregulated in human colorectal cancer (Sakamoto et al., 2007; Mani et al., 2009; Brembeck et al., 2011). These two proteins are the mammalian homologs of the *Drosophila* protein legless, and contain 6 homologous domains (HD), whilst legless only has three (Adachi et al., 2004). They have been shown to act as ß-catenin transcriptional cofactors, and are able to bind to ß-catenin via their HD2 domain (Kramps et al., 2002; Adachi et al.,

2004) . Both BCL9 and BCL9l have been shown to localise to the nucleus and co-localise with ß-catenin, and may play a role in the nuclear translocation of ß-catenin, however in the case of BCL9, this is dependent on its' binding to PYGO (Adachi et al., 2004). More recently though, a cytoplasmic role for BCL9 and BCL9l has been identified in the formation of tooth enamel in mice (Cantù et al., 2017); I am, more interested in the role that these two transcription factors play in ß-catenin mediated transcription, and colorectal cancer.

There have been a number of promising studies looking at the role of BCL9 and BCL9l in colorectal cancer and the development of potential inhibitors of the ß-catenin/BCL9/BCL9l interface. For instance, knockdown of BCL9 in Colo320 cells reduces their proliferation *in vitro*, and growth *in vivo* (Mani et al., 2009). Additionally, a peptide inhibitor that disrupted BCL9 and ß-catenin binding reduced the growth and spread of a xenograft of Colo320 cells in NOD/SCID mice (Takada et al., 2012). Overexpression of BCL9l in $Apc^{Min/+}$ mice lead to a significant increase in the number of adenomas compared with controls (Brembeck et al., 2011). On the other hand, treatment of $Apc^{Min/+}$ mice with Carnosic Acid, an inhibitor of BCL9 and BCL9l, reduced the number of tumours compared with controls (de la Roche et al., 2014). Whilst mice that are null for both BCL9 and BCL9l are embryonically lethal (Brack et al., 2009), deletion of BCL9 and BCL9l is tolerated in the mouse epithelium. Furthermore, these proteins have been shown to be required for the expression of a subset of Wnt-target genes in chemically-induced intestinal tumours (Deka et al., 2010). These studies highlight the potential therapeutic window provided by targeting BCL9 and BCL9l, and represent promising candidates, given that they are dispensable in the adult mouse intestine and colon.

Using the mice described by Deka and colleagues, I will investigate further the role of BCL9 and BCL9l in normal intestinal homeostasis, but also assess the role of these proteins in a tumourigenic setting. I aim to determine whether genes that are expressed downstream of APC-loss are dependent on BCL9 and BCL9l, using our inducible models. Similarly I wish to see whether targeting these two genes has a suppressive role in a more aggressive model such as APC KRAS mice. Finally, I aim to properly determine the therapeutic potential for BCL9 and BCL9l in our mouse models.

3.2. Results

3.2.1 BCL9 and BCL9l are dispensable for normal intestinal homeostasis

To determine the role of BCL9 and BCL9l in the murine intestine, I generated *VillinCre^{ER} Bcl9$^{fl/fl}$ Bcl9l$^{fl/fl}$* mice. I focussed on BCL9/9l conditional double knockouts, since the two proteins are thought to be functionally redundant (Deka et al., 2010) and therefore deletion of one gene could potentially be compensated for by the other. I acutely deleted both copies of BCL9 and BCL9l and sampled these mice four days post-induction. At this short time-point, there were no gross differences in intestinal morphology (Fig 3.1a) whilst proliferation was not affected in either small intestine or colon (Fig3.1e). Additionally, Lysozyme (Paneth cell marker) and Alcian Blue staining (goblet cell marker), revealed that deletion of BCL9 and BCL9l does not significantly perturb differentiation within the murine intestine (Figs 3.1c and 3.1d). This data is in agreement with what has previously been shown by Deka and colleagues – who aged tamoxifen-induced *VillinCre^{ER} Bcl9$^{fl/fl}$ Bcl9l$^{fl/fl}$* mice for 23-weeks and also reported no alterations in proliferation and intestinal lineage composition (Deka et al., 2010).

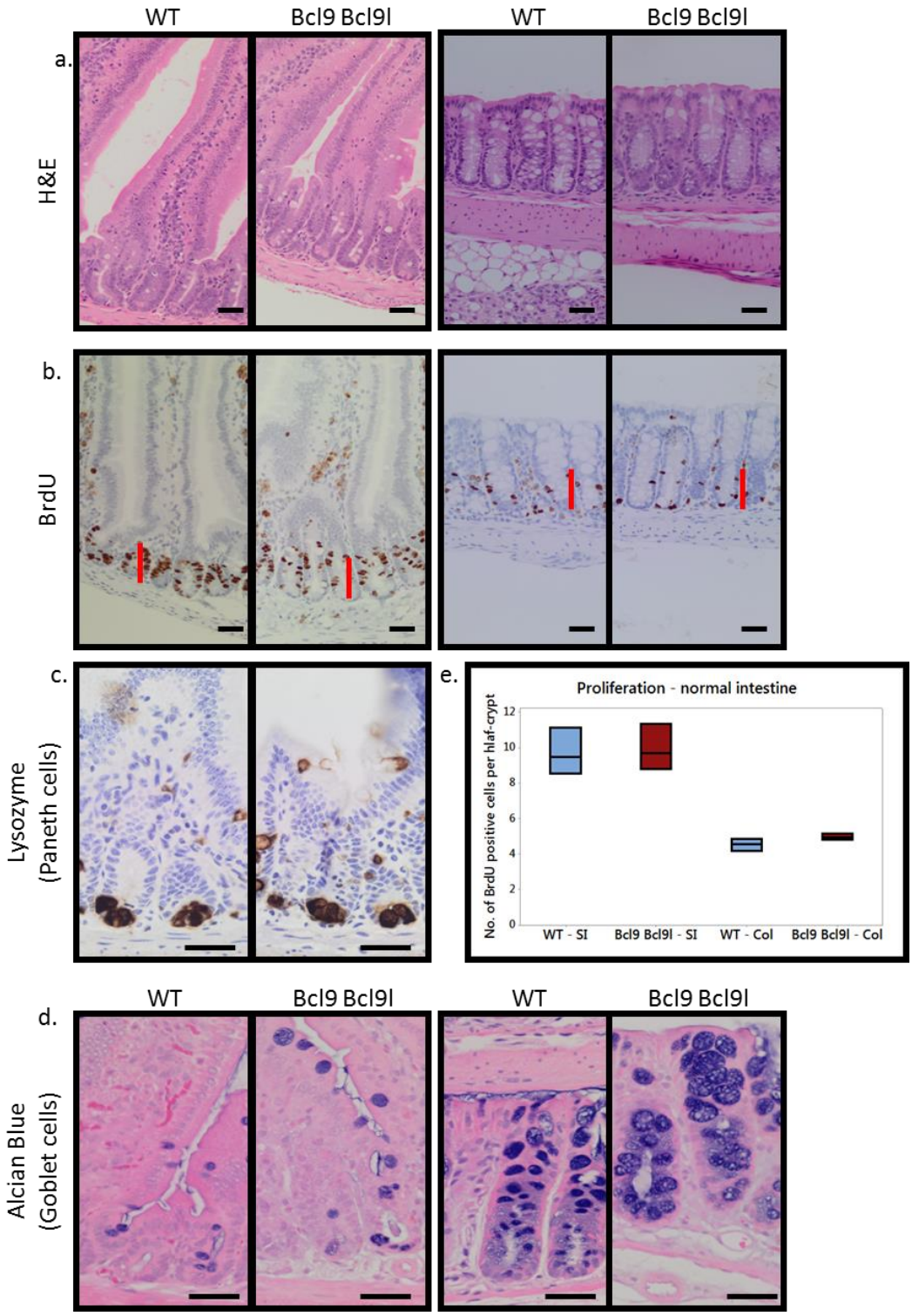

Figure 3.1: BCL9 and BCL9l are dispensable for normal intestinal homeostasis

Representative images of a. H&E b. BrdU c. Lysozyme d. Alcian Blue staining of small intestines (left) and colons (right) WT and tamoxifen-induced *VillinCre*^{ER} *Bcl9*$^{fl/fl}$ *Bcl9l*$^{fl/fl}$ (Bcl9 and Bcl9l) mice sampled 4-days post-induction, three mice per group. Red bars indicate size of proliferative zone. Scale bars =40μm e. BrdU scoring of WT and tamoxifen-induced *VillinCre*^{ER} *Bcl9*$^{fl/fl}$ *Bcl9l*$^{fl/fl}$, number of BrdU positive cells per half crypt in small intestine (SI) and colon (Col), 25 crypts per mouse, n=3 per group. One-way Mann-Whitney *U* test, p=0.331 for SI, p=0.095 for colon.

3.2.2 BCL9 and BCL9l deletion alters the cellular distribution of ß-catenin and are required for the expression of a subset of Wnt target genes

Given their potential roles in the nuclear shuttling of ß-catenin and the expression of Wnt target genes, I investigated whether deletion of BCL9 and BCL9l perturbs the distribution of ß-catenin and whether that impacts Wnt target gene expression. I observed an accumulation of nuclear ß-catenin in the base of the crypts of BCL9/9l deficient intestines, similar to WT intestines (Fig3.2a). However, when performing a Proximity Ligation Assay (PLA) for E-cadherin: ß-catenin complexes, I observed an increase in the number of E-cadherin: ß-catenin complexes in BCL9/9l-null crypts compared with WT crypts (Fig 3.2c). Importantly, there was no significant difference in the expression of ß-catenin and E-cadherin between the two groups (Fig 3.2d). The increase in the membranous pool of ß-catenin could in turn impact Wnt signalling at the transcriptional level, if there is a concomitant reduction in the nuclear pool of ß-catenin as a result. It has previously been shown that BCL9/9l are required for the expression of the intestinal stem cell marker *Lgr5* in the colonic epithelium (Deka et al., 2010). I confirmed a reduction in *Lgr5* expression following BCL9/9l deletion using *Lgr5*-RNAScope (Fig3.3a) and qRT-PCR (Fig3.3b).

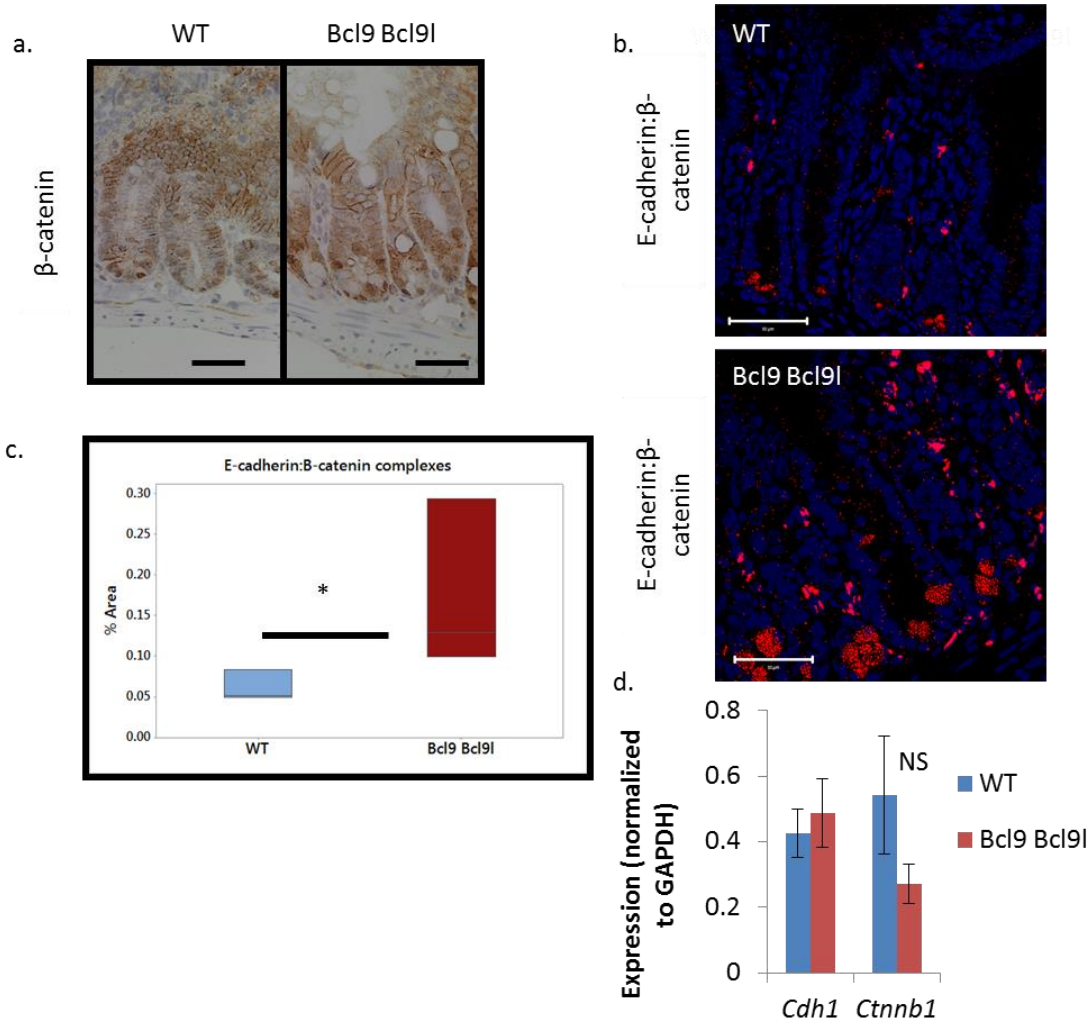

Figure 3.2: Deletion of BCL9 and BCL9l alters ß-catenin distribution

a. Immunohistochemistry staining for nuclear ß-catenin on small intestines of tamoxifen induced WT and *VillinCre*^{ER} *Bcl9*$^{fl/fl}$ *Bcl9l*$^{fl/fl}$ (Bcl9 Bcl9l) mice sampled 4-days post-induction, scale bar =40µm b. Proximity ligation assay between E-Cadherin:ß-catenin complexes (red) in tamoxifen induced WT and *VillinCre*^{ER} *Bcl9*$^{fl/fl}$ *Bcl9l*$^{fl/fl}$ (Bcl9 Bcl9l) mice sampled 4-days post-induction, nuclei stained with DAPI (blue) scale bar = 50µm, Paneth cells auto fluoresce, red granular structures at base of the crypt. c. quantification of Proximity Ligation Assay, n=3 per group, one-way Mann-Whitney *U* test, p=0.0405 (*) d. qPCR for ß-catenin (*Ctnnb1*) and E-Cadherin (*Cdh1*) (normalised to GAPDH) on intestinal tissue from tamoxifen induced WT and *VillinCre*^{ER} *Bcl9*$^{fl/fl}$ *Bcl9l*$^{fl/fl}$ (Bcl9 Bcl9l) mice sampled 4-days post-induction, n=3 per group. One-way Mann-Whitney test, p=0.331 (*Cdh1*) and p=0.191 (*Ctnnb1*), data displayed +/- SEM.

To determine whether this downregulation of *Lgr5* was specific or as a result of a global reduction in Wnt-target gene expression, we performed RNASeq analysis on intestinal tissue from *VillinCre*^{ER} *Bcl9*$^{fl/fl}$ *Bcl9l*$^{fl/fl}$ mice and WT controls. The RNASeq revealed a downregulation in a handful of Wnt target genes, including *Axin2* and *Rnf43* (Fig3.3c), however it did not appear to be a global trend – suggesting a degree of specificity of BCL9 and BCL9l for Wnt target gene expression, or that their target regulation is context dependent. This may explain why deletion of BCL9/9l is tolerated in the mouse intestinal epithelium

under normal homeostatic conditions. See tables 7.1 and 7.2 (appendix) for list of deregulated genes.

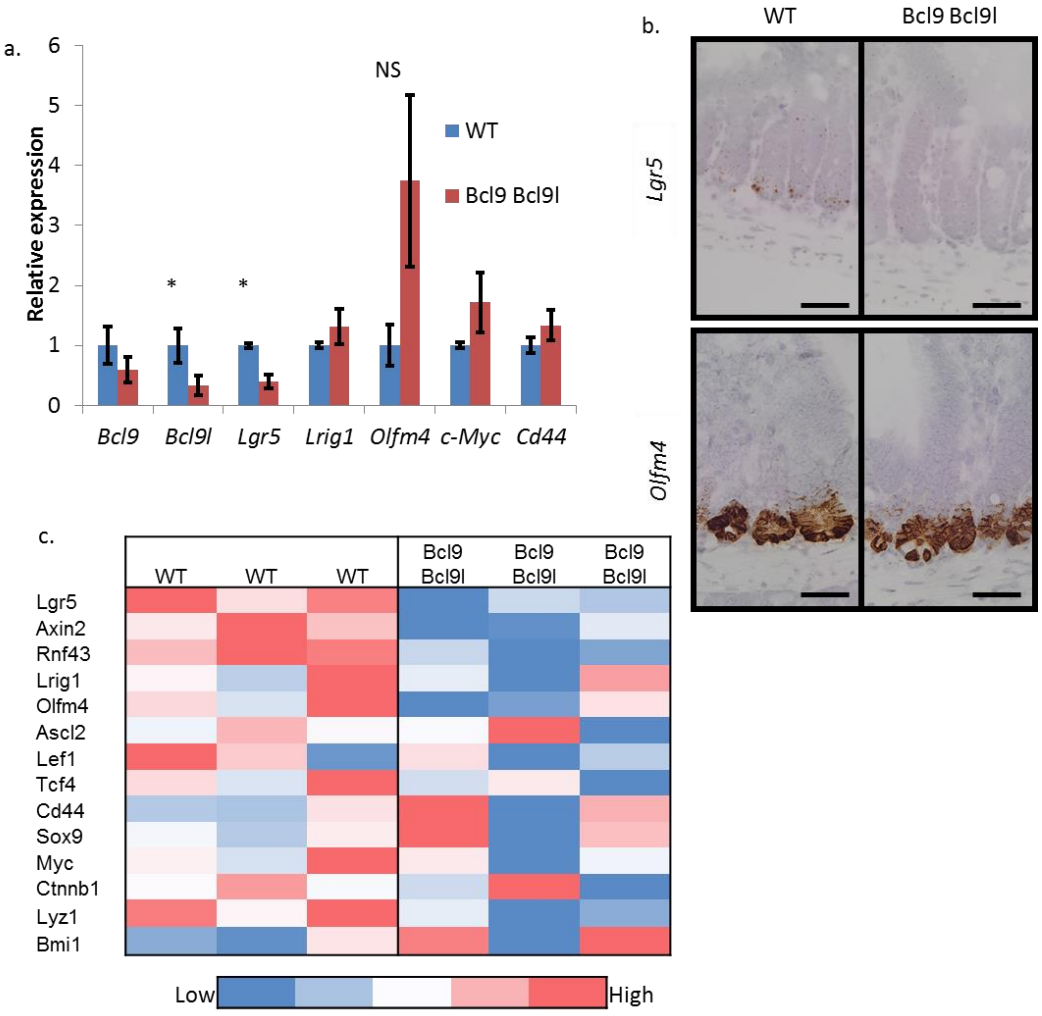

Figure 3.3: Deletion of BCL9 and BCL9l in the mouse intestine reduces the expression of a subset of Wnt-target genes

a. qPCR for Wnt-target genes and intestinal stem cell genes: *Bcl9*, *Bcl9l*, *Lgr5*, *Lrig1*, *Olfm4*, *Axin2*, *c-Myc* and *Cd44* from the small intestine of tamoxifen-induced WT and *VillinCre*^{ER} *Bcl9*$^{fl/fl}$ *Bcl9l*$^{fl/fl}$ and mice sampled 4-days post-induction, n=3 per group, one-way Mann Whitney *U* test, p=0.0405 (*).p=0.0952 (*Bcl9* and *Olfm4*), p=0.5 (*Lrgi1*), p=0.164 (*c-Myc* and *Cd44*), data displayed +/- SEM b. RNAScope for *Lgr5* and *Olfm4* staining on small intestines from tamoxifen-induced WT and *VillinCre*^{ER} *Bcl9*$^{fl/fl}$ *Bcl9l*$^{fl/fl}$ and mice sampled 4-days post-induction, scale bar =40µm. c. Heat-map for Wnt-target gene expression from the small intestine of tamoxifen-induced WT and *VillinCre*^{ER} *Bcl9*$^{fl/fl}$ *Bcl9l*$^{fl/fl}$ (Bcl9 Bcl9l) mice sampled 4-days post-induction, n=3 per group.

3.2.3 BCL9 and BCL9l are required for intestinal regeneration and the survival of intestinal crypts in the absence of Wnt ligands

Given that BCL9 and are BCL9l are thought to play a key role in the Wnt-signalling pathway, I sought to assess if *VillinCre^{ER} Bcl9$^{fl/fl}$ Bcl9l$^{fl/fl}$* mice would be more sensitive to manipulations/alterations in Wnt pathway activity. Irradiation of the mouse small intestine induces a regenerative response in intestinal crypts, accompanied by high levels of Wnt signalling. Following exposure to 10Gy γ-irradiation, small intestinal crypts from *VillinCre^{ER} Bcl9$^{fl/fl}$ Bcl9l$^{fl/fl}$* mice showed a significantly reduced capacity to regenerate compared with WT mice, when the number of regenerating crypts 72-hours post-irradiation was scored (Fig3.4a and Fig3.4b).

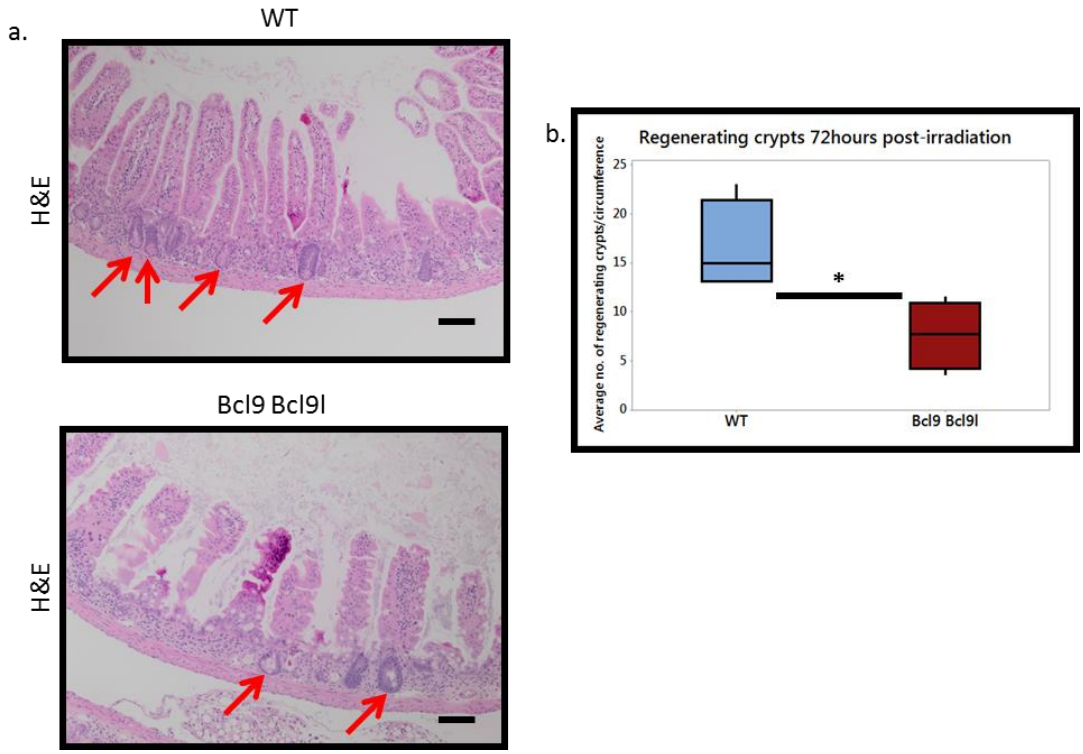

Figure 3.4: BCL9 and BCL9l are required for intestinal regeneration following irradiation

a. Representative H&Es from tamoxifen-induced WT and *VillinCre^{ER} Bcl9$^{fl/fl}$ Bcl9l$^{fl/fl}$* (Bcl9 Bcl9l) mice sampled 72 hours after irradiation (10Gy), red arrows indicate regenerating crypts Scale bar = 100μm. b. Quantification of regenerating crypts – average number of regenerating crypts per circumference in the small intestine of tamoxifen induced WT and *VillinCre^{ER} Bcl9$^{fl/fl}$ Bcl9l$^{fl/fl}$* (Bcl9 Bcl9l) mice sampled 72 hours after irradiation. One-way Mann-Whitney *U* test, p=0.0152 (*), n=4 per group.

I then investigated whether reduced Wnt-signalling is tolerated in Bcl9- and Bcl9l-deficient intestines. I treated tamoxifen-induced *VillinCre*^{ER} *Bcl9*$^{fl/fl}$ *Bcl9l*$^{fl/fl}$ mice with the Porcupine inhibitor LGK974 or vehicle. Porcupine catalyses the palmitoylation of Wnt ligands and is required for their secretion (Takada et al., 2006). Treatment with LGK974 had a profound affect upon the architecture of the mouse intestine following Bcl9 and Bcl9l deletion – ablating proliferation and intestinal crypts, when compared with vehicle treated mice (Figs3.5a-c). Importantly it has been shown that WT mice tolerate LGK974 treatment for up to 50-days; however this treatment was associated with a reduction in both *Lgr5* and *Olfm4* expression (David Huels – personal communication) in the small intestine. This may explain the observed phenotype; LGK974 treatment could be further reducing the number of intestinal stem cells in *VillinCre*^{ER} *Bcl9*$^{fl/fl}$ *Bcl9l*$^{fl/fl}$, ablating proliferation and intestinal crypts in these mice. Interestingly, when I isolate BCL9/9l-deficient small intestinal crypts and attempt to propagate them *in vitro*, these crypts fail to establish and die after seeding (Fig3.5d and Fig3.5e). Importantly, exogenous Wnt-ligands are absent from the crypt culture media used, and therefore it would be interesting to see whether addition of Wnt3a is able to rescue the growth of these crypt cultures. Altogether, this suggests that BCL9/9l-null crypts are very sensitive to perturbations in Wnt signalling.

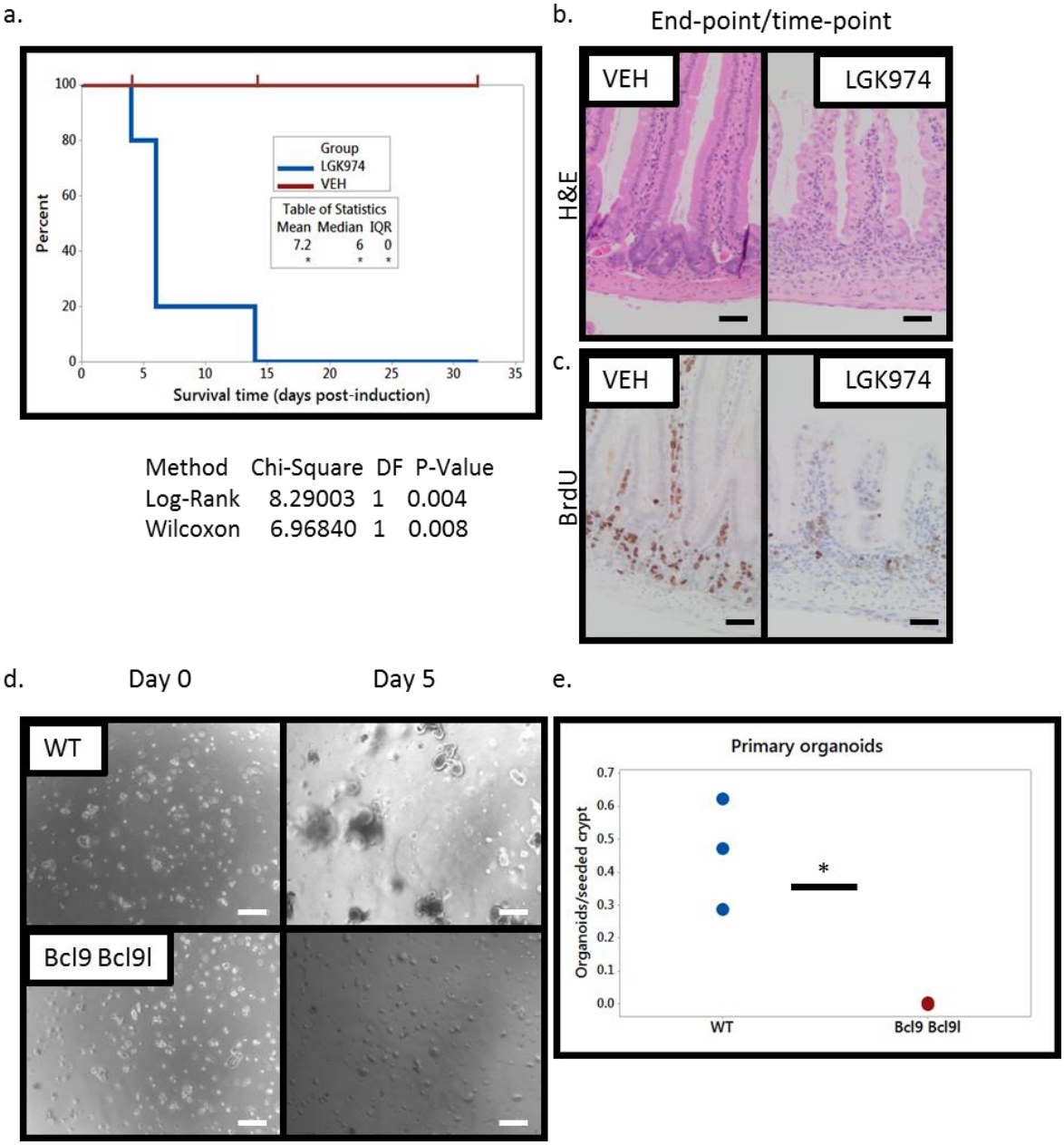

Figure 3.5: BCL9 and BCL9l-null intestinal crypts are sensitive to Porcupine inhibition

a. Survival curve for tamoxifen-induced *VillinCre^{ER} Bcl9$^{fl/fl}$ Bcl9l^{fl}* mice treated with 5mg/kg LGK974 or vehicle, twice daily, n=5 per group. Representative b. H&E c. BrdU staining from LGK974 and vehicle treated tamoxifen-induced *VillinCre^{ER} Bcl9$^{fl/fl}$ Bcl9l$^{fl/fl}$* and WT mice sampled at end-point (LGK974) or a 32-day time-point (VEH), scale bars =40μm d. Representative images of small intestinal crypts seeded in Matrigel 4-days post-induction from tamoxifen-induced *VillinCre^{ER} Bcl9$^{fl/fl}$ Bcl9l$^{fl/fl}$* (Bcl9 Bcl9l) or WT mice e. Quantification of viable organoids from WT and Bcl9 Bcl9l mice 6-days post seeding. 150 crypts seeded per well - total number of viable organoids/seeded crypt scored, one-way Mann-Whitney *U* test, p=0.0405 (*) n=3 per group.

3.2.4 BCL9 and BCL9l deletion partially suppresses the crypt progenitor phenotype following acute APC loss

Since Bcl9 and Bcl9l are both Wnt target genes and are upregulated in human Colorectal Cancer,) I generated *VillinCre^{ER} Apc$^{fl/fl}$* (APC) and *VillinCre^{ER} Apc$^{fl/fl}$ Bcl9$^{fl/fl}$ Bcl9l$^{fl/fl}$* (APC BCL9 BCL9l) mice to determine the role of these two proteins following Apc loss and whether they represent potential therapeutic targets. Deletion of BCL9/9l following acute APC loss lead to a significant reduction in proliferation in both the small intestine and colon at day 4 compared with mice WT for BCL9 and BCL9l (Figs 3.6a-c). This is not too surprising since both *Bcl9* and *Bcl9l* expression are upregulated in the mouse small intestine following the loss of both copies of APC (Fig3.6d) – suggesting a role for these two proteins following Wnt pathway hyperactivation. Given that loss of both copies of *Apc* results in a hyperactivation of the Wnt signalling pathway, I next investigated whether this reduced proliferation could be due to perturbed Wnt signalling.

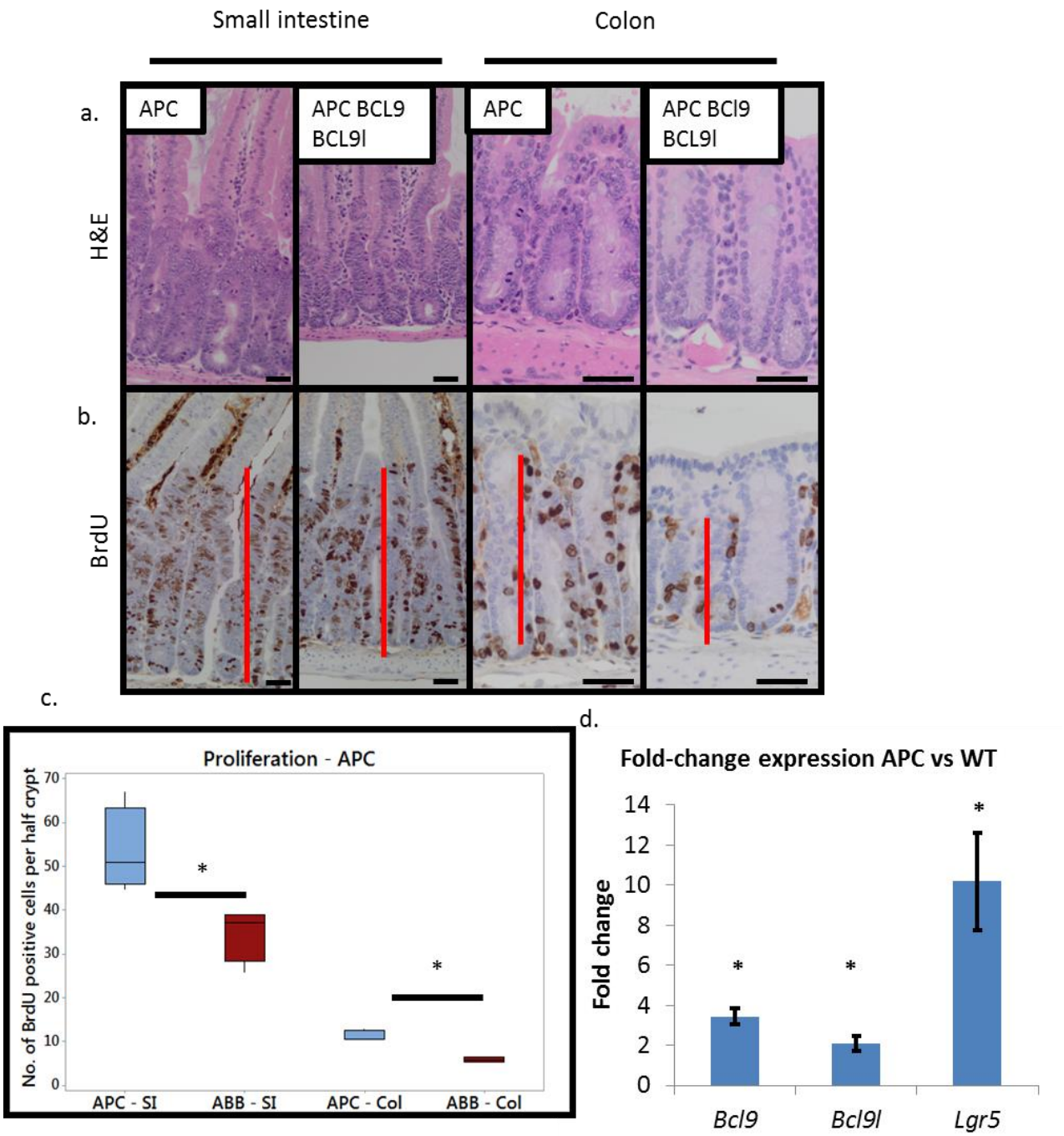

Figure 3.6: Deletion of BCL9 and BCL9l partially suppresses the Apc crypt progenitor phenotype

a. H&E b. BrdU staining of small intestine from tamoxifen-induced *VillinCre*^{ER} *Apc*$^{fl/fl}$ (APC) and *VillinCre*^{ER} *Apc*$^{fl/fl}$ *Bcl9*$^{fl/fl}$ *Bcl9l*$^{fl/fl}$ (APC BCL9 BCL9l) sampled 4-days post-induction, red bar indicates proliferative zone, scale bars = 40μm. c. quantification of BrdU positive cells per half-crypt from small intestine (SI) and colon (Col) from tamoxifen-induced VillinCre^{ER} Apc$^{fl/fl}$ (APC) and *VillinCre*^{ER} *Apc*$^{fl/fl}$ *Bcl9*$^{fl/fl}$ *Bcl9l*$^{fl/fl}$ (ABB) mice sampled 4-days post-induction. Mice were injected with BrdU intraperitoneally 2 hours prior to sampling. 25 crypt per mouse were scored, n=4. One-way Mann-Whitney U-test, p=0.0152 for both small intestine and colon. d qPCR of *Bcl9, Bcl9l* and *Lgr5* in tamoxifen-induced *VillinCre*^{ER} *Apc*$^{fl/fl}$ (APC) and WT mice sampled 4-days post-induction. Displayed as fold-change APC vs WT, n=3 (WT), n=5 (APC). One-way Mann-Whitney *U* test, p=0.0407 for *Bcl9*, p=0.0185 for *Bcl9l* and *Lgr5*. Data displayed +/- SEM

3.2.5 BCL9 and BCL9l are required for the expression of Wnt target genes following APC loss

As previously observed for WT mice, I confirmed that BCL9/9l are still required for *Lgr5* expression following APC loss via qRT-PCR and RNAScope (Fig3.7a and Fig3.7d). Additionally, I observed via qRT-PCR and immunohistochemistry that there is a significant reduction in the expression in a number of other Wnt target genes, such as *Axin2*, CD44 and SOX9 (Figs 3.7b-d). ß-catenin immunohistochemistry revealed that ß-catenin still accumulated in the nucleus following deletion of BCL9/9l (Fig3.8a). However, as determined via a PLA, there was an increase, albeit non-significant, in the number of E-cadherin: ß-catenin complexes following BCL9/9l deletion following APC loss (Fig3.8b and Fig3.8c). However, qRT-PCR reveals that *Cdh1* expression is reduced in APC BCL9 BCL9l small intestines compared with controls (Fig3.8d); suggesting that E-cadherin is limiting for the formation of E-cadherin: ß-catenin complexes in these intestines. Therefore, if E-cadherin is also reduced at the protein level following BCL9/9l deletion and APC loss, this could explain why I do not observe a significant increase E-cadherin: ß-catenin complexes in APC BCL9 BCL9l small intestines compared with APC small intestines. Since the reduced pool of E-cadherin could be saturated with bound ß-catenin, so there is no further increase in E-cadherin: ß-catenin complex formation. An immunoblot of epithelial extractions from APC and APC BCL9 BCL9l small intestines or an immunohistochemistry stain for E-cadherin would clarify differences in E-cadherin protein levels. Nonetheless, even after the cytoplasmic pool of ß-catenin is released following APC deletion, BCL9 and BCL9l are still required for the expression of some Wnt genes; either for the efficient shuttling of ß-catenin to the nucleus or transactivation of ß-catenin genes. Further work is required to elucidate this.

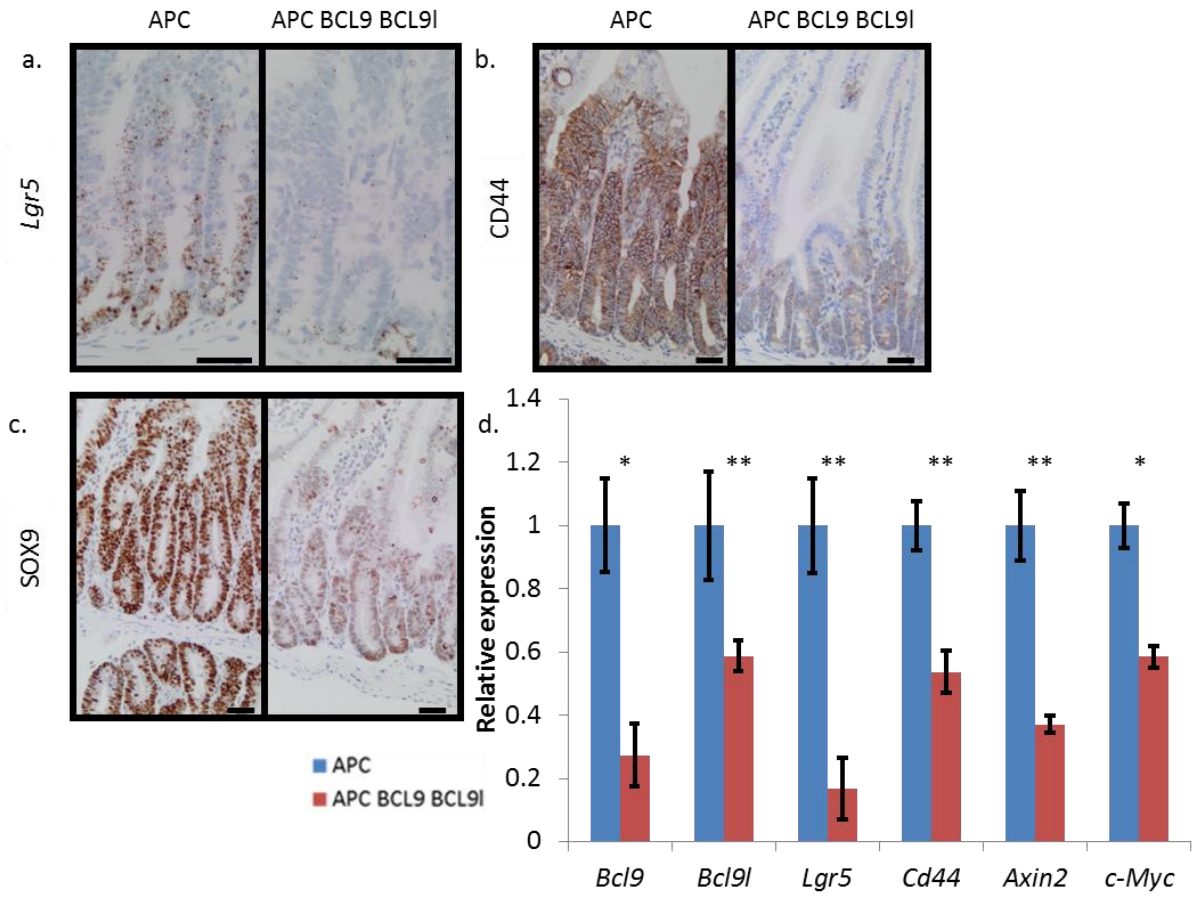

Figure 3.7: BCL9 and BCL9l are required for the expression of Wnt target genes following loss of APC in the mouse small intestine

a.*Lgr5*-RNAScope b. CD44 and c. SOX9 staining on tamoxifen induced *VillinCre*^{ER} *Apc*$^{fl/fl}$ (APC) and *VillinCre*^{ER} *Apc*$^{fl/fl}$ *Bcl9*$^{fl/fl}$ *Bcl9l*$^{fl/fl}$ (APC BLC9 BLC9l) mice sampled 4-days post-induction, scale bars = 40μm. d. qPCR for *Bcl9*, *Bcl9l*, *Lgr5*, *Cd44*, *Axin2* and *Myc* from whole pieces of small intestinal tissue isolated from on tamoxifen induced *VillinCre*^{ER} *Apc*$^{fl/fl}$ (APC) and *VillinCre*^{ER} *Apc*$^{fl/fl}$ *Bcl9*$^{fl/fl}$ *Bcl9l*$^{fl/fl}$ (APC BLC9 BLC9l) mice sampled 4-days post-induction. One-way Mann-Whitney *U* test, p=0.0108 for *Bcl9*, p=0.01 for *Myc*, p=0.0061 for *Bcl9l*, *Lgr5*, *Cd44* and *Axin2* n=5 per group. Data displayed +/- SEM

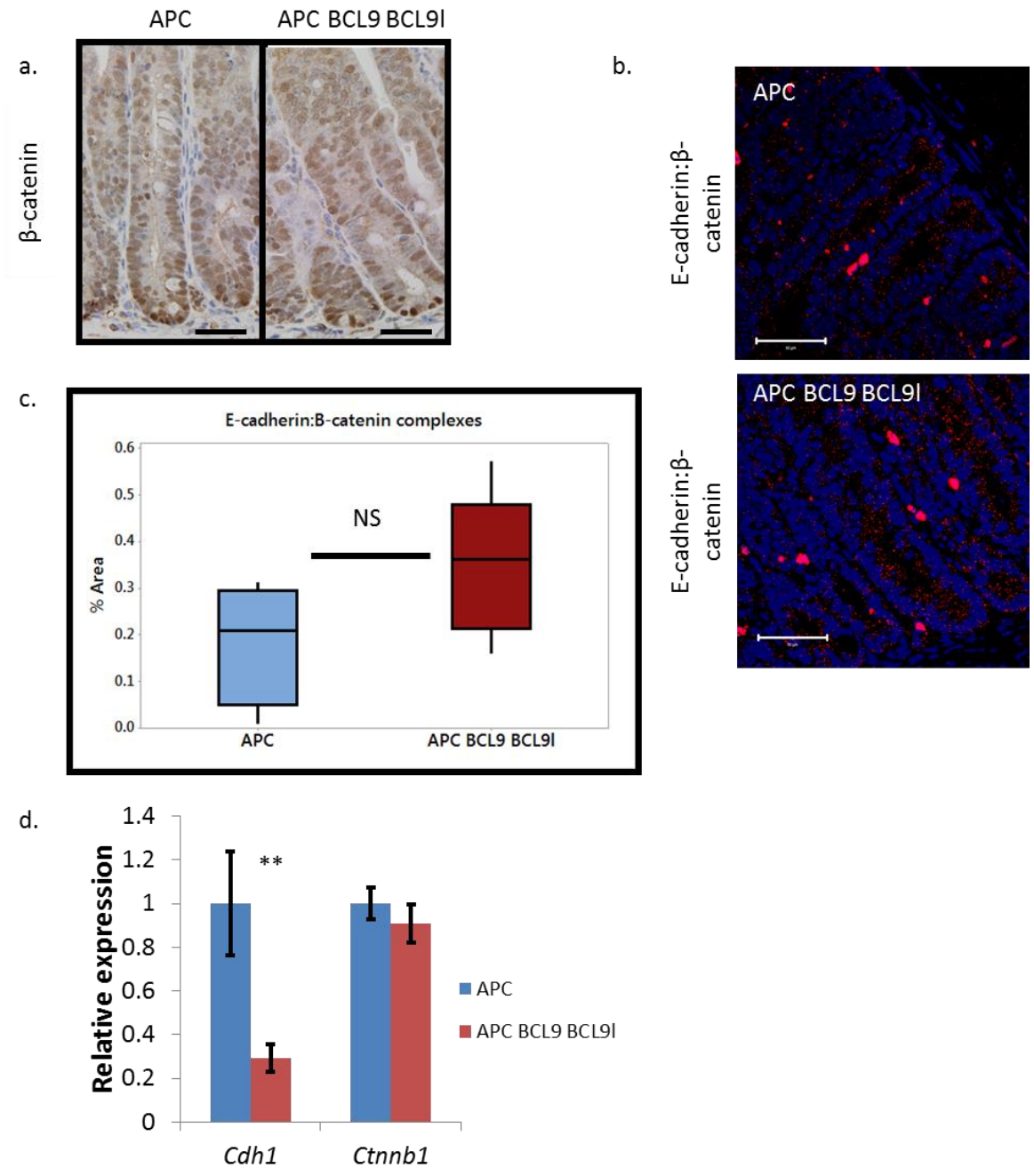

Figure 3.8 Deletion of BCL9 and BCL9l does not significantly perturb ß-catenin localisation following APC loss

a. ß-catenin staining of small intestinal crypts from tamoxifen-induced *VillinCre^{ER} Apc$^{fl/fl}$* (APC) and *VillinCre^{ER} Apc$^{fl/fl}$ Bcl9$^{fl/fl}$ Bcl9l$^{fl/fl}$* (APC BCL9 BCL9l) mice sampled four days post-induction, scale bar = 40μm. b. Proximity ligation assay between E-Cadherin:ß-catenin complexes (red) in tamoxifen induced *Villin Cre^{ER} Apc$^{fl/fl}$* (APC) and *VillinCre^{ER} Apc$^{fl/fl}$ Bcl9fl$^{/fl}$ Bcl9l$^{fl/fl}$* (APC BCL9 BCL9l) mice sampled 4-days post-induction, nuclei stained with DAPI (blue), scale bar = 20μm c. quantification of Proximity Ligation Assay, n=5 per group, one-way Mann-Whitney U-test, p=0.072. d. qPCR for E-Cadherin (*Cdh1*) and ß-catenin (*Ctnnb1*) (normalised to GAPDH) on intestinal tissue from tamoxifen induced *VilinCre^{ER} Apc$^{fl/fl}$* (APC) and *VillinCre^{ER} Apc$^{fl/fl}$ Bcl9$^{fl/fl}$ Bcl9l$^{fl/fl}$* (APC BCL9 BCL9l) mice sampled 4-days post-induction, n=5 per group. One-way Mann-Whitney *U* test, p=0.01 (*Cdh1*) (**) and p=0.27 (*Ctnnb1*). Data displayed +/- SEM.

I next took an unbiased approach to investigate the transcriptome dependent on BCL9/9l following APC loss in the mouse small intestine. I performed RNASeq on small intestinal tissue isolated from APC and APC BCL9 BCL9l mice. This RNASeq analysis revealed the profound downregulation of a large number of Wnt target genes following BCL9/9l deletion (Fig3.9a). Furthermore when I performed a Gene Set Enrichment Analysis (GSEA) on the differentially expressed genes from APC and APC BCl9 BCL9l mice, there was a negative enrichment in the APC-KO signature (Sansom et al., 2004) (Fig9.3b). This further supports the notion that BCL9 and BCL9l are required for the expression of a large number of Wnt target genes following the activation of the Wnt signalling pathway after APC loss. See tables 7.3 and 7.4 (appendix) for list of deregulated genes.

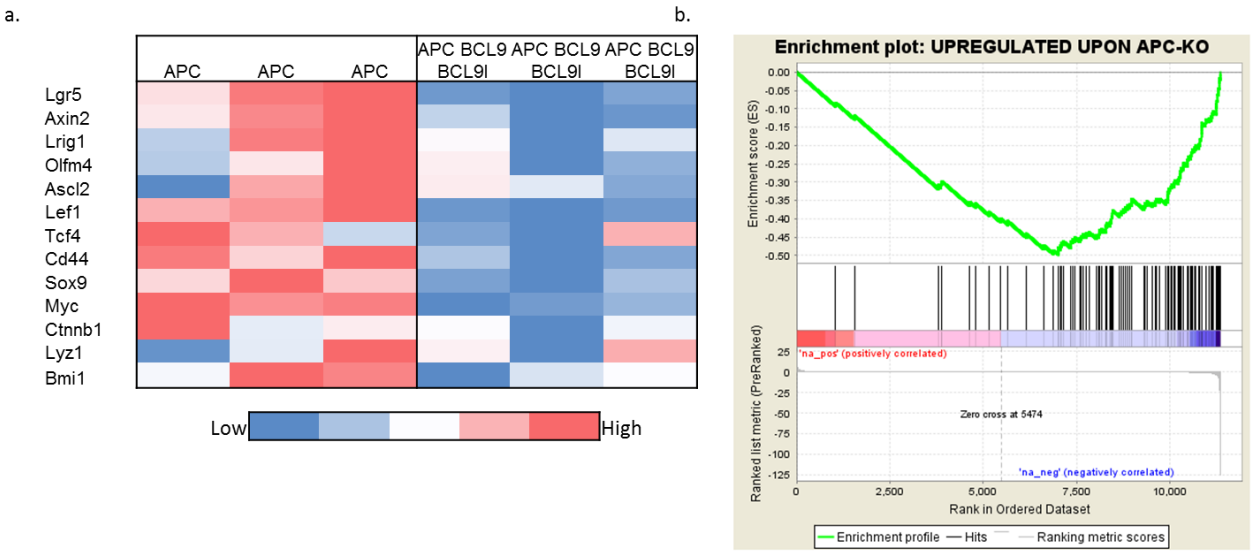

Figure 3.9: BCL9 and BCL9l are required for the expression of Wnt target genes following Apc loss in the intestine

RNASeq was performed on whole pieces of small intestinal from tamoxifen-induced *VillinCre*^{ER} *Apc*$^{fl/fl}$ (APC) and *VillinCre*^{ER} *Apc*$^{fl/fl}$ *Bcl9*$^{fl/fl}$ *Bcl9l*$^{fl/fl}$ (APC BCL9 BCL9l) sampled 4-days post induction. a. Heat-map of a Wnt-target genes and b. Gene Set Enrichment Analysis on APC-KO signature on samples, n=3 per group. Genes from RNASeq were ranked using -$\log_{10}$ (adjusted p-value) x $\log_2$ (fold change - APC BCL9 BCL9l vs APC), such that the highest ranked genes correspond to genes most downregulated in APC BCL9 BCL9l compared to APC. Ranked genes are displayed left (lowest) to right (highest) in the plot. Black lines indicate a hit within the dataset that corresponds to a gene within the data set. In this figure, black lines are skewed to the right (downregulated in APC BCL9 BCL9l compared vs APC) - hence the negative enrichment for this signature in the APC BCL9 BCL9l dataset.

3.2.6 BCL9 and BCL9l deletion partially suppresses the crypt progenitor phenotype following KRAS activation

The APC KRAS model exhibits numerous phenotypic differences compared with the APC model, and is resistant to a number of therapies. I wanted to investigate whether Bcl9/9l deletion could suppress Wnt signalling in this model and modify the phenotype.

I generated *VillinCre^{ER} Apc$^{fl/fl}$ Kras$^{G12D/+}$* (APC KRAS) and *VillinCre^{ER} Apc$^{fl/fl}$ Kras$^{G12D/+}$ Bcl9$^{fl/fl}$ Bcl9l$^{fl/fl}$* (AKBB) mice, induced them and sampled them three days post-induction. There was a significant reduction in proliferation in both the small intestines and colons of AKBB mice compared with APC KRAS mice (Figs3.10a-c). As shown before, deletion of BCL9/9l resulted in a reduction in the expression of a number of Wnt target genes – RNAScope staining and qRT-PCR showed a reduction in *Lgr5* expression (Figs 3.11a and 3.11d), whilst CD44 staining was reduced (Fig3.11b). Interestingly, the expression of some other Wnt target genes that were significantly reduced in APC BCL9 BCL9l compared with APC mice, such as *c-Myc*, *Axin2* and Sox9 were not affected in AKBB mice compared with APC KRAS mice (Fig3.11c and Fig3.11d). This would suggest that some downstream effectors of KRAS impinge upon Wnt signalling, therefore overcoming the requirement of BCL9 and BCL9l for the expression of a subset of Wnt target genes. It has been reported that oncogenic KRAS strongly cooperates with deregulated Wnt signalling following APC loss (Janssen et al., 2006; Sansom et al., 2006) hence this cooperation may, in part, explain the differential dependence of BCL9 and BCL9l for the expression of some Wnt target genes in the intestinal epithelium of APC and APC KRAS mice. Furthermore, the MAPK pathway has been shown to increase MYC expression, hence increased MYC expression may also support the expression of a number of Wnt target genes in APC KRAS small intestines.

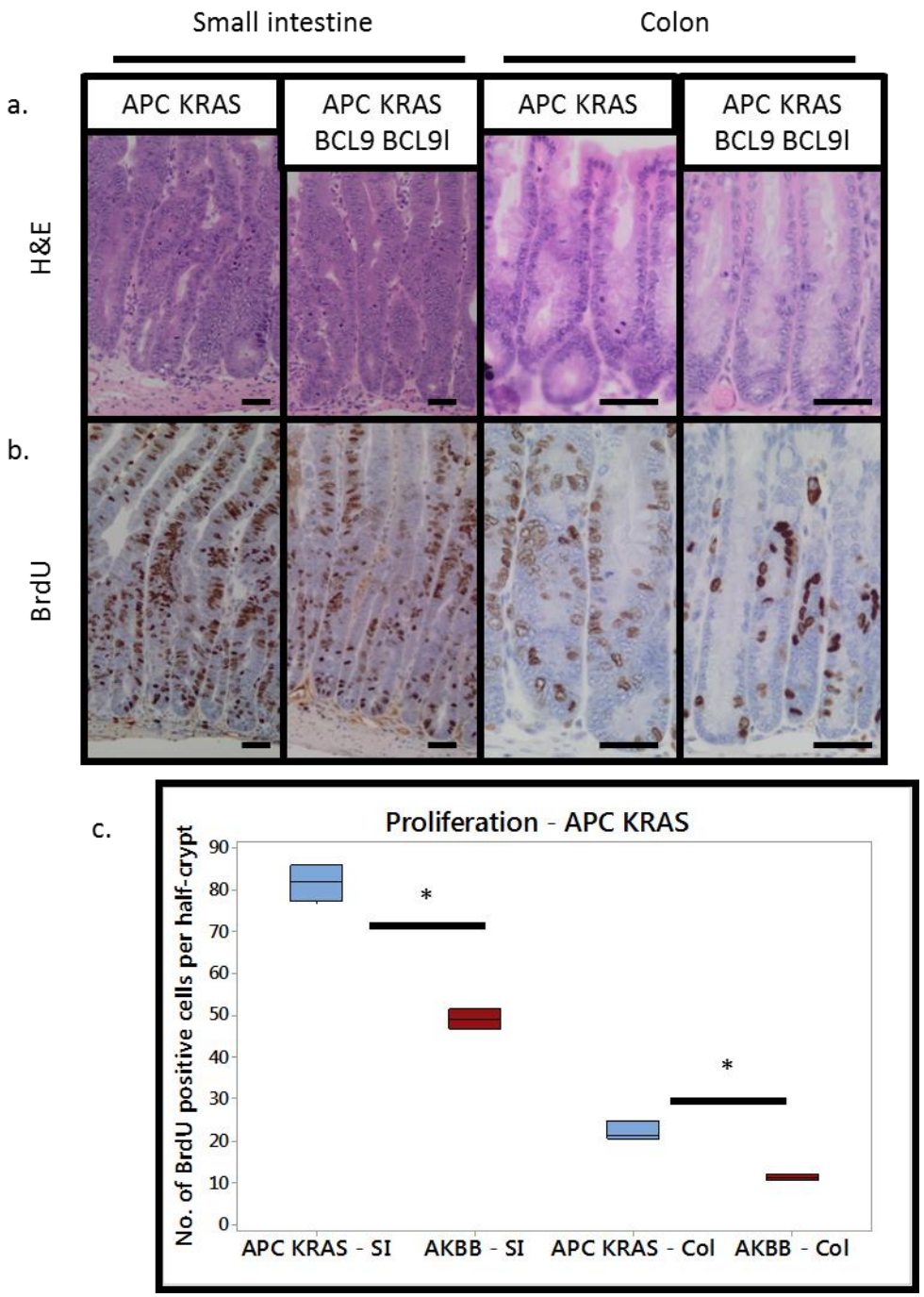

Figure 3.10: BCL9 and BCL9l deletion partially suppresses the APC KRAS phenotype

a. H&E b. BrdU staining of small intestine from tamoxifen-induced *VillinCre^{ER} Apc$^{fl/fl}$ Kras$^{G12D/+}$* (APC KRAS) and *VillinCre^{ER} Apc$^{fl/fl}$ Kras$^{G12D/+}$ Bcl9$^{fl/fl}$ Bcl9l$^{fl/fl}$* (APC KRAS BCL9 BCL9l) sampled 3-days post-induction, scale bars = 40μm. c. quantification of BrdU positive cells per half-crypt from small intestine (SI) and colon (Col) from tamoxifen-induced *VillinCre^{ER} Apc$^{fl/fl}$ Kras$^{G12D/+}$* (APC KRAS) and *VillinCre^{ER} Apc$^{fl/fl}$ Kras$^{G12D/+}$ Bcl9$^{fl/fl}$ Bcl9l$^{fl/fl}$* (AKBB) mice sampled 3-days post-induction. Mice were injected with BrdU intraperitoneally 2 hours prior to sampling. 25 crypt per mouse were scored, n=3-4 for small intestine, n=3 for colon. One-way Mann-Whitney *U* test, p=0.0259 for small intestine and p=0.0405 for colon.

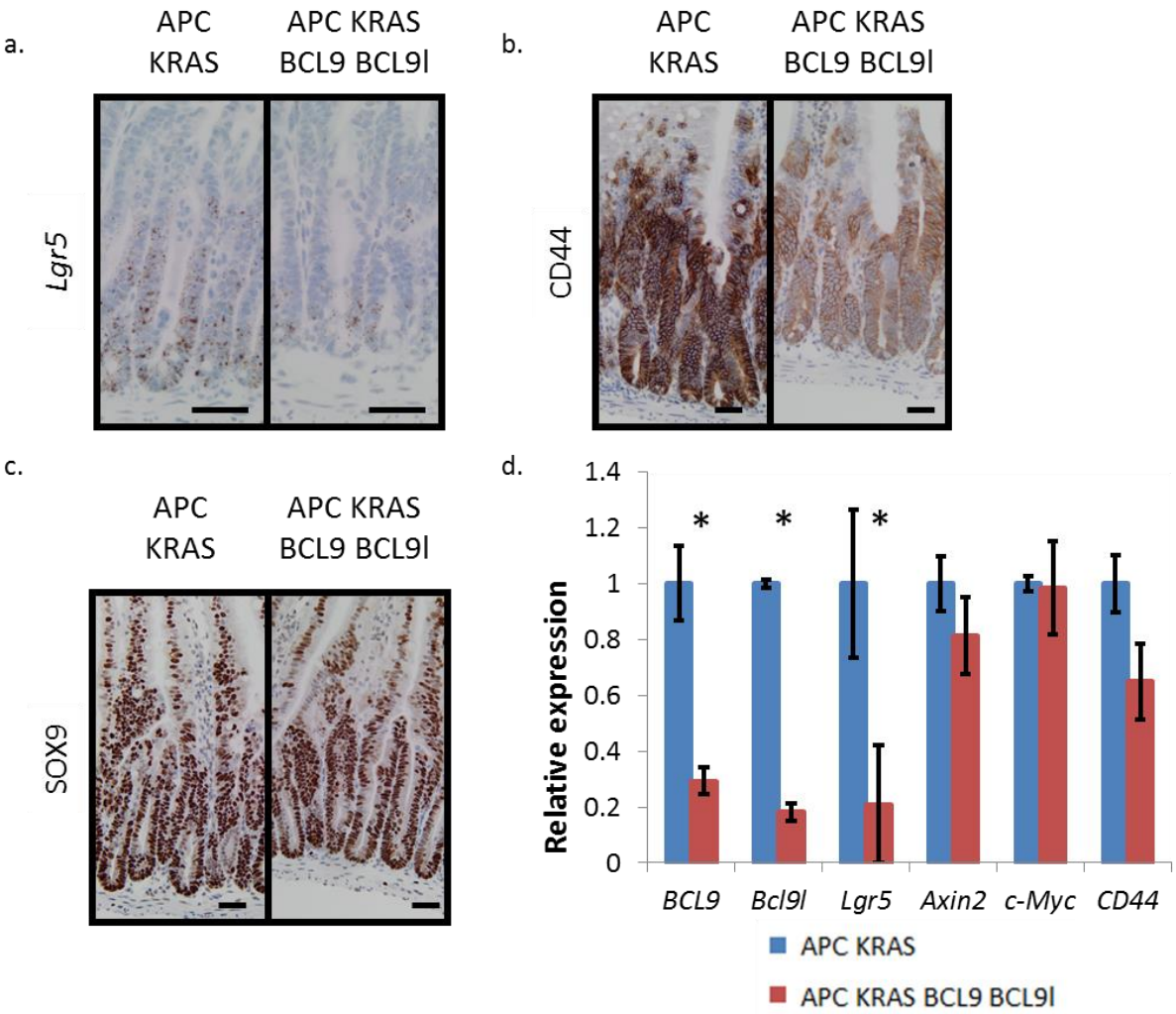

Figure 3.11: BCL9 and BCL9l are required for Lgr5 expression in APC KRAS crypts
a. *Lgr5*-RNAScope b. CD44 and c. SOX9 staining on tamoxifen induced *VillinCre*^{ER} *Apc*$^{fl/fl}$ *Kras*$^{G12D/+}$ (APC KRAS) and *VillinCre*^{ER} *Apc*$^{fl/fl}$ *Kras*$^{G12D/+}$ *Bcl9*$^{fl/fl}$ *Bcl9l*$^{fl/fl}$ (APC KRAS BLC9 BLC9l) mice sampled 3-days post-induction, scale bars = 40μm. d. qPCR for *Bcl9*, *Bcl9l*, *Lgr5*,*Axin2*, *Myc* and *Axin2* from whole pieces of intestinal tissue isolated from on tamoxifen induced *VillinCre*^{ER} *Apc*$^{fl/fl}$ *Kras*$^{G12D/+}$ (APC KRAS) and *VillinCre*^{ER} *Apc*$^{fl/fl}$ *Kras*$^{G12D/+}$ *Bcl9*$^{fl/fl}$ *Bcl9l*$^{fl/fl}$ (APC KRAS BLC9 BLC9l) mice sampled 3-days post-induction. One-way Mann-Whitney *U* test, n=3 per group, (*) p=0.0405 (for *Bcl9*, *Bcl9l* and *Lgr5*), p=0.164 (*Axin2*), p=0.331 (*c-Myc*) and p=0.0952 (*Cd44*). Data displayed +/- SEM

3.2.7 BCL9 and BCL9l are required for the dedifferentiation of villi following APC loss and KRAS activation

It has previously been shown that differentiated cells within the villi of the intestine that acquire high MAPK- and Wnt-signalling, following acute deletion of APC and KRAS activation, are able to acquire stem-cell-like properties and dedifferentiate, with tumourigenic potential (Schwitalla et al., 2013). Given that BCL9 and BCL9l regulate the expression of the intestinal stem cell marker *Lgr5*, I wanted to investigate whether BCL9 and BCL9l are required for this dedifferentiation process. I isolated both small intestinal crypts and villi from APC KRAS and AKBB mice and propagated them in culture. After five-days

post-seeding I counted the number of villi-derived spheroids from the two different genotypes, and observed a significant reduction in the number of villi-derived spheroids from AKBB mice compared to APC KRAS mice (Fig3.12a and Fig3.12b). Interestingly, I also observed that many of the small intestinal crypts isolated from AKBB mice grew with 'organoid-like' morphology, whilst those isolated from APC KRAS mice grew predominantly as spheroids (Fig3.12c). After 5-days post-seeding, I scored the number of organoid-like crypts in the APC KRAS and AKBB crypt cultures, and determined the overall percentage of the organoid-like crypts out of the total number of crypts (organoid-like and spheroid). There was a significant increase in the number of organoid-like crypts in the AKBB crypt cultures compared to the APC KRAS crypt cultures (Fig3.12d). This organoid-like morphology is reminiscent of budding WT organoids that are dependent on RSpondin for their growth; however in this instance the AKBB crypt cultures grew independently of RSpondin, suggesting that these cells have sufficient Wnt-pathway activation for growth.

Taken together, these results show that BCL9 and BCL9l are required for the dedifferentiation of villi, and the establishment of spheroids from intestinal crypts isolated from APC KRAS mice. This suggests that these epithelial cells have reduced Wnt signalling, which could in turn reduce expression of intestinal stem cell markers.

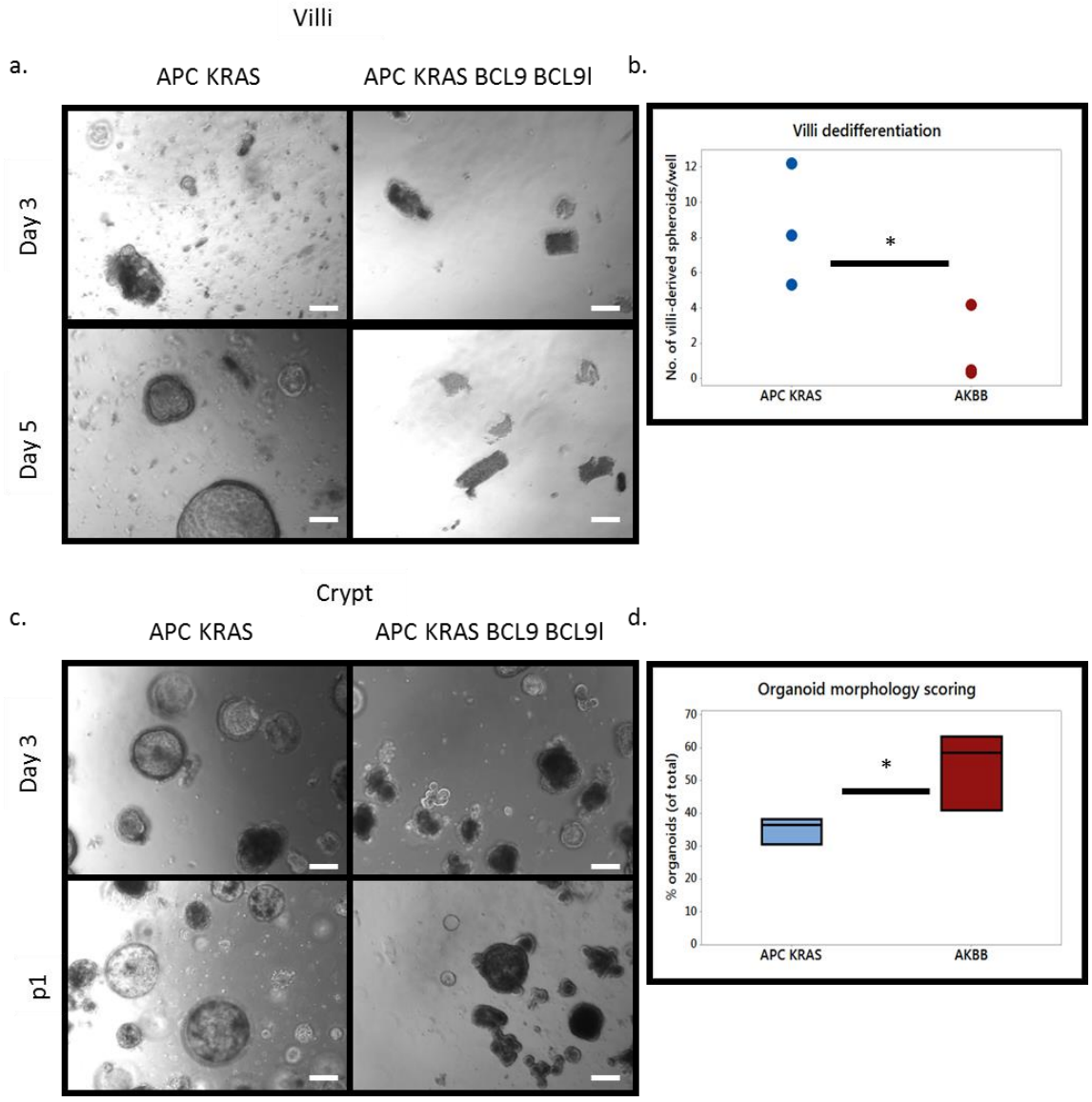

Figure 3.12: BCL9 and BCL9l are required for intestinal villi dedifferentiation

a. Representative images of intestinal villi isolated from *VillinCre^{ER} Apc$^{fl/fl}$ Kras$^{G12D/+}$* (APC KRAS) and *VillinCre^{ER} Apc$^{fl/fl}$ Kras$^{G12D/+}$ Bcl9$^{fl/fl}$ Bcl9l$^{fl/fl}$* (APC KRAS BCL9 BCL9l), 3- and 5-days post-seeding. b. Quantification of villi-derived spheroids form *VillinCre^{ER} Apc$^{fl/fl}$ Kras$^{G12D/+}$* (APC KRAS) and *VillinCre^{ER} Apc$^{fl/fl}$ Kras$^{G12D/+}$ Bcl9$^{fl/fl}$ Bcl9l$^{fl/fl}$* (APC KRAS BCL9 BCL9l) 5-days post-seeding – 70 villi/well originally seeded. One-way Mann-Whitney *U* test, p=0.0405, n=3. c. Representative images of intestinal crypt isolated from *VillinCre^{ER} Apc$^{fl/fl}$ Kras$^{G12D/+}$* (APC KRAS) and *VillinCre^{ER} Apc$^{fl/fl}$ Kras$^{G12D/+}$ Bcl9$^{fl/fl}$ Bcl9l$^{fl/fl}$* (APC KRAS BCL9 BCL9l), 3- and 5-days post-seeding. d. Quantification of % crypts with 'organoid-like morphology' form *VillinCre^{ER} Apc$^{fl/fl}$ Kras$^{G12D/+}$* (APC KRAS) and *VillinCre^{ER} Apc$^{fl/fl}$ Kras$^{G12D/+}$ Bcl9$^{fl/fl}$ Bcl9l$^{fl/fl}$* (APC KRAS BCL9 BCL9l) 5-days post-seeding. One-way Mann-Whitney *U* test, p=0.0405, n=3. Scale bars = 200μm

3.2.8 Deletion of BCL9 and BCL9l significantly accelerates tumourigenesis

Since deletion of BCL9 and BCL9l suppressed the crypt-progenitor phenotype following acute deletion of APC, regardless of KRAS activation, and also are required for the expression of the intestinal stem cell marker *Lgr5*, I was keen to investigate whether these two genes are required for the development of intestinal tumours and whether their deletion has any survival benefit. I generated cohorts of *VillinCre*^{ER} *Apc*$^{fl/+}$ *Bcl9*$^{fl/fl}$ *Bcl9l*$^{fl/fl}$ and *VillinCre*^{ER} *Apc*$^{fl/+}$ *Kras*$^{G12D/+}$ *Bcl9*$^{fl/fl}$ *Bcl9l*$^{fl/fl}$ mice, induced them and aged them until showing signs of intestinal tumour burden.

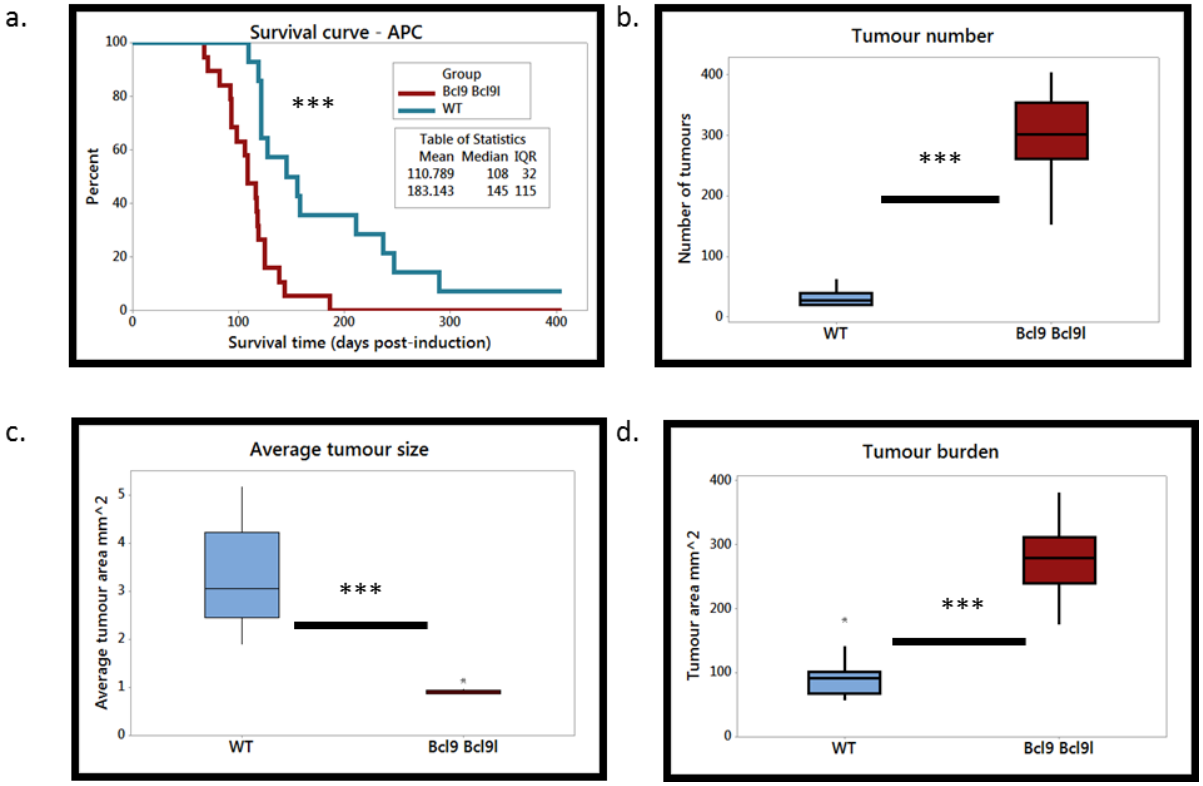

Figure 3.13 Deletion of BCL9 and BCL9l significantly accelerates intestinal tumourigenesis

a. Survival curve for tamoxifen-induced *VillinCre*^{ER} *Apc*$^{fl/+}$ (WT) and *VillinCre*^{ER} *Apc*$^{fl/+}$ *Bcl9*$^{fl/fl}$ *Bcl9l*$^{fl/fl}$ (Bcl9 Bcl9l) sampled at clinical end-point, n=16 for WT and n=19 for Bcl9 Bcl9l. Box-plots of b. Tumour-number c. Average tumour size and d. Tumour burden from tamoxifen-induced *VillinCre*^{ER} *Apc*$^{fl/+}$ (WT) and *VillinCre*^{ER} *Apc*$^{fl/+}$ *Bcl9*$^{fl/fl}$ *Bcl9l*$^{fl/fl}$ (Bcl9 Bcl9l) sampled at clinical end-point, one-way Mann-Whitney *U* test, p=0.000 for all tests. n=12 for WT, n=16 for Bcl9 Bcl9l.

Surprisingly, independent of *Kras* mutation, deletion of BCL9/9l significantly reduced tumour latency (Fig3.13a and Fig3.14a) compared with mice WT for BCL9/9l. This reduction in latency was accompanied with a significant increase in the number of intestinal tumours in the mice lacking intestinal BCL9/9l, with the mice developing a large number of small lesions (Fig 3.13b-c and Fig3.14b-c), contributing to a significantly higher tumour burden in

these mice compared with controls (Fig3.13d and Fig3.14d). Whilst tumours were uniformly distributed between the proximal and distal small intestine of *VillinCre*^{ER} *Apc*$^{fl/+}$ mice, upon BCL9/9l deletion there was a significant shift towards proximal tumours (Fig3.15a). Similarly, whilst *VillinCre*^{ER} *Apc*$^{fl/+}$ *Kras*$^{G12D/+}$ mice displayed a predominantly colonic tumour burden, there was a significant shift away from colonic tumours to proximal small intestinal tumours following deletion of BCL9/9l (Fig3.15b).

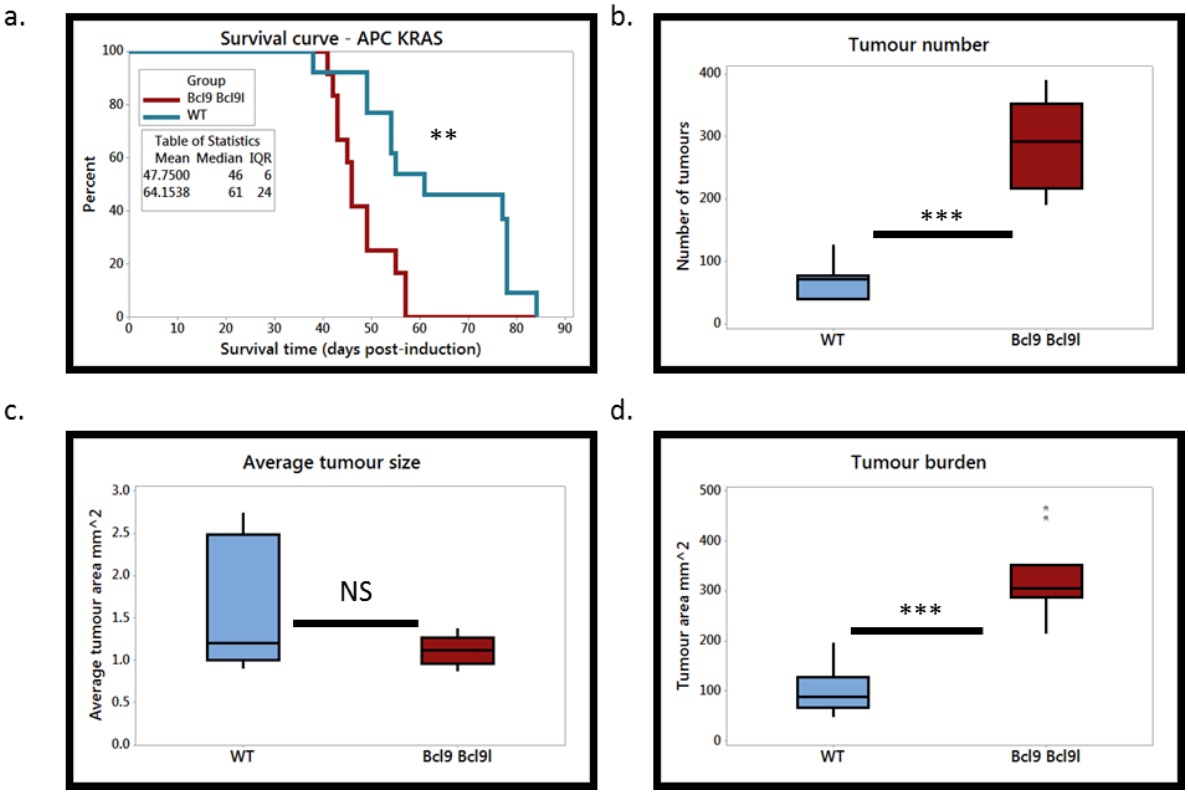

Figure 3.14 Deletion of BCL9 and BCL9l significantly accelerates tumourigenesis in a KRAS-driven model of intestinal tumourigenesis

a. Survival curve for tamoxifen-induced *VillinCre*^{ER} *Apc*$^{fl/+}$ *Kras*$^{G12D/+}$ (WT) and *VillinCre*^{ER} *Apc*$^{fl/+}$ *Kras*$^{G12D/+}$ *Bcl9*$^{fl/fl}$ *Bcl9l*$^{fl/fl}$ (Bcl9 Bcl9l) sampled at clinical end-point, n=13 for WT (1 censor) and n=13 for Bcl9 Bcl9l. Box-plots of b. Tumour number c. Average tumour size and d. Tumour burden from tamoxifen-induced *VillinCre*^{ER} *Apc*$^{fl/+}$ *Kras*$^{G12D/+}$ (WT) and *VillinCre*^{ER} *Apc*$^{fl/+}$ *Kras*$^{G12D/+}$ *Bcl9*$^{fl/fl}$ *Bcl9l*$^{fl/fl}$ (Bcl9 Bcl9l) sampled at clinical end-point, one-way Mann-Whitney *U* test, p=0.0001 for tumour number, p=0.112 for average tumour size and p=0.0002 for tumour burden. n=9 for WT, n=11 for Bcl9 Bcl9l.

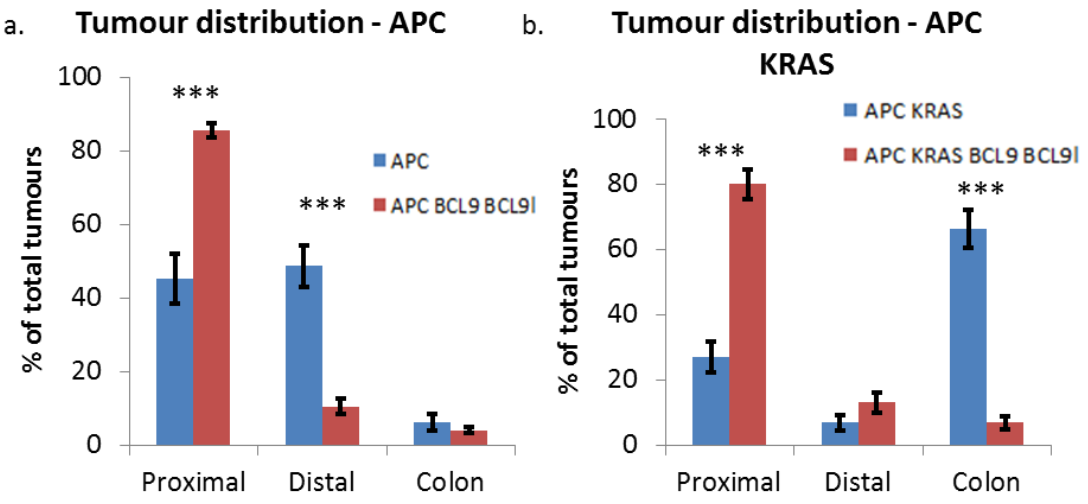

Figure 3.15 Deletion of BCL9 and BCL9l favours proximal intestinal tumour formation

Bar charts of tumour distribution along the small intestine and colon of a. VillinCre^{ER} Apc$^{fl/+}$ (APC), n=7, and VillinCre^{ER} Apc$^{fl/+}$ Bcl9$^{fl/fl}$ Bcl9l$^{fl/fl}$ (APC BCL9 BCL9l), n=14 b. VillinCre^{ER} Apc$^{fl/+}$ Kras$^{G12D/+}$ (APC KRAS), n=8 and VillinCre^{ER} Apc$^{fl/+}$ Kras$^{G12D/+}$ Bcl9$^{fl/fl}$ Bcl9l$^{fl/fl}$ (APC KRAS BCL9 BCL9l), n=9. Data displayed as % tumours per region of total tumour number, +/- SEM. One-Way Mann-Whitney *U* test – for APC: *** p=0.0002 (proximal and distal) and p=0.37 (colon). For APC KRAS, *** p=0.00015 (Proximal and colon) and p=0.089 for distal.

Importantly, the tumours that arose following BCL9/9l deletion were not escapers – IHC staining for BCL9 confirmed deletion of BCL9, whilst the tumours from control mice displayed strong nuclear staining of BCL9 (Fig3.16). The tumours lacking BCL9/9l still accumulated nuclear ß-catenin (Fig3.17a); however RNAScope confirmed that these tumours had low levels of *Lgr5* expression compared with controls (Fig3.17b), in accordance with previous findings.

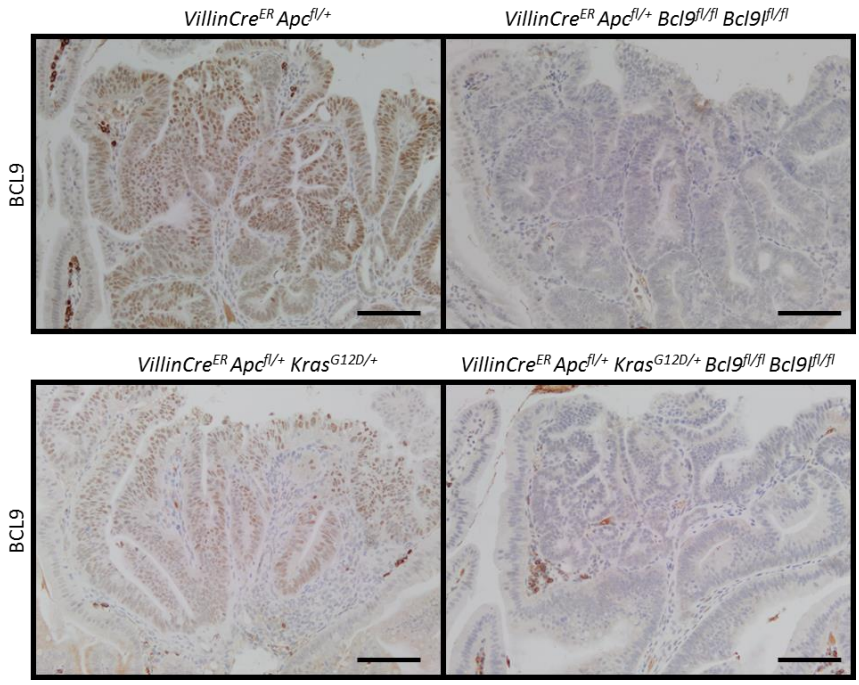

Figure 3.16: Increased tumour burden is not due to an escaper population

Representative images of BCL9 immunohistochemistry staining of intestinal tumours from *VillinCre*^{ER} *Apc*$^{fl/+}$, *VillinCre*^{ER} *Apc*$^{fl/+}$ *Bcl9*$^{fl/fl}$ *Bcl9l*$^{fl/fl}$, *VillinCre*^{ER} *Apc*$^{fl/+}$ *Kras*$^{G12D/+}$ and *VillinCre*^{ER} *Apc*$^{fl/+}$ *Kras*$^{G12D/+}$ *Bcl9*$^{fl/fl}$ *Bcl9l*$^{fl/fl}$ mice. Bcl9 accumulates in the nucleus of control tumours. Scale bars = 100μm.

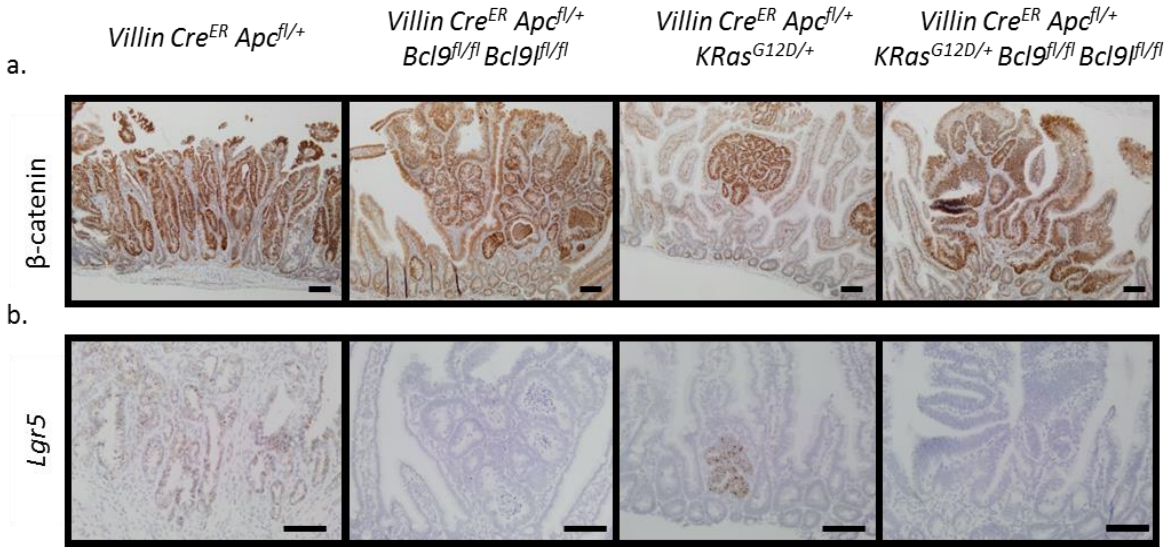

Figure 3.17 BCL9 and BCL9l-null tumours contain high levels of nuclear ß-catenin, but significantly reduced Lgr5 expression

Representative images of a. ß-catenin immunohistochemistry and b. *Lgr5*-RNAScope staining of intestinal tumours from *VillinCre*^{ER} *Apc*$^{fl/+}$, *VillinCre*^{ER} *Apc*$^{fl/+}$ *Bcl9*$^{fl/fl}$ *Bcl9l*$^{fl/fl}$, *VillinCre*^{ER} *Apc*$^{fl/+}$ *Kras*$^{G12D/+}$ and *VillinCre*^{ER} *Apc*$^{fl/+}$ *Kras*$^{G12D/+}$ *Bcl9*$^{fl/fl}$ *Bcl9l*$^{fl/fl}$ mice. Scale bars = 100μm.

These results were very much unexpected, given the previously highlighted role of these two transcription factors in Colorectal Cancer and the requirement of them for the expansion of the crypt progenitor phenotype

following acute APC deletion. There were several potential hypotheses that I had which may serve to explain these phenotypes.

3.2.9. BCL9 and BCL9l deletion does not increase DNA damage or slow cell migration

The formation of tumours in *VillinCre^{ER} Apc$^{fl/+}$* and *VillinCre^{ER} Apc$^{fl/+}$ Bcl9$^{fl/fl}$ Bcl9l$^{fl/fl}$* is dependent upon the loss of the second copy *Apc* after tamoxifen induction. Following APC deletion, cell migration along the crypt-villus axis is attenuated (Sansom et al., 2004), allowing the formation of tumours *in situ*. Hence factors that affect these pathways could increase or decrease the rate of tumourigenesis. To confirm an increased rate of tumour initiation, I induced *VillinCre^{ER} Apc$^{fl/+}$* and *VillinCre^{ER} Apc$^{fl/+}$ Bcl9$^{fl/fl}$Bcl9l$^{fl/fl}$* mice and then sampled the mice 50-days post-induction and scored the number of macroscopic and microscopic lesions. As with mice sampled at end-point; there was a significant increase in the number of both macroscopic and microscopic tumours following BCL9/9l deletion (Fig3.18b and Fig3.18c). I also scored the number of ß-catenin positive lesions – there was a significant increase in the total number of ß-catenin positive intestinal lesions in the *VillinCre^{ER} Apc$^{fl/+}$ Bcl9$^{fl/fl}$ Bcl9l$^{fl/fl}$* mice compared with control mice, particularly within the proximal region of the small intestine (Fig3.18d). A simple explanation for the increase in tumour number is that deletion of BCL9/9l results in DNA damage, either directly or due to an inhibition of the DNA damage repair pathway, resulting in increased tumour initiation. γ-H2AX staining of normal tissue from WT and *VillinCre^{ER} Bcl9$^{fl/fl}$ Bcl9l$^{fl/fl}$* mice, as well as the tumours from *VillinCre^{ER} Apc$^{fl/+}$* and *VillinCre^{ER} Apc$^{fl/+}$ Bcl9$^{fl/fl}$ Bcl9l$^{fl/fl}$* mice sampled 50-days post-induction, revealed that there was no increase in DNA damage following BCL9/9l deletion (Fig3.19). It should be noted that there have been no previous reports linking BCL9 and BCL9l to DNA damage.

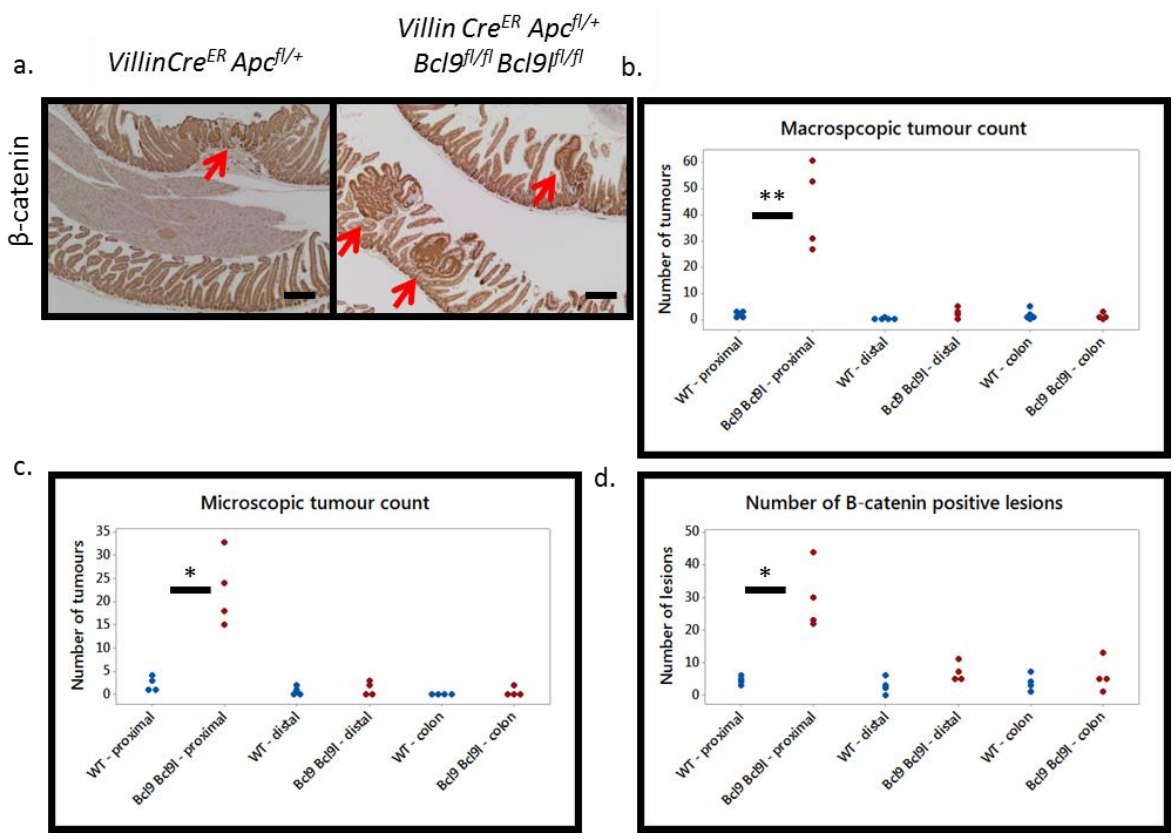

Figure 3.18: Increased tumour initiation following deletion of BCL9 and BCL9l

a. Representative ß-catenin staining of intestinal tumours from *VillinCre^{ER} Apc$^{fl/+}$* and *VillinCre^{ER} Apc$^{fl/+}$ Bcl9$^{fl/fl}$ Bcl9l$^{fl/fl}$* mice sampled 50-days post-induction, red arrows indicate tumours, scale bar = 300μm. b. Macroscopic tumour c. Microscopic tumours and d. Number of ß-catenin positive lesions counts within the intestine and colons of *VillinCre^{ER} Apc$^{fl/+}$* (WT) and *VillinCre^{ER} Apc$^{fl/+}$ Bcl9$^{fl/fl}$ Bcl9l$^{fl/fl}$* (Bcl9 Bcl9l) mice sampled 50-days post-induction, n=4-5 per group, one-way Mann-Whitney *U* test, ** p=0.01 (macroscopic proximal tumours) and * p=0.0152 (microscopic proximal tumours and proximal ß-catenin lesions).

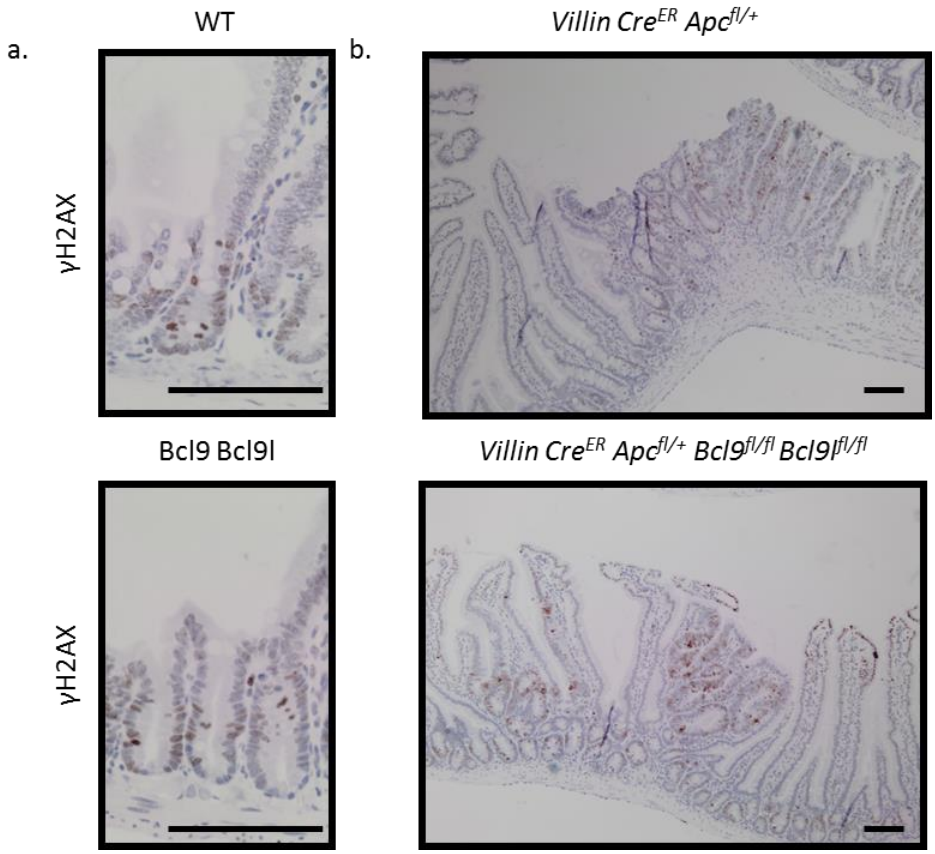

Figure 3.19: Deletion of BCL9 and BCL9l does not increase DNA damage
Representative of γH2AX staining of a. intestines from WT and *VillinCre^{ER} Bcl9$^{fl/fl}$ Bcl9l$^{fl/fl}$* (Bcl9 Bcl9l) mice sampled 4-days post-induction. b. tumours from *VillinCre^{ER} Apc$^{fl/+}$* and *VillinCre^{ER} Apc$^{fl/+}$ Bcl9$^{fl/fl}$ Bcl9l$^{fl/fl}$* sampled 50-days post-induction. Scale bars = 100μm.

Another hypothesis to explain increased lesion formation is there could be increased retention of APC-deficient cells. This could occur by two mechanisms 1) when BCL9/9l is deleted cells migrate more slowly up the crypt-villus axis, so if there is a LOH event, then APC-deficient cells are more likely to persist to form lesions. 2) The reduced number of *Lgr5*-positive stem cells following BCL9/9l deletion means there is less intestinal stem cell (ISC) competition. As a result APC-deficient cells (even after BCL9/9l loss) are more likely to replace neighbouring stem cells; producing monoclonal crypts and increasing tumour initiation.

An abrogation in migration could be supported by the morphology of the tumours I observe in these mice following Bcl9/9l deletion. Many of the intestinal tumours in *VillinCre^{ER} Apc$^{fl/+}$ Bcl9$^{fl/fl}$ Bcl9l$^{fl/fl}$* mice exhibit a 'top-down' morphology, suggesting that these tumours originally formed outside of the crypt, whilst adenomas in *VillinCre^{ER} Apc$^{fl/+}$* mice tend to exhibit a bottom-up architecture, likely arising from the crypts (Fig 3.20a).The original model for top-down tumour formation implicated high Wnt- and MAPK-signalling to initiate dedifferentiation (Schwitalla et al., 2013). Given that I have shown that BCL9

and BCL9l deletion reduces the expression of a number of Wnt target genes, but also impairs the dedifferentiation of APC KRAS villi, then the formation of these tumours could be due to perturbed migration rather than dedifferentiation.

To investigate whether deletion of BCL9/9l perturbs cell migration along the crypt-villus axis, I performed BrdU pulse-chase experiments. WT and *VillinCre^{ER} Bcl9$^{fl/fl}$ Bcl9l$^{fl/fl}$* mice were induced with tamoxifen, four days post-induction injected with BrdU, to label proliferating cells, and then sampled 2- or 48-hours later (Fig3.20b). After 2 hours BrdU injection, the labelled cells are located at the base of the crypt, as expected, however at a 48-hour time-point the labelled cells have migrated into the villi (Fig3.20c). Scoring of the cumulative distribution of BrdU positive cells at a 2-hour and 48-hour time point revealed that deletion of BCL9/9l did not significantly perturb migration along the crypt-villus axis at a 48 hour time-point (Fig3.20c). It would be interesting to determine whether deletion of BCL9/9l following Apc loss had any effect on migration too, particularly given that E-cadherin is downregulated at the transcriptional level, which may lead to perturbed migration.

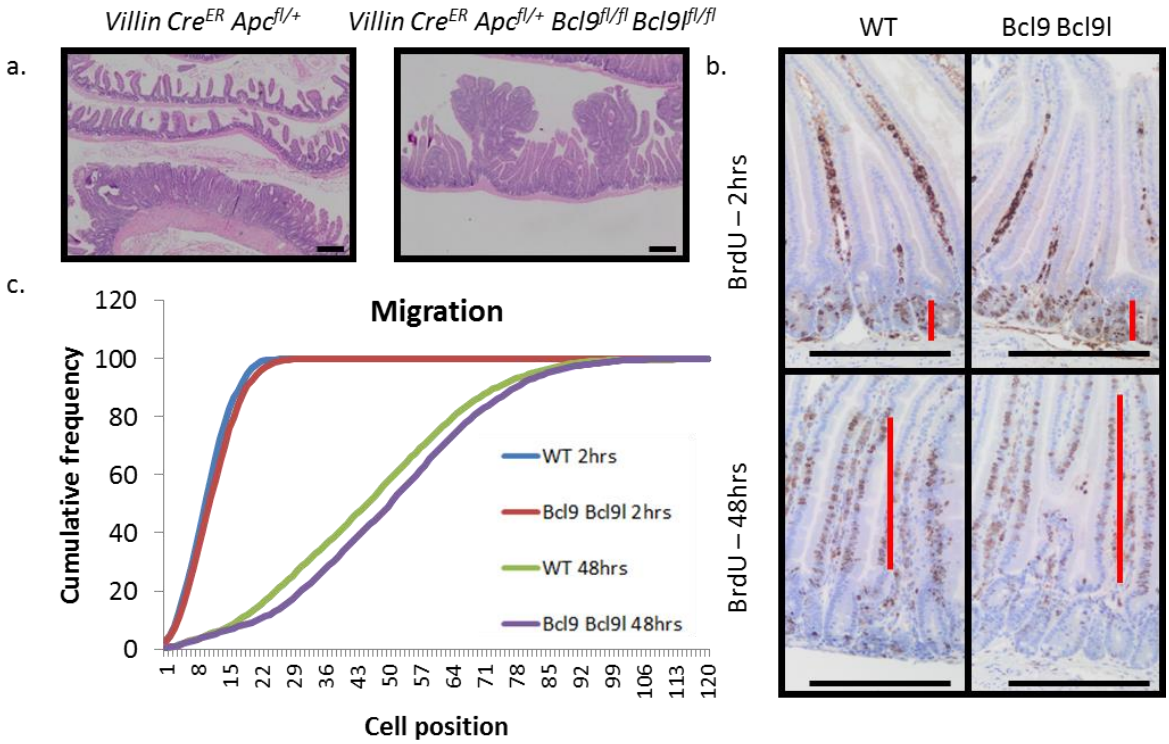

Figure 3.20: BCL9 and BCL9l deletion does not perturb migration along the crypt-villus axis

a. H&E staining of small intestinal tumours from *VillinCre*^{ER} *Apc*$^{fl/+}$ and *VillinCre*^{ER} *Apc*$^{fl/+}$ *Bcl9*$^{fl/fl}$ *Bcl9l*$^{fl/fl}$ mice sampled at clinical end-point. b. BrdU staining of small intestines from WT and *Villin Cre*^{ER} *Bcl9*$^{fl/fl}$ *Bcl9l*$^{fl/fl}$ (Bcl9 Bcl9l) mice – injected with BrdU 2 or 48 hours prior to sampling, red bars indicate BrdU-positive zone, scale bars =200μm c. Cumulative frequency of BrdU-positive cells along the crypt-villus axis of WT and *VillinCre*^{ER} *Bcl9*$^{fl/fl}$ *Bcl9l*$^{fl/fl}$ (Bcl9 Bcl9l) at a 2 hour and 48 hour time-point post BrdU injection. At least 25 half-crypts scored per mouse, n=2 for 2 hours, n=3 for 48 hours. One-way Mann-Whitney *U* test, p=0.1376, looking at the cell position at 50% cumulative frequency at the 48 hour time point.

3.2.10 BCL9 and BCL9l deletion reduces intestinal stem cell clonal potential

It has previously been reported that ISCs are the cells of origin of colorectal cancer (Barker et al., 2009), but also intestinal stem cell dynamics can play a key role in the early stages of tumour formation (Vermeulen et al., 2013). Intestinal stem cells exhibit 'neutral drift' dynamics, such that they exist as an equipotent population and that their replacement by neighbours or clonal expansion is random (Lopez-Garcia et al., 2010). However, it has also been shown that factors that contribute to 'clonal fitness' such as particular mutations, including *Kras* activation and *Apc* mutations can confer a clonal advantage, and an increased probability for a clone to repopulate a crypt (Vermeulen et al., 2013).

I have shown that BCL9/9l are required for the expression of a subset of Wnt target genes, as well as the intestinal stem cell marker, *Lgr5*, in the mouse intestinal epithelium, whilst it has also been shown that Bcl9 and Bcl9l are required for 'stemness' maintenance and tumourigenicity in APC KRAS crypt cultures (Moor et al., 2015). These observations might suggest that ISCs lacking BCL9/9l may have a clonal disadvantage compared with WT ISCs. To investigate this, I generated *Lgr5-EGFP-Cre^{ER} TdTom$^{fl/fl}$ Bcl9$^{fl/fl}$ Bcl9l$^{fl/fl}$* mice and induced them with a very low level of tamoxifen, so as to recombine in a single intestinal stem cell per crypt and then aged the mice to various time points to assess the ability of these BCL9/9l-null clones to populate the crypt. Scoring of average clone size (% of crypt Tomato positive) at various time-points revealed that intestinal stem cells lacking BCL9/9l have a reduced clone size, and that there are more partially fixed crypts compared to WT crypts (Fig3.21b and 3.21c).

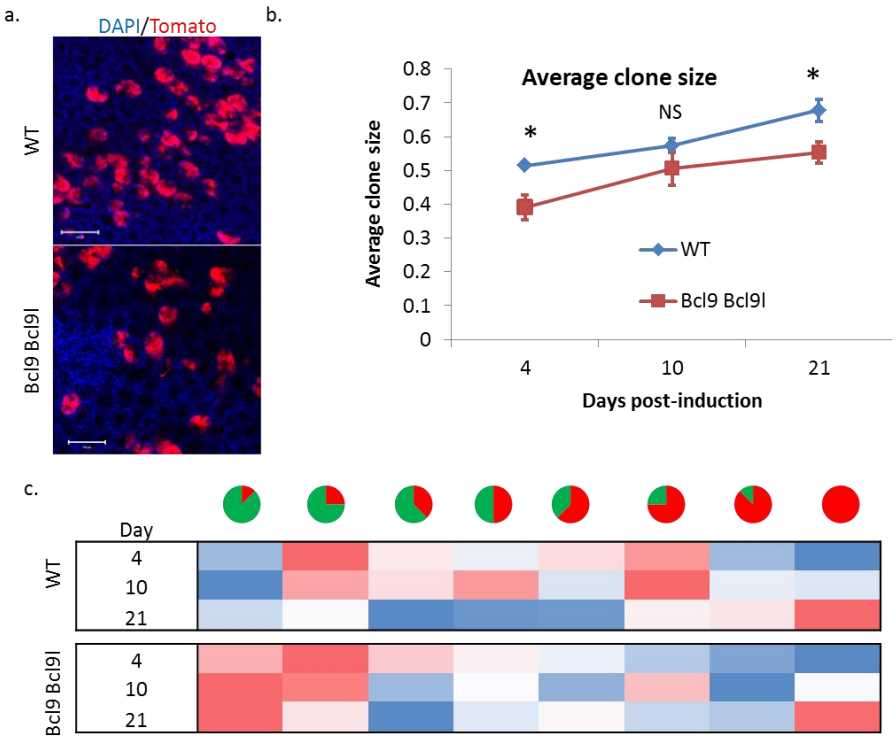

Figure 3.21: Deletion of Bcl9 and Bcl9l reduces stem cell fitness

a. Representative images of crypts from *Lgr5-EGFP-Cre^{ER} tdTom$^{fl/+}$* (WT) and *Lgr5-EGFP-Cre^{ER} Bcl9$^{fl/fl}$ Bcl9$^{fl/fl}$* (Bcl9 Bcl9l) mice injected with 0.15mg tamoxifen and sampled 10-days later, blue = DAPI (nuclei), red = tomato, scale bar = 100µm. b. Average clone size from *Lgr5-EGFP-Cre^{ER} tdTom$^{fl/+}$* (WT) and *Lgr5-EGFP-Cre^{ER} Bcl9$^{fl/fl}$ Bcl9$^{fl/fl}$* (Bcl9 Bcl9l) mice injected with 0.15mg tamoxifen and sampled 4, 10 and 21 days post-induction, data displayed +/- SEM, n=3, One way Mann-Whitney *U* test, p=0.0405 (*). c. Heat map for % distribution of clone size from *Lgr5-EGFP-Cre^{ER} tdTom$^{fl/+}$* (WT) and *Lgr5-EGFP-Cre^{ER} Bcl9$^{fl/fl}$ Bcl9$^{fl/fl}$* (Bcl9 Bcl9l) mice injected with 0.15mg tamoxifen and sampled 4, 10 and 21-days later

This result would be in agreement with the findings of Vermeulen and colleagues, however it may also serve to provide an explanation for the increased rate of tumourigenesis I observe in *VillinCre^{ER} Apc$^{fl/+}$ Bcl9$^{fl/fl}$ Bcl9l$^{fl/fl}$* and *VillinCre^{ER} Apcfl$^{/+}$ Kras$^{G12D/+}$ Bcl9$^{fl/fl}$ Bcl9l$^{fl/fl}$*. Since if BCL9 and BCL9l control the size of the ISC pool through regulation of *Lgr5* expression, then even though BCL9/9l-deficient clones have a clonal disadvantage, a reduced stem cell pool would reduce intestinal stem cell competition – leading to a faster rate of crypt fixation, tumour initiation and increased tumour number.

3.3 Discussion

In this chapter I have shown that deletion of BCL9 and BCL9l does not affect normal intestinal homeostasis, confirming previous reports (Deka et al., 2010). However, when the intestinal epithelium is challenged via irradiation or inhibition of Wnt ligand secretion, there is a dependency of the intestinal epithelium upon BCL9/9l for regeneration and growth. These phenotypes could be due to the requirement of BCL9/9l for the expression of a subset of Wnt target genes, including the intestinal stem cell marker *Lgr5*. This is in agreement with the notion that BCL9l may act as a specific modulator of Wnt signalling rather than a general component of the pathway (Brembeck et al., 2004). The reduced expression could in part be explained in part by the increase in the amount of ß-catenin present at the cell junctions, bound to E-cadherin, and hence a threshold level of nuclear ß-catenin may be required for the transcription of these Wnt target genes, since the cells at the base of the intestinal crypts from *VillinCre^{ER} Bcl9$^{fl/fl}$ Bcl9l$^{fl/fl}$* mice were positive for nuclear ß-catenin .This highlights the implicated role of BCL9 and BCL9l in the shuttling of ß-catenin into the nucleus (Adachi et al., 2004).

Interestingly when the cytoplasmic pool of ß-catenin is released following deletion of APC, thereby ablating the destruction complex, there was still a reduction in the expression of a subset Wnt target genes, suggesting that BCL9 and BCL9l play a functional role within the ß-catenin transcription complex. It has recently been shown that BCL9 is critical component of the Wnt-enhanceosome, acting as a scaffold for its' assembly (Tienen et al., 2017). In agreement with the potential role of BCL9 and BLC9l in colorectal cancer, deletion of BCL9/9l following acute loss of APC and KRAS activation significantly

reduced proliferation. Furthermore, I showed that BCL9 and BCL9l are required for the dedifferentiation of villi from APC KRAS mice, which may in part due to a reduction in expression of Wnt target genes. These results identify BCL9 and BCL9l as potential therapeutic targets in colorectal cancer, where Wnt signalling is hyperactivated and *KRAS* frequently mutated.

When assessing whether BCL9/9l deletion could suppress intestinal tumourigenesis, I observed a very surprising result; whereby deletion of these two proteins significantly increased tumour burden and reduced tumour latency compared with control mice, regardless of *Kras* mutation status. Deletion of BCL9/9l profoundly increased the number of tumours that developed in the proximal small intestine, compared with control mice. The tumours that did form, were not escapers, but also had reduced *Lgr5* expression; despite tumour cells accumulating nuclear ß-catenin, confirming that BCL9 and BCL9l are required for *Lgr5* transcription. The increased tumourigenesis was independent of DNA damage and cellular migration along the crypt-villus axis. However, the increased tumourigenesis following deletion of BCL9/9l could be due to alterations in intestinal stem cell dynamics.

I have shown that loss of BCL9/9l confers a clonal disadvantage, presumably due to the reduced Wnt signalling within these cells, and therefore there is a greater probability of these BCL9/9l-deficient stem cells being replaced by their WT neighbours. Importantly, however in the tumour models, *VillinCre*^{ER} recombines throughout the entire intestinal epithelium, and therefore all cells should be deficient for BCL9/9l, thus reduced clonal fitness should not be a factor. However, the RNASeq data suggests that the deletion of BCL9 and BCL9l could reduce the ISC pool, given the downregulation of *Lgr5* amongst other Wnt target genes. Hence, in this setting there could be reduced stem cell competition altogether, which would allow for an increased rate of clonal fixation (Fig3.22), increasing the rate of tumour formation. For instance, Vermeulen and colleagues showed that on average, 4.3 mutational hits in *Apc* are required for APC-deficient clones to repopulate crypts, due to ISC competition (Vermeulen et al., 2013), in situations where you have fewer stem cells the required number of hits could be dramatically reduced.

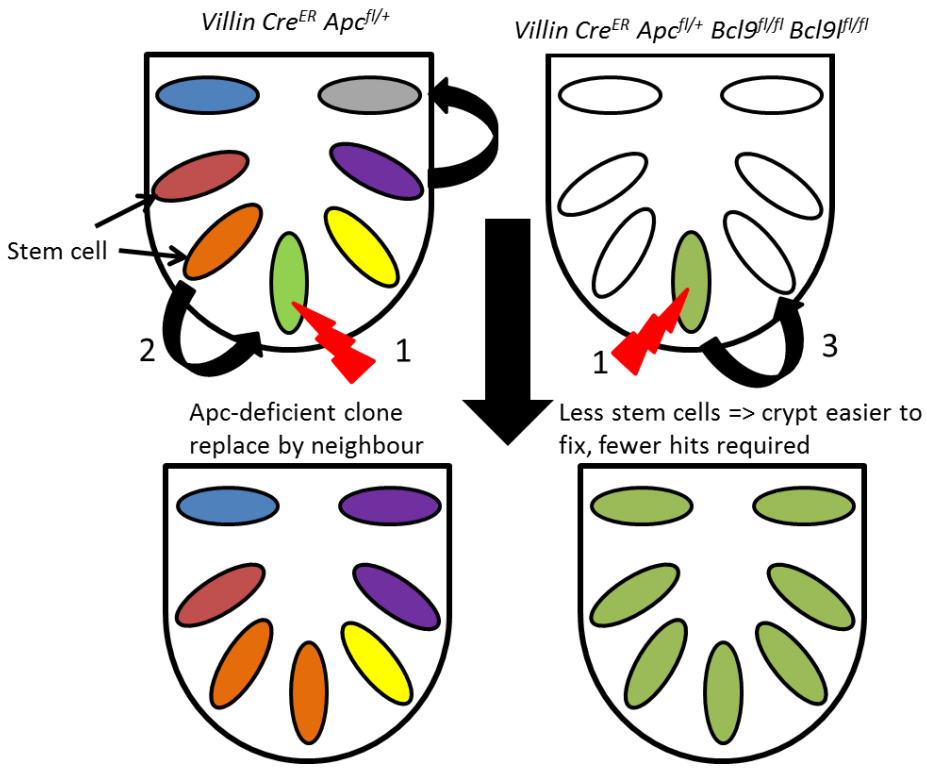

Figure 3.22: Proposed model of ISC dynamics following BCL9 and BCL9l deletion
Schematic representation of intestinal stem cells (ovals) within crypts following deletion of Bcl9/9l: 1. Second hit in *Apc* in stem cell of crypt from *VillinCre*^{ER} *Apc*$^{fl/+}$ (left) and *VillinCre*^{ER} *Apc*$^{fl/+}$ *Bcl9*$^{fl/fl}$ *Bcl9l*$^{fl/fl}$ (right) mice 2. The APC-deficient stem cell (green) is replaced by its neighbour (orange), hence additional 'hits' are required in *Apc* for crypt fixation and tumour formation. 3. The APC-deficient stem cell has reduced stem cell competition following BCL9/9l deletion; due to a reduction in *Lgr5*-expression therefore it is not replaced by its neighbour, resulting in a monoclonal crypt and increased tumour initiation.

We have also shown that lowering Wnt signalling could also accelerate tumour formation. Treatment of *Lgr5Cre*^{ER} *Apc*$^{fl/fl}$ and *Apc*$^{Min/+}$ mice with LGK974 significantly reduced tumour latency compared with vehicle controls (David Huels – personal communication). Additionally, in the *Lgr5Cre*^{ER} *Apc*$^{fl/fl}$ mice treated with LGK974 there was a profound increase in tumour formation in the proximal small intestine compared with vehicle controls. LGK974 treatment also reduces the expression of a number of stem cell markers in WT mice, including *Lgr5* and *Olfm4*, and this treatment reduced crypt fixation time. This data suggests that Wnt ligands can influence tumour initiation by controlling the number of stem cells, but also the level of Wnt signalling could potentially play a role in the location of tumour formation along the small intestine. An analogous situation could be in operation following deletion of BCL9 and BCL9l in the intestine, whereby there is reduced stem cell competition allowing for faster crypt fixation and increased tumour formation. It is important to note that mice

developed more intestinal tumours in a carcinogenesis tumour model following deletion of BCL9 and BCL9l (Deka et al., 2010).

These results raise important considerations for the application and development of BCL9 and BLC9l inhibitors in the clinic. For instance, lowering Wnt signalling may not be suitable as a chemopreventive strategy for FAP patients, since it may predispose them to further tumour formation. However, I have shown that targeting Wnt signalling at the transcriptional level in transformed epithelial cells with high Wnt- and MAPK-pathway activity can reduce proliferation, revealing a potential therapeutic opportunity for treatment of established tumours.

Chapter 4: Identification of a nutrient stress signature in APC KRAS crypts

4.1 Introduction

In the previous chapter I described how targeting Wnt signalling, which is significantly deregulated in colorectal cancer, via deletion of BCL and BCL9l, is able to partially suppress the APC KRAS phenotype following acute deletion of APC in the murine intestine. However, this did not translate into an extension in survival in an ageing model of tumourigenesis, whereby deletion of BCL9 and BCL9l significantly increased tumour burden and reduced tumour latency compared with control mice. Hence, I will now discuss the use of unbiased approaches to identify additional rewiring events in *Kras*-mutant APC-deficient intestinal epithelial cells; that could drive resistance to established therapies, to try and identify novel therapeutic targets. In this chapter I will focus on the use of proteomics, whilst also referring to the lab's RNASeq dataset – performed by David Vincent – to investigate global changes in gene expression between APC and APC KRAS intestinal epithelial cells.

4.1.1 Stable Isotope Labelling by Amino acid in Cell culture (SILAC)

Proteomics, the large scale study of the protein content of cells or tissue was traditionally performed on two-dimensional (2D) electrophoresis gels (O'Farrell, 1975). In this instance, quantitation was based on the alteration in the staining patterns of the proteins isolated from two or more tissues or cell populations (Zhou et al., 2002). However, in recent years mass spectrometry has been applied for the identification of proteins, initially for peptide sequencing (Shevchenko et al., 1997). These sequencing experiments relied upon the incorporation of ^{18}O to the c-terminus of the peptides following enzymatic digestion, resulting in a 2 mass unit shift, allowing easier identification of the peptides within the spectra (Shevchenko et al., 1997). Ong and colleagues used this principle to develop Stable Isotope Labelling by Amino acids (SILAC) to look at changes in the proteomes of differentiating myotubes (Ong et al., 2002).

SILAC relies on the incorporation of stable-isotope (^{13}C or ^{15}N) containing essential amino acids, such as Lys-8 ($^{13}C_6{}^{15}N_2$) or Arg-10 ($^{13}C_6{}^{15}N_4$), into the proteomes of a cell population (Zanivan et al., 2013). Two cell populations can be differentially labelled using 'heavy'- or 'light'-labelled amino acids. Importantly, these labelled amino acids do not affect the growth or morphology

of these cells (Ong et al., 2002). Once, labelled the two samples are collected, lysed and mixed together in a 1:1 ratio and analyzed via Mass Spectrometry, identifying peptides within the analyte. The peptides from the differentially labelled cell-populations are separated by a residue specific mass according to the number of heavy- or light-labelled amino acid residues; identifying individual signals from either cell population. Thus, the ratio of signal intensities from light and heavy labelled samples allows for the quantitative comparison of the proteome of two differentially labelled cell populations (Ong & Mann, 2006).

4.1.2 Targeting the eIF2α-signalling axis

The eIF2 complex is a critical component of the translation initiation machinery, recruiting the initiator-methionine tRNA to the 40S ribosomal subunit, in a GTP-dependent manner. eIF2 is activated by its GEF, eIF2B5. Phosphorylation of eIF2's α subunit at serine 51 leads to a reduction in global protein synthesis (Farrell et al., 1977). This phosphorylation event is in response to a variety of stresses, including uncharged tRNAs and ER stress. The downstream signalling after eIF2α-phosphorylation serves to induce a transcriptional programme, induced by ATF4 that alleviates the stress, or can lead to apoptosis. There are a number of recent studies that have highlighted the potential therapeutic window that could be afforded by targeting this pathway in colorectal cancer. For instance, transcriptional profiling of $Lgr5^{high}$ vs $Lgr5^{low}$ cells isolated from *Lgr5-eGFP* mice revealed that intestinal stem cells have very low expression of components of the ER stress pathway, compared with transit-amplifying cells (Heijmans et al., 2013). Furthermore it has been shown that by blocking eIF2α dephosphorylation in WT intestinal organoids, using Salubrinal – a GADD34 (eIF2α phosphatase) inhibitor (Boyce et al., 2005), leads to a reduction in the expression of a number of stem cell markers, such as *Lgr5* and *Olfm4* (Heijmans et al., 2013). Indeed, the authors went on to show that ER stress serves to regulates intestinal stemness, such that induction of ER stress results in a loss of stem cells *in vivo* and can be exploited for therapeutic benefit – combinatorial treatment of a xenograft model showed a strong synergy between Salubrinal and oxaliplatin (a standard of care drug for colorectal cancer) (Wielenga et al., 2015). Furthermore, deletion of GRP78 throughout the mouse intestine and colon suppresses the APC-crypt progenitor phenotype (van

Lidth de Jeude et al., 2016). These studies highlight the therapeutic window offered by targeting ER stress in colorectal cancer.

A number of PERK inhibitors have been developed recently and these show anti-cancer properties. For instance, GSK2656157 has been shown to reduce the growth of a number of human cell line xenografts (Atkins et al., 2013). However, this study revealed that two weeks of treatment with GSK2656157 lead to severe atrophy of acinar cells and degeneration of islet cells within the pancreata of these mice (Atkins et al., 2013), a similar observation has also seen in rats treated with GSK2656157. Hence further development of PERK inhibitors for humans must consider potential effects on the exocrine and endocrine functions of the pancreas. Recently, a novel screen for PERK inhibitors identified a small molecule, ISRIB (Integrated Stress Response Inhibitor) that potently reverses the effects of eIF2α phosphorylation (Sidrauski et al., 2013). ISRIB treatment was able to increase protein synthesis in cells subjected to ER stress, whilst also reducing ATF4 expression at the protein level (Sidrauski et al., 2013). Furthermore, this chronic ISRIB treatment was able to extend survival in a mouse model of Prion disease, without affecting pancreas function (Halliday et al., 2015) – making this a suitable drug to take forward into ageing studies. More recently ISRIB has been shown to synergise with gemcitabine in an orthotopic model of pancreatic cancer (Palam et al., 2015). In this chapter I will discuss the molecular implications of the use of ISRIB both *in vivo* and *in vitro*, in an attempt to target eIF2α-Atf4 signalling in colorectal cancer.

4.2 Results

4.2.1 *Kras* mutation alters the translational profile of Apc-deficient intestinal epithelial cells

To identify potential novel therapeutic targets in Apc-deficient Kras-mutant intestinal crypts I took an unbiased approach and performed SILAC on small intestinal crypts isolated from *VillinCre*^{ER} *Apc*$^{fl/fl}$ (APC) and *VillinCre*^{ER} *Apc*$^{fl/fl}$ *Kras*$^{G12D/+}$ (APC KRAS) mice, carrying out forward and reverse labelling (Fig4.1). Approximately 5000 proteins were identified, of which just under 1000 were differentially expressed between the two populations, the statistical threshold for this was a ratio >1.4 or <0.7 in both the forward and reverse labelled samples. I took these differentially expressed proteins and analysed

them with Ingenuity Pathway Analysis software (QIAGEN) to look at the top pathways and transcription factors predicted to be upregulated in APC KRAS cultures and APC cultures (Fig4.2). Interestingly, some of the top upregulated pathways were involved in protein synthesis, such as: eIF2 signalling and regulation of eIF4 and p70S6K signalling (Fig4.2).

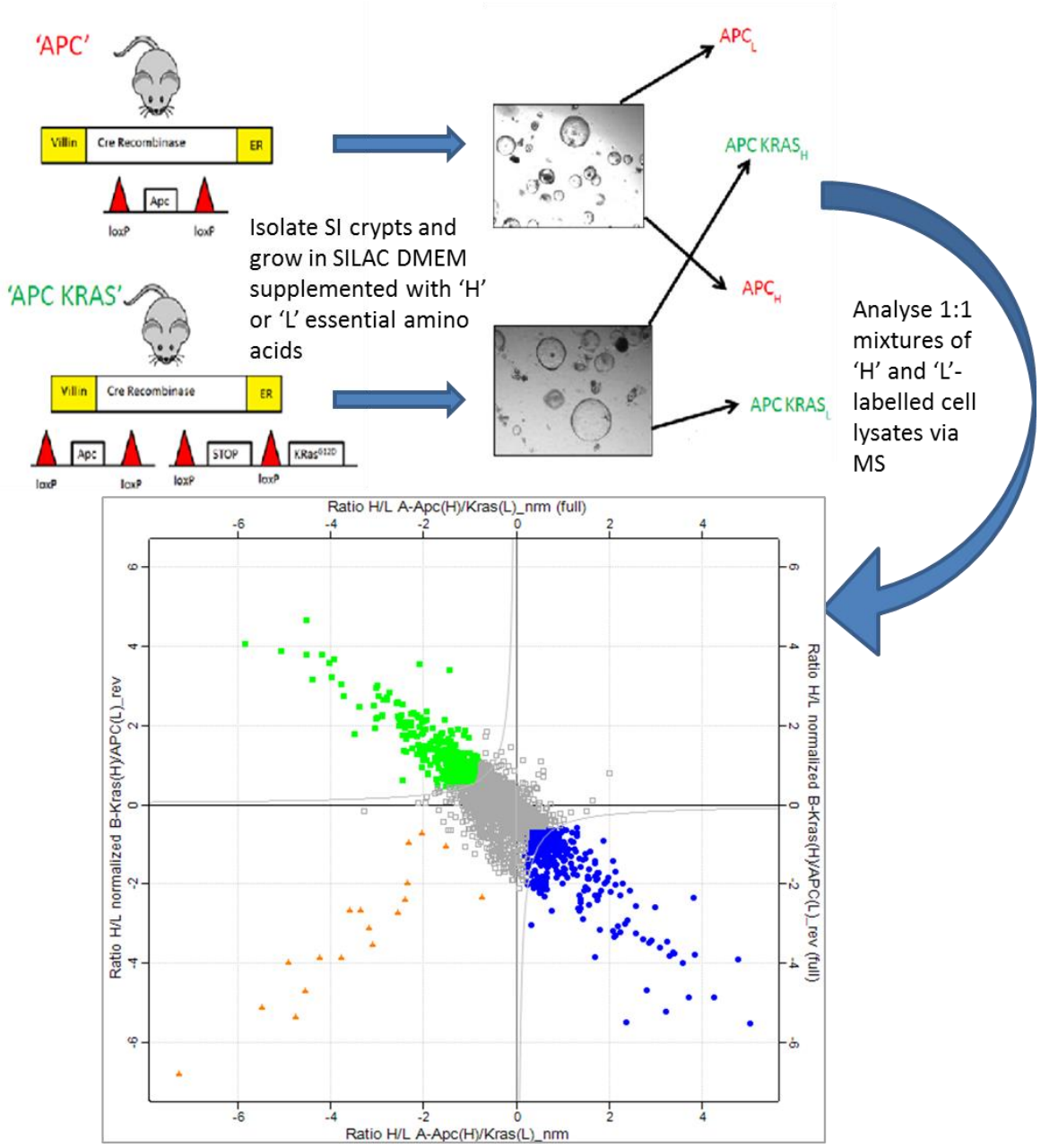

Figure 4.1: SILAC work flow

Small intestinal crypts were isolated from *VillinCre*^{ER} *Apc*$^{fl/fl}$ (APC) and *VillinCre*^{ER} *Apc*$^{fl/fl}$ *Kras*$^{G12D/+}$ (APC KRAS) mice and propagated in culture. Crypt cultures were both heavy- and light-labelled using Arg-10, Lys-8 or Arg-0 and Lys-0. After sufficient labelling, crypt cultures harvested, lysed and mixed in a 1:1 ratio of H/L samples and analysed via mass spectrometry. Scatterplot represents detected proteins – grey = no change in expression, green = upregulated in APC KRAS vs APC, blue = downregulated in APC KRAS v APC and orange = contaminants such as Matrigel components.

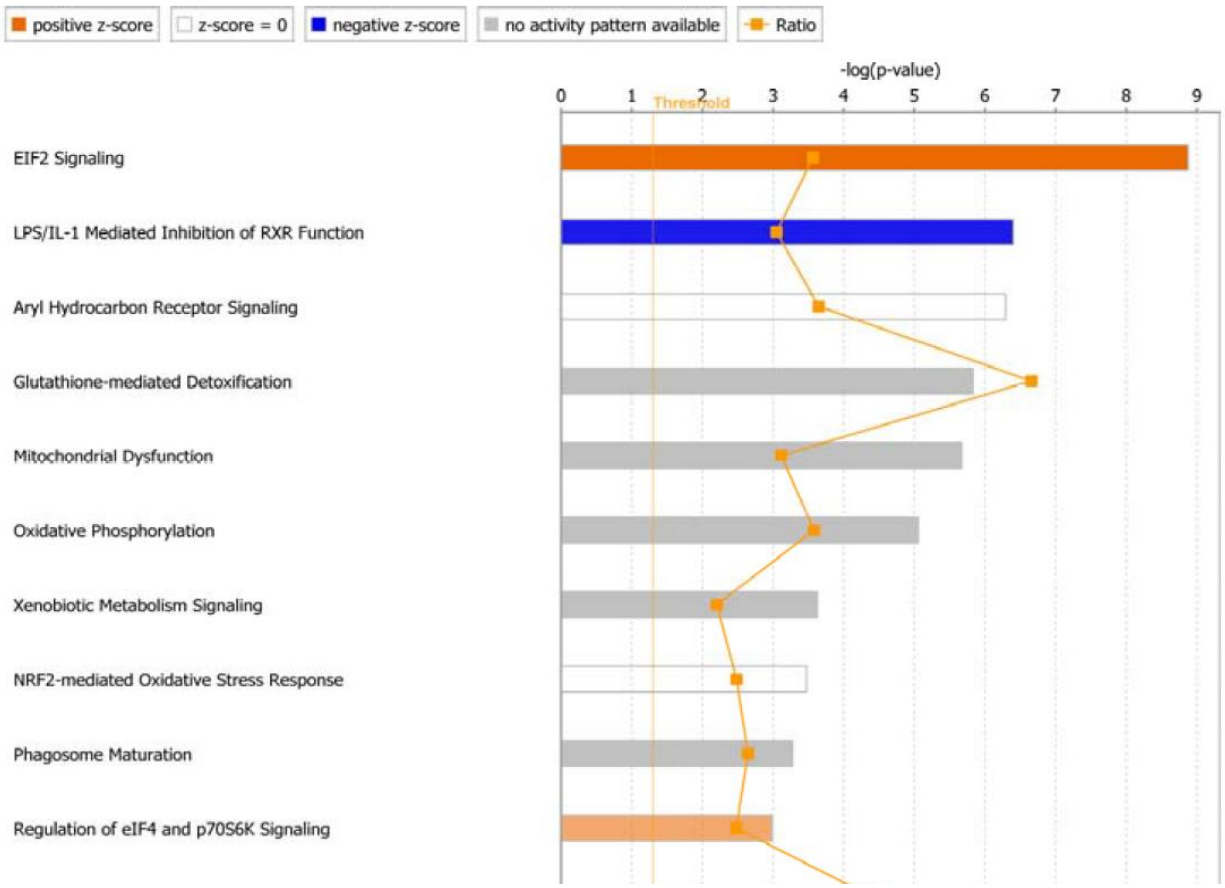

Figure 4.2: Top deregulated pathways in APC KRAS compared with APC crypt cultures

Differentially expressed proteins from APC and APC KRAS crypt cultures were analysed via Ingenuity Pathway Analysis Software (Qiagen).Bar chart displays top 10 predicted deregulated pathways.

It was confirmed by ^{35}S-methionine incorporation that APC KRAS crypt cultures produce significantly more protein than APC crypt cultures (Fig4.3a). This is not too surprising, given that APC KRAS intestinal epithelial cells proliferate significantly faster than APC intestinal epithelial cells. Hence the increase in protein synthesis could be required to drive this increase in cell growth and division. Polysome profiling also confirmed alterations in the translational profile of APC KRAS epithelial cells – there is a decrease in the sub-polysome: polysome (S: P) ratio in APC KRAS intestinal epithelial cells compared with APC (Fig4.3b). Importantly, it has previously been shown that translation elongation is rate-limiting in APC intestinal epithelial cells and that despite the increase in S: P ratio compared with WT intestinal epithelial cells, the polysomes are elongating very quickly and therefore fail to accumulate on the mRNA (Faller et al., 2015). The increased rates of protein synthesis and decreased S: P ratio in

APC KRAS intestinal epithelial cells compared with APC suggests that there is an increase in the rate of translation initiation in these cells compared with APC.

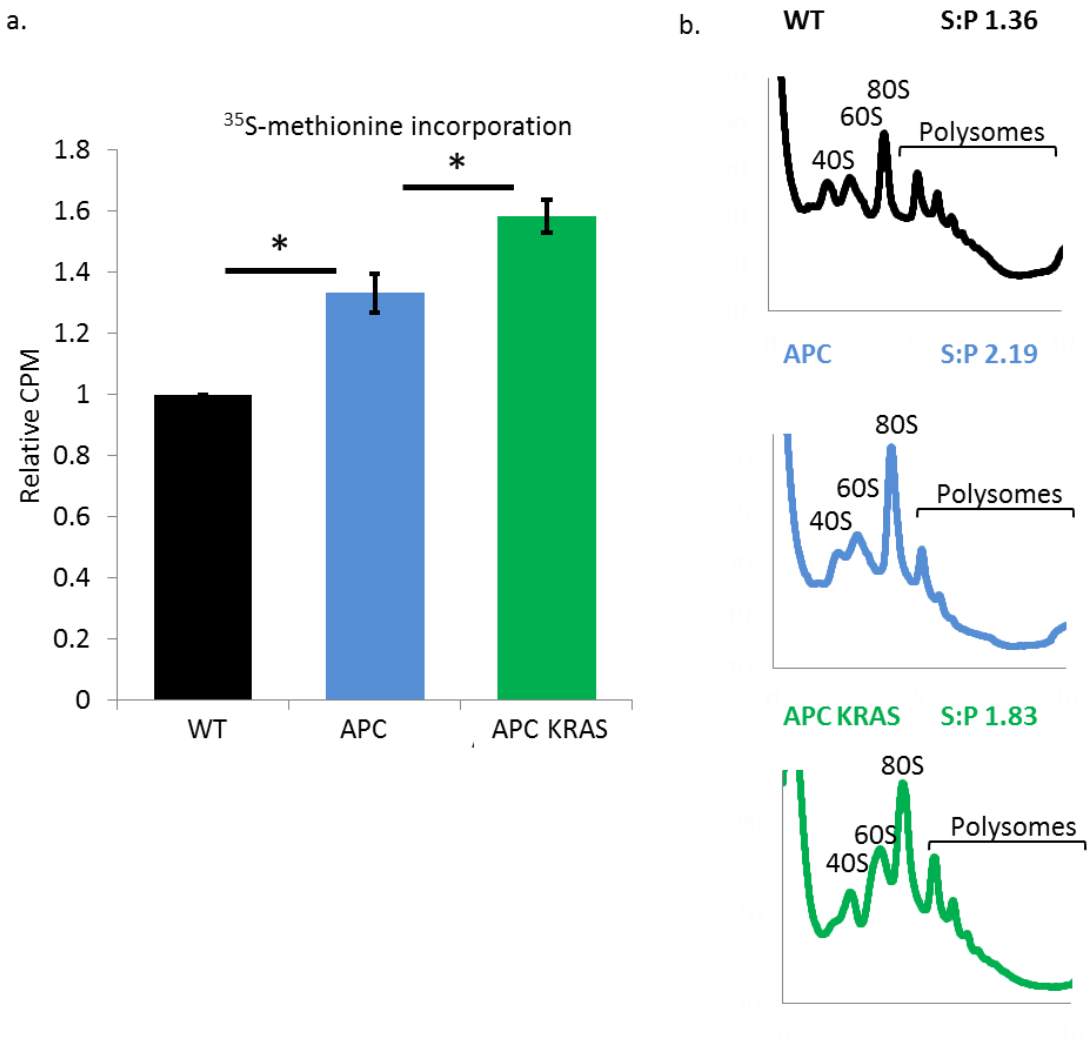

Figure 4.3: *Kras* mutation alter the translational profile of APC-deficient intestinal epithelial cells

a. ^{35}S-methionine incorporation in WT, APC and APC KRAS crypt cultures – cultures were pulsed with ^{35}S-methionine for 30 minutes. Incorporation of ^{35}S into protein was quantified by scintillation and normalized to total protein 3-technical replicates per cell line, 3-different cells lines used for each genotype. One-tailed Mann Whitney test, p=0.05. b. Polysome profiling from WT, APC and APC KRAS small intestines, S: P corresponds to sub-polysome: polysome ratio. (John Knight).

The large increase in protein synthesis in APC KRAS intestinal epithelial cells is accompanied by an increase in the expression of the translation machinery. I observe an increase in the expression of ribosomal biogenesis factors and some tRNA synthetases in the SILAC data (Table 4.1). To further validate this, I also observed a striking trend in the expression of many tRNA synthetases in RNASeq on whole intestinal tissues isolated from WT, APC and APC KRAS mice. Many of the tRNA synthetases are upregulated in APC KRAS intestinal

epithelial cells compared with APC and WT (Fig4.4). tRNA synthetases catalyse the loading of amino acids to their corresponding tRNA. Their expression can be upregulated in response to uncharged tRNAs via the evolutionarily conserved GCN2-eIF2α-ATF4 amino acid starvation response (Harding et al., 2000, D'aniello et al., 2015), this will be discussed in greater detail later. However, these results suggest that APC KRAS intestinal cells are adapting to their increase in protein synthesis by upregulating many components of the translational machinery.

Table 4.1: Fold-change protein expression of ribosome expression factors and tRNA synthetases in APC KRAS vs APC crypt cultures (SILAC data)

Gene	Fold-change	
Nop56	1.39	Ribosome biogenesis factors
Nop14	1.79	
Gar1	1.2	
Rrp9	1.28	
Rrp15	1.82	
Rrp12	1.96	
Pwp2	1.3	
Ddx18	1.75	
Nars	1.98	tRNA synthetases
Gars	1.62	
Wars	1.58	

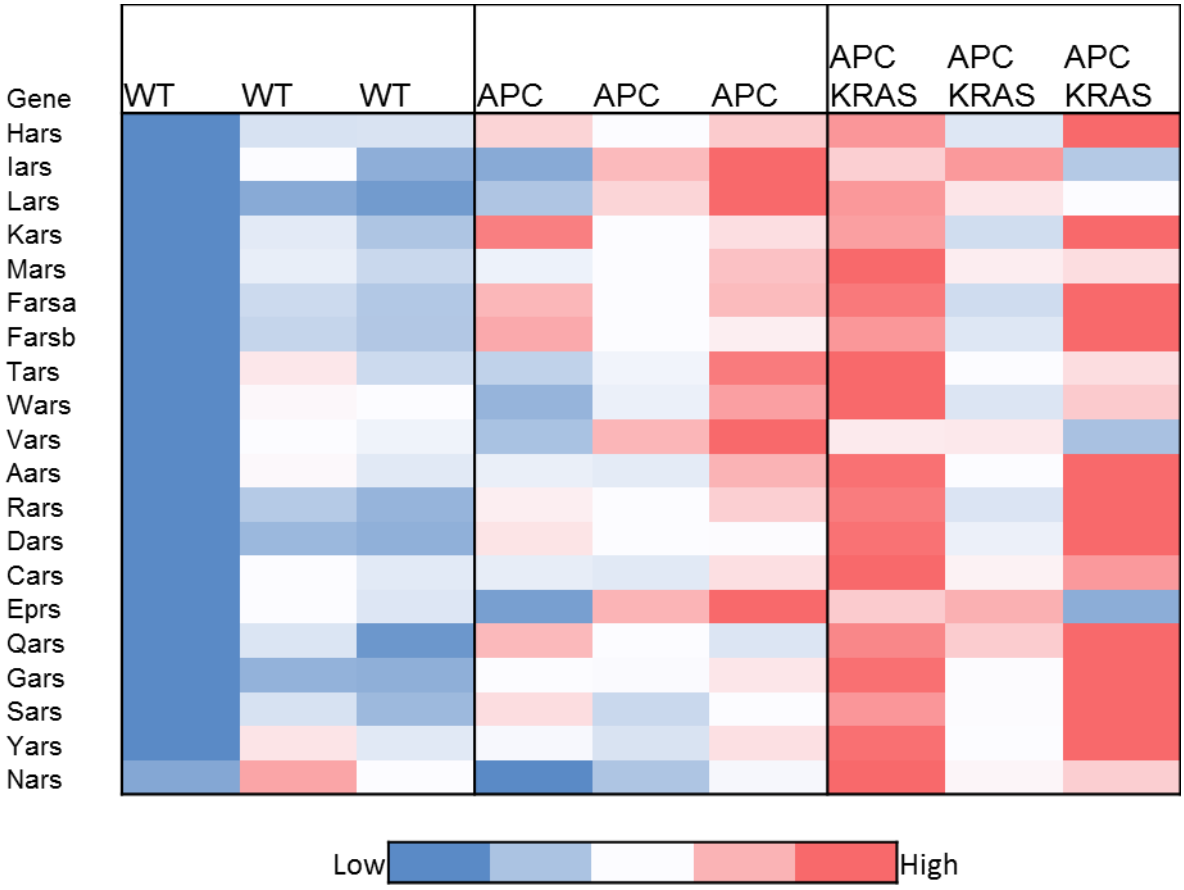

Figure 4.4: Upregulation of tRNA synthetases in APC KRAS small intestines
Heat-map (from RNASeq data) of the expression of tRNA synthetases in the small intestines of tamoxifen-induced WT, *VillinCre*^{ER} *Apc*$^{fl/fl}$ (APC) and *VillinCre*^{ER} *Apc*$^{fl/fl}$ *Kras*$^{G12D/+}$ (APC KRAS) mice. WT and APC mice sampled four days post-induction and APC KRAS mice sampled three days post-induction.

4.2.2 Predicted activation of transcription factors associated with 'nutrient stress'

From the pathway analysis data, a number of the top transcription factors that were predicted to be activated in APC KRAS crypt cultures are involved in response to various cellular stresses, such as ATF4, XBP1 and NUPR1 (Table 4.2). I confirmed upregulation of *Nupr1* in APC KRAS intestines via RNAScope (Fig4.5b). *Nupr1*, *Atf4* and *Xbp1* were all upregulated at the transcriptional level in the RNASeq data; however it is important to note that *Atf4* is regulated at the translational level (Harding et al., 2000), whilst *Xbp1* is regulated via splicing (Calfon et al., 2002). To investigate this I performed western blots on small intestinal tissue isolated (epithelial extraction – crypt fraction) from WT, APC and APC KRAS mice tissue to confirm increased expression of ATF4, and one of its' target genes Asparagine synthetase (ASNS), at the protein level in APC KRAS intestinal epithelial cells (Fig4.5c). Finally, qRT-PCR on whole small intestinal

tissue from APC and APC KRAS mice for the spliced version of *Xbp1*, *Xbp1s*, confirmed its increased activation in APC KRAS intestines (Fig3.5d). XBP1, ATF4 and NUPR1 have all been shown to play a role within the umbrella of the Endoplasmic Reticulum (ER)-stress response and the Unfolded Protein Response (UPR) (Cano et al., 2011; Walter & Ron, 2011). Hence, these results suggest that APC KRAS cells are subjected to cellular stresses that likely arise from the ER and misfolded proteins.

Table 4.2: Predicted activation states of transcription factors in APC KRAS vs APC

Upstream Regulator	Predicted Activation State	Activation z-score	p-value of overlap
TFEB	Inhibited	-3.433	2.9E-08
PPARGC1A	Inhibited	-2.867	0.00929
RB1	Inhibited	-2.295	0.000196
TFAM	Inhibited	-2	0.008
FOXO3	Inhibited	-2.288	0.00973
NFKBIA	Inhibited	-2.602	0.00201
Esrra	Inhibited	-3.5	2.96E-08
NUPR1	Activated	2.043	0.0428
XBP1	Activated	2.825	0.000751
ARNT	Activated	2.064	7.85E-05
KDM5A	Activated	3.86	0.000284
ATF4	Activated	2.777	0.00529
TRIM24	Activated	2.673	3.98E-05
MYCN	Activated	2.466	3.31E-11
MYC	Activated	2.484	1.59E-20

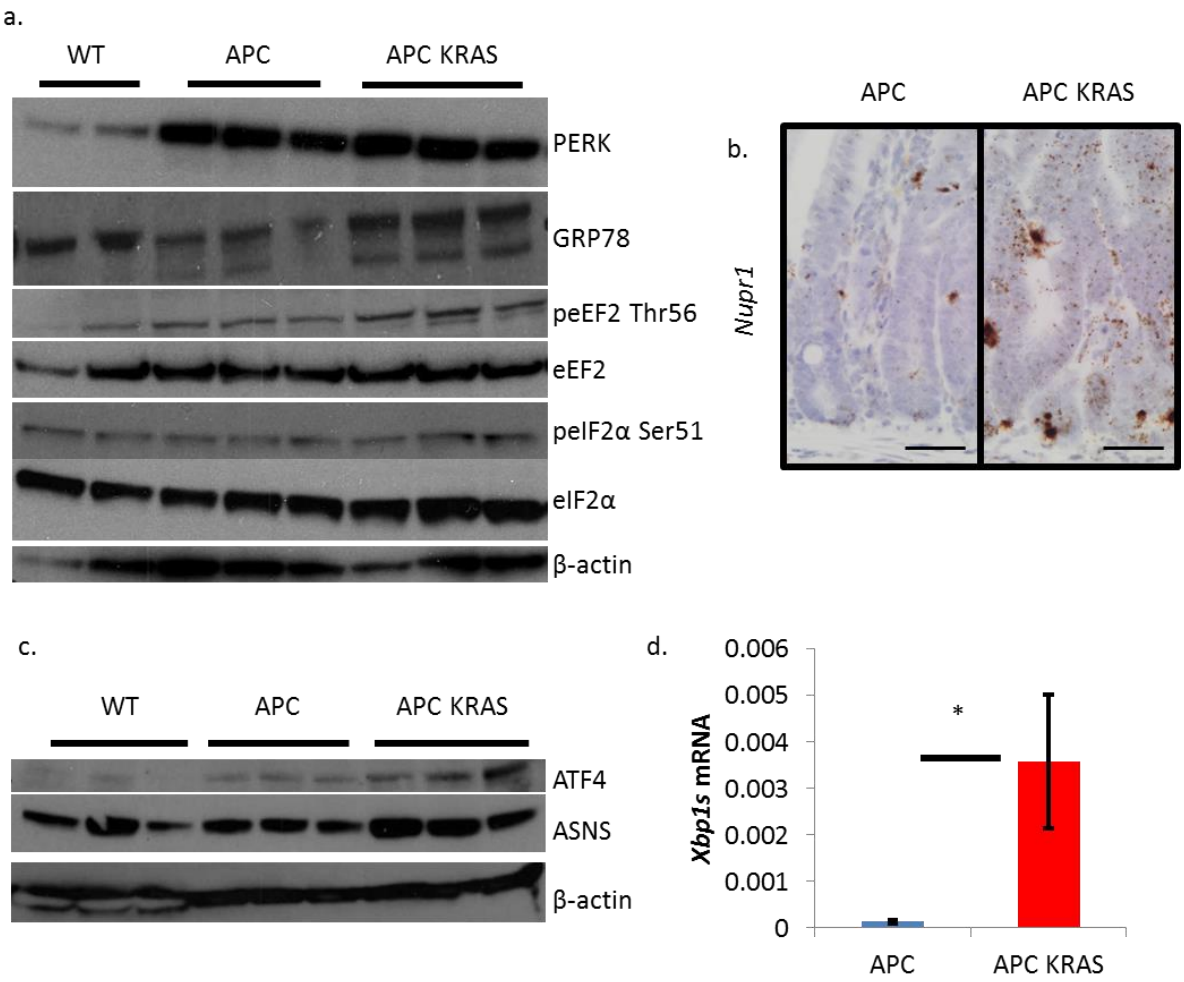

Figure 4.5: Predicted increased activation of transcription factors associated with nutrient stress in APC KRAS intestinal epithelial cells

a. Western blot for PERK, GRP78, phospho-eEF2 (Thr56), eEF2, phospho-eIF2α (Ser51), eIF2α and ß-actin from lysates from WT, APC and APC KRAS intestinal crypt cultures b. *Nupr1*-RNAScopestaining on small intestinal sections from *VillinCre*^{ER} *Apc*$^{fl/fl}$ (APC) and *VillinCre*^{ER} *Apc*$^{fl/fl}$ *Kras*$^{G12D/+}$ (APC KRAS) mice sampled four and three days post-induction respectively, scale bar = 40µm c. Immunoblot for ATF4, ASNS and ß-actin on small intestinal epithelial extractions from WT, APC and APC KRAS mice. d. qRT-PCR for spliced-Xbp1 (Xbp1s) on small intestinal tissue from APC and APC KRAS mice sampled four and three days post-induction, n=3 per group, one-way Mann-Whitney *U* test, p=0.0405.

4.2.3 Increased markers of nutrient stress in APC KRAS

The translation of ATF4 is regulated via upstream reading frames (uORFs), and is upregulated following phosphorylation of eIF2α at serine 51 (Harding et al., 2000, Harding et al., 2003), although a recent study from Brendan Manning has confirmed a noncanonical upregulation of ATF4 via mTORC1 activity (Ben-Sahra et al., 2016). Phosphorylation of eIF2α results in a global reduction in protein synthesis, whilst certain transcripts, including ATF4, are selectively translated. eIF2 signalling was the top pathway predicted to be upregulated in APC KRAS crypt cultures compared with APC cultures, this could be due to the

increased rates of protein synthesis or due to downstream activation of the pathway. It is likely to be the latter, given the increased expression of ATF4 target genes within the SILAC data. Interestingly, immunoblotting revealed an increase in eIF2α phosphorylation and total PERK levels in APC KRAS crypt cultures (Fig4.5a), whilst there was a clear increase in phoso-eIF2α staining in APC KRAS small intestines and colon compared with WT and APC mice (Fig4.6a). Furthermore, intestinal and colonic tumours from both *VillinCre*^{ER} *Apc*$^{fl/+}$ *Kras*$^{G12D/+}$ mice exhibited high levels of phospho-eIF2α compared with the surrounding normal epithelium (Fig4.6a). There was also an increase in phospho-eEF2 (Thr56) both *in vitro* (Fig4.5a) and *in vivo* (Fig4.6b). eEF2 (eukaryotic elongation factor 2) is a translation factor; it is required for translation elongation mediating the GTP dependent translocation of the ribosome. It is negatively regulated by phosphorylation at Thr56 by eEF2K (eukaryotic elongation factor 2 kinase) (Ryazanov et al., 1988). eEF2K has been shown to be critical for the adaption of cells to nutrient deprivation, following activation via AMP-activated protein kinase (AMPK), by blocking translation elongation via phosphorylation of eEF2 (Leprivier et al., 2013). Hence, increased phospho-eEF2 levels indicate a cellular, potentially metabolic, stress in APC KRAS cells.

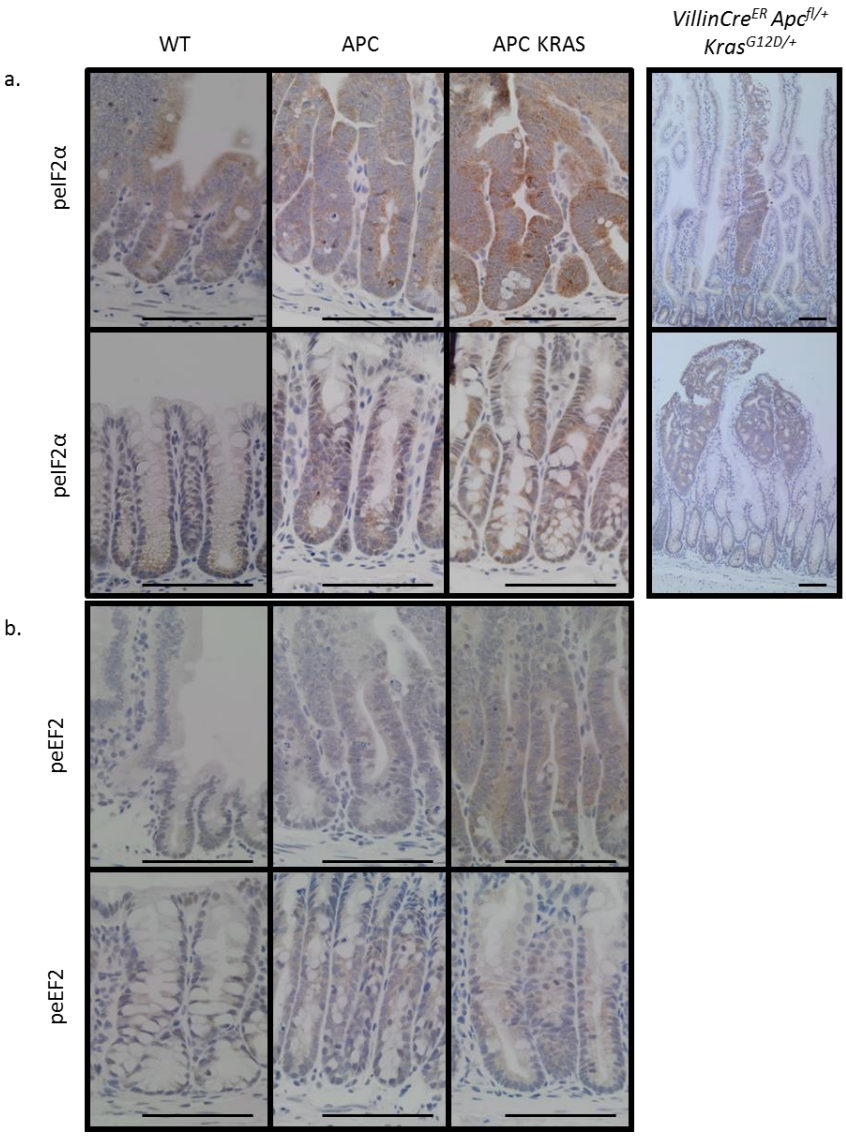

Figure 4.6: Increased phosphorylation of eIF2α and eEF2 in APC KRAS cells
a. Phospho-eIF2α (Ser51) staining of small intestinal (upper panel) and colonic sections (lower panel) of WT, *VillinCre*^{ER} *Apc*$^{fl/fl}$ (APC) and *VillinCre*^{ER} *Apc*$^{fl/fl}$ *Kras*$^{G12D/+}$ (APC KRAS) mice, and small intestinal and colonic tumours from *VillinCre*^{ER} *Apc*$^{fl/+}$ *Kras*$^{G12D/+}$ mice. b. Phospho-eEF2 (Thr56) staining of small intestinal (upper panel) and colonic sections (lower panel) of WT, APC and APC KRAS mice. Scale bar = 100μm

The phosphorylation of eIF2α and eEF2 should result in a reduction in protein synthesis, yet we know that APC KRAS crypt cultures produce more protein than APC crypt cultures, therefore it could well be that the 'nutrient stress' I observe in APC KRAS cells could be self-induced, due to fast rates of protein synthesis, given the large energetic demand of this process (Buttgereit & Brandt, 1995). One other consequence of fast rates of protein synthesis is an accumulation of misfolded proteins in the ER, activating the UPR, upregulating a transcriptional programme to overcome these misfolded proteins. Two target genes of the UPR are the ER chaperones GRP78 (BiP) and GRP94 (Bertolotti et al., 2000), immunohistochemistry showed that both of these proteins are

upregulated in the intestines of APC KRAS mice compared with APC and WT mice (Fig4.7a and 4.7b), whilst immunoblotting confirmed an upregulation of GRP78 in APC KRAS crypt cultures (Fig4.5a).

Taken together, these results suggest that the large increase in protein synthesis in APC KRAS crypt cultures is resulting in an imbalanced proteostasis such that these cells are trying to reduce protein synthesis and adapt to this large energetic burden. Phosphorylation of eIF2α and eEF2 will reduce global protein synthesis. In turn, phospho-eIF2α can drive the selective translation of ATF4, which in turn, drives a transcriptional programme of genes that serve to alleviate the UPR, including ASNS. Furthermore the increased expression of GRP78 and GRP94 will function to sequester misfolded proteins in the ER. Given this 'nutrient stress' puts a large energetic burden on cells, it would be interesting to determine whether it can be exploited for therapeutic benefit, this will be discussed in greater detail in the rest of this chapter. In order to maintain increased proliferation and protein synthesis, it is likely that APC KRAS intestinal epithelial cells have altered metabolism too, this will be discussed in chapter 5.

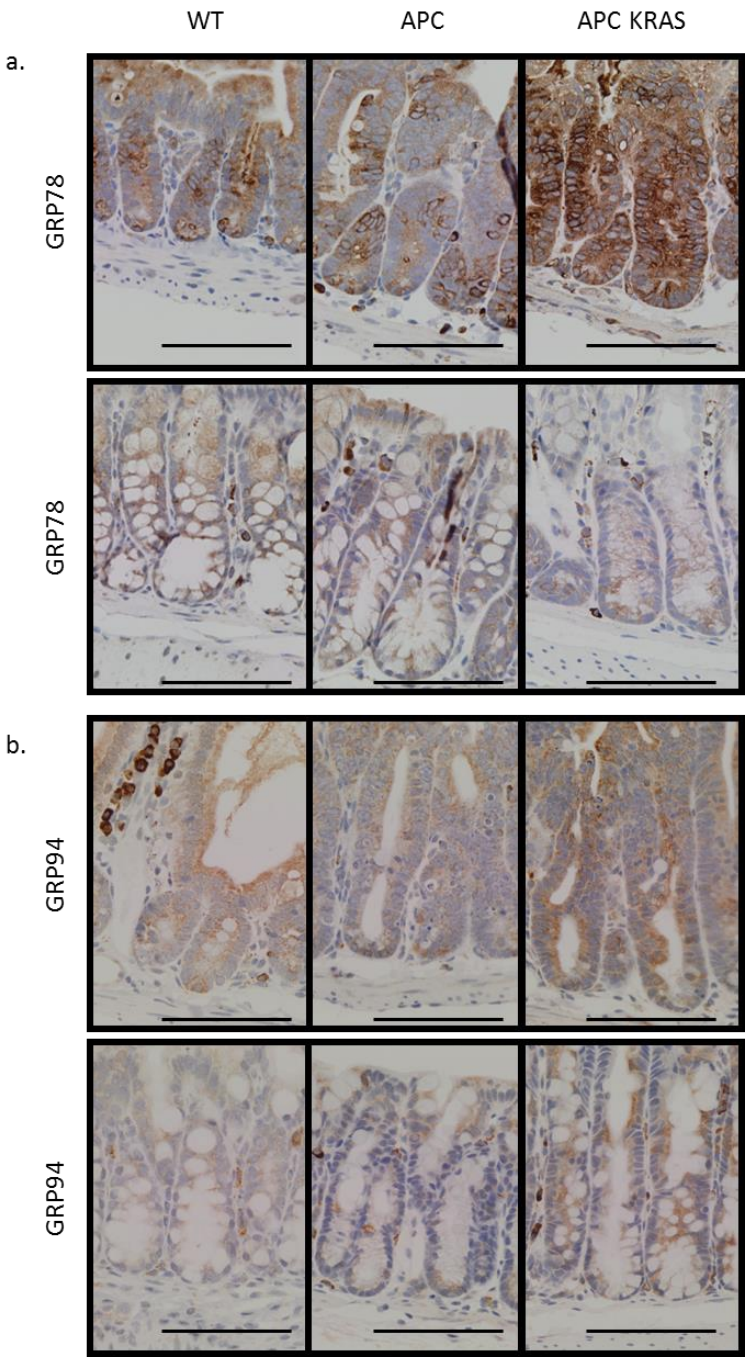

Figure 4.7: Increased expression of ER chaperones in APC KRAS intestinal epithelial cells

a. GRP78 and b. GRP94 staining of small intestinal (upper panel) and colonic sections (lower panel) of WT, *VillinCre*^{ER} *Apc*$^{fl/fl}$ (APC) and *VillinCre*^{ER} *Apc*$^{fl/fl}$ *Kras*$^{G12D/+}$ (APC KRAS) mice, WT and APC mice sampled 4-days post-induction, APC KRAS mice sampled 3-days post induction. Scale bar = 100μm

4.2.4 eIF2α phosphorylation is limiting in APC KRAS

I have shown that there is an increase in eIF2α-phosphorylation (Ser51) in APC-deficient *Kras*-mutant intestinal epithelial cells, compared with APC alone. This is an inhibitory phosphorylation event that reduces global protein synthesis, whilst selectively translating certain transcripts, such as ATF4. Given that APC KRAS crypt cultures produce more protein, I wondered whether the high levels of eIF2α phosphorylation were an artefact, rather than having a functional role in these cells. To investigate this, I used the small molecule ISRIB, which reverses the effects of eIF2α phosphorylation. I treated APC and APC KRAS crypt cultures with 500nM ISRIB and assayed nascent protein synthesis using ^{35}S-methionine labelling. Treatment of APC and APC KRAS crypt cultures with ISRIB significantly increased protein synthesis in specifically the APC KRAS crypt cultures compared with DMSO-treated controls (Fig4.8a). In parallel to this, I performed polysome profiling on APC and APC KRAS crypt cultures treated with ISRIB or DMSO (Fig4.8b). In line, with the ^{35}S-methionine labelling results, there was an increase in the polysome:sub-polysome ratios of all three APC KRAS crypt culture lines treated with ISRIB compared with DMSO controls, whilst this was not the case for the APC crypt cultures (Fig4.8c), suggesting that ISRIB treatment increases protein synthesis in APC KRAS crypt cultures. Finally, immunoblotting lysates from APC and APC KRAS crypt cultures treated with ISRIB or DMSO revealed that ISRIB does not affect phospho-eIF2α levels, whilst selectively reducing ATF4 at the protein level in APC KRAS crypt cultures (Fig4.8d). Altogether, these results indicate that eIF2α phosphorylation in APC KRAS intestinal epithelial cells does have a functional role, despite the increased rates of protein synthesis, and that the cells are trying to slow their rates of protein synthesis.

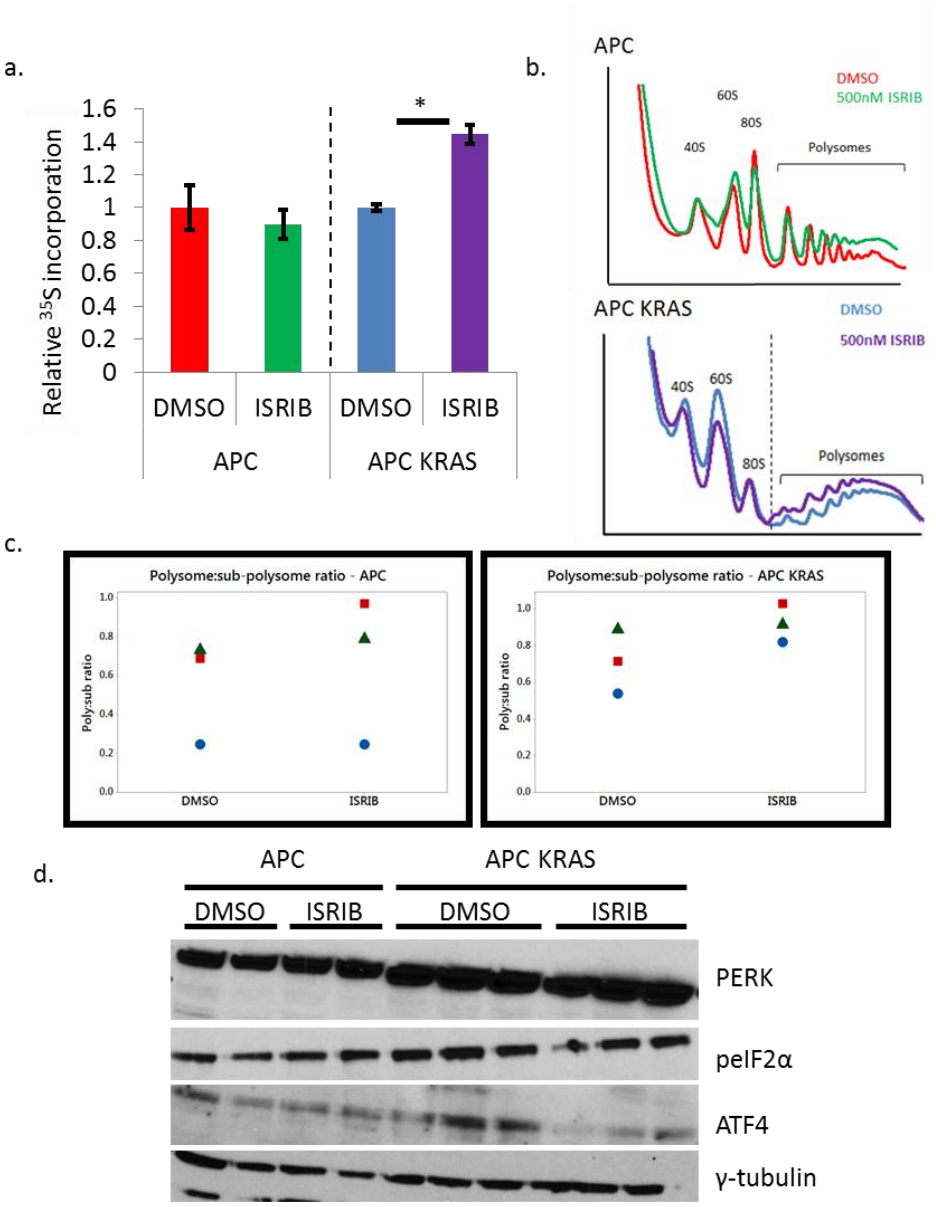

Figure 4.8: ISRIB treatment increases translation in APC KRAS cells

a. ^{35}S-methionine incorporation in APC and APC KRAS small intestinal crypt cultures – cultures were treated with 500nM or 0.1% DMSO for 4.5 hours and then pulsed with ^{35}S-labelled methionine for 30 minutes. Incorporation of ^{35}S into nascent protein was quantified by scintillation and normalized to total protein, 3-technical replicates per cell line, 3-different cells lines used for each genotype. Data expressed relative to each vehicle line, one-way Mann-Whitney *U* test, p=0.0405, data displayed +/- SEM b. Polysome profiles from APC and APC KRAS small intestinal crypt cultures treated with 500nM ISRIB or vehicle (0.1% DMSO) for 5 hours, three different cell lines used for each experiment. c. Quantification of polysome: sub-polysome ratios of APC and APC KRAS small intestinal crypt cultures treated with 0.1% DMSO or 500nM ISRIB for 5 hours – symbols represent paired cell lines. d. Immunoblot for PERK, phospho-eIF2α(Ser51), Atf4 and ß-actin on lysates from paired APC and APC KRAS crypt cultures treated with 0.1% DMSO or 500nM ISRIB for 5 hours.

4.2.5 ISRIB partially suppresses the APC KRAS phenotype

Given my *in vitro* results with ISRIB treatment, I wanted to determine whether it could reduce proliferation in our acute models – specifically APC KRAS mice. I hypothesized that if ISRIB treatment increases protein synthesis in these mice, whilst also blocking translation of ATF4 – a transcription factor required to overcome ER stress, then this could lead to reduced proliferation as the cells are 'too energetically stressed'. Treatment of APC KRAS mice with ISRIB significantly reduced proliferation in both the small intestine and colon compared with vehicle controls, whilst not affecting proliferation in APC mice (Fig4.9a-c). ISRIB treatment did not affect the levels of GRP78 or phosphorylation of eIF2α (Fig4.10b and Fig4.10c), suggesting that ER stress was not further increased, although one would not expect an increase in phosphorylation of eIF2α following ISRIB treatment.

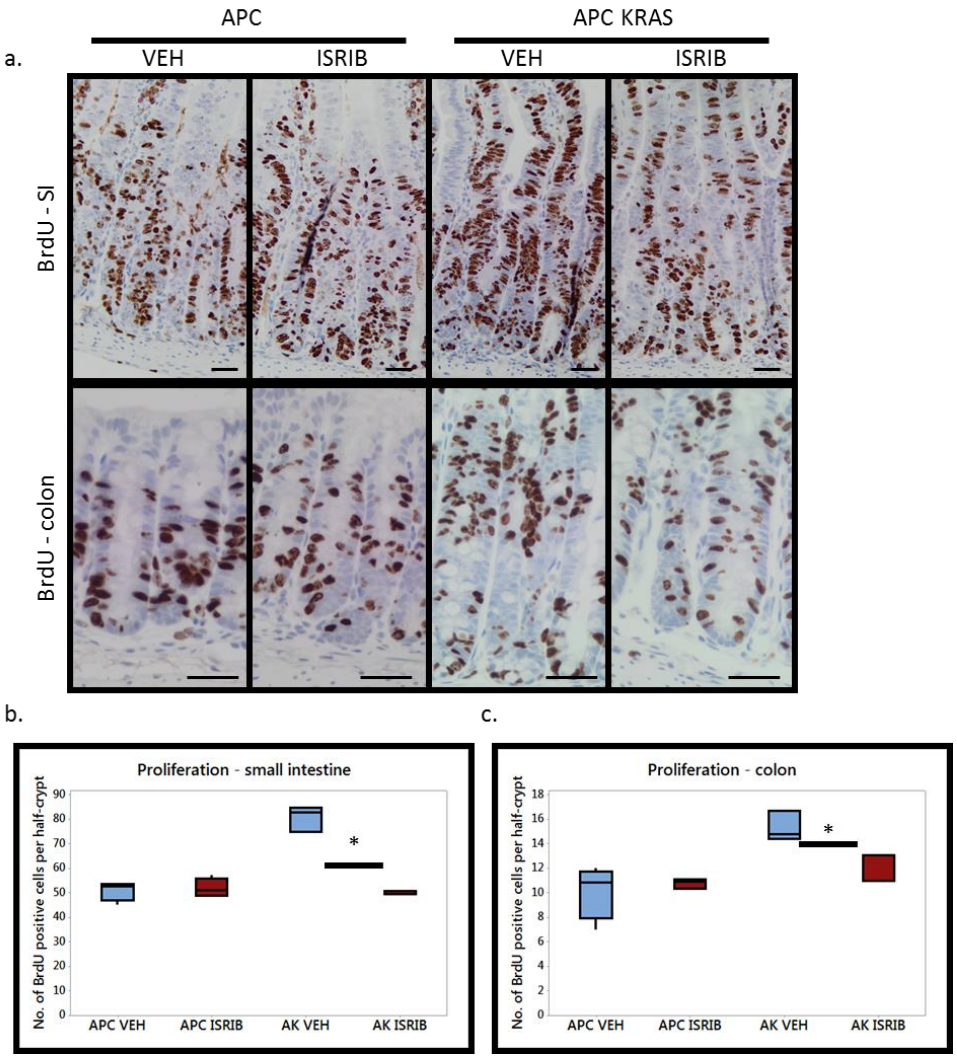

Figure 4.9: ISRIB reduces proliferation in APC KRAS mice

a. BrdU staining of small intestines (SI – upper panel) and colons (lower panel) from tamoxifen-induced *VillinCre^{ER} Apc$^{fl/fl}$* (APC) and *VillinCre^{ER} Apc$^{fl/fl}$ Kras$^{G12D/+}$* (APC KRAS) mice treated daily with 0.25mg/kg ISRIB or vehicle – sampled 4- and 3-days post induction respectively, scale bars = 40μm. BrdU scoring in b. small intestine and c. colon of tamoxifen-induced APC and APC KRAS mice treated with 0.25mg/kg ISRIB or vehicle sampled 4- and 3-days post induction respectively, 25 crypts per mouse, n=4 for APC, n=3 for APC KRAS, one-way Mann-Whitney *U* test, 0.443 (APC – SI and col), * p=0.0405 (AK- SI and col)

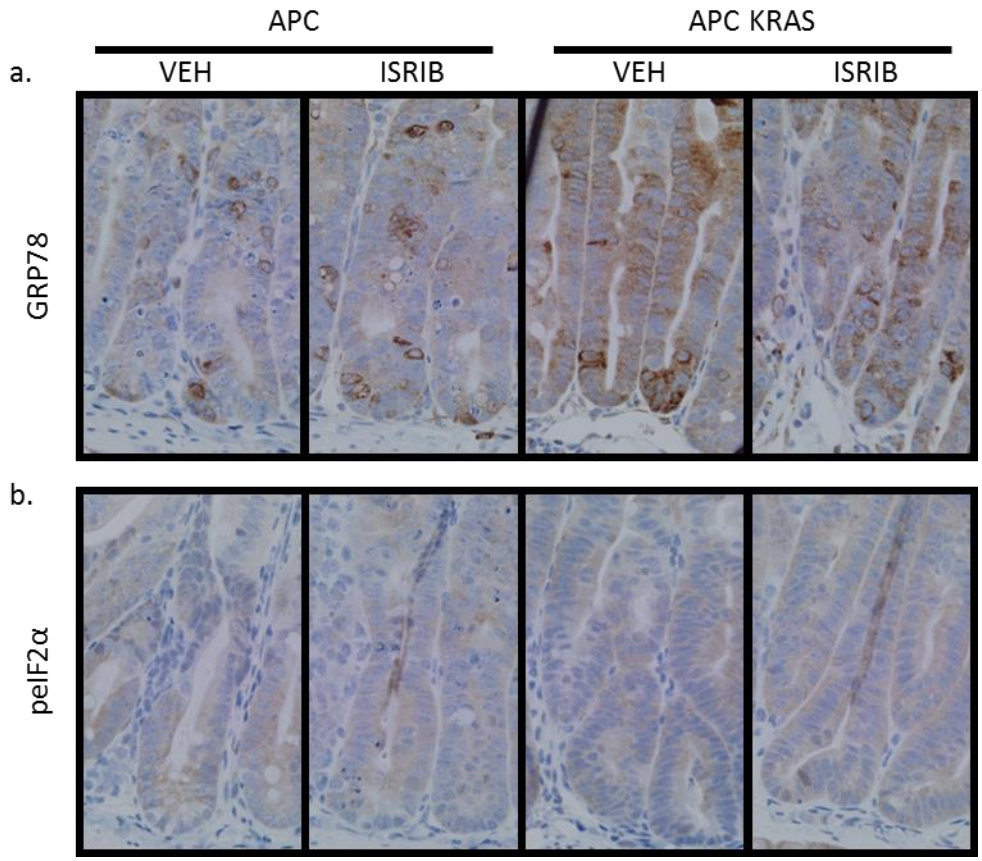

Figure 4.10: ISRIB does not increase ER stress in APC KRAS mice
a. GRP78 and b. phospho-eIF2α staining of small intestines from tamoxifen-induced *VillinCre*^{ER} *Apc*$^{fl/fl}$ (APC) and *VillinCre*^{ER} *Apc*$^{fl/fl}$ *Kras*$^{G12D/+}$ (APC KRAS) mice treated daily with 0.25mg/kg ISRIB or vehicle – sampled 4- and 3-days post induction respectively. Scale bars = 40μm

Western blot revealed that ISRIB reduces ATF4 protein levels specifically in the intestines of APC KRAS mice (Fig4.11a); however this did not correlate with reduced ATF target gene expression in these mice (Fig4.11b). To determine if ISRIB was still affecting protein synthesis, I performed polysome profiling on small intestines isolated from APC KRAS mice treated with ISRIB or vehicle (Fig4.12a). These traces suggest that there is no change in protein synthesis - there was no obvious trend in either group in the polysome: sub-polysome ratio (Fig4.12b). Further work is required to determine why ISRIB treatment reduces proliferation in APC KRAS intestines and colons *in vivo*.

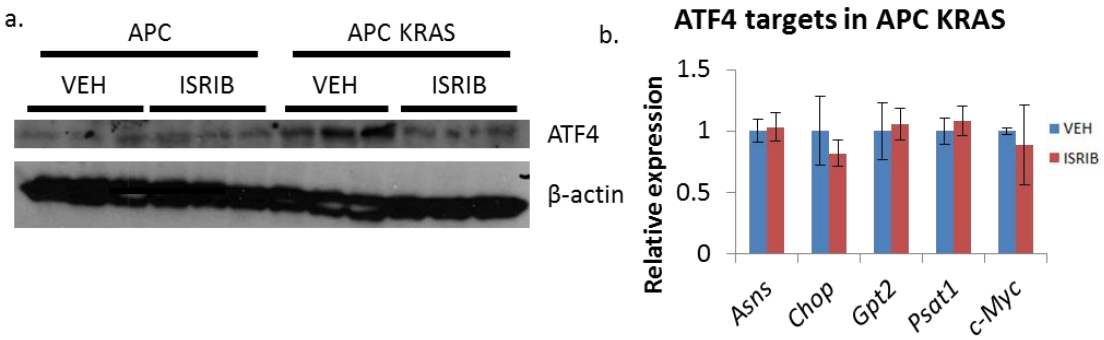

Figure 4.11: ISRIB reduces ATF4 expression, but not Atf4 target gene expression in APC KRAS intestines

a. Immunoblot for ATF4 and ß-actin on epithelial extractions (crypt fraction) from tamoxifen-induced *VillinCre*^{ER} *Apc*$^{fl/fl}$ (APC) and *VillinCre*^{ER} *Apc*$^{fl/fl}$ *Kras*$^{G12D/+}$ (APC KRAS) mice treated daily with 0.25mg/kg ISRIB or vehicle – sampled 4- and 3-days post induction respectively. b. qRT-PCR for ATF4 target genes: *Asns, Chop, Gpt2, Psat1* and also *c-Myc*, from intestinal tissue from APC KRAS mice treated daily with 0.25mg/kg ISRIB or vehicle and sampled 3-days post-induction, n=3 per group, one-way Mann-Whitney *U* test p=0.331 (*Asns* and *Chop*), p=0.5 (*Gpt2* and *c-Myc*) and p=0.191 (*Psat1*), data displayed +/- SEM.

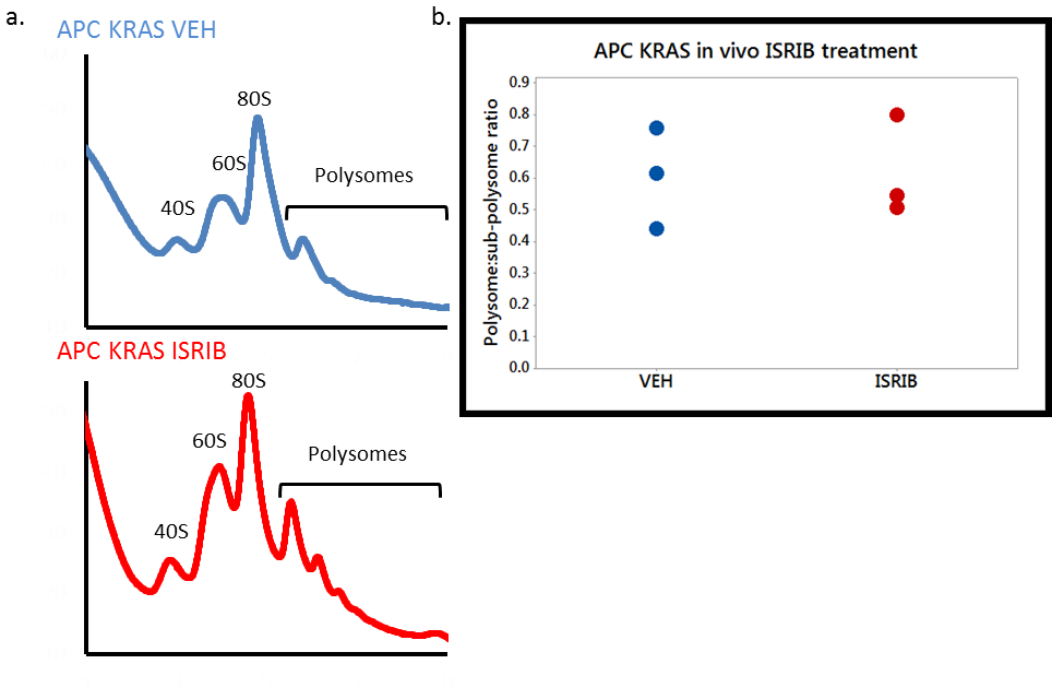

Figure 4.12: ISRIB treatment dose not significantly alter polysome profiles from small intestines of APC KRAS mice

a. Polysome profiles from the small intestines of tamoxifen-induced *VillinCre*^{ER} *Apc*$^{fl/fl}$ *Kras*$^{G12D/+}$ (APC KRAS) mice treated daily with 0.25mg/kg ISRIB or vehicle – sampled 3-days post induction. b. Quantification of polysome: sub-polysome ratios of APC KRAS mice treated with vehicle or ISRIB, n=3 per group, one-way Mann-Whitney *U* test, p=0.5

4.2.6 Neither prophylactic nor symptomatic ISRIB treatment extend survival

Having shown that ISRIB treatment significantly suppresses proliferation in the small intestine and colon following acute APC-deletion and KRAS activation, I sought to investigate whether ISRIB has any affect upon tumour growth in a KRAS-driven model of intestinal tumourigenesis. I treated *VillinCre^{ER} Apc$^{fl/+}$ Kras$^{G12D/+}$* mice with ISRIB or vehicle daily from 21-days post-induction and aged them until clinical end-point. At 21-days these mice will have small lesions throughout their small intestine and colon. There was no difference in survival between ISRIB and vehicle treated mice, and also in total tumour number and tumour burden (Fig4.13a-c). These results suggest that during the early stages of intestinal tumourigenesis, eIF2α phosphorylation does not have a functional role, or that following chronic ISRIB treatment, these tumour cells acquire resistance to ISRIB. In our acute models, there is a rapid phenotype, with a big burst of proliferation following APC-loss and KRAS activation, with limited time for transformed cells to acquire resistance to a drug. Hence these models are more reminiscent of treating an established tumour with a drug, rather than attempting to block/slow tumour development. Furthermore, given that tumours at end-point exhibit very high levels of phospho-eIF2α (Fig4.6a), I hypothesized that ISRIB treatment may have an impact when mice present with clinical symptoms. Once *VillinCre^{ER} Apc$^{fl/+}$ Kras$^{G12D/+}$* mice exhibited clinical signs, such as paling feet, weight loss and hunching, I treated them with ISRIB or vehicle until end-point. Symptomatic ISRIB treatment of *VillinCre^{ER} Apc$^{fl/+}$ Kras$^{G12D/+}$* mice had no survival benefit over vehicle controls (Fig5.6d). This result suggests that in established tumours the Integrated Stress Response does not have a functional role and therefore do not respond to ISRIB.

There is a possibility that additional stromal signals could play a role in the adaptation of tumour cells to ISRIB treatment in comparison to phenotypic changes in our acute models or that in this more complex tumours setting, you need combinatorial approaches to open a therapeutic window. To investigate this, I treated *VillinCre^{ER} Apc$^{fl/+}$ Kras$^{G12D/+}$ Nupr1$^{-/-}$* mice with ISRIB or vehicle when sick and aged them until clinical end-point. ISRIB treatment partially extended survival in these mice compared with vehicle controls (Fig4.14b). Importantly, despite its upregulation in APC KRAS intestines and its' role in ER stress signalling, NUPR1 deletion does not impact tumour latency *in VillinCre^{ER}*

Apc$^{fl/+}$ *Kras*$^{G12D/+}$ mice (Fig4.14a). This data suggests that a combinatorial approach to targeting ER stress, using ISRIB and an inhibitor of NUPR1 could potentially provide a therapeutic window in KRAS driven colon tumours.

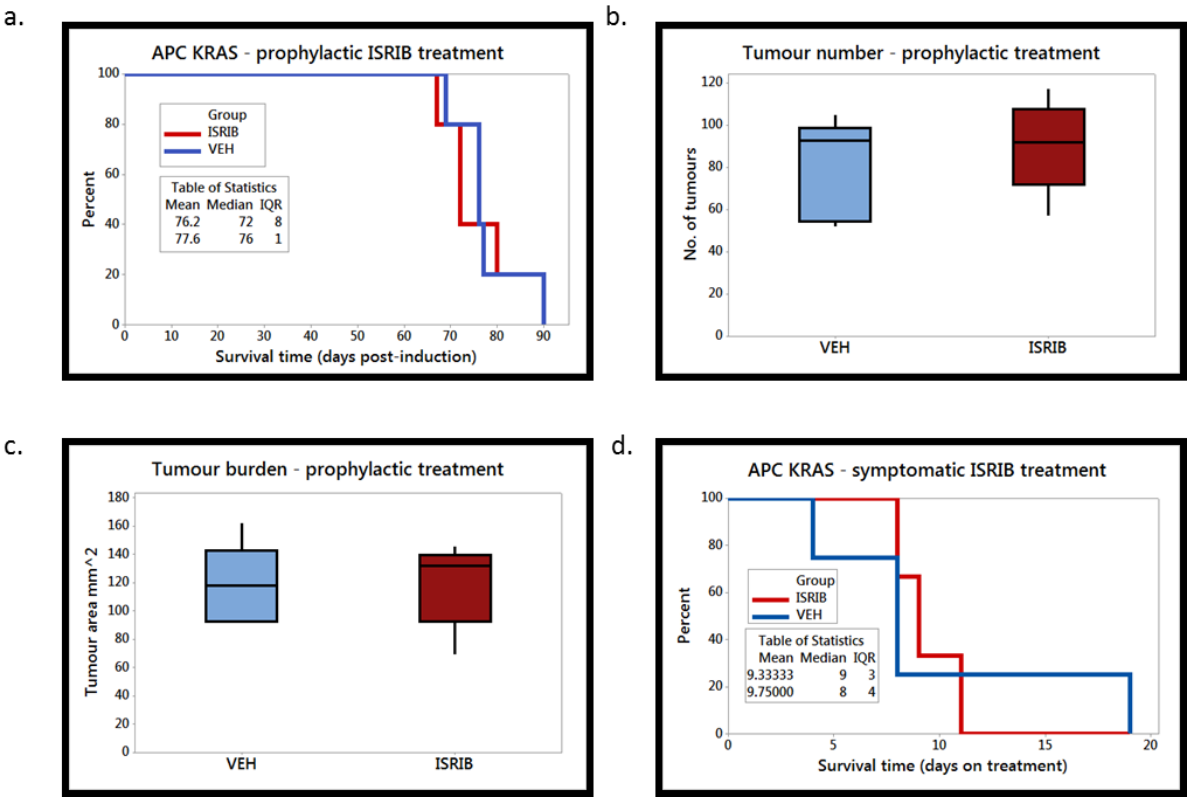

Figure 4.13: ISRIB treatment does not extend survival in a KRAS-driven model of intestinal tumourigenesis

a. Survival plot for *VillinCre*^{ER} *Apc*$^{fl/+}$ *Kras*$^{G12D/+}$ mice treated daily with 0.25mg/kg ISRIB or vehicle daily from 21-days post-induction to clinical end-point, n=5 per group, log-rank test p=0867. b. Tumour number and c. Tumour burden at end-point of *VillinCre*^{ER} *Apc*$^{fl/+}$ *Kras*$^{G12D/+}$ mice treated daily with 0.25mg/kg ISRIB or vehicle daily from 21-days post-induction, n=5 per group, one-way Mann-Whitney *U* test p=0.377 (tumour number), p=0.417 (tumour burden). d. Survival plot for *VillinCre*^{ER} *Apc*$^{fl/+}$ *Kras*$^{G12D/+}$ mice treated daily with 0.25mg/kg ISRIB or vehicle daily when showing clinical signs of intestinal tumour burden until end-point, n=4 per group.

a.

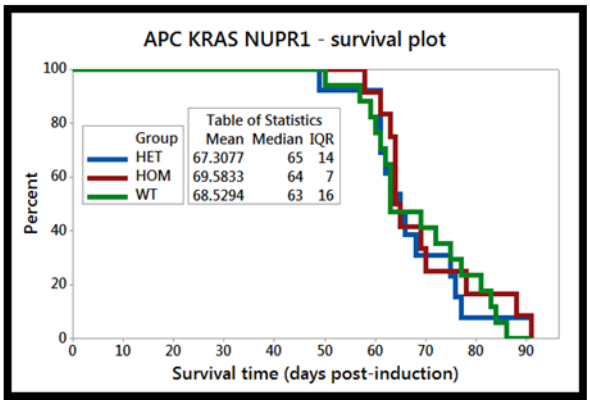

b.

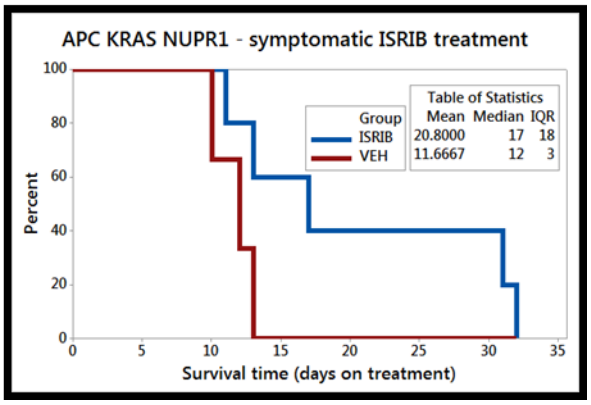

Figure 4.14: ISRIB treatment synergises with NUPR1 deletion in a KRAS-driven model of intestinal tumourigenesis

a Survival plot for VillinCre^{ER} Apc$^{fl/+}$ Kras$^{G12D/+}$ (WT), *VillinCre^{ER} Apc$^{fl/+}$ Kras$^{G12D/+}$ Nupr1$^{+/-}$* (HET) and *VillinCre^{ER} Apc$^{fl/+}$ Kras$^{G12D/+}$ Nupr1$^{-/-}$* (HOM) mice aged until showing signs of intestinal tumour burden. n=17 for WT, n=13 for HET and n=12 for HOM, log-rank test p=0.402 b. Survival plot of *VillinCre^{ER} Apc$^{fl/+}$ Kras$^{G12D/+}$ Nupr1$^{-/-}$* mice treated with 0.25mg/kg ISRIB or vehicle daily from onset of symptoms of intestinal tumour burden until end-point. n=3 for vehicle, n=5 for ISRIB. Log-rank test p=0.091.

4.2.7 eIF2B5 is required for intestinal regeneration

Whilst the exact mechanism by which ISRIB functions is unknown, it is thought to operate by either weakening the binding of phospho-eIF2α to eIF2B, thereby increasing the pool of eIF2B available to exchange GTP with GDP on eIF2. Alternatively, it enhances the basal activity of eIF2B, such that the activity of any 'free' eIF2B is sufficient to generate enough ternary complexes to sustain translation (Sidrauski et al., 2015). I sought to disrupt this GTP/GDP exchange between eIF2 and eIF2B by deleting one copy of eIF2B5, the catalytic subunit of eIF2B – using *Eif2b*$^{+/-}$ mice and investigating the role of this protein in intestinal homeostasis and intestinal tumourigenesis.

Importantly *Eif2b5*$^{+/-}$ mice do not exhibit any major phenotypes and are born at comparable ratios to their WT littermates. Furthermore there was no alteration in intestinal homeostasis in these mice (Fig4.15). To determine whether eIF2B5 has a functional role under a high Wnt- and high MAPK-pathway activation, I irradiated WT and *Eif2b5*$^{+/-}$ mice with 10Gy irradiation and then looked at the number of regenerating crypts 72 hours post-irradiation. There was a significant reduction in the number of regenerating crypts in *Eif2b5*$^{+/-}$ mice compared with WT controls (Fig4.16b). Interestingly, I observe an induction in eIF2α phosphorylation following irradiation (Fig4.16c), which could be due to a burst in protein synthesis accompanying proliferation during crypt regeneration; this may also lead to induction of ER stress, since there is an increase in GRP78 expression in regenerating crypts (Fig4.16d).

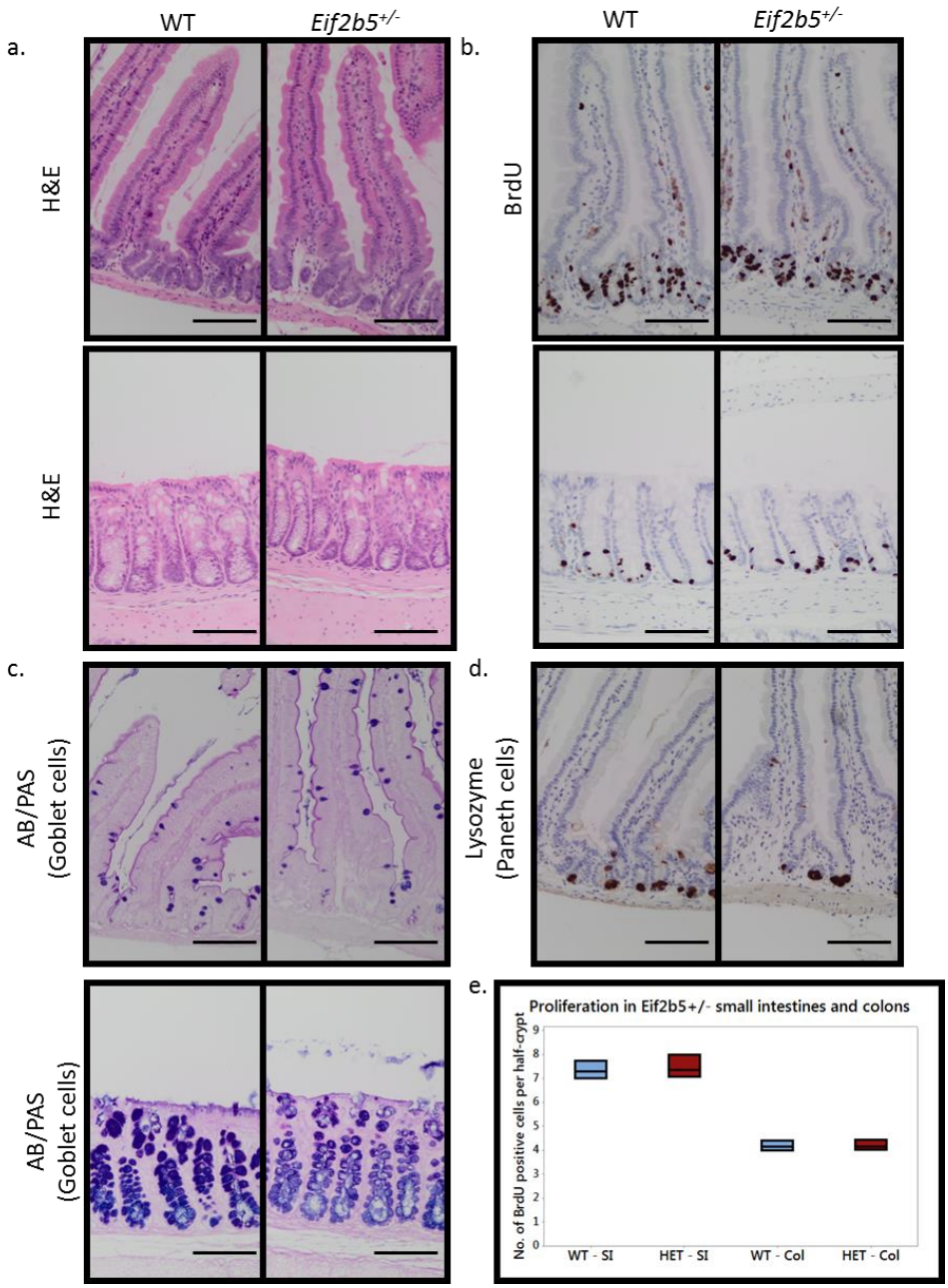

Figure 4.15 *Efi2b5*+/- mice do not exhibit an intestinal phenotype

a. H&E b. BrdU. c. Alcian Blue/Periodic acid Schiff (AB/PAS) d. Lysozyme staining (small intestine only) from small intestinal(upper panels) and colonic sections (lower panels) from WT and *Eif2b5*$^{+/-}$mice e. BrdU scoring from small intestines and colons of WT and *Eif2b5*$^{+/-}$ (HET) mice, number of BrdU-positive cells per half-crypt, 25 crypts per mouse, 3 mice per group, one-way Mann Whitney *U* test, p=0.331 (SI) and p=0.414 (col).

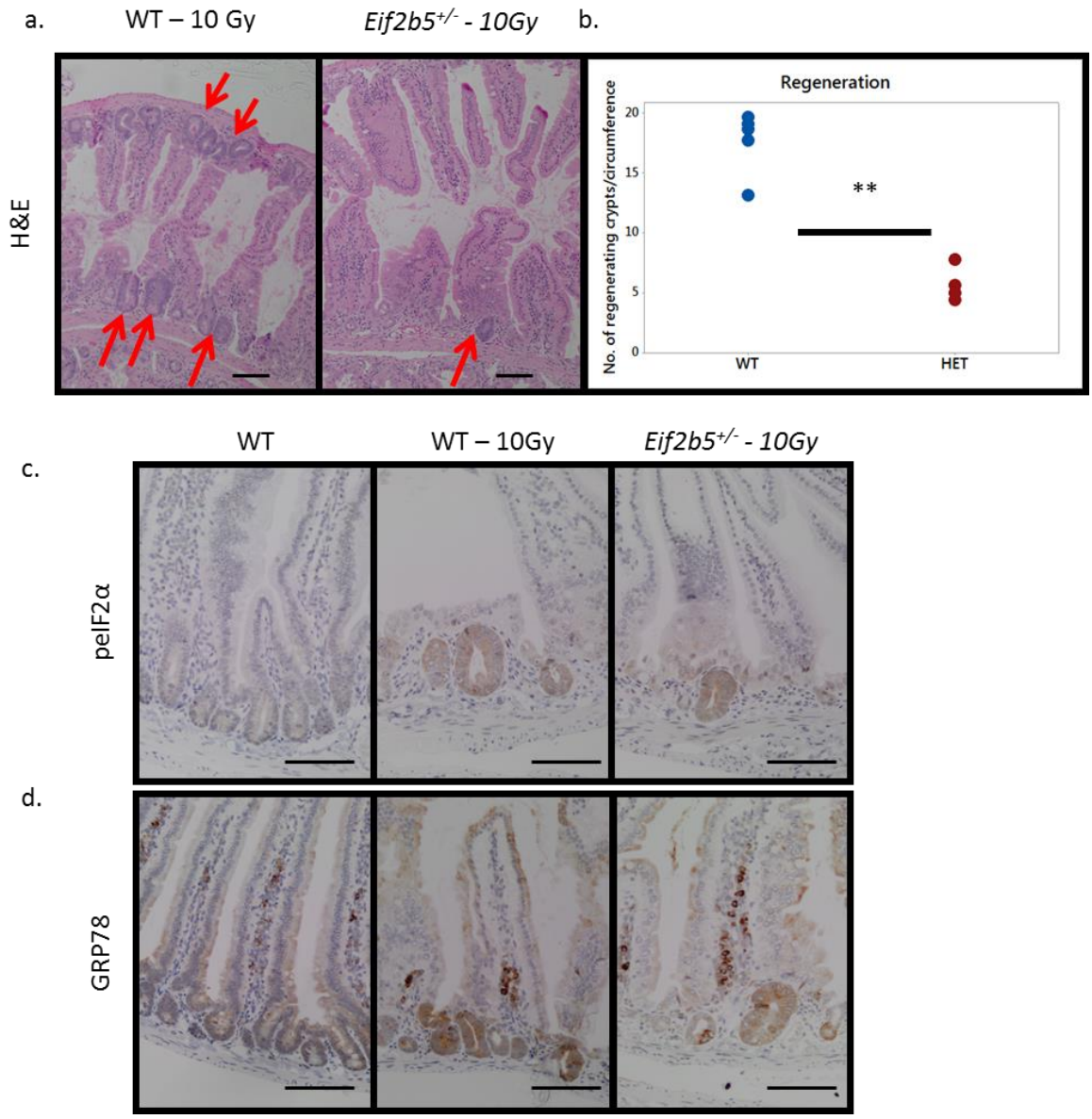

Figure 4.16: *Efi2b5*+/- mice have a reduced capacity to regenerate

a H&E staining of small intestinal sections of WT and *Eif2b5*$^{+/-}$ mice sampled 72-hours after exposure to 10Gy γ-irradiation, scale bars = 100μm b. Quantification of the number of regenerating crypts/circumference of irradiated WT and *Eif2b5*$^{+/-}$ mice, n=5 for WT and n=4 for Eif2b5$^{+/-}$ (HET), one-way Mann-Whitney *U* test, ** p=0.01.c. phospho-eIF2α and d. GRP78 staining of intestines of un-irradiated WT mice, irradiated WT and *Eif2b5*$^{+/-}$ mice sampled 72 hours after exposure to 10Gy irradiation, scale bars = 100μm.

4.2.8 Functional output of eIF2B5 in the small intestine:

To determine the functional role of eIF2B5 in the normal intestine, I isolated small intestinal crypts from WT and *Eif2b5*$^{+/-}$ mice via epithelial extraction. I confirmed a reduction in eIF2B5 protein level via immunoblotting however there was a small reduction in eIF2α phosphorylation, but not GRP78 expression, compared with WT crypts (Fig4.17a-c). Despite this decrease in expression of eIF2B5, there was no difference in rates of protein synthesis between WT and *Eif2b5*$^{+/-}$ small intestinal crypt cultures (Fig4.18a). Similarly, there was no difference in the polysome profiles obtained from the small intestines of WT and *Eif2b5*$^{+/-}$ mice (Fig4.19b and Fig4.19c). This data suggests that under normal homeostasis, loss of one copy of eIF2B5 is tolerated in the mouse intestine; however when there is a burst in proliferation or protein synthesis, such as following irradiation, eIF2B5 is required. Hence, one could imagine that in a tumour setting, eIF2B5 is required for tumour growth.

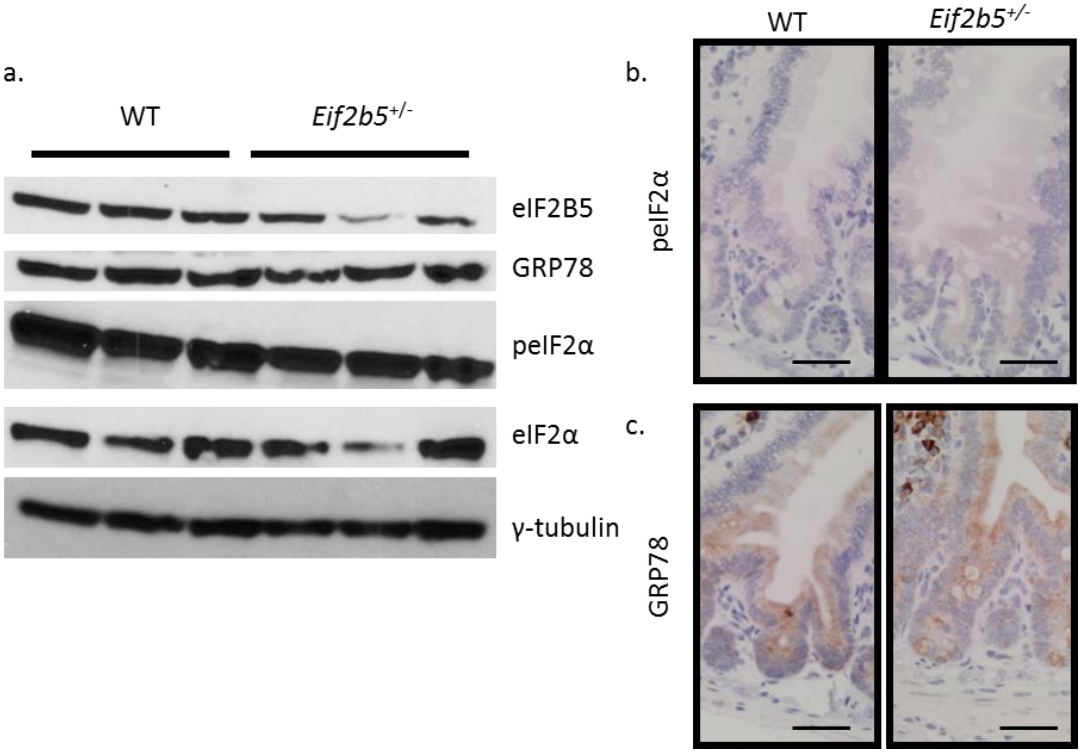

Figure 4.18: Loss of one copy of eIF2B5 does not affect ER stress in the normal intestine

a. Immunoblot for eIF2B5, GRP78, phospho-eIF2α (Ser51), eIF2α and γ-tubulin on epithelial extractions (crypt fraction) isolated from the small intestines of WT and *Eif2b5*$^{+/-}$ mice. b. phospho-eIF2α and c. GRP78 on small intestines of WT and *Eif2b5*$^{+/-}$ mice, scale bar = 40μm.

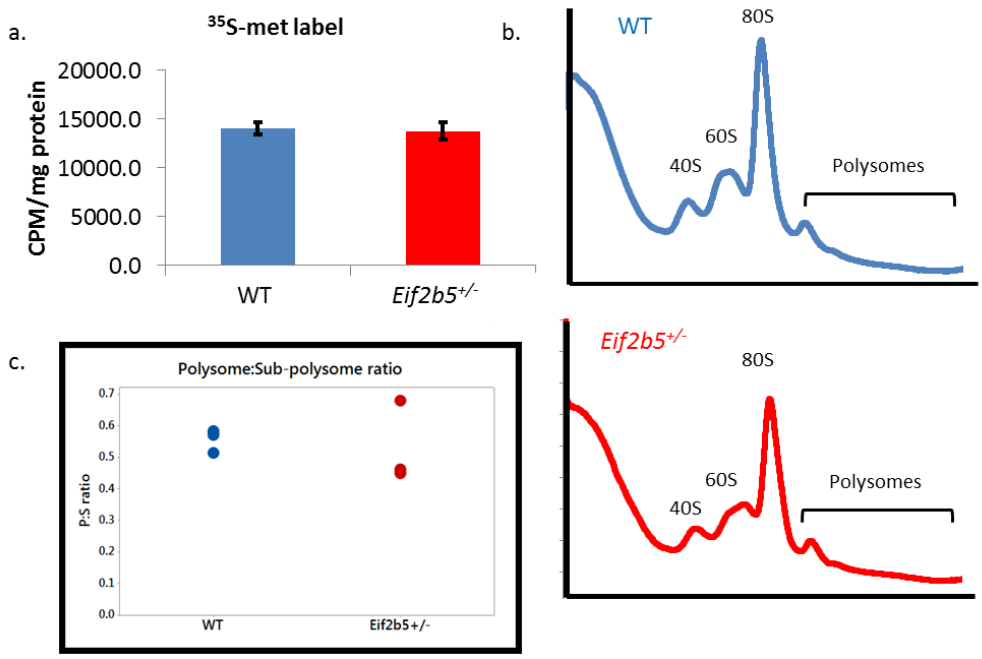

Figure 4.19: Loss of one copy of eIF2B5 does not affect protein synthesis in the normal intestine

a. ^{35}S-methionine incorporation in WT and *Eif2b5*$^{+/-}$ small intestinal crypt cultures – cultures were pulsed with ^{35}S-labelled methionine for 30 minutes. Incorporation of ^{35}S into protein was quantified by scintillation and normalized to total protein 3-technical replicates per cell line, 3-different cells lines used for each genotype, data displayed +/- SEM, one-way Mann Whitney *U* test, p=0.5. b. polysome profiles from WT and *Eif2b5*$^{+/-}$ small intestinal epithelium c. Quantification of polysome: sub-polysome ratios of profiles from WT and *Eif2b5*$^{+/-}$ small intestines, n=3 per group, one-way Mann Whitney *U* test, p=0.331.

4.2.9 eIF2B5 heterozygous deletion extends survival in *Apc*$^{Min/+}$ mice

Intestinal regeneration following irradiation is a surrogate way of inducing both high Wnt-and MAPK-pathway activity. The irradiation data suggest that eIF2B5 could play a role in high-Wnt conditions, or in proliferating cells. To investigate this I crossed *Eif2b5*$^{+/-}$ mice to *Apc*$^{Min/+}$ mice, a spontaneous intestinal tumour model, and aged them until clinical end-point. Loss of one copy of eIF2B5 significantly extended survival in *Apc*$^{Min/+}$mice, however there was no difference in the number of tumours or tumour burden between the two cohorts (Fig4.20a-c). Additionally, levels of phospho-eIF2α and GRP78 were not significantly altered (Fig4.20f and 4.20g), suggesting that there is not an increase in ER stress. Altogether, these results suggest that the tumours grow more slowly in *Apc*$^{Min/+}$ *Eif2b5*$^{+/-}$ mice. To determine whether deletion of one copy of *Eif2b5* reduces protein synthesis in intestinal tumours, I isolated intestinal tumours from *Apc*$^{Min/+}$ and *Apc*$^{Min/+}$ *Eif2b5*$^{+/-}$ mice propagated them *in vitro* and performed ^{35}S-methionine incorporation. This revealed that tumours

lacking one copy of *Eif2b5* did not have reduced protein synthesis (Fig4.21a), this was also supported by polysome profiling on the same tumour cultures – there was no difference in the polysome: sub-polysome ratio (Fig4.21c).

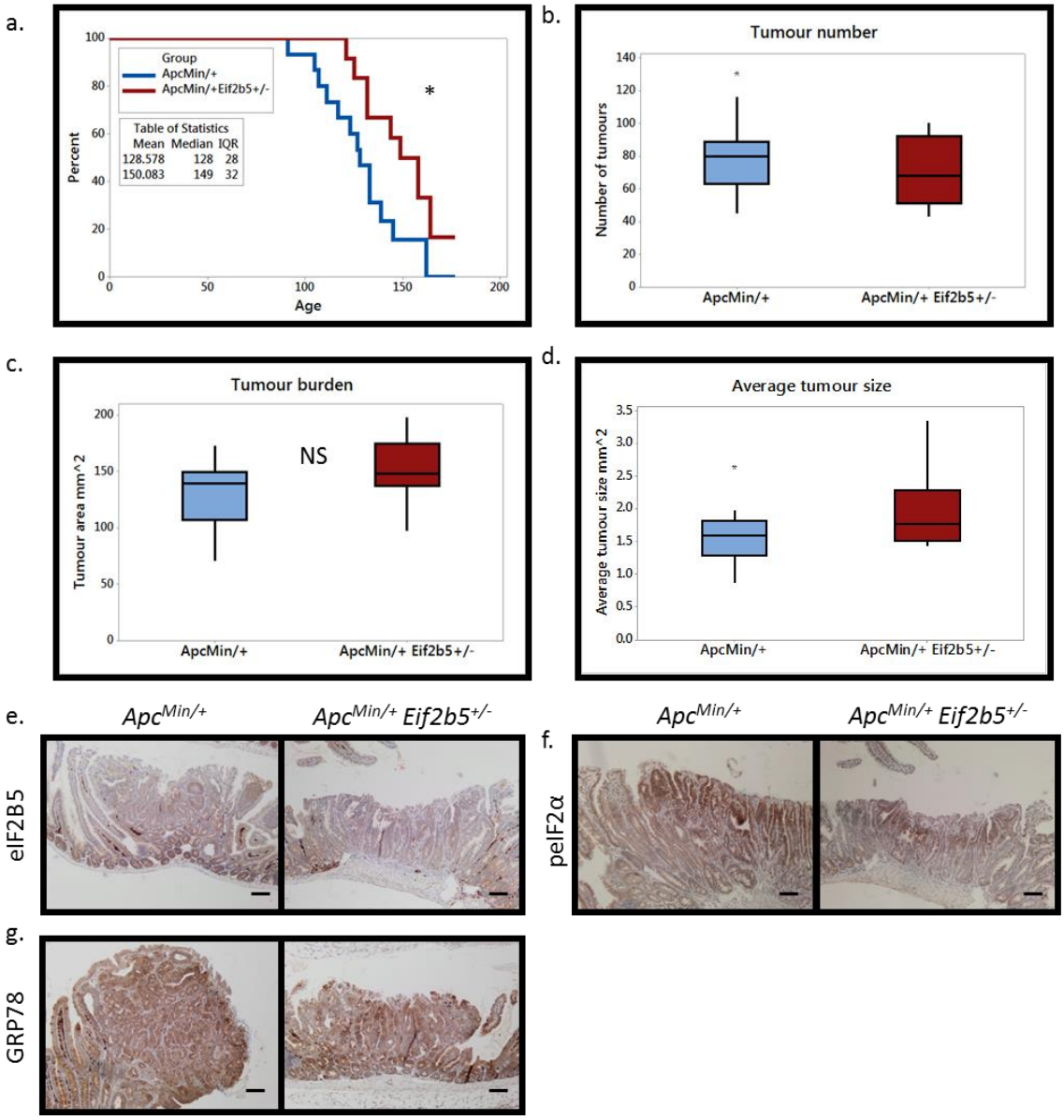

Figure 4.20: eIF2B5 is required for tumour progression in ApcMin/+ mice
a. Survival-curve for $Apc^{Min/+}$ (n=13, 2 censored) and $Apc^{Min/+}$ *Eif2b5*$^{+/-}$ (n=8, 6 censored) aged until clinical end-point, Log-rank test, p=0.024 (*) b. Tumour number, one-way Mann-Whitney *U* test p=0.246 c. Tumour burden, one-way Mann-Whitney test p=0.0598 and d. Average tumour size, one-way Mann-Whitney test p=0.105, from $Apc^{Min/+}$ (n=13) and $Apc^{Min/+}$ *Eif2B5*$^{+/-}$ (n=8) mice aged until clinical end-point. e. eIF2b5 f. phospho-eIF2α and g. GRP78 staining of small intestinal tumours from $Apc^{Min/+}$ and $Apc^{Min/+}$ *Eif2b5*$^{+/-}$ mice.

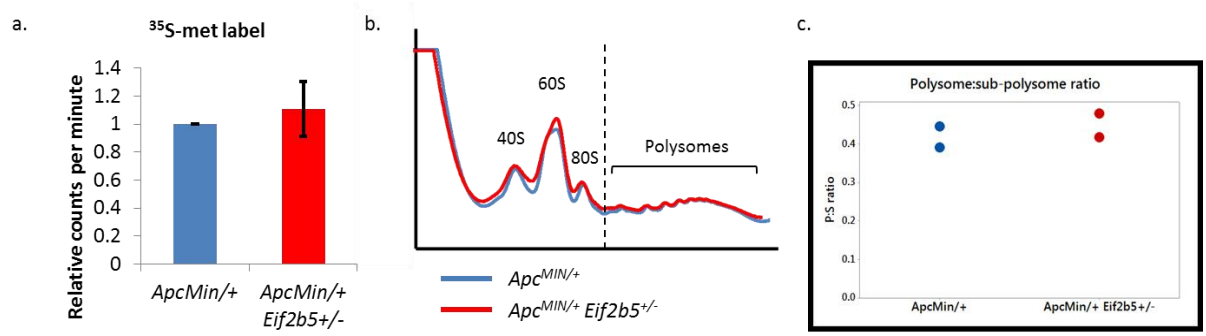

Figure 4.21: *ApcMin/+ Eif2b5+/-* tumours do not have reduced protein synthesis
a. ^{35}S-methionine incorporation in intestinal tumours cultures isolated from *Apc$^{Min/+}$ and Apc$^{Min/+}$ Eif2b5$^{+/-}$* mice – cultures were pulsed with ^{35}S-labelled methionine for 30 minutes. Incorporation of ^{35}S into nascent protein was quantified by scintillation and normalized to total protein 3-technical replicates per cell line, 2-different tumour lines used for each genotype, data displayed +/- SEM. b. polysome profiles from intestinal tumours cultures isolated from Apc$^{Min/+}$ *and Apc$^{Min/+}$ Eif2b5$^{+/-}$* mice c. Quantification of polysome: sub-polysome ratios of profiles from intestinal tumours cultures isolated from Apc$^{Min/+}$ *and Apc$^{Min/+}$ Eif2b5$^{+/-}$* mice, n=2 per group.

4.3 Discussion

In this chapter I performed quantitative proteomics on APC and APC KRAS crypt cultures to investigate differences in the APC and APC KRAS proteomes: to better understand the cooperation of APC loss and KRAS activation in colorectal cancer, so as to identify potential novel therapeutic targets.

This proteomic approach, using SILAC, identified a 'nutrient stress' signature, which is likely to be a result of increased protein synthesis. Following pathway analysis of deregulated proteins identified via SILAC - the top predicted upregulated pathway was eIF2 signalling, which is likely to be due to increased expression of many components of the translation machinery; ribosomal proteins and tRNA synthetases for instance, but also components of the UPR which signals via eIF2α, to reduce global protein synthesis. Other top hits included eIF4 and S6K signalling, which feeds into translation, indicating a pronounced increase in protein synthesis in APC KRAS compared with APC crypt cultures. It has been shown that APC KRAS crypt cultures produce significantly more protein than APC crypt cultures, and that they have different translational profiles (John Knight – personal communication).

I observe increased phosphorylation of eIF2α and eEF2 in APC KRAS cells compared with APC, both *in vitro* and *in vivo*, suggesting that APC KRAS cells are trying to reduce protein synthesis. Furthermore, there is increased expression of the ER chaperones GRP78 and GRP94, associated with ER stress, in APC KRAS

intestinal epithelial cells *in vivo*, suggesting that proteostasis is perturbed in APC KRAS. The pathway analysis also identified a number of transcription factors that are activated by the UPR, such as ATF4 and XBP1, in APC KRAS crypt cultures. I confirmed their upregulation *in vivo*, whilst analysis of RNASeq data confirmed an upregulation of a large number of ATF4 targets in APC KRAS intestines, suggesting that these cells are adapting to stress.

APC-deficient *Kras*-mutant intestinal epithelial cells have increased rates of protein synthesis, despite increased phosphorylation of eIF2α; I wanted to investigate whether this phosphorylation event had a functional role or was merely an artefact of increased protein synthesis. I used the small molecule inhibitor, ISRIB, which has been shown to reverse the effects of eIF2α phosphorylation – increase global protein synthesis and reduce ATF4 expression (Sidrauski et al., 2013). Treatment of APC and APC KRAS crypt cultures with ISRIB, significantly increased protein synthesis in APC KRAS crypt cultures, but not APC crypt cultures, compared with DMSO controls. Furthermore, this treatment did not affect phosphorylation of eIF2α, but it did reduce ATF4 expression in APC KRAS crypt cultures. This suggests that eIF2α phosphorylation is limiting in APC KRAS crypt cultures, but also that ISRIB provides a tool to target ATF4 expression at the protein level.

Given the increased expression in ATF4 targets, many of which are involved in metabolism, in APC KRAS intestinal epithelial cells compared with APC epithelial cells, I was interested to determine whether ISRIB treatment could have a therapeutic benefit *in vivo*. ISRIB treatment of our acute models reduced proliferation in APC KRAS small intestines and colons, but not APC. This reduction in proliferation was accompanied by reduced expression of ATF4 at the protein level; however, of the ATF4 targets investigated, there was no change in expression. Furthermore, polysome profiling on the small intestines of ISRIB and vehicle treated APC KRAS mice proved inconclusive as to whether there is increased protein synthesis *in vivo* following ISRIB treatment. Despite ISRIB treatment reducing proliferation in the intestines and colons of APC KRAS mice, there was no survival benefit in *VillinCre*^{ER} *Apc*$^{fl/+}$ *Kras*$^{G12D/+}$ mice treated prophylactically or symptomatically with ISRIB compared with vehicle control. However, there was a trend towards increased survival of symptomatically

treated *VillinCre*^{ER} *Apc*$^{fl/+}$ *Kras*$^{G12D/+}$ *Nupr1*$^{-/-}$ mice – hence a combinatorial approach to targeting ER stress could open up a therapeutic window.

The exact mechanism by which ISRIB functions is not entirely resolved; however it has been shown to be an activator of eIF2B - the GEF for eIF2 (Sidrauski et al., 2015). To investigate the role of eIF2B5 in intestinal tumourigenesis, I used a knock-out mouse of eIF2B5, the catalytic subunit of the eIF2B complex. Deletion of one copy of eIF2B5 did not affect normal intestinal homeostasis nor reduce rates of protein synthesis in the small intestine; however intestinal crypts from these mice have a reduced capacity to regenerate. This could be due to a reduced ability to regulate a burst in protein synthesis associated with increased proliferation in the intestinal crypts following irradiation. Since irradiated WT crypts have high levels of eIF2α phosphorylation and GRP78 expression, suggesting an increase in protein synthesis as these crypts regenerate. Additionally, this result suggests that eIF2B5 plays a key-role following Wnt-pathway activation. To investigate this, I crossed *Eif2b5*$^{+/-}$ mice to *Apc*$^{Min/+}$ mice. Loss of one copy of eIF2B5 significantly extended survival of *Apc*$^{Min/+}$ mice, however, there was no difference in tumour number or burden at end-point. The intestinal tumours that did arise in *Apc*$^{Min/+}$ *Eif2b5*$^{+/-}$ did not exhibit gross differences in GRP78 and phospho-eIF2α levels compared to control tumours. Interestingly, there was no differences in rates of protein synthesis in cultured tumours from *Apc*$^{Min/+}$ and *Apc*$^{Min/+}$ *Eif2b5*$^{+/-}$ mice. This suggests that the increased survival in *Apc*$^{Min/+}$ *Eif2b5*$^{+/-}$ mice could be due to differences in the tumours' translatomes compared to control mice, such that loss of one copy eIF2B5 affects the translation of certain mRNAs.

Chapter 5: Investigating metabolic deregulation in APC KRAS crypts

5.1 Introduction

Having identified that APC KRAS cells produce significantly more protein than APC cells and exhibit a nutrient stress phenotype; I was curious to investigate whether there are also changes in metabolism between these cells in response to the large energetic demand of protein synthesis.

5.1.1 Metabolism in cancer

Deregulated metabolism is a hallmark of cancer, and there has been a great focus on both glucose and glutamine metabolism in transformed cells. It was first reported by Otto Warburg that tumours take up significantly more glucose and release more lactate compared with normal tissue (Warburg & Wind, 1927). This has been further exploited for imaging purposes – Fludeoxyglucose (^{18}F), FDG, is used in combination with Positron Emission Tomography (PET) to look for tumours within patients. The FDG is taken up by the cancer cells and phosphorylated by hexokinase, to form FDG-6-phosphate. This cannot be metabolised further via glycolysis, and hence accumulates in tissues that are glycolytic (Som et al., 1980). Interestingly, Hexokinase 2 has been shown to be upregulated in colorectal cancer and its' higher expression correlates with a worse prognosis (Hamabe et al., 2014). Of note, Hexokinase 2 is not expressed in the normal adult intestinal epithelium (Hamabe et al., 2014), and therefore specific inhibitors may be of therapeutic benefit. Under basal conditions, glucose is converted to pyruvate in the cytoplasm, via a series of reactions, and then enters the TCA (Tricarboxylic acid) cycle) in the mitochondria for production of ATP via oxidative phosphorylation.

The large production of lactate by cancer cells highlights a shift away from oxidative phosphorylation – glucose derived pyruvate is converted to lactate and secreted, rather than entering the TCA (Tricarboxylic acid) cycle for ATP production. Lactate production is a far less efficient pathway for producing ATP than the TCA cycle (Warburg 1956). However the production of ATP via the TCA cycle is a major negative regulator of glycolysis (Pavlova & Thompson, 2016), hence this shift away from oxidative phosphorylation ensures higher rates of glycolysis. This is important since many glycolytic intermediates are used in the biosynthesis of other macromolecules required for the growth of

proliferating cells. For instance, glucose-6-phosphate, the first intermediate is used for the pentose-phosphate pathway, which produces ribose-5-phosphate, a precursor of nucleotide biosynthesis (Patra & Hay, 2014). Similarly, serine and glycine are produced from glyceraldehyde-3-phosphate.

Increased glutamine uptake is another hallmark of cancer metabolism that has emerged over the years. It was first reported by Harry Eagle, who showed that HeLa cells required significantly more glutamine in their culture medium compared with other amino acids (Eagle, 1955). Further studies have confirmed increased glutamine uptake has been reported in numerous cancers *in vivo* (Sauer et al., 1982; Yuneva et al., 2012). This dependency of many cancers on glutamine is likely to be driven by the increased expression of MYC in cancer, which has been shown to induce a transcriptional programme of genes involved in glutamine metabolism (Yunev et al., 2007), such that many cancers are 'addicted' to glutamine (Wise & Thompson, 2010). It should be noted that *c-MYC* has been identified as a target of the Wnt pathway in colorectal cancer cells (He et al., 1998) and that deletion of MYC *in vivo* suppresses the crypt progenitor phenotype following APC loss in the murine intestine (Sansom et al., 2007). Hence targeting glutamine metabolism in our mouse models may be of therapeutic benefit. As with glucose being a source of carbons for biosynthesis, cancer cells utilise the nitrogen atoms from glutamine for the biosynthesis of macromolecules, including numerous amino acids, such as asparagine (Zhang et al., 2014), and nucleotides (DeBerardinis et al., 2007) – and hence glutamine is required for cell growth and division.

5.1.2 Metabolomics

Much like proteomics, mass spectrometry has been applied to biological samples to study metabolites within those samples. Often, before samples enter the mass spectrometer they are separated by liquid chromatography, whilst this is less high-throughput than direct injection of the analyte into the mass spectrometer, it minimises signal suppression and allows for increased sensitivity (Johnson et al., 2016). The use of a mass spectrometer allows for untargeted metabolomics, however given the profound deregulation of glycolysis and glutaminolysis in many cancer types, there has been a focus on targeted metabolomics for cancer metabolomics, using a pre-determined list of

metabolites of interest (Zamboni et al., 2015). This approach can give information on absolute levels of metabolites within samples – it may be useful to look at the uptake or release of metabolites from cell lines or within tissue samples, however, it does not provide a much insight into the source of these metabolites. In order to address this, one can use stable-isotope labelled metabolites, such as ^{13}C-U-Glucose, to trace metabolites and the flux through particular metabolic pathways (Zamboni et al., 2015).

5.1.3 Targeting glutaminolysis

Since the paradigm that many cancers are 'addicted to glutamine', there has been much interest in targeting glutaminolysis. For instance, the development of GLS (glutaminase) inhibitors allows for the targeted disruption of the first step of glutaminolysis – the deamination of glutamine to glutamate. For instance, CB-839, a GLS inhibitor, has been shown to inhibit the growth of two triple negative breast cancer cell lines in a xenograft model (Gross et al., 2014). Downstream of this reaction, glutamate can be further deaminated by glutamate-pyruvate transaminase (GPT) to produce alanine and α-ketoglutarate. There are two different isozymes of GPT, a cytoplasmic form GPT1 and a mitochondrial form GPT2. GPT2 has recently been shown to catalyse the production of alanine from glutamate, and serve as a critical coupling point of the Warburg effect and glutaminolysis (Smith et al., 2016). Interestingly, GPT2 has been shown to be upregulated in human colorectal cancer, but also in response to a variety of oncogenic mutations including RAS/mutant p53 (Smith et al., 2016) and oncogenic *PIK3CA* mutations (Hao et al., 2016). Moreover, GPT2 has also been shown to be a transcriptional target of ATF4 (Salgado et al., 2014; D'Aniello et al., 2015; Hao et al., 2016), hence the upregulation of ATF4 that I observe in APC KRAS intestinal epithelial cells could lead to increased GPT2 expression and other metabolic changes in response to ER stress. In this chapter I will discuss the changes in the metabolomes of APC and APC KRAS cells, identified via ^{13}C-glucose and glutamine tracing, as well as the specific targeting of GPT2 in APC KRAS cells.

5.2 Altered metabolism between APC and APC KRAS intestinal epithelial cells

5.2.1 APC crypt cultures are highly glycolytic, whilst APC KRAS cultures are dependent on glutamine

Glucose and glutamine starvation *in vitro* revealed that APC and APC KRAS crypt cultures are both highly glycolytic, although it should be noted that glucose removal slowed the growth of WT crypt cultures also. However, APC KRAS crypt cultures were highly dependent on glutamine for growth (Fig5.1 – Fatih Ceteci). To determine a functional role for glucose and glutamine in WT, APC and APC KRAS crypts cultures, ^{13}C-U-labelled-D-glucose and ^{13}C-U-L-glutanime were traced *in vitro*. In accordance with APC and APC KRAS crypt cultures being highly glycolytic, there was a significant increase in glucose uptake by APC KRAS crypt cultures compare with APC and WT crypt cultures (Fig5.2a). This increase in glucose uptake was accompanied by a significant release of $^{13}C_3$-labelled lactate by both APC and APC KRAS crypt cultures compared with WT crypt cultures (Fig5.3b). Interestingly, there was a significant increase in the secretion of $^{13}C_3$-labelled alanine into the media specifically from APC KRAS crypt cultures and not WT or APC cultures (Fig5.3c), suggesting that APC KRAS crypt cultures are synthesising alanine from the carbons of glucose.

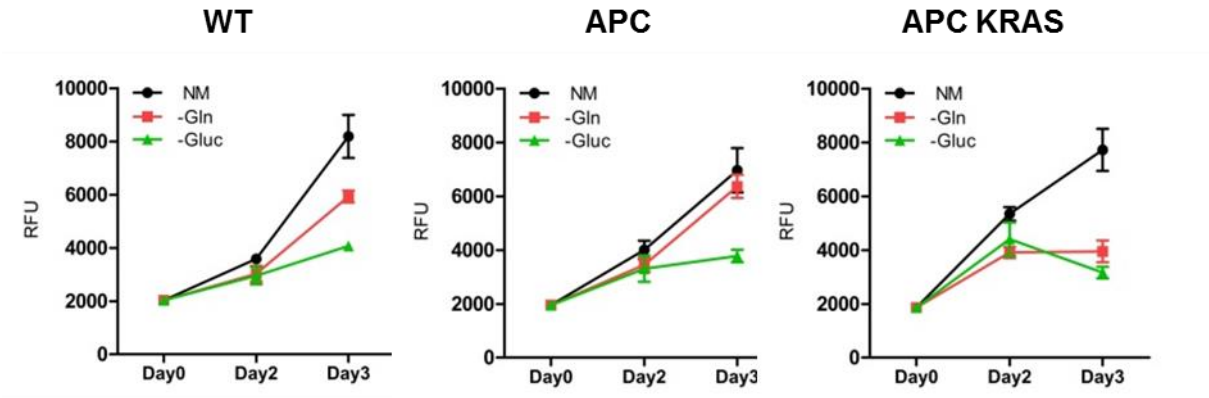

Figure 5.1: APC KRAS crypt cultures are dependent on glucose and glutamine for growth

Proliferation assay for WT, APC and APC KRAS small intestinal crypt cultures grown in response to either complete media (NM), glucose-free media (-Glc) or glutamine-free media (-Glu). Proliferation assayed via cell titre blue assay each day. (Fatih Ceteci)

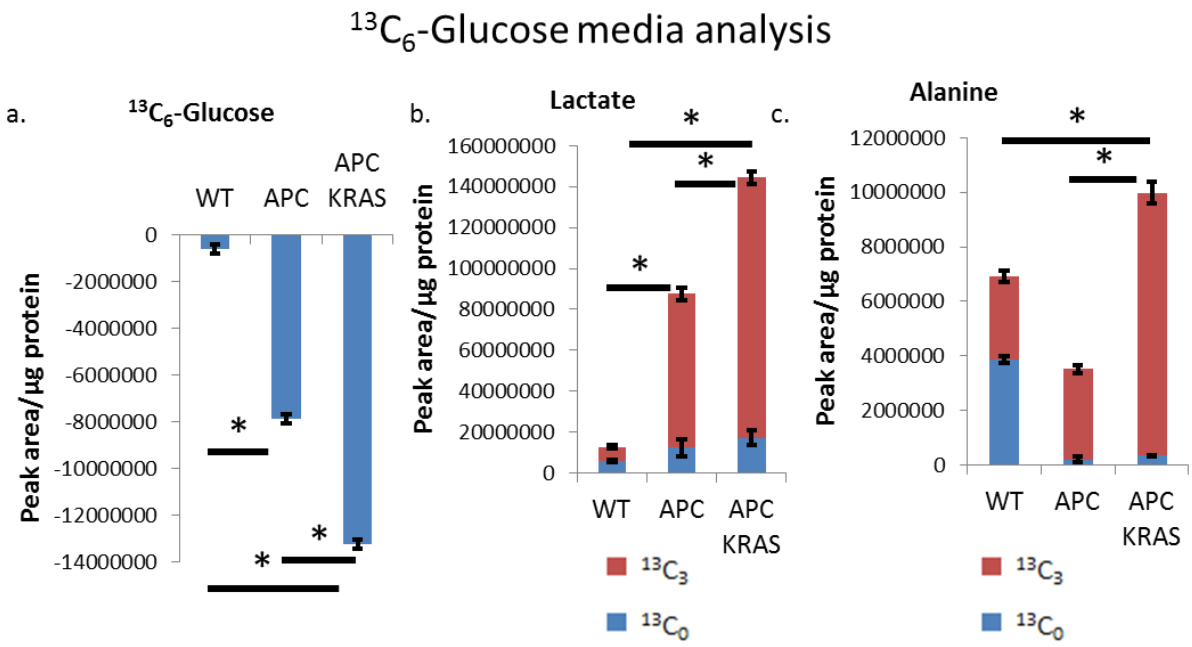

Figure 5.2: APC KRAS and APC crypt cultures are highly glycolytic

WT, APC and APC KRAS small intestinal crypts were grown in complete crypt culture media, supplemented with 10mM ^{13}C-U-Glucose for 24 hours, media and intracellular metabolites collected for analysis. Bar charts of media levels of a. $^{13}C_6$-Glucose b. $^{13}C_3/^{13}C_0$-lactate and c. $^{13}C_3/^{13}C_0$-alanine. Data displayed +/- SEM. Three cell lines for each genotype used, in technical triplicate. One-way Mann-Whitney *U* test, p=0.0405 (*). Data collected by Fatih Ceteci, analysis by David Gay

Glutamine tracing confirmed a significant increase in glutamine uptake by APC KRAS crypt cultures compared with WT and APC crypt cultures (Fig5.3a). This increased glutamine uptake was accompanied by an increase in $^{13}C_5$-glutamate secretion by APC KRAS crypt cultures, compared with APC crypt cultures (Fig5.3b), suggesting that the glutamine which is taken up by these cells is converted to glutamate. This is further supported by the observation that there is a significant increase in intracellular levels of $^{13}C_5$-glutamate in APC KRAS crypt cultures compared with WT crypt cultures (Fig5.3d), but also a significant decrease in intracellular $^{13}C_5$-glutamine in APC KRAS crypt cultures, compared with APC and WT crypt cultures (Fig5.3c), again suggesting that the glutamine which is taken up by APC KRAS crypt cultures is converted to glutamate.

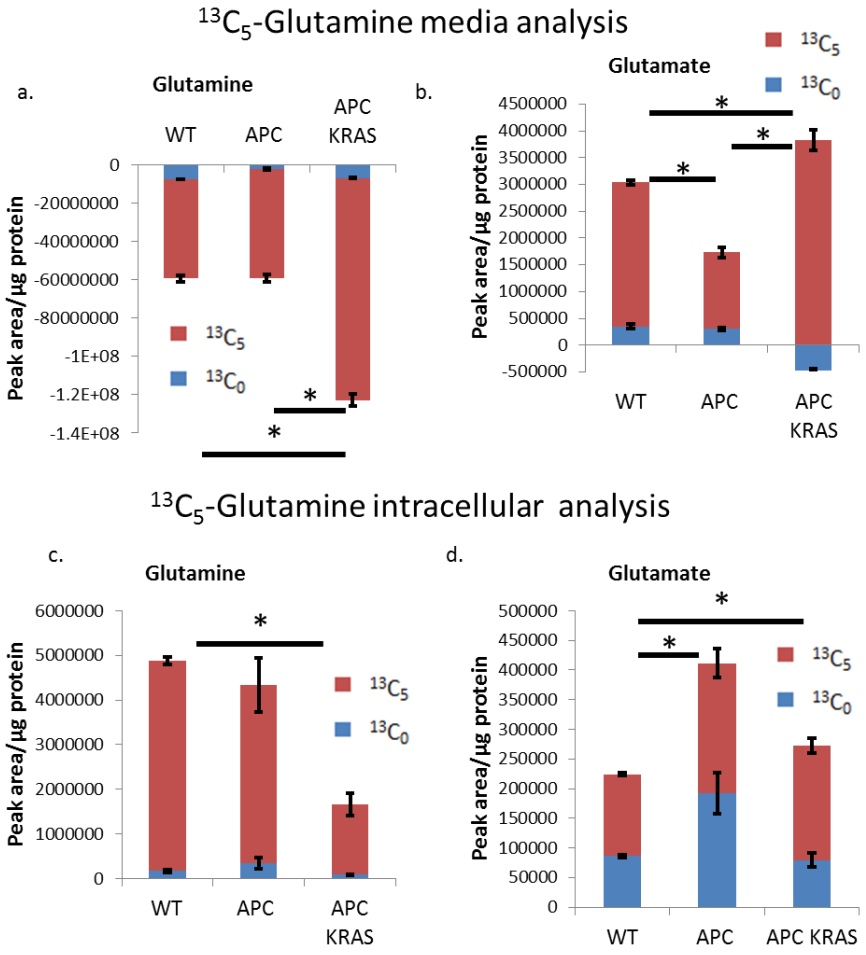

Figure 5.3: APC KRAS crypt cultures consume glutamine

WT, APC and APC KRAS small intestinal crypt cultures were grown in complete crypt culture media, supplemented with 2mM ^{13}C-U-Glutamine for 24 hours, media and intracellular metabolites collected for analysis. Bar charts of media levels of a. $^{13}C_5/^{13}C_0$-Glutamine b. $^{13}C_5/^{13}C_0$-Glutamate. Bar charts of intracellular levels of c. $^{13}C_5/^{13}C_0$-Glutamine d. $^{13}C_5/^{13}C_0$-Glutamate. Data displayed +/- SEM. Three cell lines for each genotype used, in technical triplicate. One-way Mann-Whitney *U* test, p=0.0405 (*). Data collected by Fatih Ceteci, analysis by David Gay

5.2.2 Altered expression of metabolic genes in APC KRAS compared with APC

Given that both APC and APC KRAS crypt cultures show increased glycolysis compared with WT crypt cultures, and APC KRAS cultures are dependent on glutamine, I sought to determine whether there is an increase in the expression of genes involved in glycolysis and glutaminolysis in both APC and APC KRAS intestinal epithelial cells. I mined our RNASeq data to look for the expression levels of genes involved in glycolysis and glutaminolysis in WT, APC and APC KRAS intestinal tissue. There was a strong upregulation of glycolytic genes in APC KRAS intestines, compared with APC and WT (Fig5.4a), including genes such as Hexokinase 1 (*Hk1*) and *Slc2a1*, the glucose transporter. It should be noted that HK1, SLC2A1 and Hexokinase 2 (HK2) were upregulated in APC

KRAS crypt cultures compared with APC crypt cultures in the SILAC data. The increased expression of HK1 and HK2 in APC KRAS intestinal crypt cultures was confirmed via immunoblotting (Fig5.4b). There was also a profound upregulation in the genes involved in glutaminolysis, such as *Gpt2* and *Slc1a5* – the glutamine transporter (Fig5.4a). I confirmed increased expression of *Gpt2* and *Slc1a5* via RNAScope (Fig5.4c). Interestingly, both *Gpt2* (Salgado et al., 2014) and *Slc1a5* (Timosenko et al., 2016) are ATF4 targets, thus some of the metabolic changes I observe could be driven by increased protein synthesis and ER stress, and that this is a mechanism by which the cells are able to adapt and survive.

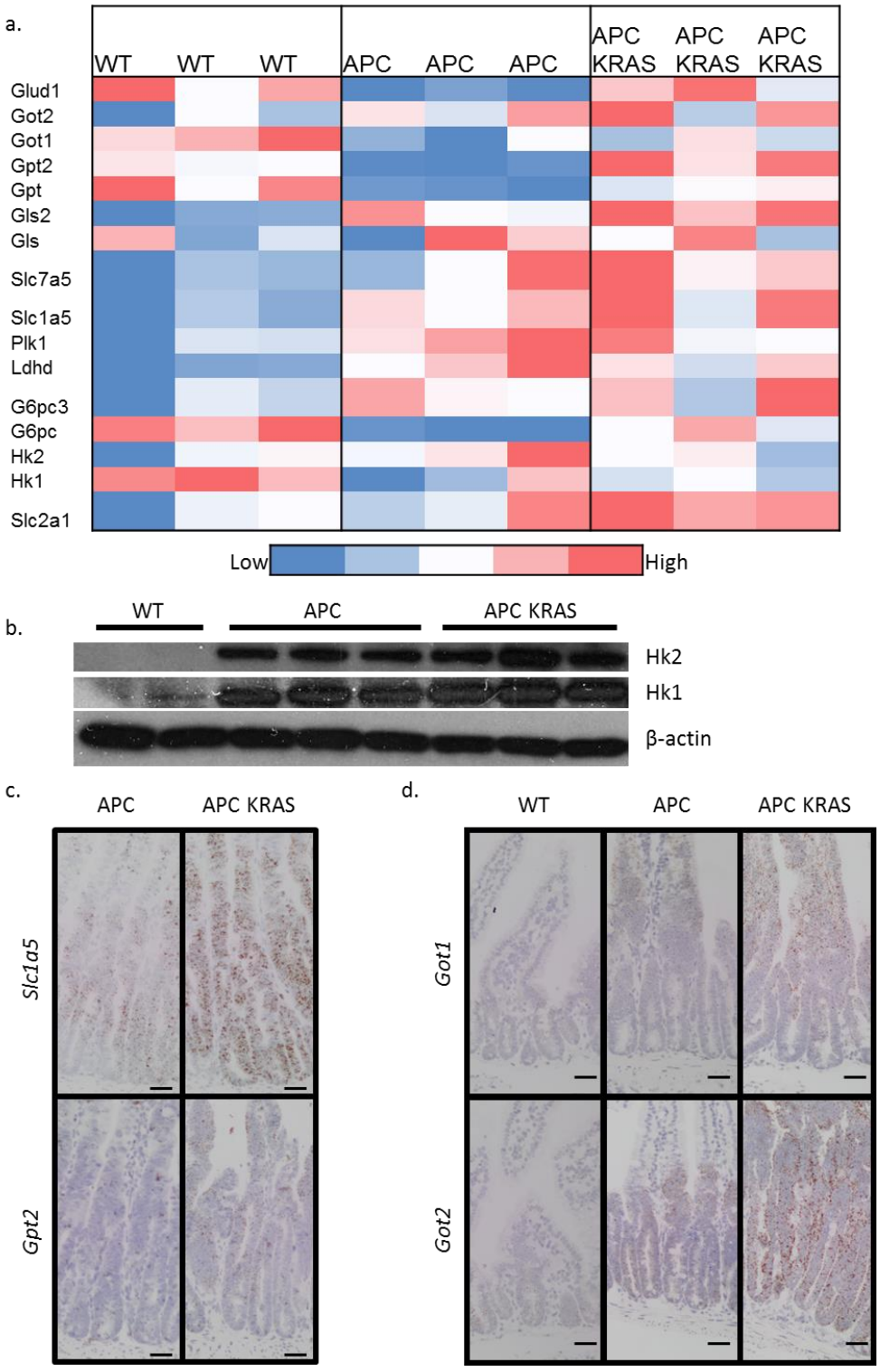

Figure 5.4: Altered expression of genes involved in glycolysis and glutaminolysis between APC and APC KRAS intestinal epithelial cells

a. Heat-map for genes involved in glutaminolysis and glycolysis from RNASeq data obtained from small intestinal tissue from WT, APC and APC KRAS mice. b. Immunoblot for HK2, HK1 and ß-actin on lysates from WT, APC and APC KRAS small intestinal crypt cultures. c. *Slc1a5* and *Gpt2* RNAScope on small intestinal sections from APC and APC KRAS mice. d. *Got1* and *Got2* RNAScope on small intestinal sections from WT, APC and APC KRAS mice. Scale bars = 40µm

Within this dataset, there is a switch in the expression in a number of enzymes that catalyse reversible reactions in different cellular compartments between the different genotypes. For instance, there is a decrease in the expression in the cytosolic gene glutamate-pyruvate transaminase 1 (*Gpt1*), whilst the mitochondrial isoform glutamate-pyruvate transaminase 2 (*Gpt2*) is upregulated in APC KRAS intestines (Fig5.4a). A similar pattern is seen with another transaminase, glutamic-oxaloacetic acid transaminase (*Got*), whereby the mitochondrial form (*Got2*) is upregulated in APC KRAS compared with APC, and there is no major change in the expression of the cytoplasmic form, *Got1*. I confirmed these changes in expression using RNAScope (Fig5.4d). The change in expression of different isoforms, in addition to the upregulation of certain metabolic genes confirms the altered metabolism in APC KRAS intestinal epithelial cells. This metabolic rewiring may provide novel therapeutic targets for intervention.

To investigate this, I analysed the expression of some of these genes in human colorectal cancer using Oncomine (Skrzypczak et al., 2010) (Fig5.5). The overall pattern of expression of these genes overlapped pretty well between the mouse data and human data, but what was very striking was that the isoform switch was also present – *GPT2* is not expressed in the normal colonic epithelium, however it is upregulated in both adenomas and adenocarcinomas, whilst *GPT1* shows that opposite expression pattern, again supporting the notion that some of these metabolic genes could prevent viable therapeutic targets, given their specific upregulation in transformed tissue. Investigating the role of GPT2 in KRAS-driven tumourigenesis will be discussed in greater detail later in this chapter

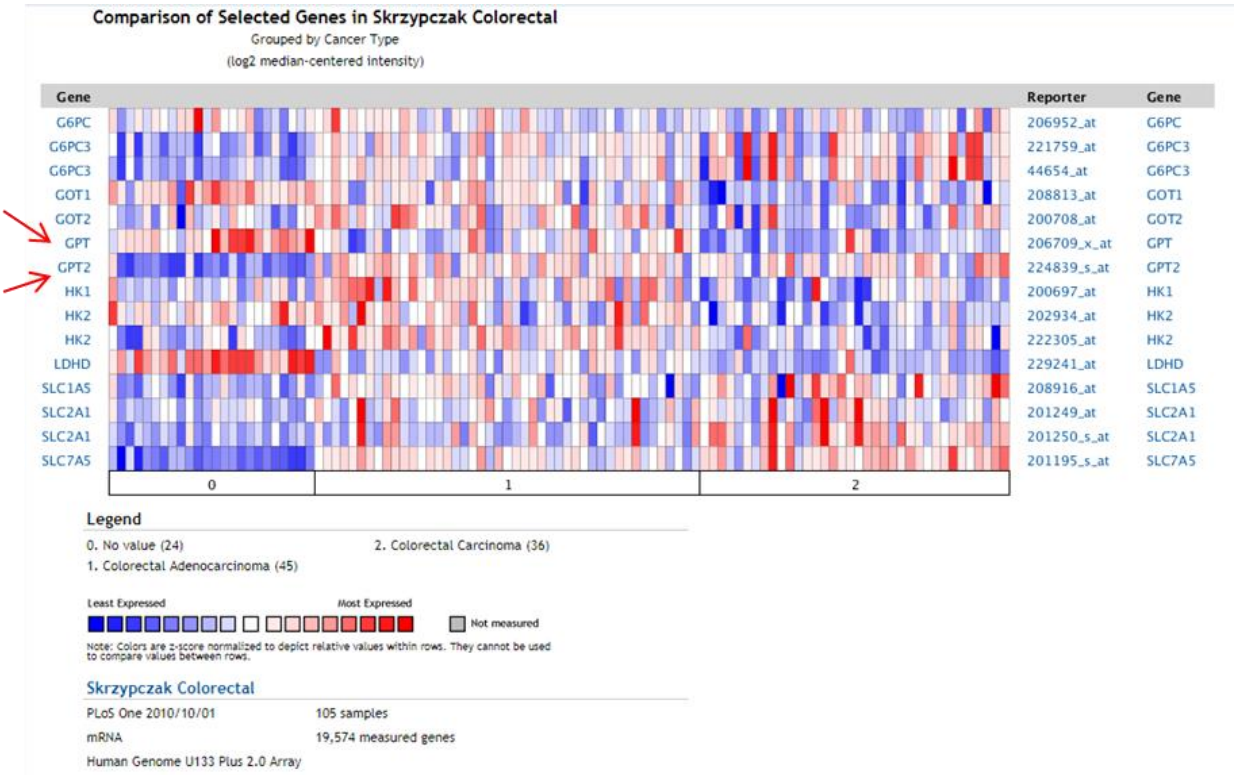

Figure 5.5: Increased expression in GPT2 in human colorectal cancer
Heatmap taken from Oncomine analysing the expression of genes involved in glycolysis and glutaminolysis in human colorectal cancer. Dataset from (Skrzypczak et al., 2010). Red arrows indicate *GPT1* and *GPT2* expression data.

5.2.3 Fasting significantly reduces proliferation in APC KRAS small intestines

I have shown that acute loss of APC along with KRAS activation in the intestinal epithelium drives a significant increase in protein synthesis, and that this is accompanied by alterations in metabolism – these cells are highly glycolytic and their growth is dependent on glutamine. Indeed, a number of markers of 'nutrient stress' are increased in these cells compared with APC-deficient intestinal epithelial cells. This suggests that these cells are trying to regulate their protein synthesis and adapt to the large energetic burden of this process. Hence, it would be interesting to try and 'stress' these cells further, for example by starving these cells of nutrients. In order to assess this *in vivo*, I fasted WT, APC and APC KRAS mice for 16 hours prior to sampling. Fasting significantly decreased proliferation in the small intestine of APC KRAS mice compared with controls on normal chow; however there was no difference in proliferation in the small intestines of WT and APC mice (Fig5.6). Interestingly, there was no effect on proliferation in the colon of APC KRAS mice, whilst proliferation is significantly reduced in the colons of WT and APC mice upon fasting (Fig5.6c).

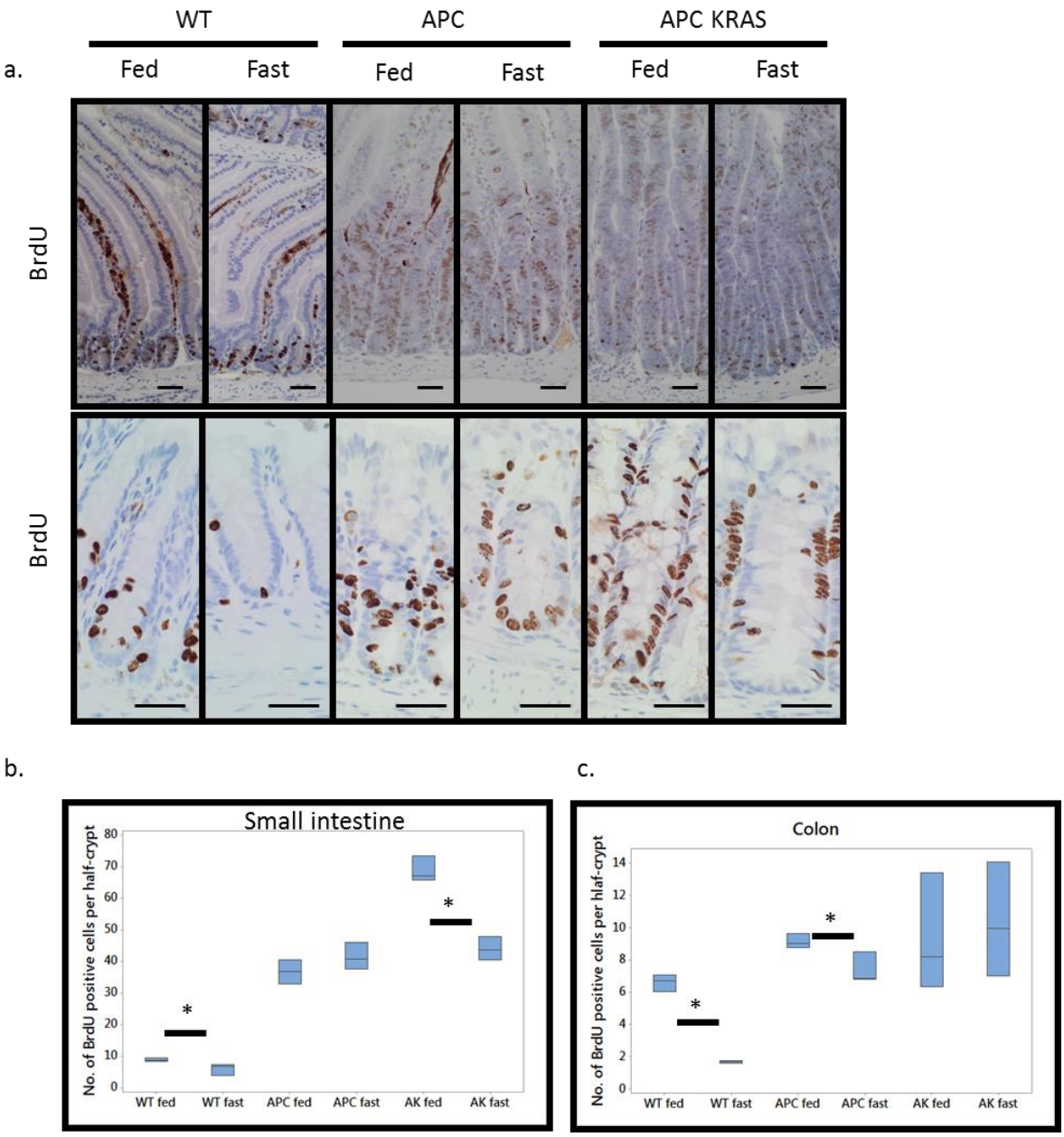

Figure 5.6: Fasting significantly reduces proliferation in APC KRAS small intestines

a. BrdU staining of WT, *VillinCre^{ER} Apc$^{fl/fl}$* (APC), *VillinCre^{ER} Apc$^{fl/fl}$ Kras$^{G12D/+}$* (APC KRAS) small intestines (upper panel) and colons (lower panel) given normal chow *ad libitum* (Fed) or fasted (Fast) for 16 hours prior to sampling, scale bars = 40μm . BrdU scoring of b. Small intestines and c. colons from WT, APC and APC KRAS that were either fed or fasted for 16 hours prior to sampling, no. of BrdU positive cells per half-crypt scored, 25 crypts per mouse scored. n=3 for each group, one-way Mann-Whitney *U* test, p=0.0405 (*).

Upon fasting in all three models, I observe a mild increase in phosphorylation of the α-subunit of AMP-activated kinase (AMPK) at Thr172, indicating activation of AMPK (Fig5.7a), indicating an increase in the AMP: ATP ratio. Given that mTORC1 is a master regulator of growth and integrates numerous signalling pathways, including nutrient sensing, I stained for one of its' downstream targets, phosphorylation of ribosomal protein S6 (S6) in the fed and

fasted mice. Fasting ng reduced phospho-S6 staining in the WT intestines, but not the intestines of APC and APC KRAS mice (Fig4.15b). This suggests that nutrient sensing and mTORC1 activity are uncoupled in APC and APC KRAS intestinal epithelial cells, or that there is significant signal rewiring following APC loss and KRAS activation to alter mTORC1 activity, since it has been shown that loss of APC leads to hyperactivation of mTORC1 (Faller et al., 2015). Furthermore, this would also suggest that activation of mTORC1 in APC and APC KRAS intestines is independent of mTORC1's nutrient sensing activity.

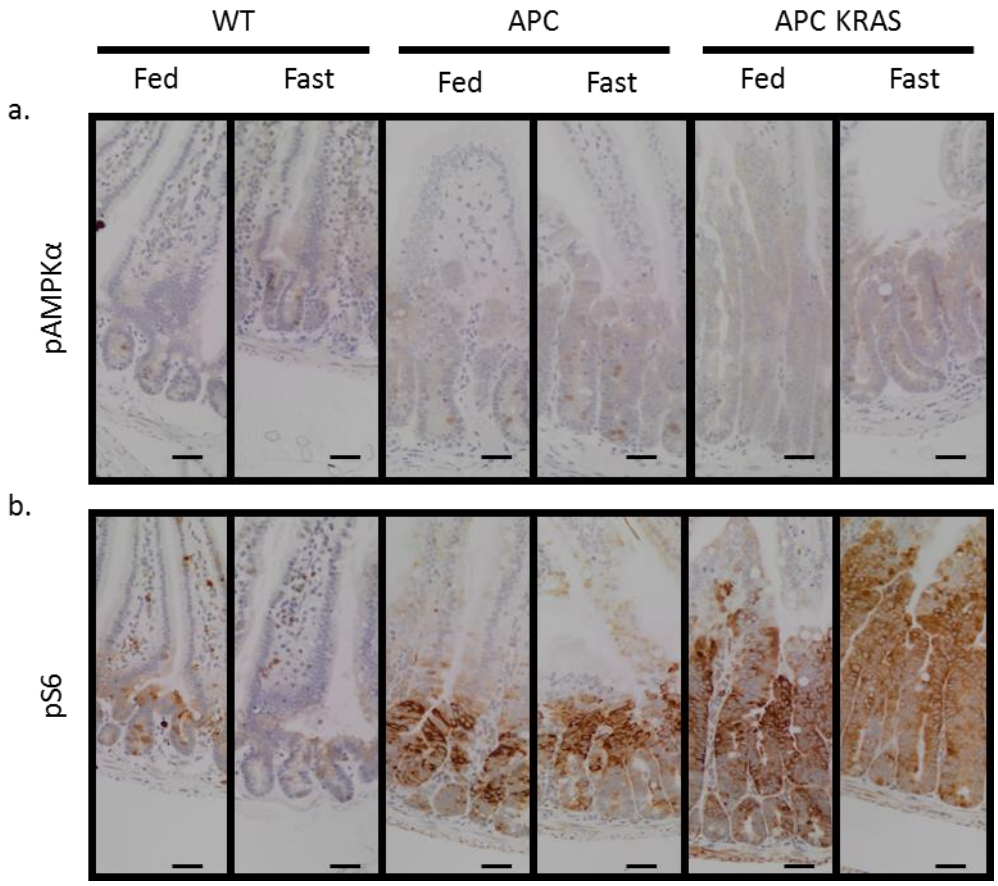

Figure 5.7: Fasting activates AMPK in the mouse intestine
a. Phospho-AMPKα (Thr172) and b. phospho-ribosomal protein S6 (Ser235/236) staining of small intestinal sections from WT, APC and APC KRAS mice that were either given food *ad libitum* (Fed) or fasted for 16 hours prior to sampling (Fast). Scale bars = 40μm

5.2.4 Dietary modulation of non-essential amino acids does not impact Kras-driven intestinal tumourigenesis

Fasting removes all nutrients from the mouse's diet, whilst this had a profound impact in intestinal proliferation in APC KRAS mice; it is not a viable therapeutic option. However, removal of dietary non-essential amino acids (NEAAs) is tolerated *in vivo* (Kamata et al., 2014), and hence provides a window

to study the role of dietary NEAAs in tumourigenesis. To investigate this, I placed *VillinCre*^{ER} *Apc*$^{fl/+}$ *Kras*$^{G12D/+}$ mice on a diet lacking 7 NEAAs: alanine, aspartic acid, asparagine, glutamate, glycine, proline and serine (-7AA) and a corresponding control diet, containing all 20 amino acids (20AA), for two weeks, induced them and aged them until clinical end-point. There was no difference in survival of the mice on these two diets, total tumour number and total tumour burden (Figs5.8a-c). However the tumours that did grow in the mice fed on the -7AA diet were smaller (Fig5.8d). This shows that whilst APC-deficient *Kras*-mutant intestinal tumours may grower slower in the absence of these seven NEAAs; they can grow independently of these seven dietary NEAAs. Amino acid profiling on the sera isolated from these mice at end-point confirmed a reduction in the circulating levels of glycine, serine and proline in the mice on the -7AA diet (Fig5.8e).

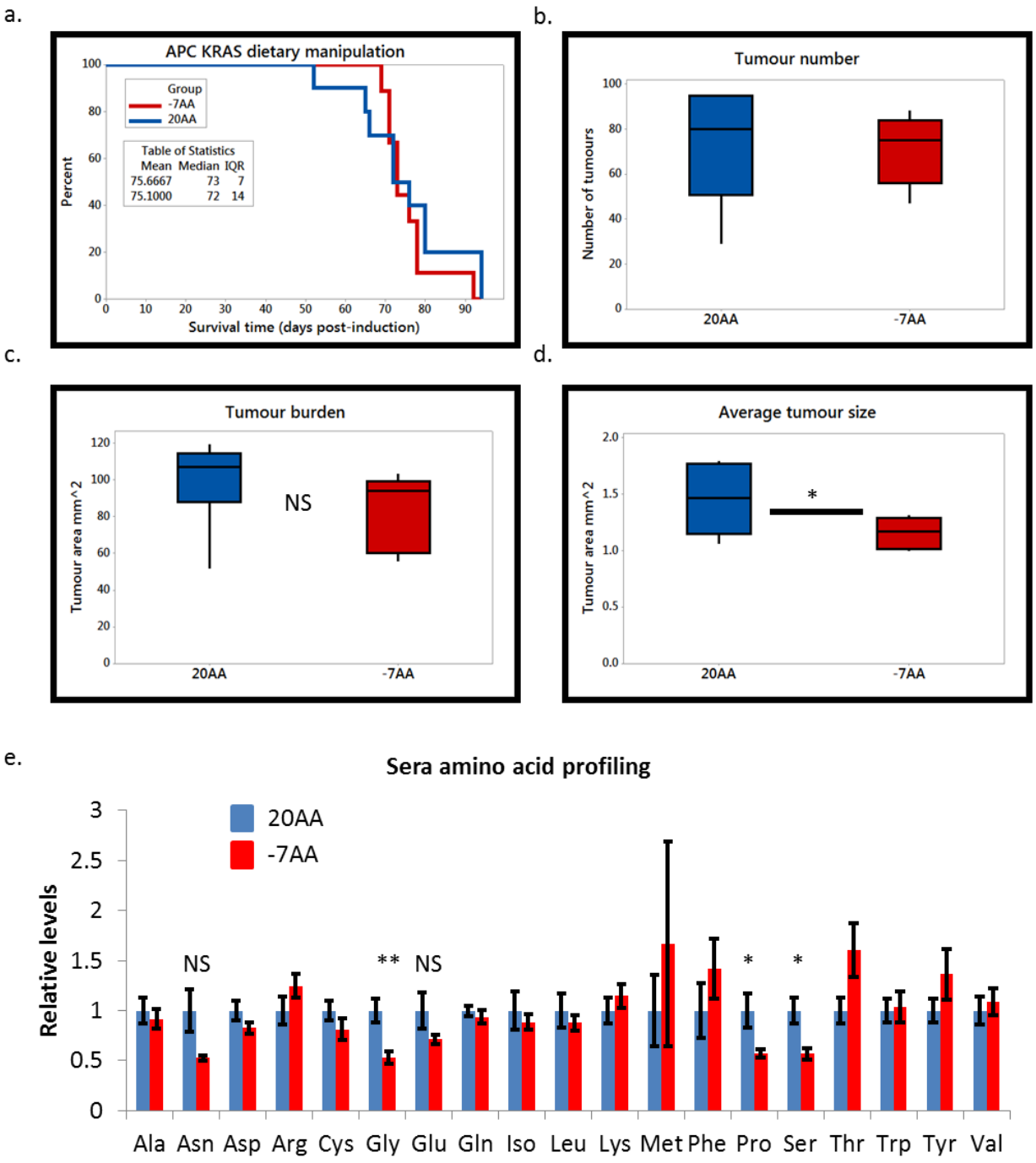

Figure 5.8: APC KRAS mice are refractory to dietary non-essential amino acid depletion

a. Survival curve (n=10 for 20AA, n=9 for -7AA), log-rank test, p=0.473 b. Tumour number c. Tumour burden and Average tumour size (n=6 for 20AA, n=7 for -7AA) for *VillinCre*^{ER} *Apc*$^{fl/+}$ *Kras*$^{G12D/+}$ mice that were placed on 20AA diet or -7AA diet (lacks alanine, asparagine, aspartic acid, glutamate, glycine, proline and serine) for two weeks, then induced and aged until clinical endpoint. One-way Mann-Whitney *U* test, p=0.26 (Tumour number), p=0.0502 (Tumour burden) and p=0.0371 * (Average tumour size). e. Amino acid profiling of sera from mice at endpoint, n=8 per group. Data displayed +/- SEM. One-way Mann-Whitney *U* test, p=0.135 for Asn, p=0.0014 for Gly, p=0.0639 for Glu, p=0.042 for Pro and p=0.012 for Ser.

5.2.5 APC KRAS crypt cultures upregulate *de novo* NEAA synthesis

Given that the -7AA diet did not impact intestinal tumourigenesis, despite a reduction in the circulating levels of these amino acids compared with mice on the control diet, I investigated whether APC KRAS crypt cultures were able to synthesize these amino acids *de novo*, since I have previously shown that APC KRAS crypt cultures can synthesize alanine from glucose (Fig5.2c), whilst exogenous glutamine is converted to glutamate (Fig5.3b). Glucose tracing confirmed that APC KRAS crypt cultures are able to synthesise both serine and glycine from glucose (Fig5.9a and Fig5.9b). Whilst glutamine tracing confirmed that proline is synthesized from glutamine by APC KRAS crypt cultures (Fig5.9c). Finally, I have previously shown that *Got1/2* and ASNS are upregulated in APC KRAS intestines (Fig5.4. and Fig4.5c), these are the transaminases that catalyse the production of aspartic acid and asparagine respectively, using the amide groups from glutamate and glutamine. Hence, it is likely that APC KRAS crypt cultures can also produce aspartic acid and asparagine *de novo*. These results show that APC KRAS intestinal epithelial cells are extremely metabolically flexible.

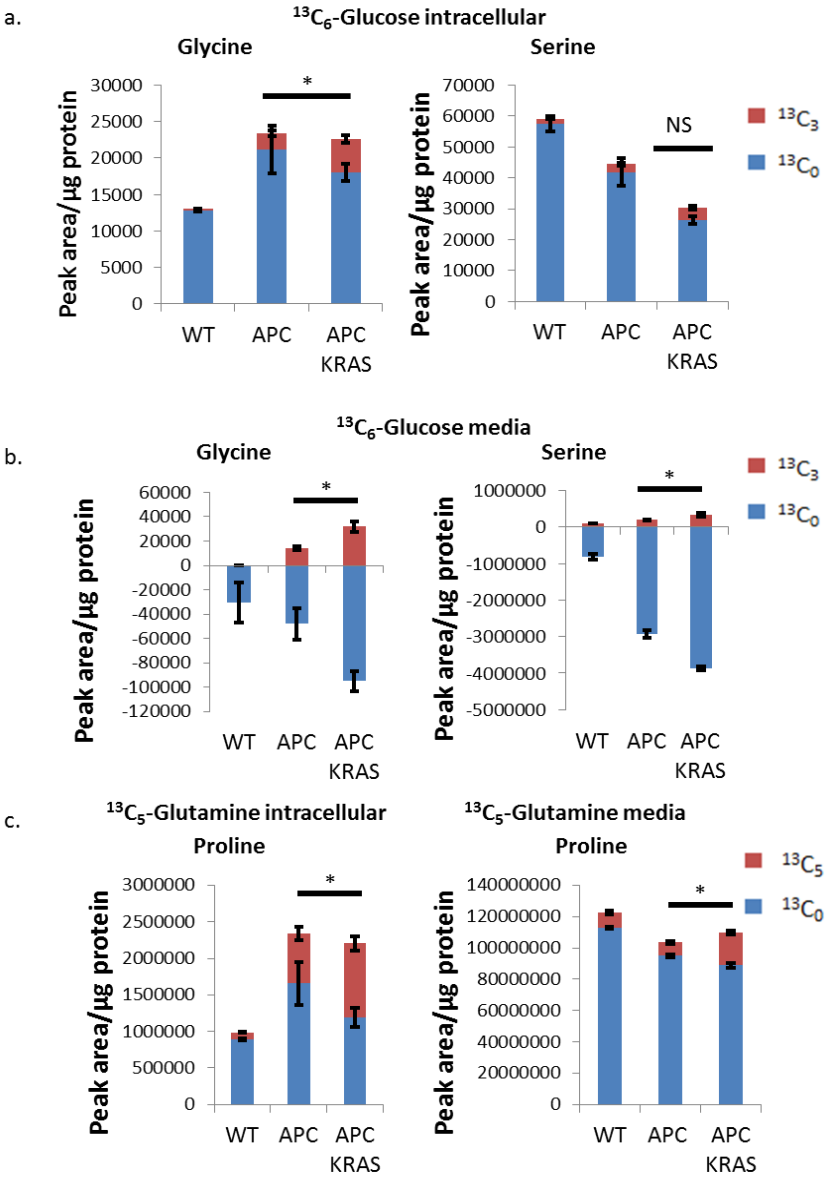

Figure 5.9: APC KRAS crypt cultures can synthesise glycine, proline and serine *de novo*

WT, APC and APC KRAS small intestinal crypt cultures were grown in complete crypt culture media, supplemented with 10mM ^{13}C-U-Glucose or 2mM ^{13}C-U-Glutamine for 24 hours, media and intracellular metabolites collected for analysis. Bar charts of intracellular levels of a. and media levels b. of $^{13}C_3/^{13}C_0$-glycine$^{13}C_3/^{13}C_0$-serine from crypt cultures grown with labelled glucose c. Bar charts of intracellular and media levels of $^{13}C_5/^{13}C_0$-proline from crypt cultures grown with labelled glutamine. Data displayed +/- SEM. Three cell lines for each genotype used, in technical triplicate. One-way Mann-Whitney *U* test, p=0.0405 (*).Data collected by Fatih Ceteci, analysis by David Gay.

5.3 Targeting GPT2 in APC KRAS cells

5.3.1 GPT2 is required for glutamine-derived and glucose-derived alanine production in APC KRAS crypt cultures

I have previously shown that APC KRAS crypt cultures produce large quantities of alanine, with the carbon backbone derived from glucose via pyruvate. It is thought that GPT2 could drive this transaminase reaction, given its' high expression in APC KRAS crypt cultures. To investigate this, I traced ^{15}N-α-L-glutamine and ^{13}C-U-D-glucose in *VillinCre^{ER} Apc$^{fl/fl}$ Kras$^{G12D/+}$* (APC KRAS) and *VillinCre^{ER} Apc$^{fl/fl}$ Kras$^{G12D/+}$ Gpt2$^{fl/fl}$* (APC KRAS GPT2) crypt cultures. There was a significant reduction in both intracellular and extracellular levels of ^{15}N-L-alanine and intracellular $^{13}C_3$-L-alanine, and an increase in $^{13}C_3$-pyruvate from the APC KRAS GPT2 crypt cultures, compared with APC KRAS crypt cultures (Fig5.10a-d). This suggests that GPT2 is the enzyme driving the production of L-alanine in APC KRAS crypt cultures, and is a nexus for both glycolysis and glutaminolysis in these cells.

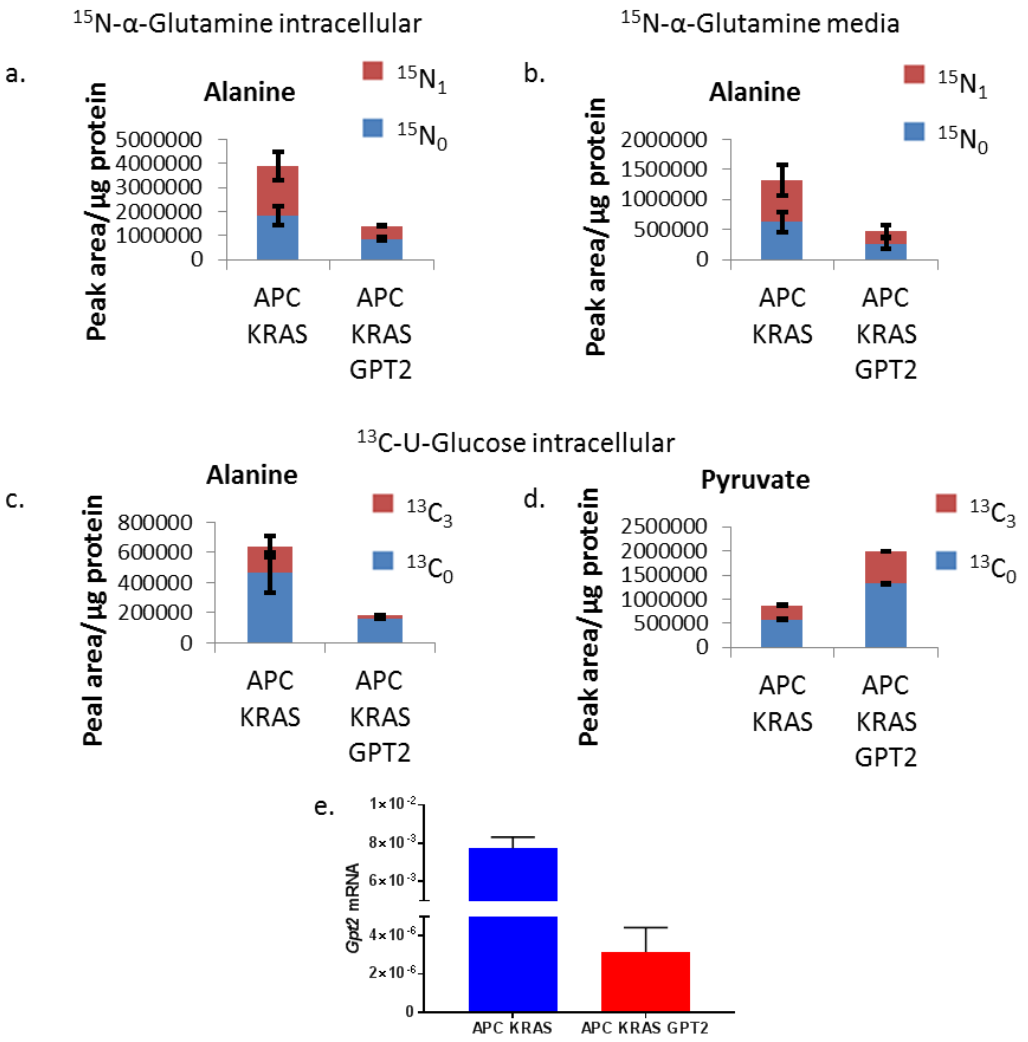

Figure 5.10: GPT2 is required for the production of glucose- and glutamine-derived alanine in APC KRAS GPT2 crypt cultures

APC KRAS and APC KRAS GPT2 small intestinal crypt cultures were grown in media containing ^{15}N-α-L-Glutamine or ^{13}C-U-D-Glucose for 24 hours and then media and intracellular metabolites were collected for analysis. Bar charts of a. intracellular levels $^{15}N_1$-L-alanine b. secreted $^{15}N_1$-L-alanine c. intracellular $^{13}C_3$-L-alanine and d. intracellular $^{13}C_3$-pyruvate from APC KRAS and APC KRAS GPT2 crypt cultures, data displayed +/- SEM, n=2 per group, four replicates for each cell line. e. qRT-PCR for *Gpt2* expression in APC KRAS and APC KRAS GPT2 small intestinal crypt cultures, n=2 per group, data displayed +/- SEM.

5.3.2 Alanine is required for the growth of GPT2-deficient APC KRAS organoids

Given the specific upregulation of GPT2 in APC KRAS intestinal epithelial cells, I hypothesized that the products of its reaction, L-alanine and α-ketoglutarate could play a functional role in the growth of these APC KRAS crypt cultures. To investigate this, I grew APC KRAS and APC KRAS GPT2 crypt cultures in alanine-free media and added back either alanine or a cell permeable form of α-ketoglutarate, dimethyl-2-oxoglutarate (DMOG). Alanine removal or addition of DMOG had no impact on the growth of APC KRAS crypt cultures; however it

was the presence of alanine in the media as opposed to DMOG that was required for the growth of APC KRAS GPT2 crypt cultures (Fig5.11a and Fig5.11b). This suggests that alanine production is required for the growth of APC KRAS crypt cultures and that they can overcome alanine starvation through *de novo* alanine synthesis via GPT2.

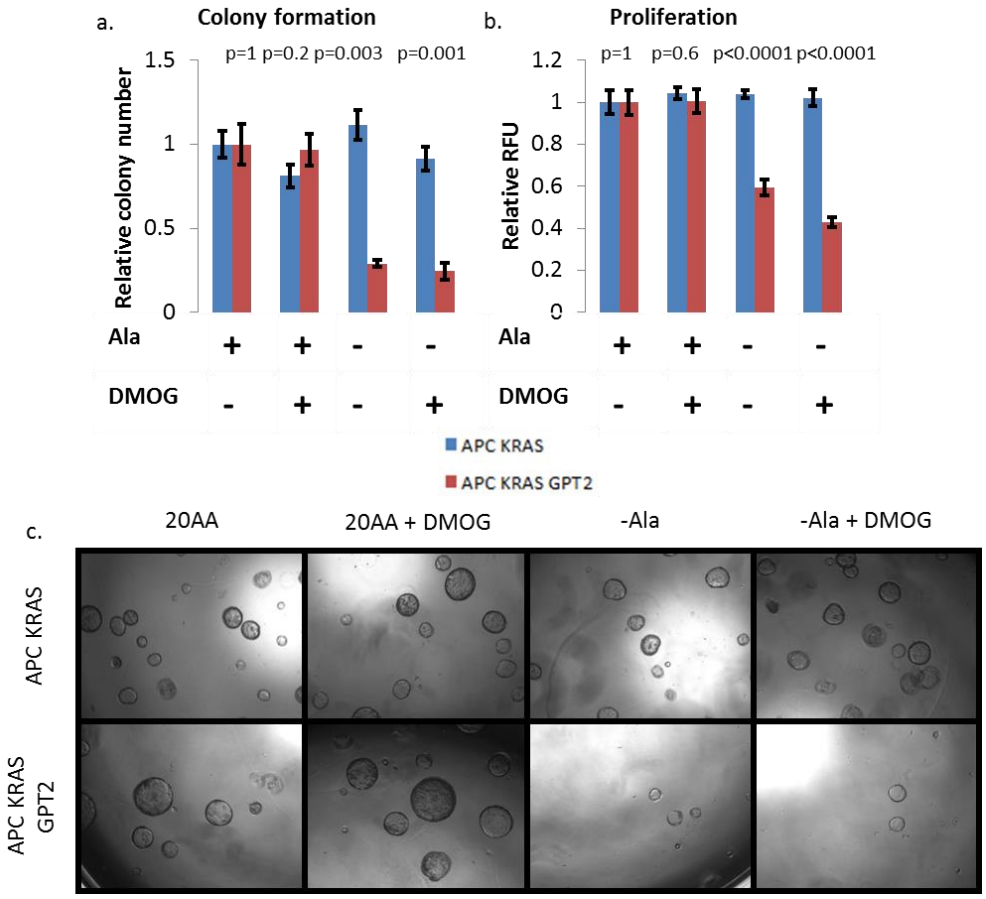

Figure 5.11: APC KRAS GPT2 crypt cultures are dependent on alanine not α-ketoglutarate for growth *in vitro*

a. Bar chart of colony formation b. Bar chart for relative viability and c. representative images of APC KRAS and APC KRAS GPT2 single cells (10,000/well) seeded in Matrigel and grown in complete ADF media (20AA) or alanine free ADF (-Ala) media with and without 1mM dimethyl-2-oxoglutarate (DMOG), scale bars = 200μm. Individual colonies were counted 72 hours post seeding and a cell titre blue assay performed 96 hours post seeding. n=1 for each genotype, with 4 technical replicates per condition. Data displayed +/- SEM. Images from 96 hours post-seeding.

5.3.3 GPT2 deletion does not affect the APC KRAS crypt progenitor phenotype

To determine whether GPT2 has a functional role in the early stages of tumourigenesis, I generated *VillinCre^{ER} Apc$^{fl/fl}$ Kras$^{G12D/+}$ Gpt2$^{fl/fl}$* (APC KRAS GPT2) mice and looked at proliferation three days post-induction compared with *VillinCre^{ER} Apc$^{fl/fl}$ Kras$^{G12D/+}$* (APC KRAS) mice. Deletion of GPT2 did not impact proliferation in the small intestine or colon compared with control mice (Fig5.12c). Interestingly I did observe an increase in apoptosis in these mice compared with controls, when scoring the number of apoptotic bodies from H&E sections, in both the small intestine and colon (Fig5.12a and Fig5.12d), highlighting a role for GPT2 in the survival of these cells following APC loss and KRAS activation. Whilst there was no difference in proliferation, the increase in apoptosis following GPT2 deletion may translate into increased survival in an intestinal model of intestinal tumourigenesis.

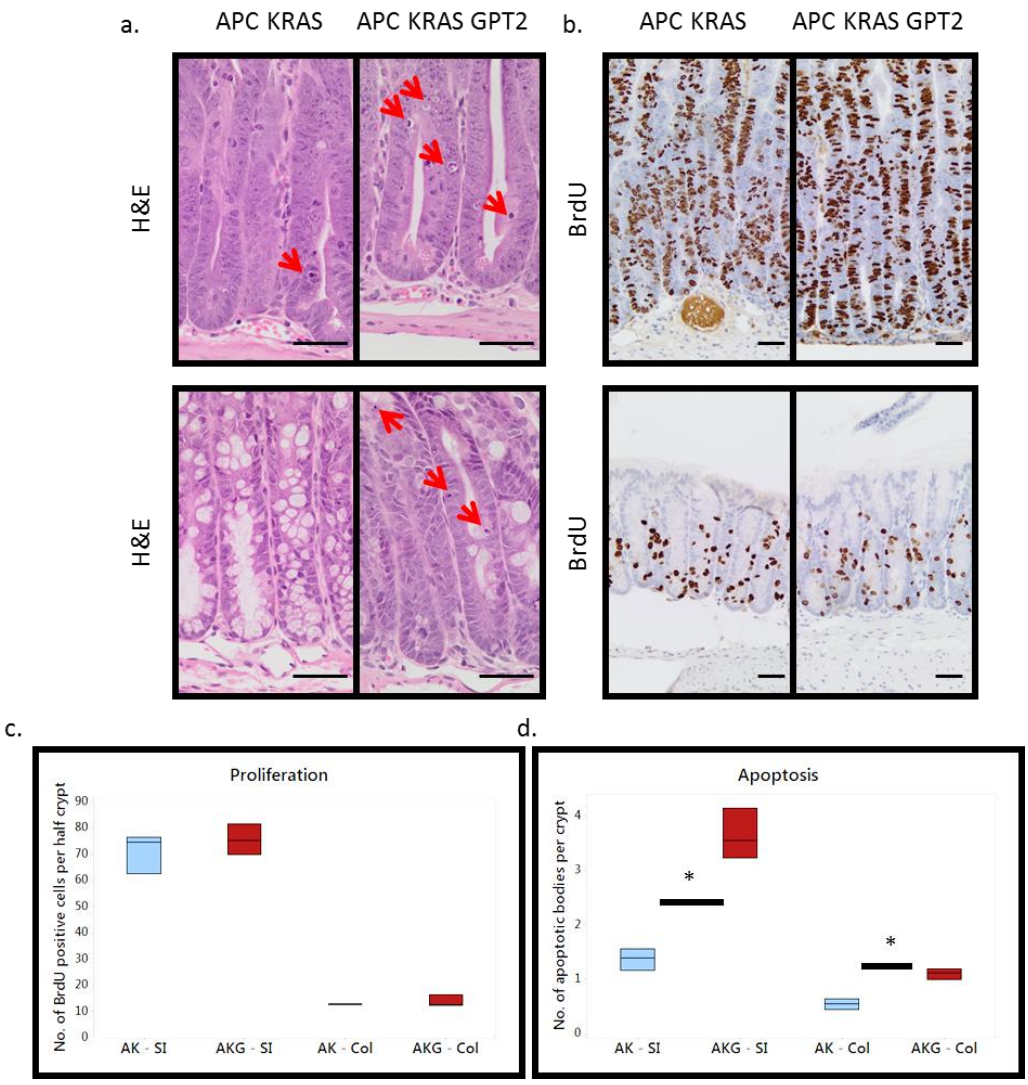

Figure 5.12: GPT2 does not suppress the APC KRAS crypt progenitor phenotype despite increasing apoptosis

a. H&E and b. BrdU staining of small intestines from tamoxifen-induced *VillinCre*^{ER} *Apc*$^{fl/fl}$ *Kras*$^{G12D/+}$ (APC KRAS) and *VillinCre*^{ER} *Apc*$^{fl/fl}$ *Kras*$^{G12D/+}$ *Gpt2*$^{fl/fl}$ (APC KRAS GPT2) mice sampled 3-days post-induction, scale bars = 40μm. c. BrdU scoring and d. apoptosis scoring of small intestines (SI) and colons (Col) from tamoxifen-induced *VillinCre*^{ER} *Apc*$^{fl/fl}$ *Kras*$^{G12D/+}$ (AK) and *VillinCre*^{ER} *Apc*$^{fl/fl}$ *Kras*$^{G12D/+}$ *Gpt2*$^{fl/fl}$ (AKG) mice sampled 3-days post-induction. Number of BrdU positive cells per half-crypt and apoptotic bodies per crypt were scored, 25 crypts per mouse, n=3, one-way Mann-Whitney *U* test, (*) p=0.0405, p=0.331 (SI proliferation) and p=0.5 (Colon proliferation)

5.3.4 GPT2 deletion accelerates intestinal tumourigenesis

To investigate whether GPT2 is required for KRAS-driven intestinal tumourigenesis, I generated *VillinCre*^{ER} *Apc*$^{fl/+}$ *Kras*$^{G12D/+}$ and *VillinCre*^{ER} *Apc*$^{fl/+}$ *Kras*$^{G12D/+}$ *Gpt2*$^{fl/fl}$ mice, induced them and aged them until clinical endpoint. Unexpectedly, GPT2 deletion actually accelerated tumourigenesis and decreased tumour latency (Fig5.13a). However, there was no difference in total tumour number or tumour burden (Fig5.13b and Fig5.13c). This would suggest that

following GPT2 deletion, the rate of tumour initiation is greater, however that these tumours do not grow significantly faster than the controls.

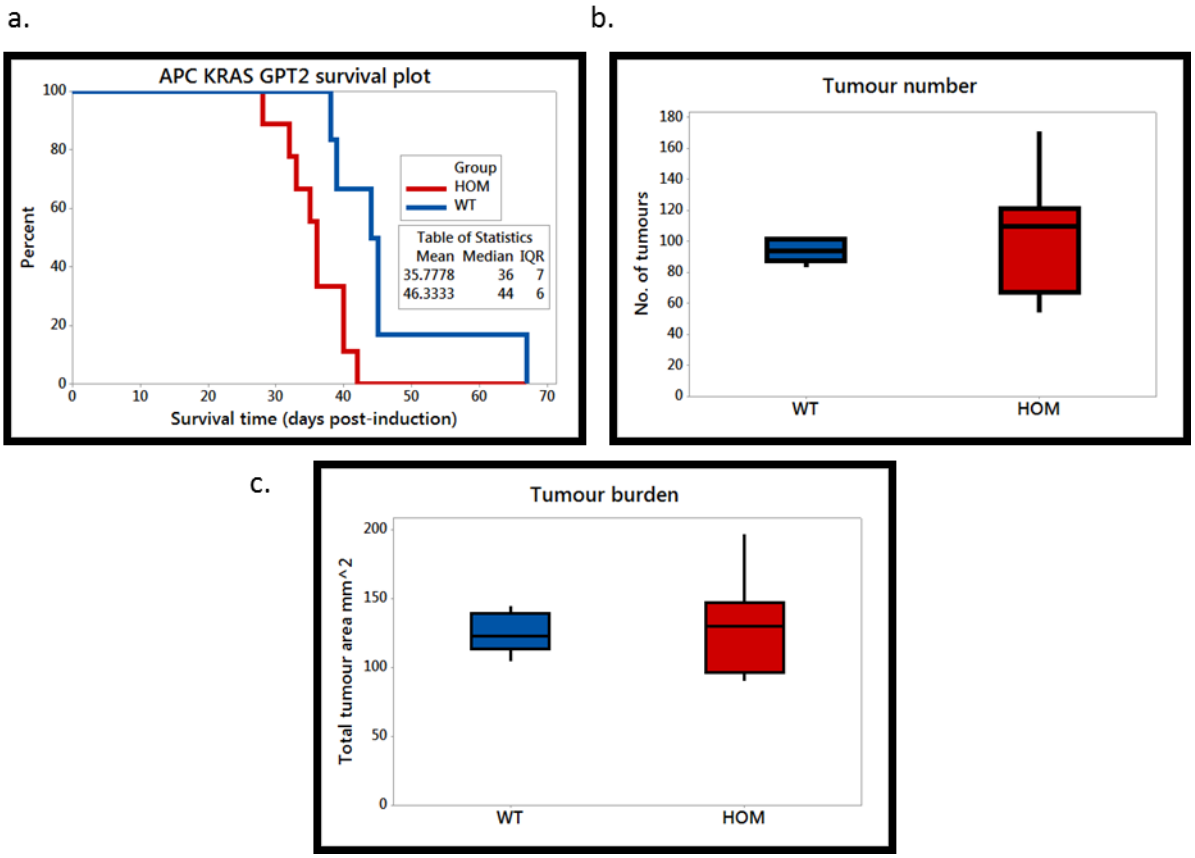

Figure 5.13: Deletion of GPT2 accelerates intestinal tumourigenesis
Tamoxifen-induced *VillinCre^{ER} Apc$^{fl/+}$ Kras$^{G12D/+}$* (WT) and *VillinCre^{ER} Apc$^{fl/+}$ Kras$^{G12D/+}$ Gpt2$^{fl/fl}$* (HOM) mice aged until clinical endpoint. a. Survival plot, n=7 (1 censor) for WT, n= 9 for HOM, log rank test p=0.008. b. Tumour number and c. Tumour burden boxplots, one-way Mann-Whitney *U* test p=0.26 (tumour number) and p=0.442 (tumour burden), n=5 for WT and n=8 for HOM.

5.3.5 Dietary manipulation extends survival of mice with GPT2-deficient tumours

Given that alanine is absolutely required for the growth of APC KRAS GPT2 crypt cultures, I sort to determine whether reducing systemic alanine levels could impact intestinal tumourigenesis in *VillinCre^{ER} Apc$^{fl/+}$ Kras$^{G12D/+}$ Gpt2$^{fl/fl}$* mice. Since alanine is a non-essential amino acid, it can be removed from the diets of mice, without significantly affecting the growth of the mice, unlike essential amino acids, such as isoleucine (Kamata et al., 2014). To investigate the role of alanine in intestinal tumourigenesis, I placed *VillinCre^{ER} Apc$^{fl/fl}$Kras$^{G12D/+}$* and *VillinCre^{ER} Apc$^{fl/+}$ Kras$^{G12D/+}$ Gpt2$^{fl/fl}$* mice on a control diet containing all 20 amino acids (20AA) or a diet lacking alanine (-5AA), along with four other non-essential amino acids: proline, aspartic acid, glutamate and

asparagine. There was no difference in survival between the *VillinCre*^{ER} *Apc*$^{fl/+}$ *Kras*$^{G12D/+}$ cohorts on the 20AA and -5AA diets, however, there was a significant extension in survival of *VillinCre*^{ER} *Apc*$^{fl/+}$ *Kras*$^{G12D/+}$ *Gpt2*$^{fl/fl}$ mice on the -5AA diet compared with the 20AA diet (Fig5.14a). Despite this extension in survival, there was no difference in tumour number or burden at end-point between these cohorts (Fig5.14b and Fig5.14c).

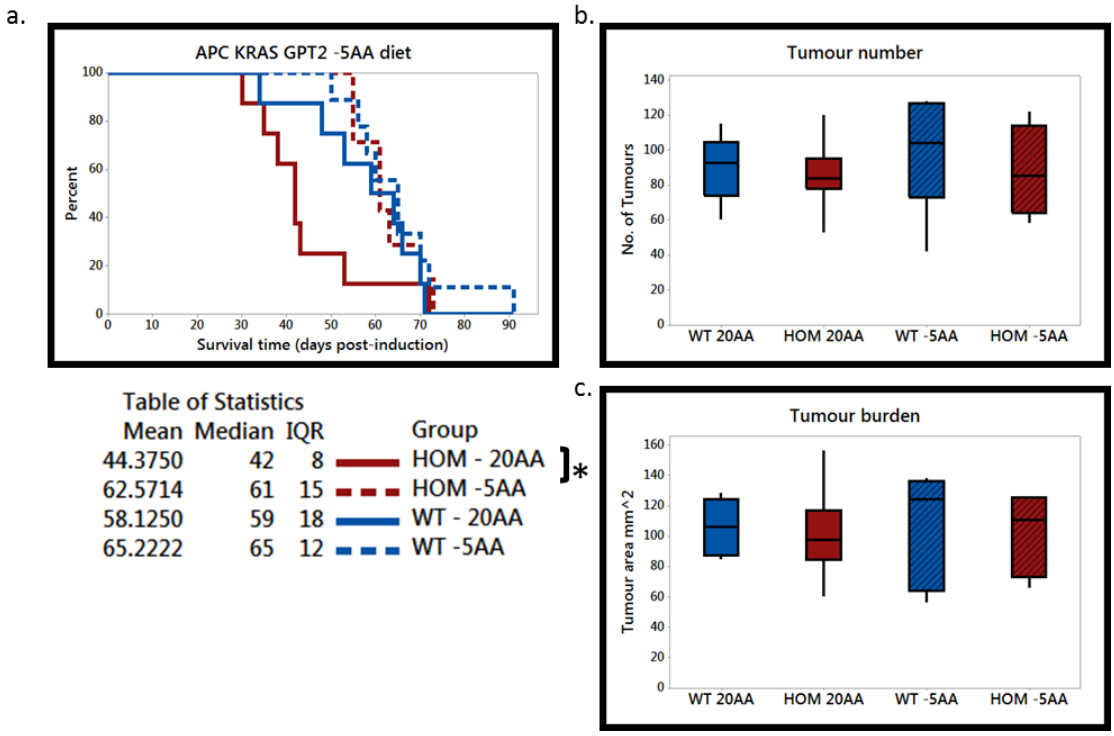

Figure 5.14: Dietary manipulation of non-essential amino acids extends survival of mice with GPT2-deficient tumours

VillinCre^{ER} *Apc*$^{fl/+}$ *Kras*$^{G12D/+}$ (WT) and *VillinCre*^{ER} *Apc*$^{fl/+}$ *Kras*$^{G12D/+}$ *Gpt2*$^{fl/fl}$ (HOM) mice were place on a control diet (20AA) or a diet lacking alanine, asparagine, aspartic acid, glutamate and proline (-5AA) two weeks prior to induction, then induced with tamoxifen and aged until clinical end-point. a. Survival curve (n=8 for WT 20AA, n=9 for WT=-5AA, n=8 for HOM 20AA and n=8 for HOM -5AA), log-rank test p=0.031 (HOM 20AA vs HOM -5AA) b. Tumour number and c. Tumour burden boxplots of mice at end-point (n=8 for WT 20AA, n=7 for WT=-5AA, n=7 for HOM 20AA and n=6 for HOM -5AA).

To determine whether this extension in survival was due to a cocktail of missing non-essential amino acids in the diet, or specifically alanine, I grew APC KRAS and APC KRAS GPT2 crypt cultures in media lacking alanine, proline, aspartic acid, glutamate and asparagine either in combination or individually. APC KRAS crypt cultures grew in all combinations; however the growth of the APC KRAS GPT2 crypt cultures was completely dependent on alanine *in vitro* (Fig5.15a). To determine whether this alanine dependency translated *in vivo*, I formulated two new diets – one diet lacking just alanine (-1AA) and another

lacking proline, aspartic acid, glutamate and asparagine (-4AA) and aged *VillinCre^{ER} Apc$^{fl/+}$ Kras$^{G12D/+}$ Gpt$^{fl/fl}$* mice on these diets. There was no survival benefit, compared with 20AA diet, of the mice place on the -1AA diet, although there was a moderate, albeit non-significant extension in survival in the mice on -4AA diet (Fig5.16a). Interestingly, there was an increase in the number of tumours in the -1AA *VillinCre^{ER} Apc$^{fl/+}$ Kras$^{g12D/+}$ Gpt$^{fl/fl}$* cohort, compared with control mice. Importantly, as per the -5AA diet, neither the -1AA or -4AA diet had affected survival in *VillinCre^{ER} Apc$^{fl/+}$ Kras$^{G12D/+}$* mice (Fig5.16a). This would suggest that despite loss of GPT2, these tumour cells are still metabolically flexible.

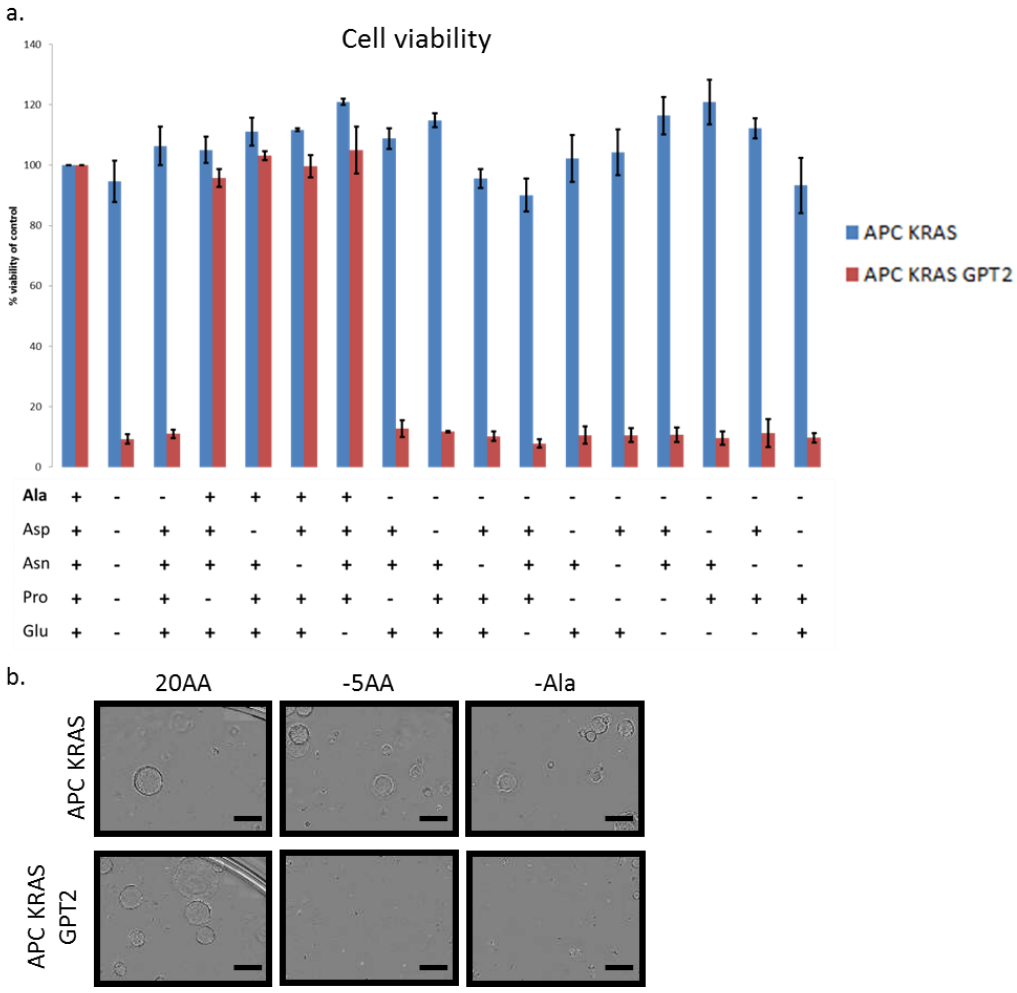

Figure 5.15: Alanine is specifically required for the growth of APC KRAS GPT2 crypt cultures

a. Bar charts of relative viability (normalised to complete media control), data displayed +/-SEM. b. Representative images of APC KRAS and APC KRAS GPT2 crypt cultures grown in media lacking certain non-essential amino acids. 10,000 cells/well were seeded in Matrigel/PBS (1:1) in Advanced D-MEM/F-12 lacking either alanine, proline, aspartic acid, glutamate or asparagine – in combination or individually. Viability was measured 96 hours post-seeding, after 4 hour incubation with Cell Titre Blue. Two biological replicates for each genotype, with four technical replicates per condition were used. Scale bars = 300μm.

a.

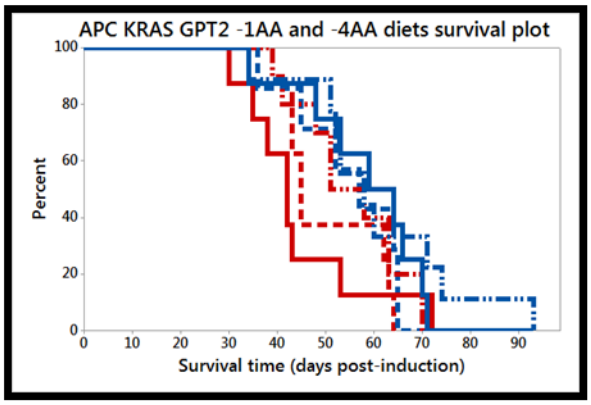

b.

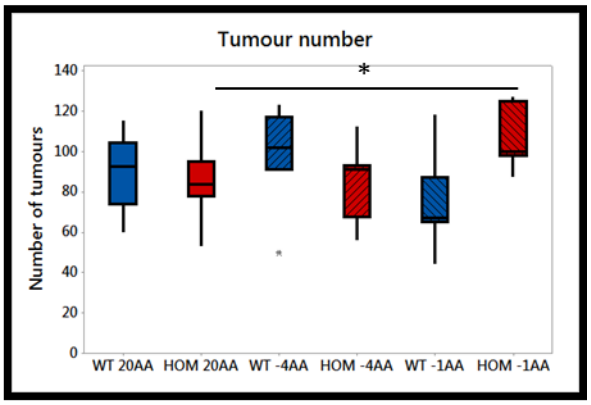

Table of Statistics

Mean	Median	IQR	Group	
50.1250	45	19	-1AA HOM	
54.8571	57	20	-1AA WT	
55.4000	51	15	-4AA HOM	NS
60.6667	58	19	-4AA WT	
44.3750	42	8	20AA HOM	
58.1250	59	18	20AA WT	

Figure 5.16: A removal cocktail of dietary NEAAs, including alanine, is required for survival benefit of *VillinCreER Apcfl/+ KrasG12D/+ Gpt2fl/*fl mice
VillinCre^{ER} *Apc*$^{fl/+}$ *Kras*$^{G12D/+}$ (WT) and *VillinCre*^{ER} *Apc*$^{fl/+}$ *Kras*$^{G12D/+}$ *Gpt2*$^{fl/fl}$ (HOM) mice were place on a control diet (20AA) or a diet lacking alanine, asparagine, aspartic acid, glutamate and proline (-5AA) two weeks prior to induction, then induced with tamoxifen and aged until clinical end-point. a. Survival curve (n=8 for WT 20AA, n=9 for WT -4AA, n=7 for WT -1AA, n=8 for HOM 20AA, n=10 for HOM -4AA and n=8 for -1AA HOM), Log-Rank for 20AA HOM vs -4AA HOM, p=0.286 b. Tumour number boxplot of mice at end-point (n=8 for WT 20AA, n=7 for WT -4AA, n=7 for WT -1AA, n=7 for HOM 20AA, n=9 for HOM -4AA and n=7 for HOM -1AA). One-way Mann-Whitney *U* test, p=0.0149.

5.4 Discussion

In this chapter I have investigated the metabolic changes between APC and APC KRAS cells, focussing on glycolysis and glutaminolysis, two metabolic pathways that are frequently deregulated in cancer.

Glucose withdrawal confirmed that both APC and APC KRAS crypt cultures are highly glycolytic. Fatih Ceteci has confirmed via FDG-PET that the intestines of both APC and APC KRAS mice are highly glycolytic (unpublished). Tracing confirmed that glucose is converted to lactate in both APC and APC KRAS, and that they exhibit a Warburg effect shift in metabolism. However, APC KRAS crypt cultures specifically utilised the carbons of glucose to produce alanine. Glutamine uptake is often deregulated in cancer, and many cancer cells are 'addicted to glutamine' (Wise & Thompson, 2010); this was the case for APC KRAS crypt cultures, whose growth is dependent on glutamine. This was

confirmed by glutamine tracing, revealing that it is taken up by APC KRAS crypt cultures and converted to glutamate following deamination. Transcriptional analysis from our RNASeq data revealed an upregulation of many genes involved in both glycolysis and glutaminolysis in APC KRAS, such as *Hk2* and *Slc1a5*. There was also a pronounced switch in the expression of certain transaminase enzymes, such as *Gpt2* is upregulated in APC KRAS, whilst *Gpt1* is suppressed. A similar switch is observed between *Got1* and *Got2*. This suggests that is significant changes in metabolism in APC KRAS intestinal epithelial cells, and that since many of these enzymes are not significantly expressed in the normal epithelium, could present potential therapeutic targets.

Given the identified 'nutrient stress' (chapter 4) and altered metabolism in APC KRAS intestinal epithelial cells, I attempted to try and stress these cells further by fasting these mice, along with WT and APC mice for 16 hours prior to sampling. Fasting significantly reduced proliferation in APC KRAS small intestines, but not in the colon, compared with 'fed' controls. Fasting in all three groups induced a mild activation of AMPK, indicating a reduction in cellular ATP levels. Following these results, I investigated whether removal of seven dietary NEAAs; alanine, aspartic acid, asparagine, glutamate, glycine, proline and serine, would extend survival of a KRAS-driven model of intestinal tumourigenesis. There was no difference in survival of mice fed a control diet with all 20 amino acids in and the mice fed the -7AA diet. However two models of APC-driven intestinal tumourigenesis display a survival benefit on this -7AA diet compared with normal chow (Maddocks et al., 2017). The resistance of APC KRAS mice to NEAA dietary restriction could be explained by the fact that APC KRAS crypt cultures can synthesise many of these NEAAs *de novo*, unlike APC crypt cultures. Given that ATF4 drives the expression of a number of the metabolic genes discussed above, such as *Gpt2*, *Slc2a5* and *Asns*, it raises the possibility that the metabolic phenotypes of APC KRAS intestinal epithelial cells could, in part, be due to the activation of the UPR and the integrated stress response.

I also investigated the role of one ATF4's target genes, *Gpt2*, in Kras-driven intestinal tumourigenesis. I showed that both glycolysis and glutaminolysis feed into the production of alanine in APC KRAS crypt cultures, and this is dependent on GPT2. Deletion of GPT2 rendered APC KRAS crypt cultures

dependent on exogenous alanine for their growth. Deletion of GPT2 did not reduce proliferation in our APC KRAS acute model, this is likely due to the fact that alanine is a non-essential amino acid, and therefore these crypts could obtain alanine from circulation. Interestingly though GPT2 deletion did increase apoptosis in the small intestines and colon of APC KRAS mice. Surprisingly, despite this increase in apoptosis, deletion of GPT2 actually decreased survival in a KRAS-driven model of tumourigenesis.

Given the striking dependency of GPT2-deficient APC KRAS crypt cultures upon exogenous alanine, I sort to target this non-essential amino acid by reducing dietary intake of alanine *VillinCre^{ER} Apc$^{fl/+}$ Kras$^{G12D/+}$ Gpt2$^{fl/fl}$* mice. When these mice are place on a diet lacking alanine, aspartic acid, asparagine, glutamate and proline (-5AA), there is a significant extension in survival compared with the mice on control diet (20AA). Importantly, this diet had no survival benefit on *VillinCre^{ER} Apc$^{fl/+}$ Kras$^{G12D/+}$* mice, which is not that surprising given that I have previously shown that these mice do not respond to a -7AA diet. I then investigated whether this effect was solely dependent on alanine or rather a removal of a combination of these amino acids; I used diets lacking aspartic acid, asparagine, glutamate and proline (-4AA) or just alanine (-1AA). In this instance there was no survival benefit for mice on the -1AA diet, whilst there was a moderate, but non-significant, increase in survival in mice placed on the -4AA diet. This suggests that these tumours are still metabolically flexible, but that it also shows that the correct dietary formulation can impact KRAS-driven intestinal tumourigenesis following GPT2 deletion. Furthermore, given that GPT2 is lowly expressed in the normal intestinal epithelium, it presents a novel drug target for colorectal cancer.

Chapter 6: Discussion

In the previous results chapters I have discussed the different approaches I used to investigate KRAS-driven tumourigenesis in mouse models of Colorectal Cancer, as well as any potential novel targets arising from these studies. I will now discuss the relevance of these findings and their wider implications for patient benefit

6.1 Targeting Wnt signalling at the transcriptional level

Since deregulated Wnt signalling is a hallmark of colorectal cancer, there has been much interest in targeting the pathway for therapeutic benefit, however this has been with limited success. I sought to investigate whether targeting Wnt signalling at the transcriptional level via deletion of BCL9 and BCL9l could impact tumourigenesis. Importantly, deletion of BCL9 and BCL9l was tolerated in the murine intestine, with no perturbation of normal intestinal homeostasis – suggesting that these could be potential drug targets. Deletion of these proteins altered the distribution of ß-catenin throughout the cell, in agreement with their previously identified role as ß-catenin shuttling proteins, resulting in an increase in the membrane associated pool of ß-catenin. This may have had an indirect effect on the transcriptional output of ß-catenin, since a number of Wnt target genes, such as *Lgr5, Axin2* and *Rnf43* were downregulated following deletion of BCL9 and BCL9l. Hence, a threshold level of nuclear ß-catenin may be required for the expression of these genes or BCL9 and BCL9l are required for the direct or indirect transactivation of ß-catenin at the promoters of these genes. E-cadherin has been shown to limit the transforming potential of mutated ß-catenin by sequestering it to the membrane (Huels et al., 2015). Therefore, I plan to delete a single copy of E-cadherin along with BCL9/9l and determine if this rescues *Lgr5* expression. If not, then this would suggest that BCL9 and BCL9l are somehow required for the transactivation of ß-catenin for *Lgr5* expression, rather than *Lgr5* requiring a threshold level of ß-catenin for its transcription. It would also be interesting to determine via some *in silico* analysis whether the genes that require BCL9/9l for their expression contain a particular motif within their promoters or enhancers. Similarly, since BCL9/9l are part of the Wnt enhanceosome (Tiene et al., 2017), a ChIP-Seq experiment for ß-catenin in intestinal crypts lacking BCL9 and BCL9l would identify

differential binding of ß-catenin to target genes in a BCL9/9l-dependent manner.

Treatment of BCL9/9l-deficient intestinal crypts with the porcupine inhibitor, LGK974, resulted in severe crypt atrophy within seven days. This could potentially be explained by the reduction in *Lgr5* expression following deletion of BCL9/9l, such that the stem cell pool is reduced and it is then further compacted following LGK974 treatment – which has been shown to reduce *Lgr5* and *Olfm4* expression in WT intestinal crypts (David Huels – personal communication). Hence, LGK974 treatment combined with BCL9/9l deletion could be directly killing off the stem cells leading to crypt atrophy. Alternatively, intestinal crypts could be sensitive to a particular level of Wnt signalling, since it has been shown that *VillinCre*^{ER} *Ctnnb1*$^{fl/+}$ mice are also very sensitive to LGK974 treatment and display a very similar phenotype to *VillinCre*^{ER} *Bcl9*$^{fl/fl}$ *Bcl9l*$^{fl/fl}$ mice treated with porcupine inhibitor (David Huels – personal communication). This notion is in agreement with some of the early Tankyrase inhibitors which exhibited severe intestinal toxicity (T. Lau et al., 2013), such that inhibition beyond a certain level of Wnt signalling is toxic for the murine intestine. These studies highlight the inherent sensitivity of the intestine to Wnt inhibition, and therefore any targeted therapies would have to be carefully considered going forward, particularly combinatorial approaches.

Many Wnt-based therapies have failed in colorectal cancer, since they target the destruction complex (Tankyrase inhibitors) or Wnt signalling upstream of the destruction complex (Porcupine inhibitors). However, 80% of colorectal cancer patients have mutations in *APC* and therefore are unlikely to respond to these treatments, hence the need for Wnt-targeted therapies that act downstream of the destruction complex. This could potentially be provided by targeting BCL9/9l, given their location within the pathway; deletion of BCL9l has been shown to resensitize colorectal cancer cell lines to Tankyrase inhibition (de la Roche et al., 2014). To investigate this I sought to determine whether deletion of BCL9/9l impacts our acute APC-deficient models.

Deletion of BCL9and BCL9l suppressed proliferation in the small intestine and colon of both *VillinCre*^{ER} *Apc*$^{fl/fl}$ (APC) and *VillinCre*^{ER} *Apc*$^{fl/fl}$ *Kras*$^{G12D/+}$ (APC KRAS) mice, as well as reducing a number of Wnt target genes, including *Lgr5*

and CD44. This would suggest that even when Wnt signalling is hyperactivated, BCL9 and BCL9l are still required for the expression of certain Wnt target genes, however this does not answer the question as to whether the reduced expression in Wnt target genes is due to reduction of nuclear ß-catenin, or whether BCL9/9l are required for the transactivation of ß-catenin. Since deletion of BCL9 and BCL9l still increased, albeit not significantly, the number of E-cadherin: ß-catenin complexes in APC-deficient small intestinal crypts. As well as reducing proliferation in intestinal and colonic crypts, deletion of BCL9/9l significantly reduced the dedifferentiation of villi isolated from APC KRAS mice. During this dedifferentiation process, these villi acquire stem-cell-like properties and are also tumourigenic (Schwitalla et al., 2013). Hence, the reduced ability of these villi to dedifferentiate following BCL9/9l deletion could be in part due to reduced *Lgr5* expression and Wnt signalling in the intestinal epithelium of APC KRAS mice. Additionally, the intestinal crypts isolated from these mice grew as organoids, rather than spheroids like the controls, again, this could in part be due to reduced Wnt signalling. A similar observation was seen by Moor and colleagues, who also went on to show that these organoid-like crypt cultures isolated from *Apc*-deficient *Kras*-mutant intestinal epithelium have reduced tumourigenicity in an allograft model, compared with BCL9- and BCL9l-WT controls (Moor et al., 2015). My data and that from Moor and colleagues shows that targeting BCL9 and BCL9l can reduce proliferation and tumourigenicity in transformed cells with both high Wnt- and high MAPK-signalling.

There was a differential requirement for BCL9/9l to drive the expression of some Wnt target genes in APC and APC KRAS intestines. For instance *Cd44*, *c-Myc* and *Axin2* were all significantly downregulated in APC BCL9 BCL9l intestines vs APC, however this was not the case in an APC KRAS setting. These genes are controlled by the RSpondin axis of Wnt signalling. Interestingly a number of human tumours harbouring RSpondin fusion mutations, resulting in RSpondin overexpression, have been identified; these tumours frequently have *KRAS* or *BRAF* mutations (Seshagiri et al., 2012). It was proposed that these RSpondin mutations behave analogously to APC loss, and hence synergise to drive tumour progression. Therefore the Wnt transcriptional programme that synergises with MAPK-pathway activation may be driven by the RSpondin-axis as opposed to the

canonical Wnt-axis, and hence deletion of BCL9/9l has a differential impact on a subset of Wnt target genes in APC KRAS intestines vs APC.

When investigating whether BCL9 and BCL9l are required for the development of intestinal tumours I observed a very striking and unexpected phenotype. Whereby, deletion of BCL9/9l actually accelerated tumourigenesis regardless of *Kras* mutation status. This reduced tumour latency was accompanied by a significant increase in tumour number, resulting in a very large tumour burden. These tumours were predominantly located within the proximal small intestine (approximately 80% of tumours) when compared to control mice. This observation could align with the 'just-right' hypothesis, which suggests that *APC* mutations in colorectal tumours are selected for to provide a 'just-right' level of Wnt signalling, even if it is sub-maximal. It has been shown that Wnt signalling decreases from the proximal intestine to the colon in mice, and that this could influence the location of tumour formation (Leedham et al., 2011). Indeed, it has been shown that proximal colonic tumours retain more 20AARs compared to tumours that arise in the distal colon (Christie et al., 2013; Leedham et al., 2011).

The Apc^{Min} allele lacks any 20AARs, required for ß-catenin binding and degradation, hence following LOH in these tumours; the tumours have very high levels of Wnt signalling, which is thought to be suboptimal for tumour formation in the proximal small intestine, due to the high underlying basal Wnt signalling within this region. Hence, $Apc^{Min/+}$ mice develop tumours in the distal small intestine, which has lower levels of Wnt signalling. Reducing Wnt signalling in tumours, such as in the $Apc^{1322T/+}$ mouse, which has sub-maximal Wnt signalling, leads to the development of tumours in the proximal small intestine (Pollard et al., 2009; Leedham et al., 2011). I used the APC-580S allele which lacks any 20AARs (Shibata et al., 1997), similar to the $Apc^{Min/+}$ allele. Therefore, upon LOH of the second copy, these tumours should have very high levels of Wnt signalling, which would favour tumour formation in the distal small intestine. However, upon deletion of BCL9/9l Wnt signalling is lowered, this in turn would be permissive for tumour formation in the proximal small intestine. This may explain the profound increase in tumour formation in the proximal small intestine following BCL9/9l deletion, but does not explain the increased tumour burden.

BCL9l mutations have been associated with aneuploidy tolerance in aneuploid human CRC (López-García et al., 2017); providing a possible link between BLC9l and DNA damage. Hence loss of BCL9l may accelerate loss of the second copy of *APC*. However, the increased tumour burden in *VillinCre^{ER} Apc$^{fl/+}$ Bcl9$^{fl/fl}$ Bcl9l$^{fl/fl}$* and *VillinCre^{ER} Apc$^{fl/+}$ Kras$^{G12D/+}$ Bcl9$^{fl/fl}$ Bcl9l$^{fl/fl}$* mice was not due to increased DNA damage. Nor did deletion of BCL9/9l perturb migration along the crypt-villus axis. As shown in the short term models, these tumours lacking BCL9 and BCL9l had very low expression of *Lgr5* compared to control tumours. This lead to the hypothesis that the increased tumourigenesis could be due to reduced intestinal stem cell competition, by virtue of reduced stem cell number. Whilst stem cells lacking both BCL9 and BCL9l have a significantly reduced clonal fitness compared with WT controls, it is important to remember that using the *Villin*Cre recombinase will result in recombination in all cells throughout the murine intestine and colon. Hence reduced clonal fitness does not come into the equation in this setting. Rather, that if deletion of BCL9 and BCL9l reduces the number of intestinal stem cells, then following a 'hit' in the second copy of *Apc* there is a greater probability of that clone to repopulate the crypt, and therefore initiate tumour formation, compared to in the control crypt. Since in a wildtype setting, it is predicted that on average, 4.3 mutational 'hits' in *Apc* are require for the formation of a monoclonal crypt due to the stochastic replacement of intestinal stem cells (Vermeulen et al., 2013).

This idea is supported by the fact that treatment of *Lgr5Cre^{ER} Apc$^{fl/fl}$* mice with LGK974 also increases tumourigenesis, and that this could be due to increased rates of clonal fixation (David Huels – personal communication). Furthermore, reducing Wnt signalling through inhibition of RSpondin signalling, reduces the stem cell pool and also leads to the rapid formation of monoclonal crypts (Yan et al., 2017). Hence, reducing Wnt signalling could indeed promote tumour formation due to be reduced intestinal stem cell competition. Interestingly, David observed a switch from a distal tumour burden in the vehicle treated mice to a proximal small intestine burden in the LGK974 treated mice – highlighting a role for Wnt signalling in the location of tumour formation.

Going forward, to investigate the idea that the increased tumourigenesis is due to reduced stem cell competition, I would like to work with the previously described *Lgr5Cre^{ER}-EGFP tdTom^{fl}* mice and treat them with a BCL9/9l inhibitor

such as Carnosic Acid (de la Roche et al., 2014) and see whether this results in a faster rate of clonal fixation. In this instance, BCL9/9l would be inhibited across the entire intestinal stem cell pool, rather than at the single cell level that I previously used, and thus would be able to determine whether the clonal dynamics are significantly perturbed following crypt-wide inhibition of BCL9 and BCL9l. One could hypothesize that this may lead to increased rates of monoclonal crypt formation in agreement with previous studies that have investigated stem cell dynamics in response to Wnt inhibition. Additionally, it would also be interesting to determine whether the reduced clonal fitness of BCL9/BCL9l deficient stem cells could translate into reduced tumour burden. By using an *Lgr5*-driven Cre one could delete BCL9 and BCL9l throughout the intestinal stem cells along with APC and age the mice for tumour studies. If the tamoxifen dose if low enough to induce a mosaic recombination pattern, then there is the potential for APC-deficient BCL9/9l-null clones to be lost from the crypt which may in turn lead to a reduction in tumour burden and extension in survival compared with controls.

It is important to remember that the *Apc* allele used in these studies, the APC-580S allele (Shibata et al., 1997), lacks any ß-catenin binding domains, however, this differs in the human scenario; with many colorectal cancer patients having mutant APC proteins that are larger and still retain some ß-catenin binding activity. Hence, if a different *Apc* allele was used, such as Apc^{1322T} mice, which have been shown to develop spontaneous tumours with sub-maximal nuclear ß-catenin (Pollard et al., 2009; Lewis et al., 2010), then deletion of BCL9/9l may have a protective effect in this tumour setting, by further reducing Wnt signalling. This is currently being investigated by Mariann Bienz – who has shown that deletion of BCL9/9l significantly delays tumour formation in $Apc^{1322T/+}$ mice (personal communication). Alternatively, one could investigate the role of BCL9 and BCL9l in models with different activating mutations within the Wnt-pathway, such as ß-catenin. To investigate this, I have generated $VillinCre^{ER}$ $Ctnnb1^{Ex3/+}$ $Bcl9^{fl/fl}$ $Bcl9l^{fl/fl}$ mice. Upon genetic recombination, a truncated form of ß-catenin that cannot be phosphorylated and degraded is expressed. This mutant ß-catenin accumulates in the cytoplasm and subsequently translocates to the nucleus and transforms the intestine (Harada et al., 1999; Leedham et al., 2011). These mice are currently ageing,

however preliminary data shows that deletion of BCL9/9l significantly delays tumour onset in these mice, compared to control mice. This would suggest that the larger the APC protein, and therefore more 20AARs that remain, the more dependent cells are upon BCL9/9l for transformation. Hence one could imagine that patients may respond differently to BCL9/9l inhibition depending on the location of their tumour within the colon and the number of 20AARs it retains.

When considering a therapeutic window, BCL9 and BLC9l may represent promising targets for treatment of human patients with established tumours, which will have already lost both copies of APC. Since, unlike other tested Wnt pathway targets, these two proteins function downstream of the destruction complex and are required for the expansion of the APC crypt progenitor phenotype. As a proof of concept, existing small molecule inhibitors of the BCL9/ß-catenin interaction have been shown to inhibit Wnt signalling and growth in colorectal cancer cell lines (Takada et al., 2012). Furthermore, the requirement of BCL9/9l for the expansion of the APC KRAS crypt progenitor phenotype underpins the role of Wnt signalling in more aggressive models of intestinal tumourigenesis. This is in agreement with the observation that restoration of APC expression, and reduction of Wnt signalling, in adenocarcinomas can drive tumour regression (Dow et al., 2015). Finally, it would be interesting to determine whether *VillinCre*^{ER} *Apc*$^{fl/fl}$ *Kras*$^{G12D/+}$ *Bcl9*$^{fl/fl}$*Bcl9l*$^{fl/fl}$ (AKBB) mice are now sensitive to particular therapies. For instance, it has been shown that APC KRAS mice are resistant to mTORC1/2 inhibition, MAPK-pathway inhibition and PI3K/AKT inhibition. Thus by treating AKBB mice with various therapeutic agents, would allow me to investigate whether these resistance mechanisms are in part driven by a cooperation of high Wnt signalling and high MAPK signalling; if these mice are now sensitive to these agents. This would in turn address the potential scope for combining these agents with novel Wnt inhibitors in patients with *KRAS* mutation.

6.2 SILAC identifies a nutrient stress signature in APC KRAS intestinal epithelial cells

Whilst targeting Wnt signalling below the destruction complex was able to suppress the APC KRAS crypt progenitor phenotype, it failed to suppress intestinal tumourigenesis. Therefore I decided to take an unbiased approach and look at global changes between the proteomes of APC KRAS crypt cultures and

APC crypt cultures, whilst referring back to the lab's *in vivo* RNASeq data (David Vincent), to try and identify potential novel therapeutic targets.

Using SILAC I was able to apply quantitative proteomics to APC and APC KRAS crypt cultures. Pathway analysis of the deregulated proteins predicted a marked increase in the rates of protein synthesis in APC KRAS and APC crypt cultures, with eIF2 signalling being the top hit in the pathway analysis. This increased rate in protein synthesis has been confirmed by John Knight, who has shown that APC KRAS crypt cultures produce approximately 20-30% more protein that APC crypt cultures. It is well known that oncogenic KRAS alters the expression of numerous ribosomal proteins and translation factors (Bhat et al., 2015), but it can also signal to the eIF4F complex, involved in translation initiation, via ERK and MNK1/2 (Scheper & Proud, 2002). The increased eIF2 signalling could be due to two causes. It could be an indicator of the increased rates of protein synthesis, since a large number of ribosomal proteins and tRNA synthetases were upregulated in the SILAC data and RNASeq data respectively. Alternatively, it could suggest that the cells are under some sort of stress, since the eIF2 complex can signal a stress response upon phosphorylation of its' α-subunit at serine 51. I believe that it is a combination of these two scenarios that enriches for eIF2 signalling within the pathway analysis, since I also observe a predicted activation of ATF4, due to an upregulation of its' target genes within both the SILAC and RNAseq data sets – the increased expression of ATF4 in APC KRAS cells at the protein level has been confirmed *in vivo*. Additionally I also observe an induction of eIF2α phosphorylation both *in vitro* and *in vivo* in APC KRAS intestinal epithelial cells.

There are four kinases that phosphorylate eIF2α at serine 51, PERK, PKR, GCN2 and HRI. PERK and GCN2 are activated by ER stress and uncharged tRNAs respectively and therefore are likely to be activated when cells are producing large amounts of protein. I also observe increased expression of the ER chaperone GRP78 in APC KRAS cells both *in vivo* and *in vitro*, suggesting that there is increased ER stress in APC KRAS cells compared to APC cells. Taken together, this suggests that the increased protein synthesis in APC KRAS cells could be leading to some sort of proteotoxic stress in APC KRAS cells, to which these cells are trying to respond to via eIF2 signalling. Importantly, I also observe predicted activation and expression of two other transcription factors,

XBP1 and NUPR1, which are activated downstream of ER stress and the UPR. Similarly, there is increased phosphorylation of eEF2 (Thr56) in APC KRAS cells compared to APC cells – again suggesting that there are activated feedback loops in these cells trying to slow/regulate protein synthesis. Altogether these results suggest that APC KRAS intestinal epithelial cells experience a nutrient stress, which may in fact be cell autonomous. This may in turn open a therapeutic window, whereby one could try and target this proteotoxic stress to induce cell death. For instance, a number of studies have attempted to target ER stress in colon cancer models. For instance Heijmans and colleagues showed that induction of ER stress induces a loss of stemness in the normal intestinal epithelium (Heijmans et al., 2013). The authors went on to show that induction of ER stress in colon cancer stem cell induces their differentiation, and that this leads to a sustained response to oxaliplatin in a xenograft model of transplanted colon cancer cells, due to the ablation of the cancer stem cell population (Wielenga et al., 2015). Finally, deletion of GRP78 supresses the APC-crypt progenitor phenotype, highlighting the importance of regulating ER stress in proliferating cells (van Lidth de Jeude et al., 2016). These studies indicate that targeting ER stress in colon cancer may open a therapeutic window in CRC. Given the high levels of ER stress I observe in APC KRAS cells, *KRAS* mutant tumours might be particularly sensitive to these therapies.

eIF2α phosphorylation has also been shown to activate autophagy (Bretin et al., 2016). Autophagy is an evolutionarily conserved process that enables cells to degrade macromolecules and organelles allowing components to be used in metabolic and catabolic processes. Thus, one could imagine that autophagy could be important in APC KRAS cells, in order to maintain pools of amino acids to drive protein synthesis and cellular growth. Recently, two studies in models of non-small-cell lung cancer and melanoma have shown that activation of the MAPK pathway following *Kras* or *Braf* mutation leads to autophagy dependent tumour growth (Guo et al., 2013; Xie et al., 2015). Furthermore, a recent study has highlighted a role for autophagy in an *Apc*-driven model of tumourigenesis, although in this study the authors showed that autophagy is important for the immune system's anti-tumour response (Lévy et al., 2015). Deletion of ATG7, a critical autophagy gene, significantly delayed intestinal tumourigenesis and reduced tumour burden in *VillinCre*^{ER} *Apc*$^{fl/+}$ *Kras*$^{G12D/+}$ mice (Fig 6.1). It remains

to be seen however if this requirement of autophagy for KRAS-driven intestinal tumourigenesis is due to a requirement for autophagy to fuel protein synthesis or metabolism, or potentially both. I plan to study protein synthesis in crypt cultures isolated from *VillinCre^{ER} Apc$^{fl/fl}$ Kras$^{G12D/+}$ Atg7$^{fl/fl}$* mice and also perform metabolomics on these culture too.

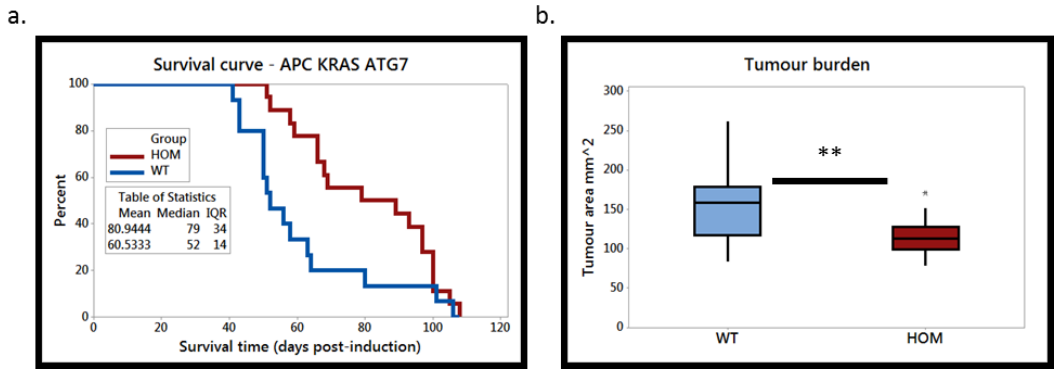

Figure 6.1: Autophagy is required for KRAS-driven intestinal tumourigenesis
a. survival curve for *VillinCre^{ER} Apc$^{fl/+}$ Kras$^{G12D/+}$* (WT, n=15) and *VillinCre^{ER} Apc$^{fl/+}$ Kras$^{G12D/+}$ Atg7$^{fl/fl}$* (HOM, n=18), Log-rank test p=0.031. b. Box plot for tumour burden from *VillinCre^{ER} Apc$^{fl/+}$ Kras$^{G12D/+}$* (WT, n=15) and *VillinCre^{ER} Apc$^{fl/+}$ Kras$^{G12D/+}$ Atg7$^{fl/fl}$* (HOM, n=14) sampled at clinical end-point. One-way Mann Whitney test, ** p =0.00685.

6.3 Investigating the role of eIF2 signalling in intestinal tumourigenesis and homeostasis

Given that eIF2 signalling was the top pathway upregulated in APC KRAS crypt cultures in the pathway analysis, and that there could be a potential link to this and the metabolic flexibility of APC KRAS intestinal epithelial cells I wanted to try and target eIF2 signalling, as well as one of its' potential downstream targets.

There has been much interest in targeting eIF2 signalling in neurodegenerative diseases – focusing on PERK inhibitors. Whilst numerous PERK inhibitors have been developed, they have been shown to impair endocrine and exocrine functions within the pancreas (Atkins et al., 2013; Moreno et al., 2013), limiting their use to acute treatments. Recently a novel small molecule inhibitor, ISRIB, was identified in a screen for PERK inhibitors, which was shown to reverse the effects of eIF2α phosphorylation and did not display pancreatic toxicity (Sidrauski et al., 2013; Halliday et al., 2015). Using ISRIB I was able to show that eIF2α phosphorylation is playing a functional role APC KRAS cells, since ISRIB treatment significantly increased protein synthesis in APC KRAS crypt

cultures, but not APC crypt cultures, without affecting phospo-eIF2α levels, but reduced ATF4 expression in APC KRAS crypt cultures. This confirms that APC KRAS cells are trying to regulate/slow their rates of protein synthesis, and that translation initiation is limiting in APC KRAS cells, as opposed to elongation, which is limiting in APC cells (Faller et al., 2015).

ISRIB treatment suppressed proliferation in the small intestines and colons of APC KRAS mice, but not APC mice. This reduction in proliferation was accompanied by a reduction in ATF4 at the protein level in ISRIB treated APC KRAS mice, but not APC ISRIB treated mice, although I did not observe a reduction in the expression of ATF4 target genes in ISRIB treated APC KRAS mice. This could be why the reduced proliferation following ISRIB treatment in the acute APC KRAS model did not translate into a survival benefit in an ageing model of KRAS-driven intestinal tumourigenesis. It was recently shown that mTORC1 is able to regulate ATF4 protein levels independently of eIF2α signalling (Ben-Sahra et al., 2016); therefore it would be interesting to see whether an ISRIB/rapamycin treatment was able to reduce ATF4 target gene expression in APC KRAS mice. However, at the translational level the two drugs would be acting differently, with ISRIB known to increase protein synthesis and rapamycin to decrease protein synthesis in APC KRAS crypt cultures (John Knight – personal communication). Although, the polysome profiles from the ISRIB treated APC KRAS mice suggest that there is no change in rates of protein synthesis compared to vehicle treated mice. Going forward it would be useful to have an additional technique to quantify rates of protein synthesis *in vivo*, particularly in tumours. For instance, a puromycin analog, O-propargyl-puromycin (OP-Puro) has been developed to assay protein synthesis *in vivo* (Li et al., 2012) and could potentially be used to look at protein synthesis within tumours.

ISRIB is thought to function by either increasing the dissociation of phospho-eIF2α and eIF2B, or somehow activate eIF2B (Sidrauski et al., 2015). I have genetically deleted one cope of the catalytic subunit of eIF2B, eIF2B5. Loss of one copy of *Eif2b5* significantly delays tumour latency in $Apc^{Min/+}$ mice, although there was no difference in tumour number or burden between $Apc^{Min/+}$ and $Apc^{Min/+}$ $Eif2b5^{+/-}$ mice at end-point. Therefore it could be that the tumours in the $Apc^{Min/+}$ $Eif2b5^{+/-}$ mice grow more slowly than those in the control cohort – I plan to check this by quantifying the number of BrdU-positive cells in the

tumours of the mice of the two cohorts. Alternatively, tumourigenesis could be slowed due to a reduction in protein synthesis, however I have shown that loss of one copy of *Eif2b5* does not reduce protein synthesis in intestinal tumours or non-transformed intestinal epithelium. Recently, it has been shown that the translation of oncogenic genes can be driven by alternative upstream uORFs (Sendoel et al., 2017). Given that levels of the ternary complex can control the translation of genes with uORFs in their 5' UTRs, such as ATF4, it could be that loss of one copy of *Eif2b5* is affecting the translatome of $Apc^{Min/+}$ tumours. Interestingly, high levels of phospho-eIF2α have been shown to promote a switch to CUG start codons for non-canonical translation initiation mediated by eIF2A (Sendoel et al., 2017). The proto-oncogene c-MYC, which is required for the APC-crypt progenitor phenotype (Sansom et al., 2007), is known to have be translated from both an AUG and CUG promoter (Blackwood et al., 1994). Hence loss of a single copy of *Eif2b5* may affect MYC translation and consequently slow tumour growth in $Apc^{Min/+}$ mice.

I intend to investigate this by using both SILAC on tumour-derived cultures, but also ribosome profiling, to see if there are differences in the translatomes of these tumours and if so to try to understand why. Additionally, I am also investigating whether loss of one copy of *Eif2b5* also has an impact upon KRAS-driven intestinal tumourigenesis and proliferation in our acute models – preliminary data shows that proliferation is reduced in both the small intestines and colons of $VillinCre^{ER}$ $Apc^{fl/fl}$ $Kras^{G12D/+}$ $Eif2b5^{+/-}$ mice compared with controls, however ageing tumour studies are still ongoing. Importantly, I have shown that $Eif2b5^{+/-}$ mice do not have perturbed intestinal homeostasis, therefore eIF2B5 could provide a therapeutic window.

6.4 Altered metabolism in APC KRAS intestinal epithelial cells

Protein synthesis is an extremely energetically demanding process and therefore one could imagine that APC KRAS intestinal epithelial cells adapt their metabolism to meet these energetic requirements. Recently, there have been great advances in understanding cancer metabolism and how it differs from the metabolism of non-transformed cells – identifying potential therapeutic targets. The greatest focus has been on glucose and glutamine – cancer cells have been shown to take up high concentrations of both of these metabolites. Fatih Ceteci

previously showed that both APC and APC KRAS crypt cultures are dependent on glucose for growth, whilst APC KRAS cultures are highly dependent on glutamine for their growth. These high rates of glycolysis and glutaminolysis were confirmed via tracing experiments *in vitro*. The high rates of glutaminolysis in APC KRAS crypt cultures could be explained by increased MYC expression. MYC was the top predicted activated transcription factor in the pathway analysis of the SILAC data and there are many studies showing that MYC drives a transcriptional programme of genes involved in glutaminolysis (Wise & Thompson, 2010; Yuneva et al., 2007). RNASeq data confirmed increased expression of a number of glycolysis and glutaminolysis genes, which was further validated by RNAScope and Western Blot. These transcriptional changes in metabolic changes were also seen in human datasets.

This transcriptional profiling also identified a number of metabolic enzymes that are specifically expressed in transformed intestinal epithelial cells – such as Hexokinase II which is not expressed in WT cells, whilst *Gpt2* is specifically expressed in APC KRAS cells. Hence, identifying these enzymes as potential therapeutic targets – Hexokinase II has been shown to be required for the progression of mouse models of non-small-lung cancer and breast cancer (Patra et al., 2014), highlighting the potential benefit of targeting glycolysis. Given the large changes in metabolism between APC and APC KRAS crypt cultures, as well as the previously identified nutrient stress in APC KRAS intestinal epithelial cells, I tried to try and exploit this via fasting and dietary manipulation. 16 hours fasting specifically reduced proliferation in the small intestines of APC KRAS mice, but not APC mice. Interestingly, the opposite was seen when quantifying proliferation in the colons of these mice, this could be due to differences in metabolism between the small intestinal and colonic epithelium. In the future it would be worth investigating whether this is the case, by tracing glucose and glutamine in colonic crypt cultures, as well as investigating their response to glucose and glutamine starvation and whether this overlies with results obtained on small intestinal crypt cultures.

Whilst the fasting result highlighted the potential targeting of the nutrient stress signature in APC KRAS mice, it is not a feasible approach going forward - as it cannot be translated into the clinic. Alternatively, one could try and manipulate the diet of patients to try and affect systemic levels of circulating

amino acids which may in turn effect tumour growth. To investigate this I placed *VillinCre^{ER} Apc$^{fl/+}$ Kras$^{G12D/+}$* mice on a diet (-7AA) lacking seven non-essential amino acids: alanine, aspartic acid, asparagine, glutamate, glycine, proline and serine or a diet containing all amino acids (20AA), and aged them until clinical end-point. Despite a reduction of circulating levels of glycine, serine and proline in the -7AA mice, there was no difference in survival or tumour number between mice on 20AA and -7AA diet. This suggests that these tumours are metabolically flexible and can synthesise various non-essential amino acids *de novo*. Confirmation of '*in vivo*' metabolic flexibility was shown in a recent study that I was involved in. We showed that APC KRAS crypt cultures can synthesise serine and glycine *de novo* from glucose, and are resistant to serine/glycine deprivation, whilst APC crypt cultures had impaired growth following serine/glycine starvation due to an inability to synthesise the amino acids *de novo* (Maddocks et al., 2017)

I was able to confirm this result from our own tracing experiments – APC KRAS crypt cultures have increased synthesis of serine, glycine and alanine from glucose, and proline and glutamate from glutamine, compared to APC crypt cultures. I also observed an increase in the expression of the transaminases responsible for the synthesis of asparagine and aspartic acid from glutamine-derived amide groups – ASNS and GOT1/2 in the SILAC and RNASeq data. Altogether this data highlights the metabolic flexibility of APC KRAS intestinal epithelial cells. The metabolic flexibility of APC KRAS cells, which includes increase glucose and glutamine uptake as well as increased NEAA biosynthesis, may have a critical role in tumour growth. Vogelstein and Fearon showed that *KRAS* mutations are found in approximately 60% of tumours greater than 1cm, but only 10% of tumours less than 1cm (Fearon & Vogelstein, 1990). Hence, these metabolic adaptations driven by APC loss and *KRAS* mutation may be critical for tumour growth in hypoxic and nutrient depleted conditions as the tumours begin to outgrow their existing blood supplies. Furthermore, *KRAS* mutations are known to activate scavenging pathways such as micropinocytosis and autophagy (Bar-Sagi & Feramisco, 1986; Guo et al., 2013; Kamphorst et al., 2013). This may also explain the dependency of APC KRAS cells on autophagy too.

Interestingly, many of these amino acid biosynthesis enzymes, such as GPT2, ASNS and PSAT1 are ATF4 targets (Park et al., 2017; Salgado et al., 2014; Ye et al., 2010). Since ATF4 has been shown to have a key role in the adaptation of cells to NEAA depletion (Ye et al., 2010), it would be interesting to see whether deletion of ATF4 in APC KRAS crypt cultures or *in vivo*, not only reduces the ability of APC KRAS cells to synthesise these non-essential amino acids, but also resensitises them to serine/glycine deprivation or to the -7AA diet. Furthermore, given that canonical ATF4 activation is via phosphorylation of eIF2α, this could potentially provide a direct link between the increased rates of protein synthesis and altered metabolism in APC KRAS intestinal epithelial cells and hence provide another therapeutic window.

Despite the ability of APC KRAS intestinal epithelial cells to synthesise numerous non-essential amino acids, fasting of APC KRAS mice significantly reduced proliferation in the small intestines of these mice compared with controls. This suggests that the proliferation of APC KRAS intestinal epithelial cells is dependent on nutrients that can only be obtained from the diet, such as essential amino acids. Within the transcriptomic analysis for genes involved in glutaminolysis I identified a marked upregulation of *Slc7a5* expression in APC KRAS intestinal epithelial cells, but also human tumours. SLC7A5 mediates the exchange of intracellular glutamine for extracellular leucine and isoleucine - two essential amino acids. Deletion of SLC7A5 significantly reduces proliferation in APC KRAS mice and nearly doubles the lifespan of $VillinCre^{ER}$ $Apc^{fl/+}$ $Kras^{G12D/+}$, but has no impact on proliferation in the acute APC model or upon normal intestinal homeostasis (Arafath Najumdeen, personal communication – Fig 6.2). This highlights the requirement of leucine and isoleucine for KRAS-driven intestinal tumourigenesis. Whilst dietary deprivation of leucine/isoleucine is not tolerated by mice (Kamata et al., 2014), the development of a small molecule inhibitor or a blocking antibody against SLC7A5 could provide great therapeutic benefit in human colorectal cancer patients.

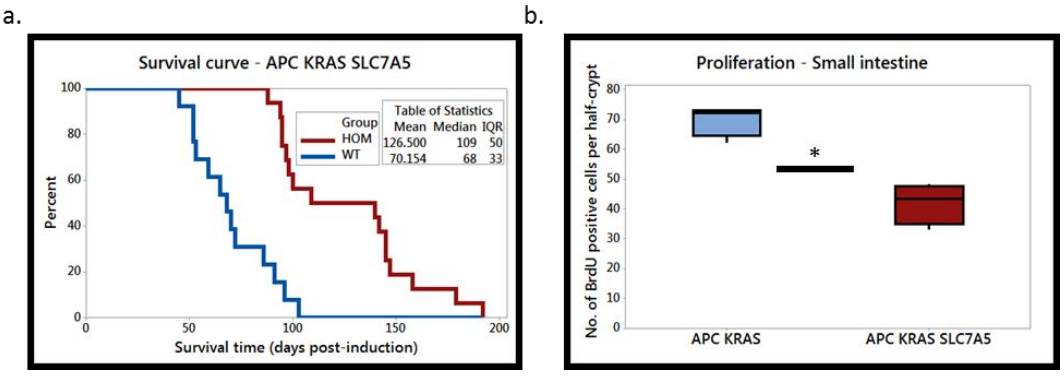

Figure 6.2: SLC7A5 is required for KRAS driven intestinal tumourigenesis
a. Survival curve for *VillinCre*^{ER} *Apc*$^{fl/+}$ *Kras*$^{G12D/+}$ (WT, n=13) and *VillinCre*^{ER} *Apc*$^{fl/+}$ *Kras*$^{G12D/+}$ *Slc7a5*$^{fl/fl}$ (HOM, n=16) mice, Log-rank test p<0.0001 b.Box-plot of scoring of proliferation of in small intestines of *VillinCre*^{ER} *Apc*$^{fl/fl}$ *Kras*$^{G12D/+}$ (APC KRAS) and *VillinCre*^{ER} *Apc*$^{fl/fl}$ *Kras*$^{G12D/+}$ *Slc7a5*$^{fl/fl}$ (APC KRAS SLC7A5) mice, sampled 3-days post-induction. Mice were injected with BrdU 2 hours prior to culling. Number of BrdU positive cells per half-crypt counted, 25 crypts per mouse scored. One-way Mann-Whitney test, * p=0.0152, n=4 per group. (Arafath Najumdeen)

6.5 Investigating the role of GPT2 in intestinal tumourigenesis

An additional target that emerged from the RNASeq data and metabolic data was GPT2. I showed that *Gpt2* is specifically upregulated in APC KRAS intestines, whilst its' isozyme, *Gpt1* is downregulated. This switch in expression is also observed in human datasets. GPT2 catalyses the transamination of pyruvate using the nitrogen group of glutamate, to produce alanine and α-ketoglutarate, and it has recently been shown to be a nexus of both glycolysis and glutaminolysis (Smith et al., 2016). I confirmed that APC KRAS crypt cultures consume both glucose and glutamine to produce alanine in a GPT2 dependent manner. Furthermore, this production of alanine is required for the growth of these crypt cultures, since *VillinCre*^{ER} *Apc*$^{fl/fl}$ *Kras*$^{G12D/+}$ *Gpt2*$^{fl/fl}$ (APC KRAS GPT2) derived crypt cultures are dependent on exogenous alanine for their growth.

Deletion of GPT2 *in vivo* did not alter proliferation in the small intestines and colons of APC KRAS mice, however there was an increase in apoptosis in both tissues following GPT2 deletion. It is important to remember that alanine is a non-essential amino acid and can therefore be synthesised *de novo*; hence circulating alanine would be able to support the growth of APC KRAS GPT2 intestinal epithelial cells, potentially explaining why there was no significant change in proliferation. Despite the increase in apoptosis, deletion of GPT2 in a KRAS-driven model of intestinal tumourigenesis actually reduced survival compared to control mice WT for GPT2, although there was no significant change in tumour burden or number of tumours. The increase in apoptosis in the

short term models suggests that the levels of alanine in circulation do not meet a threshold concentration required to avoid apoptosis in APC KRAS GPT2 intestinal epithelial cells, which would presumably be met by *de novo* alanine synthesis. Hence, reduction of circulating levels of alanine could potentially have therapeutic benefit in *VillinCre^{ER} Apc$^{fl/+}$ Kras$^{G12D/+}$ Gpt2$^{fl/fl}$* mice.

I placed *VillinCre^{ER} Apc$^{fl/+}$ Kras$^{G12D/+}$* and *VillinCre^{ER} Apc$^{fl/+}$ Kras$^{G12D/+}$ Gpt2$^{fl/fl}$* mice on a control diet containing all 20 amino acids (20AA) and a diet lacking 5 non-essential amino acids: alanine, asparagine, aspartic acid, glutamate and proline (-5AA), and aged them until clinical endpoint. There was no difference in survival of *VillinCre^{ER} Apc$^{fl/+}$ Kras$^{G12D/+}$* cohorts on either diet, however, there was a significant extension in survival in *VillinCre^{ER} Apc$^{fl/+}$ Kras$^{G12D/+}$ Gpt$^{fl/fl}$* mice on the -5AA diet compared to those on the 20AA diet. To confirm that this effect was due to removal of dietary alanine, I took two approaches. Firstly I performed a series of amino acid depletion experiments *in vitro* with different combinations of the amino acids missing in the -5AA diet, and in this setting, alanine was critical for the growth of APC KRAS GPT2 crypt cultures, whilst the others were dispensable for their growth. Secondly, I used a diet lacking just alanine (-1AA) and a diet lacking asparagine, aspartic acid, glutamate and proline (-4AA), and placed our ageing models on these diets. Surprisingly, neither diet affected survival of *VillinCre^{ER} Apc$^{fl/+}$ Kras$^{G12D/+}$ Gpt2$^{fl/fl}$* or control mice. This suggests that whilst alanine is absolutely critical for the growth of APC KRAS GPT2 crypt cultures, *in vivo*, additional non-essential amino acids must be removed to further stress these cells to affect their growth, this may in part be due to additional signalling pathways *in vivo* or provision of amino acids from the stroma. For instance pancreatic stellate cells have been shown to provide alanine for the growth of pancreatic cancer cells (Sousa et al., 2016). In this instance the pancreatic cancer cells used the stellate cell-derived alanine as an alternative carbon source for the TCA cycle to drive tumour growth in a nutrient poor environment (Sousa et al., 2016).

One key question arising from these studies is the role of alanine in these APC KRAS GPT2 cells. Preliminary results from tracing ^{15}N-L-alanine *in vitro* shows that in the absence of GPT2, APC KRAS cells are unable to synthesise glutathione from alanine, and that this pool of alanine-derived glutathione represents a significant fraction of cellular glutathione. This raises several

interesting thoughts. Firstly, that GPT2 can catalyse the reverse reaction to alanine synthesis, since glutathione is derived from glutamate and cysteine. Hence it is likely that the nitrogen group of alanine is used in glutamate synthesis and then glutathione production. Secondly, that this reduced pool of glutathione could explain why APC KRAS GPT2 crypt cultures die in the absence of alanine - since they're unable to quench reactive oxygen species (ROS), which may explain the increase in apoptosis that I observe in the small intestines and colons of APC KRAS GPT2 mice, since there is limited time for the cells to adapt in the acute setting. Finally, in a tumourigenesis model, if there are sub-lethal levels of ROS, this could lead to DNA damage, but not apoptosis, accelerating the loss of the second copy of *Apc*, initiating tumourigenesis. These are merely hypotheses and more work is required to investigate and validate them going forward, such as investigating whether exogenous glutathione rescues the dependency of APC KRAS GPT2 crypt cultures upon alanine.

I have shown that GPT2 represents a potential novel target in colorectal cancer since it is not expressed in the normal intestinal epithelium, whilst it is upregulated in both human datasets, as well as a number of human colorectal cancer cell lines following *RAS* or *PIK3CA* mutations (Hao et al., 2016; Smith et al., 2016). These studies, like my *in vitro* experiments showed that GPT2 is required for the growth of human colorectal cancer cell lines *in vitro* (Hao et al., 2016; Smith et al., 2016). However, this did not translate to an *in vivo* therapeutic benefit, for reasons that we're still trying to understand – although dietary manipulation suggests that this could be due to tumours relying on circulating non-essential amino acids or additional signalling pathways that are present *in vivo*.

Whilst there has been much interest in targeting glutaminolysis in cancer, due to the observation that many cancers are 'addicted to glutamine' – there has been limited efficacy *in vivo* for targeting this pathway. Recently, a study highlighted how differences in the environment can impact the metabolic phenotype of cancer cells. For instance, glutamine tracing in a mouse model of Non-Small Cell Lung Cancer revealed that both the tumour cells and normal lung tissue use glutamine minimally and are not sensitive to Glutaminase (GLS) knockdown or inhibition with CB-839 (Davidson et al., 2016). However, culturing these same tumour cells *in vitro* revealed that they consume large amounts of

glutamine, and are sensitive to glutamine withdrawal or CB-839 treatment (Davidson et al., 2016). This highlights how the environment can impact the metabolic phenotype of cancer cells.

To a certain extent, the Sansom lab has shown something similar. For instance, I have shown that APC KRAS crypt cultures consume large amounts of glutamine *in vitro* and are dependent on glutamine for growth (Fatih Ceteci), however treatment of APC KRAS mice with a GLS inhibitor (with Arafath Najumdeen and Andrew Campbell) does not affect proliferation in either the small intestine or colon compared to vehicle treated mice. Whilst I have shown GPT2 to be a nexus for glycolysis and glutaminolysis *in vitro*, and its' deletion sensitises APC KRAS crypt cultures to alanine deprivation – *in vivo*, GPT2 deletion did not have any major impact on the proliferation of APC KRAS intestinal epithelial cells, unless the diets of these mice are altered. Hence, these data highlight that metabolic phenotypes *in vitro* do not necessarily translate to an equivalent *in vivo* phenotype. Therefore going forward, we need to develop better predictive models and techniques for assaying metabolism *in vivo* to better identify and target metabolic vulnerabilities in cancer. For instance tracing labelled glucose and glutamine in our acute models and also within in tumours will give an insight into *in vivo* metabolism. Additionally, the application of Mass Spec Imaging (MSI) to tissue sections allows the spatial resolution and quantification of metabolites within these tissue samples (Goodwin et al., 2016). Crucially, MSI is not dependent on labelling and thereby allows untargeted data collection, generating a greater overview of any metabolic phenotypes compared to targeted tracing experiments. Application of MSI and *in vivo* labelled-metabolite tracing in parallel will aid our understanding and targeting of tumour metabolism.

Summary diagrams:

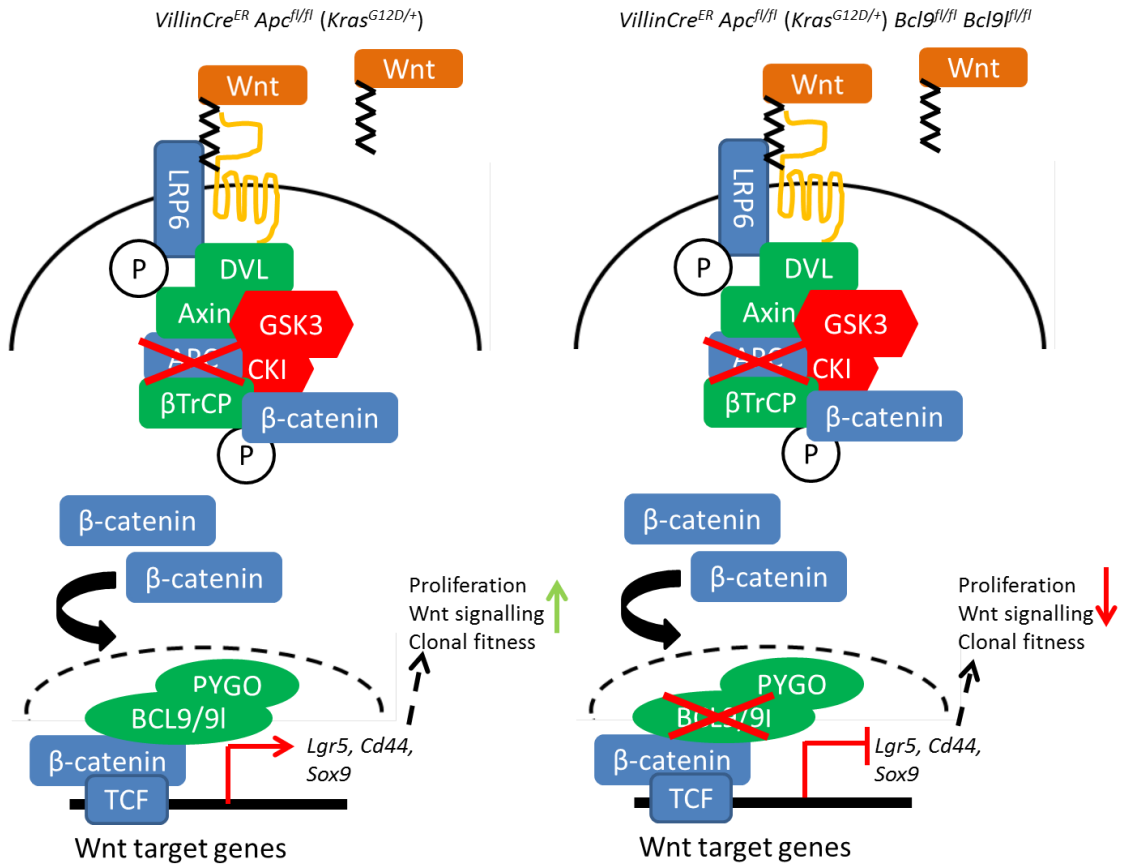

Figure 6.3: BCL9/9l represent promising drug targets in APC-deficient intestinal epithelial cells

Left panel: following deletion of both copies of APC (with or without expression of oncogenic Kras), the Wnt destruction complex is inactivated, such that ß-catenin can be phosphorylated, but not degraded. Stabilised ß-catenin subsequently translocates to the nucleus binds to additional transcription factors, such as TCF, BCL9/9l and PYGO, driving the expression of a large number of Wnt target genes, including *Lgr5*, *Sox9* and *Cd44*. This transcriptional programme in turn drives increased proliferation in the crypt. Right panel: upon deletion of BLC9 and BLC9l concomitantly with APC, there is a reduction in a large number of Wnt target genes in intestinal crypts, which in turn is associated with a reduction in proliferation. The reduced expression of Wnt target genes has a profound impact in the 'clonal fitness' of the Lgr5-positive intestinal stem cells in the normal intestinal epithelium.

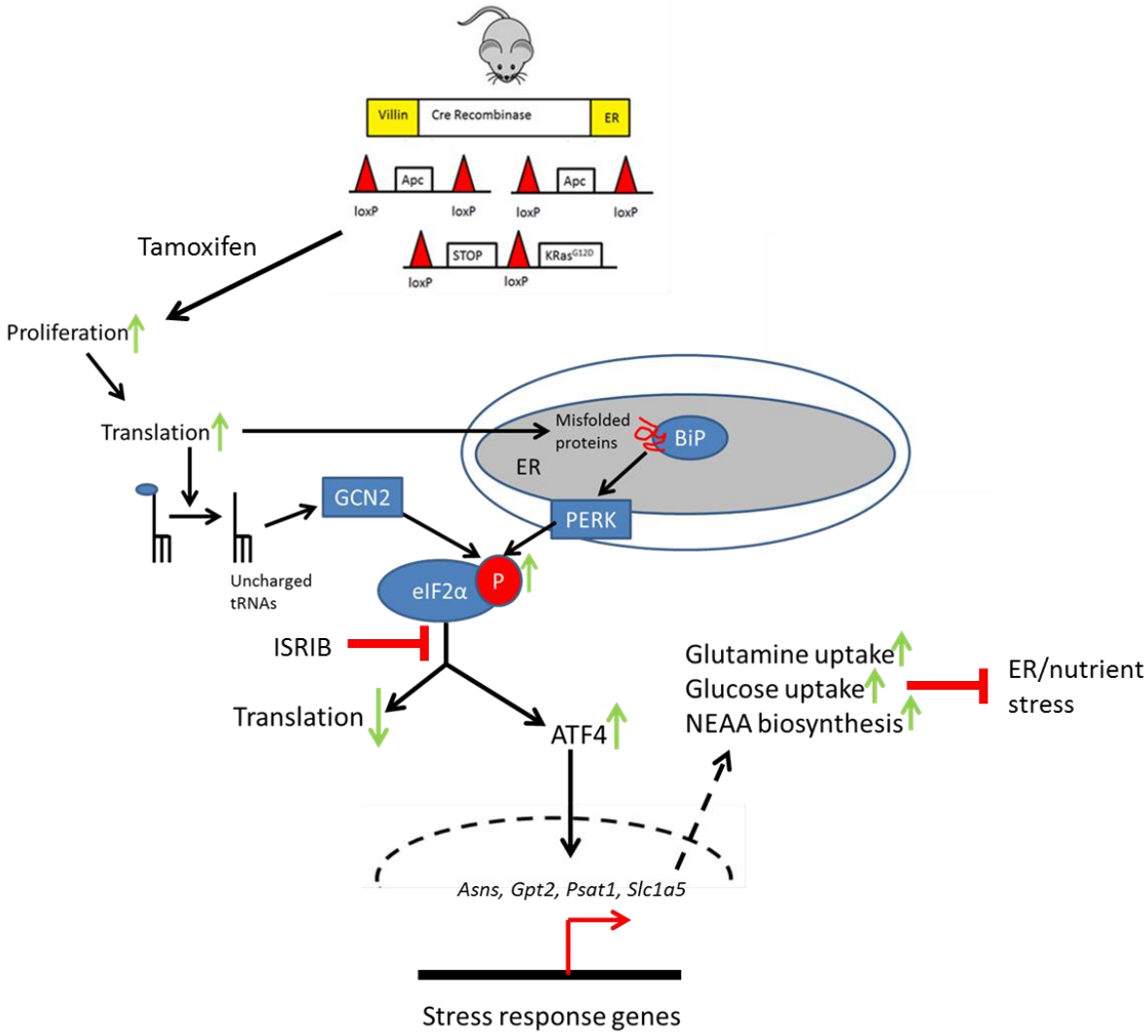

Figure 6.4: Cross-talk between translation and metabolism in APC KRAS cells

Upon deletion of APC and activation of oncogenic KRAS, there is a significant increase in proliferation in the murine intestine – this in turn leads to a large demand increase in protein synthesis. This increase in translation in turn leads to an increase in misfolded proteins in the ER, which are sequestered by the ER chaperone BiP (GRP78), which in turn activates PERK. Higher rates of protein synthesis may also lead to an accumulation of uncharged tRNAs. PERK or GCN2 phosphorylate eIF2α, this in turn reduces protein synthesis and induces ATF4 translation. This process can be inhibited by the small molecule, ISRIB. When expressed, ATF4 translocates to the nucleus and induces a transcriptional programme of enzymes involved in amino acid uptake and non-essential amino acid (NEAA) biosynthesis. The metabolic changes I observe in APC KRAS cells, namely increased glycolysis, glutaminolysis and NEAA biosynthesis may be a direct or indirect effect of increased protein synthesis to provide sufficient amino acids and energy for the translation machinery to sustain protein synthesis, suppressing ER stress.

Chapter 7: Appendix

Table 7.1 Genes downregulated in BCL9 BCL9l vs WT

Symbol	Gene name	Fold Change	p-adj
Gstm1	glutathione S-transferase, mu 1	-2.25543	1.29E-05
Defa2	defensin, alpha, 2	-5.22898	8.53E-04
Gm21002	predicted gene, 21002	-5.22898	8.53E-04
Gstm3	glutathione S-transferase, mu 3	-2.57168	2.53E-03
Cyp2c66	cytochrome P450, family 2, subfamily c, polypeptide 66	-2.77149	5.00E-03
S100g	S100 calcium binding protein G	-1.92941	2.38E-02
Rps3a1	ribosomal protein S3A1	-31.0928	6.06E-107
Capza1	capping protein (actin filament) muscle Z-line, alpha 1	-2.32991	9.56E-25
Amica1	adhesion molecule, interacts with CXADR antigen 1	-2.89769	2.90E-16
Tifa	TRAF-interacting protein with forkhead-associated domain	-5.0602	6.95E-13
Mansc1	MANSC domain containing 1	-2.00145	9.62E-11
Sorl1	sortilin-related receptor, LDLR class A repeats-containing	-1.83356	2.37E-07
Gm15315	predicted gene 15315	-3.89462	3.08E-04
Defa1	defensin, alpha 1	-2.90363	3.54E-04
Defa3	defensin, alpha, 3	-2.90363	3.54E-04
Defa17	defensin, alpha, 17	-2.90363	3.54E-04
Gm15284	predicted gene 15284	-2.90363	3.54E-04
Defa1	defensin, alpha 1	-2.90363	3.54E-04
Gm15284	predicted gene 15284	-2.90363	3.54E-04
Defa1	defensin, alpha 1	-2.90363	3.54E-04
Defa3	defensin, alpha, 3	-2.90363	3.54E-04
Defa17	defensin, alpha, 17	-2.90363	3.54E-04
Gm15284	predicted gene 15284	-2.90363	3.54E-04
Ptk6	PTK6 protein tyrosine kinase 6	-3.21581	1.38E-03
Hsd3b3	hydroxy-delta-5-steroid dehydrogenase, 3 beta- and steroid delta-isomerase 3	-6.29078	1.58E-03
Bcl3	B cell leukemia/lymphoma 3	-1.68086	3.90E-03
Pla2g2a	phospholipase A2, group IIA (platelets, synovial fluid)	-2.79005	4.67E-03
Axin2	axin2	-1.983	1.15E-02
Scnm1	sodium channel modifier 1	-1.46739	1.67E-02
Pfkfb3	6-phosphofructo-2-kinase/fructose-2,6-biphosphatase 3	-1.90765	2.27E-02
Pla2g2f	phospholipase A2, group IIF	-2.00405	3.38E-02
Mrpl9	mitochondrial ribosomal protein L9	-1.32533	4.06E-02
Lgr5	leucine rich repeat containing G protein coupled receptor 5	-2.3198	4.07E-02
Pdgfc	platelet-derived growth factor, C polypeptide	-1.70637	4.07E-02
Rnf43	ring finger protein 43	-1.38022	4.67E-02
Tmprss4	transmembrane protease, serine 4	-1.87996	6.10E-11
Itln1	intelectin 1 (galactofuranose binding)	-3.90916	2.37E-07

Itlnb	intelectin b	-3.90916	2.37E-07
Habp2	hyaluronic acid binding protein 2	-2.83344	1.47E-05
Hist2h2be	histone cluster 2, H2be	-2.77669	1.74E-05
Ces2a	carboxylesterase 2A	-3.33538	1.81E-04
Cubn	cubilin (intrinsic factor-cobalamin receptor)	-3.60788	3.06E-04
Gm14851	predicted gene 14851	-2.7629	3.20E-04
Gsdmc2	gasdermin C2	-4.66427	4.37E-04
Defa26	defensin, alpha, 26	-3.90023	4.70E-04
Gsdmc4	gasdermin C4	-3.45998	9.81E-04
Sc5d	sterol-C5-desaturase (fungal ERG3, delta-5-desaturase) homolog (S. cerevisae)	-1.58347	1.12E-03
Rnf145	ring finger protein 145	-1.76748	1.12E-03
AY761184	cDNA sequence AY761184	-2.94207	1.59E-03
Foxo6	forkhead box O6	-2.41695	1.76E-03
Ybx2	Y box protein 2	-2.56676	1.76E-03
Akr1b7	aldo-keto reductase family 1, member B7	-2.61393	1.87E-03
Clps	colipase, pancreatic	-3.18134	1.93E-03
Lyz1	lysozyme 1	-2.69469	2.66E-03
Ncald	neurocalcin delta	-1.80446	2.67E-03
Defa6	defensin, alpha, 6	-2.93032	3.90E-03
Defa24	defensin, alpha, 24	-2.93032	3.90E-03
Rnase1	ribonuclease, RNase A family, 1 (pancreatic)	-2.87722	4.70E-03
Cpb1	carboxypeptidase B1 (tissue)	-5.20607	4.70E-03
Ctrl	chymotrypsin-like	-5.5575	5.00E-03
Vwf	Von Willebrand factor homolog	-2.29885	5.51E-03
Pnliprp1	pancreatic lipase related protein 1	-5.37976	5.98E-03
Osbpl9	oxysterol binding protein-like 9	-1.35606	6.30E-03
Pycr1	pyrroline-5-carboxylate reductase 1	-2.18183	6.43E-03
Wnt2b	wingless-type MMTV integration site family, member 2B	-1.92861	6.52E-03
Dock7	dedicator of cytokinesis 7	-1.50073	1.18E-02
Elf3	E74-like factor 3	-1.58862	1.18E-02
Mptx2	mucosal pentraxin 2	-4.19714	1.22E-02
Tnfsf13b	tumor necrosis factor (ligand) superfamily, member 13b	-2.20469	1.35E-02
Myo19	myosin XIX	-1.49533	1.49E-02
Cbl	Casitas B-lineage lymphoma	-1.82077	1.57E-02
Hsd3b2	hydroxy-delta-5-steroid dehydrogenase, 3 beta- and steroid delta-isomerase 2	-4.70312	1.67E-02
Slc37a2	solute carrier family 37 (glycerol-3-phosphate transporter), member 2	-2.10145	1.67E-02
Irf8	interferon regulatory factor 8	-1.44071	1.79E-02
Defa21	defensin, alpha, 21	-3.63754	2.47E-02
LOC102639045	uncharacterized LOC102639045	-1.99438	2.53E-02
Tram2	translocating chain-associating membrane protein 2	-1.51946	2.58E-02
Wfdc10	WAP four-disulfide core domain 10	-4.38773	2.66E-02
Cyb5a	cytochrome b5 type A (microsomal)	-1.57633	2.68E-02
Aspg	asparaginase homolog (S. cerevisiae)	-1.76986	2.69E-02

Cyp2c55	cytochrome P450, family 2, subfamily c, polypeptide 55	-3.51936	2.72E-02
Sycn	syncollin	-4.39959	2.82E-02
Ces2b	carboxyesterase 2B	-2.37239	2.96E-02
D030028A08Rik	RIKEN cDNA D030028A08 gene	-1.94766	3.17E-02
Krt17	keratin 17	-4.21057	3.59E-02
Bcl9l	B cell CLL/lymphoma 9-like	-1.50643	3.70E-02
Xlr3a	X-linked lymphocyte-regulated 3A	-4.05232	3.95E-02
Fam107b	family with sequence similarity 107, member B	-1.8448	4.48E-02
Bhlha15	basic helix-loop-helix family, member a15	-2.03287	4.63E-02
Hsd17b4	hydroxysteroid (17-beta) dehydrogenase 4	-1.41443	4.93E-02
Hao2	hydroxyacid oxidase 2	-4.10493	4.93E-02

Table 7.2 – Genes upregulated in BCL9 BCL9l vs WT

Symbol	Gene name	Fold change	P-adj
Serpinb5	serine (or cysteine) peptidase inhibitor, clade B, member 5	2.180802	1.19E-02
E130012A19Rik	RIKEN cDNA E130012A19 gene	2.529961	1.81E-02
Mapk4	mitogen-activated protein kinase 4	1.85625	3.92E-02
Gpnmb	glycoprotein (transmembrane) nmb	2.31552	4.87E-02
Tchh	trichohyalin	10.49176	1.13E-13
Hist1h2al	histone cluster 1, H2al	16.62528	3.28E-11
Hinfp	histone H4 transcription factor	2.184706	3.28E-11
Tstd1	thiosulfate sulfurtransferase (rhodanese)-like domain containing 1	1.757146	4.95E-08
Hist2h2bb	histone cluster 2, H2bb	9.872563	6.11E-07
Acta1	actin, alpha 1, skeletal muscle	3.988028	1.13E-06
Hist1h1c	histone cluster 1, H1c	2.052511	7.65E-06
4930481B07Rik	RIKEN cDNA 4930481B07 gene	3.18442	1.32E-04
Dnah2	dynein, axonemal, heavy chain 2	2.358756	1.54E-04
Akr1c19	aldo-keto reductase family 1, member C19	2.983476	4.63E-04
Bcl2l15	BCLl2-like 15	2.416613	9.86E-04
Sct	secretin	1.761861	1.81E-03
Tmem116	transmembrane protein 116	4.007275	2.00E-03
C87977	expressed sequence C87977	4.305002	2.64E-

			03
Akr1c13	aldo-keto reductase family 1, member C13	2.108023	4.70E-03
Crebrf	CREB3 regulatory factor	1.497102	5.98E-03
Gstp2	glutathione S-transferase, pi 2	1.415342	2.72E-02
Gm3934	predicted gene 3934	1.415342	2.72E-02
Esr1	estrogen receptor 1 (alpha)	19.78518	1.03E-80
Pianp	PILR alpha associated neural protein	3.652625	5.25E-10
Sike1	suppressor of IKBKE 1	1.983325	2.11E-07
1500015A07Rik	RIKEN cDNA 1500015A07 gene	3.533533	4.54E-07
Gm156	predicted gene 156	3.669142	8.59E-07
C1s2	complement component 1, s subcomponent 2	6.862705	2.81E-06
C1rb	complement component 1, r subcomponent B	7.386748	3.94E-06
Apol9b	apolipoprotein L 9b	3.334812	5.02E-06
Pik3r3	phosphatidylinositol 3 kinase, regulatory subunit, polypeptide 3 (p55)	2.200377	2.85E-04
Klri2	killer cell lectin-like receptor family I member 2	4.57857	7.42E-04
Slc4a7	solute carrier family 4, sodium bicarbonate cotransporter, member 7	1.971297	9.81E-04
Hebp1	heme binding protein 1	1.917878	1.19E-03
Ctxn3	cortexin 3	2.954566	1.21E-03
Ifi44	interferon-induced protein 44	1.845908	1.61E-03
Ppp1r3g	protein phosphatase 1, regulatory (inhibitor) subunit 3G	5.677127	2.53E-03
Zmat4	zinc finger, matrin type 4	2.817032	2.56E-03
Clec2j	C-type lectin domain family 2, member J	5.233391	2.66E-03
Rbpms2	RNA binding protein with multiple splicing 2	2.044175	4.66E-03
Gm3470	predicted gene 3470	2.044175	4.66E-03
Acot1	acyl-CoA thioesterase 1	3.018551	5.00E-03
Rsad2	radical S-adenosyl methionine domain containing 2	2.393193	5.00E-03
Unc93a	unc-93 homolog A (C. elegans)	2.709171	5.48E-03
Ppme1	protein phosphatase methylesterase 1	1.52698	6.30E-03
Lpcat4	lysophosphatidylcholine acyltransferase 4	2.474251	6.43E-03
Lrrc3	leucine rich repeat containing 3	2.605904	6.48E-03

Smtn	smoothelin	1.724543	6.62E-03
Gpr151	G protein-coupled receptor 151	3.351399	7.86E-03
Crebl2	cAMP responsive element binding protein-like 2	1.443319	1.04E-02
Adam2	a disintegrin and metallopeptidase domain 2	4.229464	1.18E-02
Nipal2	NIPA-like domain containing 2	1.598145	1.35E-02
Ppp1r14a	protein phosphatase 1, regulatory (inhibitor) subunit 14A	2.022239	1.38E-02
Lmna	lamin A	1.807013	1.38E-02
Chrm2	cholinergic receptor, muscarinic 2, cardiac	2.095462	1.52E-02
Nr0b2	nuclear receptor subfamily 0, group B, member 2	2.497343	1.55E-02
Hcn3	hyperpolarization-activated, cyclic nucleotide-gated K+ 3	1.592397	1.65E-02
Apoc2	apolipoprotein C-II	1.761004	1.67E-02
D130043K22Rik	RIKEN cDNA D130043K22 gene	1.570282	1.69E-02
Rspo1	R-spondin homolog (Xenopus laevis)	4.066397	1.76E-02
Oas1g	2'-5' oligoadenylate synthetase 1G	2.257348	1.78E-02
Trim30a	tripartite motif-containing 30A	1.625961	1.78E-02
Mfge8	milk fat globule-EGF factor 8 protein	1.461762	1.81E-02
Phlda2	pleckstrin homology-like domain, family A, member 2	2.895465	1.85E-02
Kcnh2	potassium voltage-gated channel, subfamily H (eag-related), member 2	1.712857	2.17E-02
Slc25a4	solute carrier family 25 (mitochondrial carrier, adenine nucleotide translocator), member 4	1.785673	2.21E-02
Fbxl22	F-box and leucine-rich repeat protein 22	1.894663	2.22E-02
Gabarapl1	gamma-aminobutyric acid (GABA) A receptor-associated protein-like 1	1.481445	2.24E-02
Slc6a20b	solute carrier family 6 (neurotransmitter transporter), member 20B	3.003887	2.24E-02
Upb1	ureidopropionase, beta	2.048144	2.28E-02
Jph2	junctophilin 2	2.036142	2.29E-02
Bbc3	BCL2 binding component 3	1.895039	2.46E-02
Sptssb	serine palmitoyltransferase, small subunit B	3.936605	2.47E-02
1810037I17Rik	RIKEN cDNA 1810037I17 gene	1.547292	2.53E-02
Gm2036	predicted gene 2036	1.547292	2.53E-02
Nkx3-2	NK3 homeobox 2	2.917222	2.82E-02

Ckm	creatine kinase, muscle	2.358263	2.92E-02
Synm	synemin, intermediate filament protein	2.148719	2.96E-02
S100a6	S100 calcium binding protein A6 (calcyclin)	2.572725	3.15E-02
Pfkl	phosphofructokinase, liver, B-type	1.694715	3.16E-02
Ddit4l	DNA-damage-inducible transcript 4-like	3.337599	3.19E-02
Acadl	acyl-Coenzyme A dehydrogenase, long-chain	1.705547	3.25E-02
Egr1	early growth response 1	2.186315	3.42E-02
Pde4c	phosphodiesterase 4C, cAMP specific	1.993235	3.59E-02
Slc10a2	solute carrier family 10, member 2	3.576377	3.89E-02
Rasal1	RAS protein activator like 1 (GAP1 like)	3.482197	4.05E-02
Nme1	NME/NM23 nucleoside diphosphate kinase 1	1.684553	4.07E-02
Oas2	2'-5' oligoadenylate synthetase 2	2.331887	4.13E-02
Apol9a	apolipoprotein L 9a	1.79196	4.29E-02
Krt23	keratin 23	2.00667	4.47E-02
Oas1f	2'-5' oligoadenylate synthetase 1F	3.677794	4.71E-02
Hhatl	hedgehog acyltransferase-like	2.337317	4.93E-02
Tacr2	tachykinin receptor 2	3.025784	4.93E-02
Trim50	tripartite motif-containing 50	3.866943	4.93E-02
4931429I11Rik	RIKEN cDNA 4931429I11 gene	3.732122	4.93E-02

Table 7.3 Genes downregulated in APC BCL9 BCL9l vs APC

Symbol	Gene name	Fold Change	p-adj
Serpinb5	serine (or cysteine) peptidase inhibitor, clade B, member 5	-1.77591	3.39E-02
E130012A19Rik	RIKEN cDNA E130012A19 gene	-2.38567	5.04E-04
Mapk4	mitogen-activated protein kinase 4	-1.9539	6.84E-04
Gpnmb	glycoprotein (transmembrane) nmb	-2.5075	6.31E-03
Rps3a1	ribosomal protein S3A1	-16.375	1.10E-89
Capza1	capping protein (actin filament) muscle Z-line, alpha 1	-2.45369	2.57E-31
Amica1	adhesion molecule, interacts with CXADR antigen 1	-5.61048	2.11E-46

Tifa	TRAF-interacting protein with forkhead-associated domain	-4.59559	9.74E-12
Mansc1	MANSC domain containing 1	-1.52065	2.31E-04
Sorl1	sortilin-related receptor, LDLR class A repeats-containing	-1.46679	3.18E-03
Gm15315	predicted gene 15315	-3.77731	9.04E-05
Defa1	defensin, alpha 1	-3.61861	6.01E-04
Defa3	defensin, alpha, 3	-3.61861	6.01E-04
Defa17	defensin, alpha, 17	-3.61861	6.01E-04
Gm15284	predicted gene 15284	-3.61861	6.01E-04
Defa1	defensin, alpha 1	-3.61861	6.01E-04
Gm15284	predicted gene 15284	-3.61861	6.01E-04
Defa1	defensin, alpha 1	-3.61861	6.01E-04
Defa3	defensin, alpha, 3	-3.61861	6.01E-04
Defa17	defensin, alpha, 17	-3.61861	6.01E-04
Gm15284	predicted gene 15284	-3.61861	6.01E-04
Ptk6	PTK6 protein tyrosine kinase 6	-3.65449	5.22E-05
Hsd3b3	hydroxy-delta-5-steroid dehydrogenase, 3 beta- and steroid delta-isomerase 3	-3.97412	2.26E-02
Bcl3	B cell leukemia/lymphoma 3	-1.5082	2.24E-02
Pla2g2a	phospholipase A2, group IIA (platelets, synovial fluid)	-4.41971	1.26E-07
Axin2	axin2	-1.70178	4.59E-02
Scnm1	sodium channel modifier 1	-1.4454	8.91E-03
Pfkfb3	6-phosphofructo-2-kinase/fructose-2,6-biphosphatase 3	-1.88927	1.01E-02
Pla2g2f	phospholipase A2, group IIF	-3.50651	4.95E-09
Mrpl9	mitochondrial ribosomal protein L9	-1.27557	4.73E-02
Lgr5	leucine rich repeat containing G protein coupled receptor 5	-8.40323	2.16E-16
Pdgfc	platelet-derived growth factor, C polypeptide	-1.66482	1.94E-02
Rnf43	ring finger protein 43	-2.00067	4.85E-12
Scn2b	sodium channel, voltage-gated, type II, beta	-3.41631	1.26E-07
Rnf149	ring finger protein 149	-2.46486	1.41E-16
Ncs1	neuronal calcium sensor 1	-2.66606	1.61E-05
Ubash3b	ubiquitin associated and SH3 domain containing, B	-1.97895	3.29E-03

Tbx3os2	T-box 3, opposite strand 2	-2.42179	1.31E-03
Prom1	prominin 1	-1.62909	9.87E-04
Esrrg	estrogen-related receptor gamma	-2.93776	1.36E-03
Arhgdig	Rho GDP dissociation inhibitor (GDI) gamma	-2.19997	8.31E-04
Slc14a1	solute carrier family 14 (urea transporter), member 1	-5.87005	5.12E-06
Hebp2	heme binding protein 2	-1.93156	2.73E-03
Slc9a3	solute carrier family 9 (sodium/hydrogen exchanger), member 3	-2.26189	2.92E-02
Adamts4	a disintegrin-like and metallopeptidase (reprolysin type) with thrombospondin type 1 motif, 4	-2.25012	1.86E-02
Reg3d	regenerating islet-derived 3 delta	-3.17477	7.81E-03
Nlrx1	NLR family member X1	-1.52926	3.73E-02
Ampd3	adenosine monophosphate deaminase 3	-1.60609	4.80E-03
Tns4	tensin 4	-1.79127	1.59E-03
Slc23a2	solute carrier family 23 (nucleobase transporters), member 2	-1.6242	1.09E-03
Trappc4	trafficking protein particle complex 4	-1.37702	1.89E-02
Hspa8	heat shock protein 8	-1.56622	2.95E-02
Fzd9	frizzled homolog 9 (Drosophila)	-2.97038	1.51E-03
Igfbp4	insulin-like growth factor binding protein 4	-1.75528	2.33E-02
C2cd4b	C2 calcium-dependent domain containing 4B	-7.49564	6.86E-06
Adcy8	adenylate cyclase 8	-1.9038	1.35E-03
Bcl9	B cell CLL/lymphoma 9	-1.52749	6.92E-03
Ffar4	free fatty acid receptor 4	-1.69917	2.40E-03
Hk2	hexokinase 2	-2.37391	1.18E-03
Exph5	exophilin 5	-1.66292	2.45E-02
Anxa9	annexin A9	-5.37891	1.34E-14
Mmp10	matrix metallopeptidase 10	-1.47109	5.01E-03
Mmp20	matrix metallopeptidase 20 (enamelysin)	-2.43436	4.64E-02
Snx10	sorting nexin 10	-2.10319	2.77E-09
Il4ra	interleukin 4 receptor, alpha	-1.7332	3.86E-02
Nrn1	neuritin 1	-2.03907	4.52E-02

Sdr16c5	short chain dehydrogenase/reductase family 16C, member 5	-6.04887	5.07E-05
Ctxn1	cortexin 1	-1.82015	1.28E-02
Bex1	brain expressed gene 1	-5.29762	1.48E-07
Tgif2	TGFB-induced factor homeobox 2	-1.63441	1.90E-02
Card14	caspase recruitment domain family, member 14	-2.30513	5.40E-03
Rasd1	RAS, dexamethasone-induced 1	-5.34648	2.18E-03
Phtf1	putative homeodomain transcription factor 1	-1.29702	4.79E-02
Gramd1a	GRAM domain containing 1A	-1.66344	1.76E-03
Cers2	ceramide synthase 2	-1.51365	4.68E-04
Tirap	toll-interleukin 1 receptor (TIR) domain-containing adaptor protein	-1.41242	1.50E-02
Plxnb1	plexin B1	-1.95897	2.61E-05
Arid5a	AT rich interactive domain 5A (MRF1-like)	-2.31183	1.09E-03
Rgs12	regulator of G-protein signaling 12	-1.47624	3.67E-02
Syne4	spectrin repeat containing, nuclear envelope family member 4	-2.79161	3.81E-06
Wipf1	WAS/WASL interacting protein family, member 1	-1.32394	1.13E-02
B4galnt4	beta-1,4-N-acetyl-galactosaminyl transferase 4	-1.66673	2.91E-03
Hmces	5-hydroxymethylcytosine (hmC) binding, ES cell specific	-1.32973	1.19E-02
Dusp4	dual specificity phosphatase 4	-2.49981	2.83E-13
Vangl2	vang-like 2 (van gogh, Drosophila)	-1.90591	2.12E-04
Slc41a1	solute carrier family 41, member 1	-1.97045	1.02E-03
Mecom	MDS1 and EVI1 complex locus	-2.54851	9.71E-03
Soat1	sterol O-acyltransferase 1	-1.39018	1.56E-04
Celsr1	cadherin, EGF LAG seven-pass G-type receptor 1 (flamingo homolog, Drosophila)	-1.98681	4.39E-02
Hpn	hepsin	-1.97116	6.54E-03
Lgr6	leucine-rich repeat-containing G protein-coupled receptor 6	-13.7798	2.50E-19
Kctd1	potassium channel tetramerisation domain containing 1	-1.77016	2.42E-02
6030419C18Rik	RIKEN cDNA 6030419C18 gene	-3.54827	3.86E-16
Slc7a2	solute carrier family 7 (cationic amino acid transporter, y+ system), member 2	-3.40394	4.03E-04
Btg3	B cell translocation gene 3	-1.61648	3.83E-02

Gm7334	B-cell translocation gene 3 pseudogene	-1.61648	3.83E-02
Marcksl1	MARCKS-like 1	-2.51648	8.68E-10
Nptx1	neuronal pentraxin 1	-3.16199	2.25E-02
Gif	gastric intrinsic factor	-3.70985	3.39E-02
Adcy1	adenylate cyclase 1	-2.59465	2.90E-04
Cnp	2',3'-cyclic nucleotide 3' phosphodiesterase	-1.29395	1.15E-02
Klhdc2	kelch domain containing 2	-1.34756	1.83E-02
Zdhhc15	zinc finger, DHHC domain containing 15	-1.7746	1.59E-03
Ajuba	ajuba LIM protein	-1.70666	4.27E-02
Atp2c2	ATPase, Ca++ transporting, type 2C, member 2	-1.6421	2.47E-02
Tat	tyrosine aminotransferase	-11.9667	6.01E-08
Tnfrsf11b	tumor necrosis factor receptor superfamily, member 11b (osteoprotegerin)	-2.16002	1.19E-02
Celsr2	cadherin, EGF LAG seven-pass G-type receptor 2 (flamingo homolog, Drosophila)	-1.64142	3.21E-02
Cml2	camello-like 2	-2.09687	3.82E-03
Slc40a1	solute carrier family 40 (iron-regulated transporter), member 1	-2.63927	7.79E-03
Mfng	MFNG O-fucosylpeptide 3-beta-N-acetylglucosaminyltransferase	-1.62161	1.63E-02
Col9a3	collagen, type IX, alpha 3	-2.94643	6.06E-05
Gm15293	predicted gene 15293	-7.48909	8.63E-08
Vangl1	vang-like 1 (van gogh, Drosophila)	-1.94116	5.55E-05
Rcor2	REST corepressor 2	-2.13782	4.70E-04
Fosl1	fos-like antigen 1	-2.57568	3.31E-03
Notum	notum pectinacetylesterase homolog (Drosophila)	-8.77447	2.51E-20
Otop2	otopetrin 2	-4.39219	1.17E-02
Spry4	sprouty homolog 4 (Drosophila)	-2.07503	2.60E-02
Tead2	TEA domain family member 2	-2.57461	5.66E-08
Cers3	ceramide synthase 3	-2.94785	2.57E-02
Saa1	serum amyloid A 1	-7.29493	4.43E-05
Vwa2	von Willebrand factor A domain containing 2	-3.15924	2.03E-04
Trib1	tribbles homolog 1 (Drosophila)	-1.42012	3.99E-03
Cenpm	centromere protein M	-	2.92E-

		1.87164	02
Afap1l1	actin filament associated protein 1-like 1	-1.84867	3.68E-03
Wnt10a	wingless-type MMTV integration site family, member 10A	-5.32648	2.15E-03
Cbs	cystathionine beta-synthase	-3.15359	5.79E-05
1700066B19Rik	RIKEN cDNA 1700066B19 gene	-1.80232	2.84E-02
Wfdc18	WAP four-disulfide core domain 18	-3.57629	2.00E-02
Ldlrad3	low density lipoprotein receptor class A domain containing 3	-1.89484	3.07E-05
Cic	capicua homolog (Drosophila)	-1.21561	6.57E-03
Socs3	suppressor of cytokine signaling 3	-2.96243	2.06E-02
Camk2b	calcium/calmodulin-dependent protein kinase II, beta	-4.98501	2.87E-06
Tmc5	transmembrane channel-like gene family 5	-1.65459	4.90E-02
Ggh	gamma-glutamyl hydrolase	-2.77208	3.89E-03
1500009C09Rik	RIKEN cDNA 1500009C09 gene	-5.43473	2.52E-04
Hif1a	hypoxia inducible factor 1, alpha subunit	-1.70735	2.56E-02
Dlgap4	discs, large homolog-associated protein 4 (Drosophila)	-1.26294	2.91E-02
Amotl2	angiomotin-like 2	-1.36254	4.94E-02
Atp7a	ATPase, Cu++ transporting, alpha polypeptide	-1.48413	4.07E-02
Med13l	mediator complex subunit 13-like	-1.26881	2.18E-02
Dok7	docking protein 7	-2.20893	4.94E-02
Nkd1	naked cuticle 1 homolog (Drosophila)	-3.01251	8.17E-08
Pgs1	phosphatidylglycerophosphate synthase 1	-1.56819	2.31E-02
Piwil2	piwi-like RNA-mediated gene silencing 2	-2.01823	2.25E-04
Cited1	Cbp/p300-interacting transactivator with Glu/Asp-rich carboxy-terminal domain 1	-6.54692	7.81E-08
Neb	nebulin	-2.4001	2.30E-02
Rgcc	regulator of cell cycle	-2.68927	2.28E-04
Samd5	sterile alpha motif domain containing 5	-2.97649	9.71E-03
Runx1	runt related transcription factor 1	-1.7379	4.66E-02
Prox1	prospero homeobox 1	-5.57212	3.31E-24
Ubc	ubiquitin C	-2.10034	2.88E-02
Myo5c	myosin VC	-1.47218	1.18E-02

B3gnt7	UDP-GlcNAc:betaGal beta-1,3-N-acetylglucosaminyltransferase 7	-2.4368	1.74E-02
Iffo2	intermediate filament family orphan 2	-1.67258	8.12E-03
Tnnc1	troponin C, cardiac/slow skeletal	-2.87346	2.94E-02
Sav1	salvador homolog 1 (Drosophila)	-1.19292	4.77E-02
Atoh8	atonal homolog 8 (Drosophila)	-1.56467	3.38E-02
Ttc9	tetratricopeptide repeat domain 9	-3.56135	5.94E-04
Camsap1	calmodulin regulated spectrin-associated protein 1	-1.36652	3.61E-03
Fam222a	family with sequence similarity 222, member A	-1.90679	3.12E-02
4933406C10Rik	RIKEN cDNA 4933406C10 gene	-2.67997	3.87E-03
Inf2	inverted formin, FH2 and WH2 domain containing	-2.24243	3.38E-02
Sdc1	syndecan 1	-1.52779	1.94E-02
Slco5a1	solute carrier organic anion transporter family, member 5A1	-3.33137	1.10E-03
Akap13	A kinase (PRKA) anchor protein 13	-1.44021	1.49E-02
Serpina10	serine (or cysteine) peptidase inhibitor, clade A (alpha-1 antiproteinase, antitrypsin), member 10	-4.17349	1.48E-02
Smo	smoothened homolog (Drosophila)	-1.6438	3.28E-02
Nrtn	neurturin	-1.55526	4.58E-02
Ldhd	lactate dehydrogenase D	-3.03763	2.44E-02
Tmed2	transmembrane emp24 domain trafficking protein 2	-1.46774	2.95E-02
Gm21540	predicted gene, 21540	-1.46774	2.95E-02
Gga2	golgi associated, gamma adaptin ear containing, ARF binding protein 2	-1.45348	1.49E-02
Mex3d	mex3 homolog D (C. elegans)	-1.65597	9.97E-03
Tpbg	trophoblast glycoprotein	-2.20963	2.23E-06
Pbx1	pre B cell leukemia homeobox 1	-1.43052	2.81E-02
Inhbb	inhibin beta-B	-2.26819	2.91E-02
Ubxn10	UBX domain protein 10	-1.86346	2.31E-02
Lrrc4	leucine rich repeat containing 4	-2.96921	1.59E-04
Fmnl2	formin-like 2	-2.81324	1.31E-09
Arl4c	ADP-ribosylation factor-like 4C	-3.01902	9.37E-14
Pim3	proviral integration site 3	-2.43477	2.71E-04

Fam89a	family with sequence similarity 89, member A	-4.12943	1.15E-11
Pacsin3	protein kinase C and casein kinase substrate in neurons 3	-2.25746	2.26E-03
Adamts16	a disintegrin-like and metallopeptidase (reprolysin type) with thrombospondin type 1 motif, 16	-5.06832	3.60E-03
Stra6	stimulated by retinoic acid gene 6	-5.12005	5.96E-04
Adam8	a disintegrin and metallopeptidase domain 8	-3.3708	1.47E-11
Pdgfrl	platelet-derived growth factor receptor-like	-4.79734	1.49E-10
Sox4	SRY (sex determining region Y)-box 4	-2.03551	2.87E-05
Nav1	neuron navigator 1	-1.51679	3.55E-05
L3mbtl3	l(3)mbt-like 3 (Drosophila)	-1.27605	4.15E-02
Tnfrsf19	tumor necrosis factor receptor superfamily, member 19	-9.56132	1.95E-34
Msx1	msh homeobox 1	-15.5665	3.48E-32
Ttc39a	tetratricopeptide repeat domain 39A	-1.59919	1.77E-05
Foxred2	FAD-dependent oxidoreductase domain containing 2	-2.13285	8.64E-04
Nsmce1	non-SMC element 1 homolog (S. cerevisiae)	-1.39488	5.98E-03
Zfp703	zinc finger protein 703	-1.3213	1.14E-02
Agap3	ArfGAP with GTPase domain, ankyrin repeat and PH domain 3	-1.24555	2.92E-02
Fggy	FGGY carbohydrate kinase domain containing	-1.68797	4.48E-02
Tmem173	transmembrane protein 173	-2.43722	2.65E-04
Sema4c	sema domain, immunoglobulin domain (Ig), transmembrane domain (TM) and short cytoplasmic domain, (semaphorin) 4C	-1.47994	9.78E-03
S100a11	S100 calcium binding protein A11 (calgizzarin)	-2.18237	3.64E-02
Gm5068	predicted gene 5068	-2.18237	3.64E-02
Gm12854	predicted gene 12854	-2.18237	3.64E-02
Mex3a	mex3 homolog A (C. elegans)	-3.24259	6.02E-07
Gpr171	G protein-coupled receptor 171	-1.9468	3.97E-02
Myh9	myosin, heavy polypeptide 9, non-muscle	-1.20026	4.87E-02
Fgfrl1	fibroblast growth factor receptor-like 1	-2.34578	9.93E-07
Rraga	Ras-related GTP binding A	-1.22178	2.50E-02
Zfhx3	zinc finger homeobox 3	-1.43511	1.84E-02
Patz1	POZ (BTB) and AT hook containing	-	3.93E-

	zinc finger 1	1.41236	02
Gadd45g	growth arrest and DNA-damage-inducible 45 gamma	-3.1032	1.51E-06
Cd24a	CD24a antigen	-1.67453	1.03E-03
Lancl3	LanC lantibiotic synthetase component C-like 3 (bacterial)	-3.0061	4.89E-02
Sox17	SRY (sex determining region Y)-box 17	-2.052	1.28E-03
Ier3	immediate early response 3	-2.34621	5.22E-05
Sema3c	sema domain, immunoglobulin domain (Ig), short basic domain, secreted, (semaphorin) 3C	-2.20449	1.36E-03
Pthlh	parathyroid hormone-like peptide	-2.05402	3.95E-02
Ica1	islet cell autoantigen 1	-1.51949	1.32E-02
Afap1	actin filament associated protein 1	-1.57879	4.64E-02
Fkbp1a	FK506 binding protein 1a	-1.33633	4.16E-03
Tmem132a	transmembrane protein 132A	-1.84037	7.92E-05
Sidt1	SID1 transmembrane family, member 1	-1.48332	4.59E-02
Fam69b	family with sequence similarity 69, member B	-1.83381	3.26E-04
Clic4	chloride intracellular channel 4 (mitochondrial)	-1.40502	1.85E-02
Ahsg	alpha-2-HS-glycoprotein	-4.65033	5.25E-03
Gjb4	gap junction protein, beta 4	-3.5826	3.28E-02
Hid1	HID1 domain containing	-1.51187	1.64E-02
Hrg	histidine-rich glycoprotein	-5.1289	2.30E-03
1700001O22Rik	RIKEN cDNA 1700001O22 gene	-2.50334	3.46E-03
Slc39a6	solute carrier family 39 (metal ion transporter), member 6	-1.51333	1.26E-02
Arhgef26	Rho guanine nucleotide exchange factor (GEF) 26	-1.70138	4.83E-05
Ecscr	endothelial cell surface expressed chemotaxis and apoptosis regulator	-2.34992	5.70E-04
Fmod	fibromodulin	-3.60621	3.82E-02
Rem2	rad and gem related GTP binding protein 2	-2.22079	4.62E-02
Cfi	complement component factor i	-2.15837	3.29E-04
Dsg3	desmoglein 3	-4.623	9.23E-04
Thbs1	thrombospondin 1	-2.29074	3.89E-03
Sik1	salt inducible kinase 1	-1.46908	1.50E-02
Mtcl1	microtubule crosslinking factor 1	-2.41418	2.47E-02

Igfbp3	insulin-like growth factor binding protein 3	-2.05172	4.76E-02
Chic2	cysteine-rich hydrophobic domain 2	-1.31857	6.93E-03
Nnt	nicotinamide nucleotide transhydrogenase	-1.86973	2.51E-05
Sp5	trans-acting transcription factor 5	-2.15028	9.25E-06
Rtn4	reticulon 4	-1.42108	4.24E-02
Dusp1	dual specificity phosphatase 1	-1.97413	1.82E-02
Prss22	protease, serine 22	-3.51957	4.62E-02
Jag2	jagged 2	-1.96813	2.11E-03
Rasal2	RAS protein activator like 2	-1.47489	7.49E-03
Lef1	lymphoid enhancer binding factor 1	-8.77801	3.77E-19
Sypl	synaptophysin-like protein	-1.58095	1.84E-02
Vldlr	very low density lipoprotein receptor	-2.12129	1.67E-02
Laptm4b	lysosomal-associated protein transmembrane 4B	-1.38923	4.52E-05
Kansl1l	KAT8 regulatory NSL complex subunit 1-like	-2.17298	6.15E-05
Rps6kl1	ribosomal protein S6 kinase-like 1	-2.08867	1.90E-04
Nxpe3	neurexophilin and PC-esterase domain family, member 3	-1.82444	3.94E-04
Kif12	kinesin family member 12	-2.34313	6.05E-04
Zfp184	zinc finger protein 184 (Kruppel-like)	-1.93938	8.26E-03
Hpx	hemopexin	-4.29202	1.03E-02
Gm11978	predicted gene 11978	-4.14254	1.17E-02
Entpd3	ectonucleoside triphosphate diphosphohydrolase 3	-3.07934	1.64E-02
Rhobtb3	Rho-related BTB domain containing 3	-1.44215	1.69E-02
Cited4	Cbp/p300-interacting transactivator, with Glu/Asp-rich carboxy-terminal domain, 4	-1.93129	1.90E-02
Trim35	tripartite motif-containing 35	-1.5571	2.07E-02
Flot2	flotillin 2	-1.68554	2.46E-02
Ncmap	noncompact myelin associated protein	-2.36071	2.47E-02
Trim10	tripartite motif-containing 10	-3.73336	2.91E-02
Ly6c1	lymphocyte antigen 6 complex, locus C1	-1.73309	3.26E-02
Aqp5	aquaporin 5	-3.67621	3.39E-02
Nebl	nebulette	-2.29299	3.86E-02

Il11	interleukin 11	-2.97134	3.95E-02
Sh3pxd2b	SH3 and PX domains 2B	-1.77592	4.07E-02
Kdm1a	lysine (K)-specific demethylase 1A	-1.2035	4.77E-02
Sh2d5	SH2 domain containing 5	-2.70984	4.89E-02
Lrrc58	leucine rich repeat containing 58	-1.32458	1.82E-04
Gpsm1	G-protein signalling modulator 1 (AGS3-like, C. elegans)	-1.50305	2.95E-02
Faim2	Fas apoptotic inhibitory molecule 2	-7.00088	1.55E-33
Ccdc3	coiled-coil domain containing 3	-2.96859	1.48E-07
Kif26b	kinesin family member 26B	-3.66765	1.48E-06
Vash2	vasohibin 2	-2.73182	1.35E-05
Klhl8	kelch-like 8	-2.19134	1.95E-04
Phldb2	pleckstrin homology-like domain, family B, member 2	-1.78668	3.13E-04
Siglec15	sialic acid binding Ig-like lectin 15	-6.06229	7.41E-04
Lamc2	laminin, gamma 2	-2.56052	9.87E-04
Ptpn9	protein tyrosine phosphatase, non-receptor type 9	-1.35493	2.78E-03
Krt4	keratin 4	-4.51719	9.71E-03
Alb	albumin	-4.22789	1.28E-02
Phlda1	pleckstrin homology-like domain, family A, member 1	-2.23928	1.66E-02
Lpo	lactoperoxidase	-3.87074	1.69E-02
Dio2	deiodinase, iodothyronine, type II	-3.34104	3.17E-02
Ildr1	immunoglobulin-like domain containing receptor 1	-2.04937	3.52E-02
Gpc2	glypican 2 (cerebroglycan)	-1.73757	4.29E-02
Cblb	Casitas B-lineage lymphoma b	-1.53605	4.09E-03
Pls3	plastin 3 (T-isoform)	-1.78881	8.24E-03
Krt36	keratin 36	-2.93968	1.40E-05
St3gal1	ST3 beta-galactoside alpha-2,3-sialyltransferase 1	-1.56016	7.11E-03
Mpzl1	myelin protein zero-like 1	-1.35325	8.44E-03
Ly6g	lymphocyte antigen 6 complex, locus G	-4.47678	9.97E-03
Col11a1	collagen, type XI, alpha 1	-4.48655	9.79E-03
Zc3h12c	zinc finger CCCH type containing 12C	-1.8654	4.46E-02
Fam115a	family with sequence similarity 115,	-	3.04E-

	member A	1.75192	04
Cyp26b1	cytochrome P450, family 26, subfamily b, polypeptide 1	-1.83281	1.40E-02
Mdfi	MyoD family inhibitor	-2.45075	1.73E-04
Pde4dip	phosphodiesterase 4D interacting protein (myomegalin)	-1.41448	4.02E-03
Cdk17	cyclin-dependent kinase 17	-1.57689	1.40E-02
D630045J12Rik	RIKEN cDNA D630045J12 gene	-2.26444	1.11E-02
Cpne2	copine II	-2.04637	2.88E-04
Asb4	ankyrin repeat and SOCS box-containing 4	-7.94958	1.53E-12
Igsf11	immunoglobulin superfamily, member 11	-3.43597	1.67E-08
Zfp503	zinc finger protein 503	-2.82469	4.72E-08
Sox21	SRY (sex determining region Y)-box 21	-4.01815	1.60E-04
Ptk7	PTK7 protein tyrosine kinase 7	-1.7324	2.74E-04
Mamld1	mastermind-like domain containing 1	-2.34249	5.01E-04
Tbpl1	TATA box binding protein-like 1	-1.32551	1.63E-03
Grip2	glutamate receptor interacting protein 2	-3.24599	3.97E-03
Slc7a6	solute carrier family 7 (cationic amino acid transporter, y+ system), member 6	-1.76131	7.48E-03
Chit1	chitinase 1 (chitotriosidase)	-4.06054	8.20E-03
Wnt5b	wingless-type MMTV integration site family, member 5B	-2.04356	8.46E-03
Llgl1	lethal giant larvae homolog 1 (Drosophila)	-1.33202	1.02E-02
Fga	fibrinogen alpha chain	-3.58668	2.43E-02
Rab15	RAB15, member RAS oncogene family	-1.53896	3.39E-02
Cgnl1	cingulin-like 1	-2.01126	3.60E-02
Hs2st1	heparan sulfate 2-O-sulfotransferase 1	-1.27456	3.66E-02
Csrnp1	cysteine-serine-rich nuclear protein 1	-1.96395	3.96E-02
Ccdc112	coiled-coil domain containing 112	-1.69965	4.34E-02
5430416N02Rik	RIKEN cDNA 5430416N02 gene	-1.52912	4.46E-02
Slc29a4	solute carrier family 29 (nucleoside transporters), member 4	-1.76583	4.49E-02
Mal	myelin and lymphocyte protein, T cell differentiation protein	-2.79032	4.78E-02
Tspan33	tetraspanin 33	-2.04584	4.80E-02
Padi2	peptidyl arginine deiminase, type II	-2.21459	4.63E-02

Ap1s2	adaptor-related protein complex 1, sigma 2 subunit	-1.49163	4.02E-02
Evl	Ena-vasodilator stimulated phosphoprotein	-1.6944	1.39E-07
Slc45a3	solute carrier family 45, member 3	-2.1859	2.31E-02
Igfbp1	insulin-like growth factor binding protein 1	-4.63669	6.55E-03
Naa30	N(alpha)-acetyltransferase 30, NatC catalytic subunit	-1.42867	1.02E-02
Gm12603	predicted gene 12603	-3.82795	2.06E-02
Foxq1	forkhead box Q1	-1.63291	2.34E-02
Chsy1	chondroitin sulfate synthase 1	-1.43299	4.21E-02
Bckdhb	branched chain ketoacid dehydrogenase E1, beta polypeptide	-1.77139	2.34E-02
Fstl4	follistatin-like 4	-5.36945	4.33E-06
Cybrd1	cytochrome b reductase 1	-2.51283	2.47E-04
Nfe2l3	nuclear factor, erythroid derived 2, like 3	-2.94259	1.44E-02
Plcd3	phospholipase C, delta 3	-2.75625	3.55E-04
Tead4	TEA domain family member 4	-2.05853	1.55E-02
Rab11fip5	RAB11 family interacting protein 5 (class I)	-2.68788	8.63E-04
Echdc2	enoyl Coenzyme A hydratase domain containing 2	-1.35999	8.86E-03
Rnf217	ring finger protein 217	-1.63544	2.15E-02
Fbf1	Fas (TNFRSF6) binding factor 1	-1.30188	2.16E-02
B630005N14Rik	RIKEN cDNA B630005N14 gene	-1.3453	5.64E-03
Cxxc5	CXXC finger 5	-1.48447	1.15E-02
Tacstd2	tumor-associated calcium signal transducer 2	-5.01626	8.22E-07
Prr18	proline rich 18	-5.57043	3.77E-06
Tubb2b	tubulin, beta 2B class IIB	-2.53447	7.02E-06
Wtip	WT1-interacting protein	-2.50019	4.45E-05
Snn	stannin	-1.80181	2.52E-04
Plat	plasminogen activator, tissue	-2.72446	1.51E-03
Ptprg	protein tyrosine phosphatase, receptor type, G	-1.41198	1.58E-03
Map4k4	mitogen-activated protein kinase kinase kinase kinase 4	-1.31029	2.59E-03
Sgpp1	sphingosine-1-phosphate phosphatase 1	-2.75809	7.03E-03
Fut2	fucosyltransferase 2	-4.49123	7.71E-03
Akt2	thymoma viral proto-oncogene 2	-	9.97E-

		1.37158	03
Stom	stomatin	-2.49503	1.27E-02
Nme7	NME/NM23 family member 7	-1.45431	1.50E-02
Hamp	hepcidin antimicrobial peptide	-3.33952	2.61E-02
Msantd3	Myb/SANT-like DNA-binding domain containing 3	-1.57404	2.88E-02
Chst4	carbohydrate (chondroitin 6/keratan) sulfotransferase 4	-2.916	4.07E-02
Gm766	predicted gene 766	-3.24881	4.22E-02
Wif1	Wnt inhibitory factor 1	-2.51159	4.73E-02
Sox9	SRY (sex determining region Y)-box 9	-2.04841	2.88E-02
Zdhhc8	zinc finger, DHHC domain containing 8	-1.55346	1.18E-02
Tns3	tensin 3	-1.38667	4.30E-02
Csnk1e	casein kinase 1, epsilon	-1.52244	1.66E-04
Gdf11	growth differentiation factor 11	-2.01924	2.34E-03
Vill	villin-like	-2.49526	7.25E-03
Smim3	small integral membrane protein 3	-1.97234	1.46E-02
Btbd17	BTB (POZ) domain containing 17	-3.4844	2.41E-03
Abtb2	ankyrin repeat and BTB (POZ) domain containing 2	-1.99239	1.89E-02

Table 7.4 - Genes upregulated in APC BCL9 BCL9l vs APC

Symbol	Gene name	Fold Change	p-adj
Gstm1	glutathione S-transferase, mu 1	1.689535	1.45E-02
Defa2	defensin, alpha, 2	5.885585	7.70E-05
Gm21002	predicted gene, 21002	5.885585	7.70E-05
Gstm3	glutathione S-transferase, mu 3	3.445339	2.35E-06
Cyp2c66	cytochrome P450, family 2, subfamily c, polypeptide 66	4.225231	5.15E-06
S100g	S100 calcium binding protein G	2.451775	9.29E-05
Tchh	trichohyalin	2.474049	2.19E-02
Hist1h2al	histone cluster 1, H2al	6.522704	3.02E-05
Hinfp	histone H4 transcription factor	1.401805	2.48E-02
Tstd1	thiosulfate sulfurtransferase (rhodanese)-like domain containing 1	1.589304	1.75E-05

Hist2h2bb	histone cluster 2, H2bb	8.978008	3.56E-07
Acta1	actin, alpha 1, skeletal muscle	2.510933	2.34E-03
Hist1h1c	histone cluster 1, H1c	1.535783	2.31E-02
4930481B07Rik	RIKEN cDNA 4930481B07 gene	3.705657	1.04E-07
Dnah2	dynein, axonemal, heavy chain 2	2.104403	1.23E-03
Akr1c19	aldo-keto reductase family 1, member C19	4.248832	5.94E-08
Bcl2l15	BCLl2-like 15	2.214544	1.60E-03
Sct	secretin	1.885254	6.15E-05
Tmem116	transmembrane protein 116	7.590506	1.67E-08
C87977	expressed sequence C87977	6.12295	7.68E-05
Akr1c13	aldo-keto reductase family 1, member C13	2.240226	4.48E-04
Crebrf	CREB3 regulatory factor	1.517633	1.51E-03
Gstp2	glutathione S-transferase, pi 2	1.403174	1.64E-02
Gm3934	predicted gene 3934	1.403174	1.64E-02
Cntnap1	contactin associated protein-like 1	1.86442	2.65E-03
Afp	alpha fetoprotein	2.898207	4.06E-09
Ctso	cathepsin O	1.47218	1.06E-02
Tmem151a	transmembrane protein 151A	1.971401	2.09E-02
Thnsl2	threonine synthase-like 2 (bacterial)	1.921996	6.06E-05
Htatip2	HIV-1 tat interactive protein 2, homolog (human)	1.453831	1.43E-02
Abca8a	ATP-binding cassette, sub-family A (ABC1), member 8a	1.801451	7.96E-03
Nudcd3	NudC domain containing 3	1.355882	1.66E-02
Aldh1a7	aldehyde dehydrogenase family 1, subfamily A7	1.784763	3.46E-03
Reg4	regenerating islet-derived family, member 4	2.964311	3.94E-06
Sycp1	synaptonemal complex protein 1	6.015414	8.11E-04
Styxl1	serine/threonine/tyrosine interacting-like 1	3.270465	2.36E-04
Gm7120	predicted gene 7120	2.705497	3.23E-02
Gm7120	predicted gene 7120	2.705497	3.23E-02
Ms4a10	membrane-spanning 4-domains, subfamily A, member 10	1.750058	4.49E-02
Fmo1	flavin containing monooxygenase 1	1.950987	2.16E-02
Trim72	tripartite motif-containing 72	2.326642	6.38E-

			04
Rbp2	retinol binding protein 2, cellular	1.847147	1.18E-03
H1f0	H1 histone family, member 0	1.36439	1.67E-02
Ros1	Ros1 proto-oncogene	3.091572	4.53E-03
Vstm2l	V-set and transmembrane domain containing 2-like	1.870148	4.35E-02
Hmcn2	hemicentin 2	1.740593	1.71E-03
Rorc	RAR-related orphan receptor gamma	2.421253	1.14E-06
Pxmp4	peroxisomal membrane protein 4	1.819787	5.73E-05
4930552P12Rik	RIKEN cDNA 4930552P12 gene	2.93591	2.20E-03
Mmd	monocyte to macrophage differentiation-associated	1.412839	4.50E-02
Me2	malic enzyme 2, NAD(+)-dependent, mitochondrial	1.490309	4.58E-02
Plin2	perilipin 2	1.318122	4.31E-02
Akr1c12	aldo-keto reductase family 1, member C12	1.804294	1.25E-02
Gm15299	predicted pseudogene 15299	5.35883	2.09E-03
Actc1	actin, alpha, cardiac muscle 1	2.036217	1.54E-02
Lipa	lysosomal acid lipase A	1.489877	4.62E-02
Ppp1r3b	protein phosphatase 1, regulatory (inhibitor) subunit 3B	1.780291	4.76E-02
Ugdh	UDP-glucose dehydrogenase	1.766232	1.91E-05
Cdkn1c	cyclin-dependent kinase inhibitor 1C (P57)	1.572191	3.83E-04
Bche	butyrylcholinesterase	2.106371	9.75E-06
Ugt2b5	UDP glucuronosyltransferase 2 family, polypeptide B5	3.139375	5.14E-03
Fabp1	fatty acid binding protein 1, liver	2.139007	7.51E-09
Sh3rf2	SH3 domain containing ring finger 2	1.593324	1.16E-02
Cyb5b	cytochrome b5 type B	1.382478	1.79E-02
Cyp4a10	cytochrome P450, family 4, subfamily a, polypeptide 10	3.355446	4.58E-02
Car13	carbonic anhydrase 13	1.283026	1.23E-02
Acot4	acyl-CoA thioesterase 4	2.150097	1.05E-03
Gdf9	growth differentiation factor 9	2.2854	4.12E-02
Tldc2	TBC/LysM associated domain containing 2	1.825268	1.32E-06
Ugt2b36	UDP glucuronosyltransferase 2 family, polypeptide B36	3.199629	6.42E-04
Rec8	REC8 meiotic recombination protein	1.654617	3.54E-02

Mro	maestro	1.931174	2.87E-02
Slc2a8	solute carrier family 2, (facilitated glucose transporter), member 8	1.447884	4.49E-02
Cyp2c44	cytochrome P450, family 2, subfamily c, polypeptide 44	2.336762	2.18E-02
Erp29	endoplasmic reticulum protein 29	1.454424	6.51E-04
Rnase6	ribonuclease, RNase A family, 6	1.699118	2.02E-02
Rab30	RAB30, member RAS oncogene family	2.651253	2.42E-02
Kcnk3	potassium channel, subfamily K, member 3	2.092507	4.79E-03
Wfdc1	WAP four-disulfide core domain 1	1.794553	2.03E-04
6330403A02Rik	RIKEN cDNA 6330403A02 gene	2.020447	2.32E-03
Rbm46	RNA binding motif protein 46	2.368278	2.81E-02
Gpd1	glycerol-3-phosphate dehydrogenase 1 (soluble)	1.391013	3.14E-02
Slc26a10	solute carrier family 26, member 10	1.990899	6.32E-05
Tcea3	transcription elongation factor A (SII), 3	1.971189	3.80E-03
Pld1	phospholipase D1	1.428203	4.05E-03
Sybu	syntabulin (syntaxin-interacting)	2.013976	1.71E-02
Ralgps1	Ral GEF with PH domain and SH3 binding motif 1	1.559915	2.95E-02
1810046K07Rik	RIKEN cDNA 1810046K07 gene	3.060989	1.42E-03
Cyp2s1	cytochrome P450, family 2, subfamily s, polypeptide 1	2.65166	1.53E-12
Gstp1	glutathione S-transferase, pi 1	1.56183	3.17E-04
Aldh3a2	aldehyde dehydrogenase family 3, subfamily A2	1.536647	2.80E-03
Erlin1	ER lipid raft associated 1	1.543004	2.07E-02
BC021614	cDNA sequence BC021614	2.032736	5.96E-04
Fxyd2	FXYD domain-containing ion transport regulator 2	3.638058	1.67E-04
Itpka	inositol 1,4,5-trisphosphate 3-kinase A	1.971442	5.67E-04
Bco1	beta-carotene oxygenase 1	3.41586	2.99E-02
Acer1	alkaline ceramidase 1	3.592603	5.11E-05
Paqr7	progestin and adipoQ receptor family member VII	2.004716	1.30E-02
Lrmp	lymphoid-restricted membrane protein	1.465045	2.06E-02
Naaa	N-acylethanolamine acid amidase	1.477538	2.39E-06
Fabp2	fatty acid binding protein 2, intestinal	2.007891	4.48E-02
Tm4sf5	transmembrane 4 superfamily	1.625192	2.92E-

	member 5		02
Cyp2u1	cytochrome P450, family 2, subfamily u, polypeptide 1	2.054534	4.26E-02
Zfyve1	zinc finger, FYVE domain containing 1	1.436207	3.74E-02
Acp6	acid phosphatase 6, lysophosphatidic	1.536285	1.12E-02
Ces2g	carboxylesterase 2G	1.646284	2.43E-02
Rbp7	retinol binding protein 7, cellular	2.230702	2.34E-02
Adh4	alcohol dehydrogenase 4 (class II), pi polypeptide	2.937525	1.88E-03
Col6a5	collagen, type VI, alpha 5	1.81802	3.62E-02
Mfsd7a	major facilitator superfamily domain containing 7A	1.870446	3.68E-04
Cyp2b10	cytochrome P450, family 2, subfamily b, polypeptide 10	3.334616	2.19E-02
3110070M22Rik	RIKEN cDNA 3110070M22 gene	4.601167	3.05E-05
Enpp7	ectonucleotide pyrophosphatase/phosphodiesterase 7	2.888838	6.42E-03
Acaa2	acetyl-Coenzyme A acyltransferase 2 (mitochondrial 3-oxoacyl-Coenzyme A thiolase)	1.469705	4.58E-02
Abcc2	ATP-binding cassette, sub-family C (CFTR/MRP), member 2	2.316982	1.24E-02
Smlr1	small leucine-rich protein 1	1.930257	3.61E-03
Ghrl	ghrelin	1.853403	3.30E-02
Cyp3a25	cytochrome P450, family 3, subfamily a, polypeptide 25	3.215591	9.88E-06
Cyp2c65	cytochrome P450, family 2, subfamily c, polypeptide 65	2.408679	6.29E-08
Ugt1a1	UDP glucuronosyltransferase 1 family, polypeptide A1	4.033208	1.82E-06
Ace	angiotensin I converting enzyme (peptidyl-dipeptidase A) 1	2.606958	3.26E-04
Evi2a	ecotropic viral integration site 2a	1.567696	1.23E-02
Entpd5	ectonucleoside triphosphate diphosphohydrolase 5	1.8373	1.18E-03
Clec3b	C-type lectin domain family 3, member b	1.950893	8.18E-04
Cd302	CD302 antigen	1.523039	9.11E-03
Pde3a	phosphodiesterase 3A, cGMP inhibited	1.912577	2.12E-05
Slc4a5	solute carrier family 4, sodium bicarbonate cotransporter, member 5	2.031592	1.09E-04
Fam132a	family with sequence similarity 132, member A	1.775703	2.92E-02
Plbd1	phospholipase B domain containing 1	1.574463	2.31E-02
Fsd1	fibronectin type 3 and SPRY domain-containing protein	2.382816	4.52E-02

Sh2d7	SH2 domain containing 7	3.800131	3.65E-10
Lpin2	lipin 2	1.814419	3.36E-03
Slc6a20a	solute carrier family 6 (neurotransmitter transporter), member 20A	2.741163	1.96E-03
Maob	monoamine oxidase B	2.987034	3.71E-05
Sema4g	sema domain, immunoglobulin domain (Ig), transmembrane domain (TM) and short cytoplasmic domain, (semaphorin) 4G	2.707875	2.98E-08
Acad10	acyl-Coenzyme A dehydrogenase family, member 10	1.646246	1.08E-02
Gm10768	predicted gene 10768	2.234777	2.45E-02
Slc2a9	solute carrier family 2 (facilitated glucose transporter), member 9	1.59253	2.73E-02
Lypd8	LY6/PLAUR domain containing 8	1.719774	1.59E-02
9030617O03Rik	RIKEN cDNA 9030617O03 gene	1.727153	2.57E-05
Lgals2	lectin, galactose-binding, soluble 2	1.705575	5.07E-03
Lrat	lecithin-retinol acyltransferase (phosphatidylcholine-retinol-O-acyltransferase)	2.119783	1.03E-02
Dclk1	doublecortin-like kinase 1	1.631499	4.33E-04
Ccl25	chemokine (C-C motif) ligand 25	1.689231	5.70E-04
Ogn	osteoglycin	2.005588	8.99E-05
Rhebl1	Ras homolog enriched in brain like 1	1.558919	4.02E-02
Igsf10	immunoglobulin superfamily, member 10	2.08753	3.14E-02
Tmem86a	transmembrane protein 86A	2.308334	7.81E-08
Slc5a4b	solute carrier family 5 (neutral amino acid transporters, system A), member 4b	3.429134	8.13E-04
Abat	4-aminobutyrate aminotransferase	1.788117	1.22E-03
Pycard	PYD and CARD domain containing	1.798338	2.53E-02
Emc9	ER membrane protein complex subunit 9	1.662615	1.26E-02
Tango2	transport and golgi organization 2	1.441142	2.13E-02
Nfe2l2	nuclear factor, erythroid derived 2, like 2	1.377806	1.62E-02
Aldob	aldolase B, fructose-bisphosphate	2.022339	1.09E-03
Kcnj16	potassium inwardly-rectifying channel, subfamily J, member 16	2.334796	4.76E-02
Ube4a	ubiquitination factor E4A	1.289226	3.82E-02
Rasgef1b	RasGEF domain family, member 1B	1.914451	4.23E-04

B4galnt1	beta-1,4-N-acetyl-galactosaminyl transferase 1	1.598734	2.20E-04
Slc52a2	solute carrier protein 52, member 2	1.577661	3.45E-02
Col14a1	collagen, type XIV, alpha 1	1.675716	3.26E-04
Tnip1	TNFAIP3 interacting protein 1	1.509288	1.38E-02
Plac8	placenta-specific 8	1.391327	3.14E-02
Reep6	receptor accessory protein 6	1.543608	7.74E-03
Clcn1	chloride channel 1	2.043531	3.39E-02
Ces1g	carboxylesterase 1G	3.505717	1.23E-05
Zhx1	zinc fingers and homeoboxes 1	1.339086	2.61E-02
Otc	ornithine transcarbamylase	2.658859	2.15E-04
Tmem139	transmembrane protein 139	1.846263	1.66E-02
Cdc42ep5	CDC42 effector protein (Rho GTPase binding) 5	1.748703	3.81E-03
Neurl1b	neuralized homolog 1b (Drosophila)	2.129594	1.50E-03
Apba3	amyloid beta (A4) precursor protein-binding, family A, member 3	1.382911	4.36E-02
Ano7	anoctamin 7	1.914072	1.16E-02
Hcn1	hyperpolarization-activated, cyclic nucleotide-gated K+ 1	6.792101	3.56E-07
Abca8b	ATP-binding cassette, sub-family A (ABC1), member 8b	1.857035	2.92E-02
Slc9a9	solute carrier family 9 (sodium/hydrogen exchanger), member 9	1.764211	8.55E-04
4933421O10Rik	RIKEN cDNA 4933421O10 gene	1.460814	3.66E-02
Frat2	frequently rearranged in advanced T cell lymphomas 2	2.051665	1.07E-03
Trpv3	transient receptor potential cation channel, subfamily V, member 3	2.554226	2.30E-03
Fam83e	family with sequence similarity 83, member E	1.701316	2.34E-04
Slco2b1	solute carrier organic anion transporter family, member 2b1	2.085757	1.72E-03
Adtrp	androgen dependent TFPI regulating protein	1.682574	2.20E-03
Cbr1	carbonyl reductase 1	1.547333	2.78E-02
Klc4	kinesin light chain 4	1.438464	4.15E-02
Gcnt4	glucosaminyl (N-acetyl) transferase 4, core 2 (beta-1,6-N-acetylglucosaminyltransferase)	1.448729	2.62E-02
Gm1123	predicted gene 1123	1.929311	1.69E-08
Marc2	mitochondrial amidoxime reducing component 2	1.436991	1.21E-02

Btd	biotinidase	1.352883	2.78E-02
Spns3	spinster homolog 3	1.877808	3.08E-02
Sgms2	sphingomyelin synthase 2	1.298124	4.41E-02
Ugt1a6a	UDP glucuronosyltransferase 1 family, polypeptide A6A	2.464362	3.38E-07
Fam98c	family with sequence similarity 98, member C	1.666817	6.52E-03
Gm11651	predicted gene 11651	3.443785	1.74E-02
Ces1e	carboxylesterase 1E	3.521867	4.61E-06
Arg2	arginase type II	2.152044	8.62E-03
B430010I23Rik	RIKEN cDNA B430010I23 gene	1.72437	1.36E-02
Slc17a1	solute carrier family 17 (sodium phosphate), member 1	2.649948	1.15E-02
Nags	N-acetylglutamate synthase	1.950644	2.65E-03
Ctns	cystinosis, nephropathic	1.375953	2.47E-02
D2hgdh	D-2-hydroxyglutarate dehydrogenase	1.628657	2.88E-02
Ihh	Indian hedgehog	1.420691	2.95E-02
Zfp92	zinc finger protein 92	1.984582	4.64E-02
BC147527	cDNA sequence BC147527	7.07895	1.35E-05
Ces1f	carboxylesterase 1F	2.700164	2.12E-05
Insrr	insulin receptor-related receptor	2.375898	2.95E-02
Sis	sucrase isomaltase (alpha-glucosidase)	2.198921	7.93E-04
Fam213b	family with sequence similarity 213, member B	1.996453	5.98E-03
Tmem236	transmembrane protein 236	1.703961	2.93E-02
Mme	membrane metallo endopeptidase	2.207982	5.33E-03
Dqx1	DEAQ RNA-dependent ATPase	1.601111	3.18E-03
Lipe	lipase, hormone sensitive	1.79857	3.74E-02
Enpp5	ectonucleotide pyrophosphatase/phosphodiesterase 5	1.365793	8.44E-03
Itga8	integrin alpha 8	1.962246	2.81E-02
Hcar1	hydrocarboxylic acid receptor 1	2.41583	1.74E-03
Sepp1	selenoprotein P, plasma, 1	2.590662	2.35E-03
Mgst3	microsomal glutathione S-transferase 3	1.722367	5.32E-03
Siglec5	sialic acid binding Ig-like lectin 5	1.682274	1.71E-02

2610528J11Rik	RIKEN cDNA 2610528J11 gene	1.376344	2.44E-02
Micalcl	MICAL C-terminal like	1.455643	2.52E-02
Tinag	tubulointerstitial nephritis antigen	1.683303	4.07E-02
Calb2	calbindin 2	1.905647	1.87E-02
Cck	cholecystokinin	1.725785	3.56E-04
Rab27b	RAB27B, member RAS oncogene family	1.405764	2.80E-02
Sh2d6	SH2 domain containing 6	2.395775	2.90E-04
Abcc6	ATP-binding cassette, sub-family C (CFTR/MRP), member 6	3.423998	1.66E-04
Nqo1	NAD(P)H dehydrogenase, quinone 1	2.139418	8.57E-11
Gstm6	glutathione S-transferase, mu 6	1.723751	8.85E-03
Slc39a5	solute carrier family 39 (metal ion transporter), member 5	1.907672	2.41E-03
Retsat	retinol saturase (all trans retinol 13,14 reductase)	1.498696	3.03E-03
Tro	trophinin	2.302972	1.28E-02
Mroh7	maestro heat-like repeat family member 7	2.493336	3.73E-04
Itih5	inter-alpha (globulin) inhibitor H5	1.490781	1.17E-03
Nid2	nidogen 2	1.509966	1.29E-03
Mgst2	microsomal glutathione S-transferase 2	1.772416	1.35E-03
Emid1	EMI domain containing 1	1.75694	3.97E-03
Nyap1	neuronal tyrosine-phosphorylated phosphoinositide 3-kinase adaptor 1	1.864938	8.13E-03
Fgfbp1	fibroblast growth factor binding protein 1	2.290693	1.84E-02
Rdh7	retinol dehydrogenase 7	2.317233	2.27E-02
Mocs1	molybdenum cofactor synthesis 1	1.640096	2.41E-02
Shpk	sedoheptulokinase	1.578791	2.56E-02
Agr2	anterior gradient 2	1.631695	2.77E-02
Dopey2	dopey family member 2	1.448756	3.49E-02
Clic5	chloride intracellular channel 5	1.594388	3.74E-02
Cyb5r4	cytochrome b5 reductase 4	1.40377	4.34E-02
Gli1	GLI-Kruppel family member GLI1	1.820703	4.67E-02
Fam101b	family with sequence similarity 101, member B	1.416902	4.67E-02
Ptprn2	protein tyrosine phosphatase, receptor type, N polypeptide 2	1.691927	1.41E-02
Ugt1a7c	UDP glucuronosyltransferase 1	2.457914	6.44E-

	family, polypeptide A7C		11
Maoa	monoamine oxidase A	2.571102	4.66E-05
Atp6v0a2	ATPase, H+ transporting, lysosomal V0 subunit A2	1.480781	1.28E-03
Acaa1b	acetyl-Coenzyme A acyltransferase 1B	2.310085	1.97E-03
Acad11	acyl-Coenzyme A dehydrogenase family, member 11	1.699587	3.43E-03
Gucd1	guanylyl cyclase domain containing 1	1.646949	3.61E-03
Shisa3	shisa homolog 3 (Xenopus laevis)	2.13481	1.97E-02
Slc10a5	solute carrier family 10 (sodium/bile acid cotransporter family), member 5	1.811627	2.95E-02
Gm11437	predicted gene 11437	1.978639	3.93E-02
Abcg5	ATP-binding cassette, sub-family G (WHITE), member 5	1.962614	4.58E-02
Fbln5	fibulin 5	1.439165	4.67E-02
Phgr1	proline/histidine/glycine-rich 1	1.473833	4.82E-02
Amacr	alpha-methylacyl-CoA racemase	1.365473	4.99E-02
4833420G17Rik	RIKEN cDNA 4833420G17 gene	2.087736	5.07E-12
Akap7	A kinase (PRKA) anchor protein 7	1.447596	2.71E-02
Acbd4	acyl-Coenzyme A binding domain containing 4	1.491543	2.93E-02
Acsl1	acyl-CoA synthetase long-chain family member 1	1.591822	4.45E-02
Brsk1	BR serine/threonine kinase 1	1.472343	4.48E-02
Plgrkt	plasminogen receptor, C-terminal lysine transmembrane protein	1.578815	2.44E-03
Gal3st1	galactose-3-O-sulfotransferase 1	1.437448	4.51E-02
Gnpda1	glucosamine-6-phosphate deaminase 1	1.758079	8.91E-03
Pbld2	phenazine biosynthesis-like protein domain containing 2	2.364812	2.12E-05
Cmbl	carboxymethylenebutenolidase-like (Pseudomonas)	1.780843	3.16E-03
BC024139	cDNA sequence BC024139	2.373112	3.79E-03
Cd180	CD180 antigen	2.079081	8.44E-03
Grtp1	GH regulated TBC protein 1	1.414333	2.93E-02
Gsta1	glutathione S-transferase, alpha 1 (Ya)	2.581293	1.80E-02
Gm3776	predicted gene 3776	2.581293	1.80E-02
2310001H17Rik	RIKEN cDNA 2310001H17 gene	1.508564	1.21E-02
Rasa4	RAS p21 protein activator 4	1.547231	3.39E-02

Fzd5	frizzled homolog 5 (Drosophila)	1.663945	1.77E-05
Tpsg1	tryptase gamma 1	1.961409	1.75E-05
Npc1l1	NPC1-like 1	1.907943	3.81E-02
Zc3h12d	zinc finger CCCH type containing 12D	1.428072	1.74E-05
Slc17a4	solute carrier family 17 (sodium phosphate), member 4	3.309069	3.07E-05
Papln	papilin, proteoglycan-like sulfated glycoprotein	1.649621	4.26E-04
Atp2a3	ATPase, Ca++ transporting, ubiquitous	1.51723	5.72E-04
Vdr	vitamin D receptor	2.257566	4.47E-03
G630090E17Rik	RIKEN cDNA G630090E17 gene	2.003816	8.95E-03
Selenbp1	selenium binding protein 1	1.511187	1.04E-02
Ky	kyphoscoliosis peptidase	2.217493	1.28E-02
Rragd	Ras-related GTP binding D	1.834238	2.06E-02
Trim38	tripartite motif-containing 38	2.507511	2.24E-02
Ank2	ankyrin 2, brain	1.682746	3.25E-02
Fbxo25	F-box protein 25	1.633026	3.29E-02
Dll1	delta-like 1 (Drosophila)	1.502509	3.62E-02
Sesn1	sestrin 1	1.816397	2.20E-02
Hal	histidine ammonia lyase	4.799098	2.00E-04
Aadac	arylacetamide deacetylase (esterase)	2.483035	2.96E-10
Cyp4f40	cytochrome P450, family 4, subfamily f, polypeptide 40	2.162223	1.68E-05
Abhd11os	abhydrolase domain containing 11, opposite strand	1.620146	3.00E-03
Lpin1	lipin 1	1.561129	2.61E-02
Isl1	ISL1 transcription factor, LIM/homeodomain	2.283287	3.56E-02
Hdhd3	haloacid dehalogenase-like hydrolase domain containing 3	2.031348	1.35E-03
Rgs13	regulator of G-protein signaling 13	2.595102	2.91E-03
Cndp1	carnosine dipeptidase 1 (metallopeptidase M20 family)	1.855308	1.47E-02
Pcsk5	proprotein convertase subtilisin/kexin type 5	1.344226	1.54E-02
9130230L23Rik	RIKEN cDNA 9130230L23 gene	1.833632	1.11E-02
Slc26a3	solute carrier family 26, member 3	2.527542	6.99E-08
Gpr110	G protein-coupled receptor 110	2.285961	5.72E-04
Nrarp	Notch-regulated ankyrin repeat	1.528729	3.45E-

	protein		02
Ms4a18	membrane-spanning 4-domains, subfamily A, member 18	2.21276	1.74E-05
Hepacam2	HEPACAM family member 2	2.326161	5.66E-20
Rep15	RAB15 effector protein	2.616639	5.17E-09
Aoc1	amine oxidase, copper-containing 1	2.586012	8.68E-05
Ctdspl	CTD (carboxy-terminal domain, RNA polymerase II, polypeptide A) small phosphatase-like	1.497359	1.09E-03
Als2cr12	amyotrophic lateral sclerosis 2 (juvenile) chromosome region, candidate 12 (human)	2.24055	1.30E-03
Ddc	dopa decarboxylase	2.221694	1.70E-03
Tmem45b	transmembrane protein 45b	1.612747	5.53E-03
Ugt2b34	UDP glucuronosyltransferase 2 family, polypeptide B34	1.717969	6.87E-03
Pmp22	peripheral myelin protein 22	2.685667	8.62E-03
Thrb	thyroid hormone receptor beta	1.789298	8.86E-03
Aldh9a1	aldehyde dehydrogenase 9, subfamily A1	1.482639	1.09E-02
Tmem82	transmembrane protein 82	1.460061	1.10E-02
Capn9	calpain 9	2.308491	1.47E-02
Plcd1	phospholipase C, delta 1	1.41508	2.98E-02
Akr1c14	aldo-keto reductase family 1, member C14	2.902282	3.14E-02
Cldn15	claudin 15	1.652622	3.53E-02
Prpsap1	phosphoribosyl pyrophosphate synthetase-associated protein 1	1.416571	3.73E-02
Nkx6-3	NK6 homeobox 3	3.580058	4.07E-02
Dapp1	dual adaptor for phosphotyrosine and 3-phosphoinositides 1	1.282027	4.26E-02
Tnxb	tenascin XB	1.79973	1.03E-02
Gna11	guanine nucleotide binding protein, alpha 11	1.519156	2.31E-02
Prkca	protein kinase C, alpha	1.508413	6.44E-03
Aldh1a1	aldehyde dehydrogenase family 1, subfamily A1	1.841514	1.24E-02
Grin2a	glutamate receptor, ionotropic, NMDA2A (epsilon 1)	3.439492	3.29E-02
Neurl3	neuralized homolog 3 homolog (Drosophila)	1.631125	1.46E-03

Bibliography:

Aberle, H., Bauer, A., Kispert, A., & Kemler, R. (1997). ß -catenin is a target for the ubiquitin – proteasome pathway. *The EMBO Journal*, *16*(13), 3797–3804.

Adachi, S., Jigami, T., Yasui, T., Nakano, T., Ohwada, S., Omori, Y., … Akiyama, T. (2004). Role of a BCL9-Related ß -Catenin-Binding Protein , B9L , in Tumorigenesis Induced by Aberrant Activation of Wnt Signaling by Aberrant Activation of Wnt Signaling, 8496–8501.

Ahmed, D., Eide, P. W., Eilertsen, I. A., Danielsen, S. A., Eknæs, M., Hektoen, M., … Lothe, R. A. (2013). Epigenetic and genetic features of 24 colon cancer cell lines. *Oncogenesis*, *2*, 1–8. https://doi.org/10.1038/oncsis.2013.35

Albuquerque, C., Breukel, C., Luijt, R. Van Der, Fidalgo, P., Lage, P., Fodde, R., … Leita, C. N. (2002). The " just-right " signaling model : APC somatic mutations are selected based on a specific level of activation of the b - catenin signaling cascade, *11*(13), 1549–1560.

ATCC Standards Development Organization Workgroup ASN-0002. (2010). Perspectives: Cell line misidentification : the beginning of the end. *Nature Reviews Cancer*, *10*(June), 441–448. https://doi.org/10.1038/nrc2852

Atkins, C., Liu, Q., Minthorn, E., Zhang, S.-Y., Figueroa, D. J., Moss, K., … Kumar, R. (2013). Characterization of a novel PERK kinase inhibitor with antitumor and antiangiogenic activity. *Cancer Research*, *73*(6), 1993–2002. https://doi.org/10.1158/0008-5472.CAN-12-3109

B'chir, W., Maurin, A., Carraro, V., Averous, J., Jousse, C., Muranishi, Y., … Bruhat, A. (2013). The eIF2a/ATF4 pathway is essential for stress-induced autophagy gene expression. *Nucleic Acids Research*, *41*(16), 7683–7699. https://doi.org/10.1093/nar/gkt563

Baker, S. J., Fearon, E. R., Nigro, J. M., Hamilton, S. R., Preisinger, A. N. N. C., Jessup, J. M., … April, I. I. (1989). Chromosome 17 Deletions and p53 Gene Mutations in Colorectal Carcinomas. *Science*, *244*, 217–221.

Bar-sagi, D., & Feramisco, J. R. (1986). Induction of Membrane Ruffling and Fluid-Phase Pinocytosis in Quiescent Fibroblasts by ras Proteins. *Science*, *233*, 1061–1068.

Barker, N., Ridgway, R. a, van Es, J. H., van de Wetering, M., Begthel, H., van den Born, M., … Clevers, H. (2009). Crypt stem cells as the cells-of-origin of intestinal cancer. *Nature*, *457*(7229), 608–11. https://doi.org/10.1038/nature07602

Barker, N., van Es, J. H., Kuipers, J., Kujala, P., van den Born, M., Cozijnsen, M., … Clevers, H. (2007). Identification of stem cells in small intestine and colon by marker gene Lgr5. *Nature*, *449*(7165), 1003–7. https://doi.org/10.1038/nature06196

Batlle, E., Henderson, J. T., Beghtel, H., van den Born, M. M. W., Sancho, E., Huls, G., … Clevers, H. (2002). B-Catenin and TCF Mediate Cell Positioning in the Intestinal Epithelium by Controlling the Expression of EphB / EphrinB.

Cell, *111*, 251–263.

Batzer, A. G., Rotin, D., Urena, J. M., Skolnik, E. Y., & Schlessinger, J. (1994). Hierarchy of Binding Sites for Grb2 and Shc on the Epidermal Growth Factor Receptor. *Molecular and Cellular Biology*, *14*(8), 5192–5201.

Behrens, J., Jerchow, B., Wurtele, M., Grimm, J., Asbrand, C., Wirtz, R., … Birchmeier, W. (1998). Functional Interaction of an Axin Homolog , Conductin , with ᴺᴸ -Catenin , APC , and GSK3 ᴺᴸ. *Science*, *280*(April), 596–599.

Behrens, J., von Kries, J., Kuhl, M., Bruhn, L., Wedlich, D., Grossched, R., & Birchmeier, W. (1996). Functional interaction of B-catenin with the transcription factor LEF-1. *Natire*, *382*, 638–642.

Belenkaya, T. Y., Han, C., Standley, H. J., Lin, X., Houston, D. W., Heasman, J., & Lin, X. (2002). pygopus encodes a nuclear protein essential for Wingless / Wnt signaling. *Development*, *4101*, 4089–4101.

Ben-Sahra Issam, Hoxhaj Gerta, Ricoult Stephane J. H., A. J. M. & M. B. D. (2016). mTORC1 induces purine synthesis through control of the mitochondrial tetrahydrofolate cycle. *Science*, *351*(6274), 728–733.

Berkel, H. J., Turbat-Herrera, E. A., Shi, R., & De Benedetti, A. (2001). Expression of the translation initiation factor eIF4E in the polyp-cancer sequence in the colon. *Cancer Epidemiology Biomarkers and Prevention*, *10*(6), 663–666.

Bertolotti, A., Zhang, Y., Hendershot, L. M., Harding, H. P., & Ron, D. (2000). Dynamic interaction of BiP and ER stress transducers in the unfolded-protein response. *Nature Cell Biology*, *2*(June).

Bhanot, P., Brink, M., Harryman Samos, C., Hsieh, J.-C., Wang, Y., Macke, J., … Nusse, R. (1996). A new member of the frizzled family from Drosophila functiosn as a a Wingless receptor. *Nature*, *382*, 225–230.

Bhat, M., Robichaud, N., Hulea, L., Sonenberg, N., Pelletier, J., & Topisirovic, I. (2015). Targeting the translation machinery in cancer. *Nature Publishing Group*, *14*(4), 261–278. https://doi.org/10.1038/nrd4505

Biechele, S., Cox, B. J., & Rossant, J. (2011). Porcupine homolog is required for canonical Wnt signaling and gastrulation in mouse embryos. *Developmental Biology*, *355*(2), 275–285. https://doi.org/10.1016/j.ydbio.2011.04.029

Blackwood, E. M., Lugo, T. G., Kretzner, L., King, M. W., Street, A. J., Witte, O. N., & Eisenman, R. N. (1994). Functional analysis of the AUG- and CUG-initiated forms of the c-Myc protein. *Molecular Biology of the Cell*, *5*(5), 597–609. https://doi.org/10.1091/mbc.5.5.597

Brack, A. S., Murphy-Seiler, F., Hanifi, J., Deka, J., Keller, C., Aguet, M., & Rando, T. A. (2009). BCL9 is an essential component of canonical Wnt signaling that mediates the differentiation of myogenic progenitors during muscle regeneration. *Developmental Biology*, *335*(1), 93–105. https://doi.org/10.1016/j.ydbio.2009.08.014.BCL9

Bray, S. J. (2006). Notch signalling: a simple pathway becomes complex. *Nature Reviews Molecular Cell Biology*, *7*(9), 678–689. https://doi.org/10.1038/nrm2009

Brembeck, F. H., Schwarz-Romond, T., Bakkers, J., Wilhelm, S., Hammerschmidt, M., & Birchmeier, W. (2004). Essential role of BCL9-2 in the switch between beta-catenin's adhesive and transcriptional functions. *Genes & Development*, *18*(18), 2225–30. https://doi.org/10.1101/gad.317604

Brembeck, F. H., Wiese, M., Zatula, N., Grigoryan, T., Dai, Y., Fritzmann, J., & Birchmeier, W. (2011). BCL9-2 promotes early stages of intestinal tumor progression. *Gastroenterology*, *141*(4), 1359–70, 1370–3. https://doi.org/10.1053/j.gastro.2011.06.039

Bretin, A., Carriere, J., Dalmasso, G., Bergougnoux, A., B'chir, W., Maurin, A.-C., … Nguyen, H. (2016). Activation of the EIF2AK4-EIF2A / eIF2 a -ATF4 pathway triggers autophagy response to Crohn disease-associated adherent-invasive Escherichia coli infection. *Autophagy*, *12*(5), 770–783. https://doi.org/10.1080/15548627.2016.1156823

Brown, E. J., Albers, M. W., Shin, T. B., Ichikawa, K., Keith, C. T., Lane, W. S., & Schreiber, S. L. (1994). A mammalian protein targeted by G1-arresting rapamycin-receptor complex. *Nature*, *369*(6483), 756–758. https://doi.org/10.1038/369756a0

Brunn, G. J., Hudson, C. C., Sekulic, A., Williams, J. M., Hosoi, H., Houghton, P. J., … Abraham, R. T. (1997). Phosphorylation of the Translational Repressor PHAS-I by the Mammalian Target of Rapamycin. *Science*, *277*(July), 99–102.

Bruno, P. M., Liu, Y., Park, G. Y., Murai, J., Koch, C. E., Eisen, T. J., … Hemann, M. T. (2017). A subset of platinum-containing chemotherapeutic agents kills cells by inducing ribosome biogenesis stress. *Nature Medicine*, *23*(4), 461–471. https://doi.org/10.1038/nm.4291

Bushell, M., Wood, W., Carpenter, G., Pain, V. M., Morley, S. J., & Clemens, M. J. (2001). Disruption of the Interaction of Mammalian Protein Synthesis Eukaryotic Initiation Factor 4B with the Poly (A) -binding Protein by Caspase- and Viral Protease-mediated Cleavages. *The Journal of Biological Chemistry*, *276*(26), 23922–23928. https://doi.org/10.1074/jbc.M100384200

Buttgereit, F., & Brandt, M. D. (1995). A hierarchy of ATP-consuming processes in mammalian cells. *Biochemical Journal*, *167*, 163–167.

Calfon, M., Zeng, H., Urano, F., Till, J. H., Hubbard, S. R., Harding, H. P., … Ron, D. (2002). IRE1 couples endoplasmic reticulum load to secretory capacity by processing the XBP-1 mRNA. *Nature*, *415*(January), 1–6.

Cammareri, P., Vincent, D. F., Hodder, M. C., Ridgway, R. A., Murgia, C., Nobis, M., … Sansom, O. J. (2017). TGF ß pathway limits dedifferentiation following WNT and MAPK pathway activation to suppress intestinal tumourigenesis. *Cell Death and Differentiation*, 1–13. https://doi.org/10.1038/cdd.2017.92

Cano, C. E., Hamidi, T., Sandi, M. J., & Iovanna, J. L. (2011). Nupr1: the Swiss-

knife of cancer. *Journal of Cellular Physiology*, *226*(6), 1439–43. https://doi.org/10.1002/jcp.22324

Cantù, C., Pagella, P., Shajiei, T. D., Zimmerli, D., Valenta, T., Hausmann, G., … Mitsiadis, T. A. (2017). A cytoplasmic role of Wnt / b -catenin transcriptional cofactors Bcl9 , Bcl9l , and Pygopus in tooth enamel formation, *4598*(February), 1–10.

Cavallo, R., Cox, R., Moline, M., Roose, J., Polevoy, G. A., & Clevers, H. (1998). Drosophila Tcf and Groucho interact to repress Wingless signalling activity. *Nature*, *395*(October), 604–608.

Cervantes, S., Yamaguchi, T., & Hebrok, M. (2009). Wnt5a is essential for intestinal elongation in mice. *Developmental Biology*, *326*(2), 285–294. https://doi.org/10.1016/j.ydbio.2008.11.020.Wnt5a

Chardin, P., Camonis, J. H., Gale, N. W., Aelst, L. Van, Schlessinger, J., Wigler, M. H., & Bar-Sagi, D. (1993). Human Sos1: A Guanine Nucleotide Exchange Factor for Ras That Binds to GRB2. *Science*, *260*(May), 1338–1343.

Chen, B., Dodge, M. E., Tang, W., Lu, J., Ma, Z., Fan, C., … Lum, L. (2009). Small molecule – mediated disruption of Wnt-dependent signaling in tissue regeneration and cancer, *5*(2), 100–107. https://doi.org/10.1038/nchembio.137

Cheng, H., & Leblond, C. P. (1974). Origin , Differentiation and Renewal o f the Four Main Epithelial Cell Types in the Mouse Small Intestine V. Unitarian theory of the origin of the four epithelial cell tyoes. *American Journal of Anatomy*, *141*, 537–562.

Cheung, A. F., Carter, A. M., Kostova, K. K., Woodruff, J. F., Crowley, D., Bronson, R. T., … Jacks, T. (2009). Complete deletion of Apc results in severe polyposis in mice. *Oncogene*, *29*(12), 1857–1864. https://doi.org/10.1038/onc.2009.457

Christie, M., Jorissen, R. N., Mouradov, D., Sakthianandeswaren, A., Li, S., Day, F., … Sieber, O. M. (2013). Different APC genotypes in proximal and distal sporadic colorectal cancers suggest distinct WNT/β-catenin signalling thresholds for tumourigenesis. *Oncogene*, *32*(39), 4675–4682. https://doi.org/10.1038/onc.2012.486

Church, D. M., Schneider, V. A., Graves, T., Auger, K., Cunningham, F., Chen, H., … Hubbard, T. (2011). Modernizing Reference Genome Assemblies, *9*(7), 1–5. https://doi.org/10.1371/journal.pbio.1001091

Cliffe, A., Hamada, F., & Bienz, M. (2003). A Role of Dishevelled in Relocating Axin to the Plasma Membrane during Wingless Signaling. *Current Biology*, *13*, 960–966. https://doi.org/10.1016/S

Crabtree, M., Sieber, O. M., Lipton, L., Hodgson, S. V, Lamlum, H., Thomas, H. J. W., … Heinimann, K. (2003). Refining the relation between " first hits " and " second hits " at the APC locus : the " loose fit " model and evidence for differences in somatic mutation spectra among patients. *Oncogene*, *22*, 4257–4265. https://doi.org/10.1038/sj.onc.1206471

Cullough, K. D. M. C., Martindale, J. L., Klotz, L., Aw, T., & Holbrook, N. J. (2001). Gadd153 Sensitizes Cells to Endoplasmic Reticulum Stress by Down-Regulating Bcl2 and Perturbing the Cellular Redox State. *Molecular and Cellular Biology*, *21*(4), 1249–1259. https://doi.org/10.1128/MCB.21.4.1249

D'Aniello, C., Fico, a, Casalino, L., Guardiola, O., Di Napoli, G., Cermola, F., … Minchiotti, G. (2015). A novel autoregulatory loop between the Gcn2-Atf4 pathway and L-Proroline metabolism controls stem cell identity. *Cell Death and Differentiation*, 1094–1105. https://doi.org/10.1038/cdd.2015.24

Davies, H., Bignell, G. R., Cox, C., Stephens, P., Edkins, S., Clegg, S., … Futreal, P. A. (2002). Mutations of the BRAF gene in human cancer. *Nature*, *417*, 949–954.

Davis, H., Irshad, S., Bansal, M., Rafferty, H., Boitsova, T., Bardella, C., … Leedham, S. J. (2015). Aberrant epithelial GREM1 expression initiates colonic tumorigenesis from cells outside the stem cell niche. *Nature Medicine*, *21*(1), 62–70. https://doi.org/10.1038/nm.3750

De Benedetti, A., & Graff, J. R. (2004). eIF-4E expression and its role in malignancies and metastases. *Oncogene*, *23*(18), 3189–3199. https://doi.org/10.1038/sj.onc.1207545

de la Roche, M., Ibrahim, A. E., Mieszczanek, J., & Bienz, M. (2014). LEF1 and B9L shield ß-catenin from inactivation by Axin, desensitizing colorectal cancer cells to tankyrase inhibitors. *Cancer Research*. https://doi.org/10.1158/0008-5472.CAN-13-2682

DeBerardinis, R. J., Mancuso, A., Daikhin, E., Nissim, I., Yudkoff, M., Wehrli, S., & Thompson, C. B. (2007). Beyond aerobic glycolysis : Transformed cells can engage in glutamine metabolism that exceeds the requirement for protein and nucleotide synthesis. *Proceedings of the National Academy of Sciences of the United States of America*, *104*(49), 19345–19350.

Deka, J., Wiedemann, N., Anderle, P., Murphy-Seiler, F., Bultinck, J., Eyckerman, S., … Aguet, M. (2010a). Bcl9/Bcl9l are critical for Wnt-mediated regulation of stem cell traits in colon epithelium and adenocarcinomas. *Cancer Research*, *70*(16), 6619–28. https://doi.org/10.1158/0008-5472.CAN-10-0148

Deka, J., Wiedemann, N., Anderle, P., Murphy-Seiler, F., Bultinck, J., Eyckerman, S., … Aguet, M. (2010b). Bcl9/Bcl9l are critical for Wnt-mediated regulation of stem cell traits in colon epithelium and adenocarcinomas. *Cancer Research*, *70*(16), 6619–28. https://doi.org/10.1158/0008-5472.CAN-10-0148

Dever, T. E., & Green, R. (2012). Phases of Translation in Eukaryotes. *Cold Spring Harbor Perspectives in Biology*, 1–16.

Di Nicolantonio, F, Martini, M, Molinari, F, Sartore-Bianchi, A, Arena, S, Saletti, P, De Dosso, S, Mazzucchelli, L, Frattini, M, Siena, S And Bardelli, A. (2017). Wild-Type BRAF Is Required for Response to Panitumumab or Cetuximab in Metastatic Colorectal Cancer. *Journal of Clinical Oncology*, *26*(35). https://doi.org/10.1200/JCO.2008.18.0786

Dow, L. E., O'Rourke, K. P., Simon, J., Tschaharganeh, D. F., van Es, J. H., Clevers, H., & Lowe, S. W. (2015). Apc Restoration Promotes Cellular Differentiation and Reestablishes Crypt Homeostasis in Colorectal Cancer. *Cell*, *161*(7), 1539–1552. https://doi.org/10.1016/j.cell.2015.05.033

Drost, J., van Jaarsveld, R. H., Ponsioen, B., Zimberlin, C., van Boxtel, R., Buijs, A., … Clevers, H. (2015). Sequential cancer mutations in cultured human intestinal stem cells. *Nature*, *521*, 43–47. https://doi.org/10.1038/nature14415

Durand, A., Donahue, B., Peignon, G., Letourneur, F., Cagnard, N., Slomianny, C., … Romagnolo, B. (2012). Functional intestinal stem cells after Paneth cell ablation induced by the loss of transcription. *Proceedings of the National Academy of Sciences of the United States of America*, *1*(21), 1–6. https://doi.org/10.1073/pnas.1201652109

Eagle, B. H. (1955). The Minimum vitamin requirements of the L and HeLa cells in tissue culture, the production of specific vitamin deficienies, and their cure.

el Marjou, F., Janssen, K.-P., Chang, B. H.-J., Li, M., Hindie, V., Chan, L., … Robine, S. (2004). Tissue-specific and inducible Cre-mediated recombination in the gut epithelium. *Genesis*, *39*(3), 186–93. https://doi.org/10.1002/gene.20042

Ettenberg, S. A., Charlat, O., Daley, M. P., Liu, S., Vincent, K. J., Stuart, D. D., … Schmitz, R. (2010). Inhibition of tumorigenesis driven by different Wnt proteins requires blockade of distinct ligand-binding regions by LRP6 antibodies, 1–6. https://doi.org/10.1073/pnas.1007428107

Faller, W. J., Jackson, T. J., Knight, J. R. P., Ridgway, R. a., Jamieson, T., Karim, S. a., … Sansom, O. J. (2015). mTORC1-mediated translational elongation limits intestinal tumour initiation and growth. *Nature*, *517*(7535), 497–500. https://doi.org/10.1038/nature13896

Farin, H. F., van Es, J. H., & Clevers, H. (2012). Redundant Sources of Wnt Regulate Intestinal Stem Cells and Promote Formation of Paneth Cells. *Gastroenterology*, *143*(6), 1518–1529.e7. https://doi.org/10.1053/j.gastro.2012.08.031

Farrell, P., Balkow, K., Hunt, T., Jackson, R. J., & Trachsel, H. (1977). Phosphorylation of initiation factor elF-2 and the control of reticulocyte protein synthesis. *Cell*, *11*(1), 187–200. https://doi.org/10.1016/0092-8674(77)90330-0

Fearon, E. F., & Vogelstein, B. (1990). A Genetic Model for Colorectal Tumorigenesis. *Cell*, *61*, 759–767.

Feigenblum, D., & Schneider, R. J. (1996). Cap-Binding Protein (Eukaryotic Initiation Factor 4E) and 4E-Inactivating Protein BP-1 Independently Regulate Cap-Dependent Translation. *Molecular and Cellular Biology*, *16*(10), 5450–5457.

Feng, Y., Bommer, G. T., Zhao, J., Green, M., Sands, E., Zhai, Y., … Fearon, E. R. (2011). Mutant KRAS promotes hyperplasia and alters differentiation in

the colon epithelium but does not expand the presumptive stem cell pool. *Gastroenterology*, *141*(3), 1003-1013–10. https://doi.org/10.1053/j.gastro.2011.05.007

Ferlay, J., Steliarova-foucher, E., Lortet-tieulent, J., & Rosso, S. (2013). Cancer incidence and mortality patterns in Europe : Estimates for 40 countries in 2012. *European Journal of Cancer*, *49*(6), 1374–1403. https://doi.org/10.1016/j.ejca.2012.12.027

Fisher, S., Barry, A., Abreu, J., Minie, B., Nolan, J., Delorey, T. M., … Nusbaum, C. (2011). A scalable, fully automated process for construction of sequence-ready human exome targeted capture libraries. *Genome Biology*, *12*(1), 1–15. https://doi.org/10.1186/gb-2011-12-1-r1

Flogge, R. D., Karlovich, C. A., & Banerjee, U. (1991). Genetic Dissection of a Neurodevelopmental Pathway : Son of sevenless Functions Downsbarn of the sevenless and EGF Receptor Tyrosine Kinases. *Cell*, *64*(1987), 39–48.

Flynn, G., Pohl, J., Flocco, M., & Jame, R. (1991). Peptide-binding specificity of the molecular chaperone BiP. *Nature*, *353*, 726–730.

Fodde, R., Edelmannt, W., Yangt, K. A. N., Leeuwen, C. V. A. N., Carlsont, C., Renault, B., … Khan, P. M. (1994). A targeted chain-termination mutation in the mouse Apc gene results in multiple intestinal tumors. *Proceedings of the National Academy of Sciences of the United States of America*, *91*(September), 8969–8973.

Fumagalli, A., Drost, J., Suijkerbuijk, S. J. E., Boxtel, R. Van, & Ligt, J. De. (2017). Genetic dissection of colorectal cancer progression by orthotopic transplantation of engineered cancer organoids. *Proceedings of the National Academy of Sciences of the United States of America*, 2357–2364. https://doi.org/10.1073/pnas.1701219114

Galiatsatos, P., & Foulkes, W. D. (2006). Familial Adenomatous Polyposis. *American Journal of Gastroenterology*, *101*, 385–398. https://doi.org/10.1111/j.1572-0241.2006.00375.x

Gerbe, F., Brulin, B., Makrini, L., Legraverend, C., & Jay, P. (2009). DCAMKL-1 Expression Identifies Tuft Cells Rather Than Stem Cells in the. *Gastroenterology*, *137*(6), 2179–2180. https://doi.org/10.1053/j.gastro.2009.06.072

Gerbe, F., Es, J. H. Van, Makrini, L., Brulin, B., Mellitzer, G., Robine, S., … Jay, P. (2011). Distinct ATOH1 and Neurog3 requirements define tuft cells as a new secretory cell type in the intestinal epithelium. *Journal of Cell Biology*, *192*(5), 767–780. https://doi.org/10.1083/jcb.201010127

Ghoos, Y., & Vantrappen, G. (1971). The cytochemical localization of lysozyme in Paneth cell granules. *Histochemical Journal*, *3*, 175–178.

Goodwin, R. J. A., Nilsson, A., Mackay, C. L., Swales, J. G., Johansson, M. K., Billger, M., … Iverson, S. L. (2016). Exemplifying the Screening Power of Mass Spectrometry Imaging over Label-Based Technologies for Simultaneous Monitoring of Drug and Metabolite Distributions in Tissue Sections. *Journal of Biomolecular Screening*, *21*(2), 187–193.

https://doi.org/10.1177/1087057115623740

Greenman, C., Stephens, P., Smith, R., Dalgliesh, G. L., Hunter, C., Bignell, G., … Stratton, M. R. (2007). Patterns of somatic mutation in human cancer genomes. *Nature*, *446*(March). https://doi.org/10.1038/nature05610

Groden, J., Thliveris, A., Samowitz, W., Carlson, M., Gelbert, L., Albertsen, H., … Leppert, M. (1991). Identification and Characterization of the Familial Adenomatous Polyposis Coli Gene. *Cell*, *66*, 589–600.

Gross, M. I., Demo, S. D., Dennison, J. B., Chen, L., Chernov-rogan, T., Goyal, B., … Bennett, M. K. (2014). Antitumor Activity of the Glutaminase Inhibitor CB-839 in Triple-Negative Breast Cancer, *13*(April), 890–902. https://doi.org/10.1158/1535-7163.MCT-13-0870

Guinney, J., Dienstmann, R., Wang, X., de Reyniès, A., Schlicker, A., Soneson, C., … Tejpar, S. (2015). The consensus molecular subtypes of colorectal cancer. *Nature Medicine*, (October). https://doi.org/10.1038/nm.3967

Guo, J. Y., Karsli-uzunbas, G., Mathew, R., Aisner, S. C., Kamphorst, J. J., Strohecker, A. M., … White, E. (2013). Autophagy suppresses progression of K-ras-induced lung tumors to oncocytomas and maintains lipid homeostasis, 1447–1461. https://doi.org/10.1101/gad.219642.113.Essential

Haghighat, A., Mader, S., Pause, A., & Sonenberg, N. (1995). Repression of cap-dependent translation by 4E-binding protein 1 : competition with p220 for binding to eukaryotic initiation factor-4E. *The EMBO Journal*, *14*(22), 5701–5709.

Haigis, K. M., Kendall, K. R., Wang, Y., Cheung, A., Haigis, M. C., Glickman, J. N., … Jacks, T. (2008). Differential effects of oncogenic K-Ras and N-Ras on proliferation , differentiation and tumor progression in the colon. *Nature Genetics*, *40*(5), 600–608. https://doi.org/10.1038/ng.115

Halliday, M., Radford, H., Sekine, Y., Moreno, J., Verity, N., le Quesne, J., … Mallucci, G. R. (2015). Partial restoration of protein synthesis rates by the small molecule ISRIB prevents neurodegeneration without pancreatic toxicity. *Cell Death & Disease*, *6*(3), e1672. https://doi.org/10.1038/cddis.2015.49

Hamabe, A., Yamamoto, H., Konno, M., Uemura, M., Nishimura, J., Hata, T., … Ishii, H. (2014). Combined evaluation of hexokinase 2 and phosphorylated pyruvate dehydrogenase-E1α in invasive front lesions of colorectal tumors predicts cancer metabolism and patient prognosis. *Cancer Science*, *105*(9), 1100–8. https://doi.org/10.1111/cas.12487

Hao, Y., Samuels, Y., Li, Q., Krokowski, D., Guan, B., Wang, C., … Wang, Z. (2016). Oncogenic PIK3CA mutations reprogram glutamine metabolism in colorectal cancer. *Nature Communications*, *7*(May), 1–13. https://doi.org/10.1038/ncomms11971

Hara, K., Yonezawa, K., Kozlowski, M. T., Sugimoto, T., Andrabi, K., Weng, Q., … Avruch, J. (1997). Regulation of eIF-4E BP1 Phosphorylation by mTOR. *The Journal of Biological Chemistry*, *272*(42), 26457–26463.

Harada, N., Tamai, Y., Ishikawa, T., Sauer, B., Takaku, K., Oshima, M., & Taketo, M. M. (1999). Intestinal polyposis in mice with a dominant stable mutation of the ß -catenin gene. *The EMBO Journal*, *18*(21), 5931–5942.

Haramis, A. G., Begthel, H., van den Born, M., van Es, J., & Jonkheer, S. (2004). De Novo Crypt Formation and Juvenile Polyposis on BMP Inhibition in Mouse Intestine. *Science*, *303*(March), 1684–1686.

Harding, H. P., Novoa, I., Zhang, Y., Zeng, H., Wek, R., Schapira, M., & Ron, D. (2000). Regulated Translation Initiation Controls Stress-Induced Gene Expression in Mammalian Cells, *6*, 1099–1108.

Harding, H. P., Zhang, Y., Ron, D., Harding, H. P., Zhang, Y., & Ron, D. (1999). Protein translation and folding are coupled by an resident kinase letters to nature Protein translation and folding are coupled by an resident kinase. *Nature*, *398*(March), 271–274.

Harding, H. P., Zhang, Y., Zeng, H., Novoa, I., Lu, P. D., Calfon, M., … Carolina, N. (2003). An Integrated Stress Response Regulates Amino Acid Metabolism and Resistance to Oxidative Stress National Institute of Environmental Health Sciences, *11*, 619–633.

Hart, M. J., Santos, R. D. L., Albert, I. N., Rubinfeld, B., & Polakis, P. (1998). Downregulation of B-catenin by human Axin and its association with the APC tumor suppressor , B-catenin and GSK3B. *Current Biology*, *8*, 573–581.

Harvey, J. (1964). An Unidentified Virus which causes the Rapid Production of Tumours in Mice. *Nature*, *204*, 1104–1105.

Hasty, P., Livi, C. B., Dodds, S. G., Jones, D., Strong, R., Javors, M., … Sharp, Z. D. (2014). ERapa restores a normal life span in a FAP mouse model. *Cancer Prevention Research*, *7*(1), 169–178. https://doi.org/10.1158/1940-6207.CAPR-13-0299

Haze, K., Yoshida, H., Yanagi, H., Yura, T., & Mori, K. (1999). Mammalian Transcription Factor ATF6 Is Synthesized as a Transmembrane Protein and Activated by Proteolysis in Response to Endoplasmic Reticulum Stress. *Molecular Biology of the Cell*, *10*(November), 3787–3799.

He, T. Sparks, A., Rago, C., Hermeking, H. Zawel, L. da Costa, L. Morin, P. Vogelstein, B. Kinzler, K. (1998). Identification of c-MYC as a Target of the APC Pathway. *Science*, *281*(5382), 1509–1512. https://doi.org/10.1126/science.281.5382.1509

Heijmans, J., van Lidth de Jeude, J. F., Koo, B.-K., Rosekrans, S. L., Wielenga, M. C. B., van de Wetering, M., … van den Brink, G. R. (2013). ER stress causes rapid loss of intestinal epithelial stemness through activation of the unfolded protein response. *Cell Reports*, *3*(4), 1128–39. https://doi.org/10.1016/j.celrep.2013.02.031

Hinoue, T., Weisenberger, D. J., Lange, C. P. E., Shen, H., Byun, H., Berg, D. Van Den, … Laird, P. W. (2012). Genome-scale analysis of aberrant DNA methylation in colorectal cancer. *Genome Research*, *22*, 271–282. https://doi.org/10.1101/gr.117523.110.22

Hocker, M., & Wiedenmann, B. (1998). Molecular Mechanisms of Enteroendocrine Differentiation. *Annals of the New York Acadmey of Sciences*, *859*, 160–174.

Hofer, F., Fields, S., Schneider, C., & Martin, G. S. (1994). Activated Ras interacts with the Ral guanine nucleotide dissociation stimulator. *Proceedings of the National Academy of Sciences of the United States of America*, *91*(November), 11089–11093.

Houck, S. A., Ren, H. Y., Madden, V. J., Bonner, J. N., Conlin, M. P., Janovick, J. A., … Cyr, D. M. (2015). Quality control autophagy degrades soluble ERAD-resistant conformers of the misfolded membrane GnRHR. *Molecular Cell*, *54*(1), 166–179. https://doi.org/10.1016/j.molcel.2014.02.025.Quality

Howe, J. R., Bair, J. L., Sayed, M. G., Anderson, M. E., Mitros, F. A., Gloria, M., … Vogelstein, B. (2001). Germline mutations of the gene encoding bone morphogenetic protein receptor 1A in juvenile polyposis. *Nature Genetics*, *28*(june), 184–187.

Howe, J. R., Roth, S., Ringold, J. C., Summers, R. W., Ja, H. J., Sistonen, P., … Aaltonen, L. A. (1998). Mutations in the SMAD4 / DPC4 Gene in Juvenile Polyposis. *Science*, *280*(May), 15–18.

Huang, S.-M. a, Mishina, Y. M., Liu, S., Cheung, A., Stegmeier, F., Michaud, G. a, … Cong, F. (2009). Tankyrase inhibition stabilizes axin and antagonizes Wnt signalling. *Nature*, *461*(7264), 614–20. https://doi.org/10.1038/nature08356

Huels, D. J., Ridgway, R. A., Radulescu, S., Leushacke, M., Campbell, A. D., Biswas, S., … Sansom, O. J. (2015). E-cadherin can limit the transforming properties of activating b -catenin mutations, *34*(18), 2321–2333.

Hurwitz, H., Fehrenbacher, L., Novotny, W., Cartwright, T., Hainsworth, J., Heim, W., … Kabbinavar, F. (2004). Bevacizumab plus Irinotecan, Fluorouracil, and Leucovorin for Metastatic Colorectal Cancer Herbert. *The New England Journal of Medicine*, *350*(23), 2335–2342.

Imperiale, Thomas F., Ransohoff, David F., Itzkowitz, Steven H., Levin, Theodore R., D., Lavin, PhilipLidgard, G. P., Ahlquist, D. A., & Berger, B. M. (2014). Multitarget Stool DNA Testing for Colorectal-Cancer Screening. *The New England Journal of Medicine*, *370*(14), 1287–1297. https://doi.org/10.1056/NEJMoa1311194

Inomata, M., Ochiai, A., Akimoto, S., Kitano, S., & Hirohashi, S. (1996). Alteration of B-Catenin Expression in Colonic Epithelial Cells of Familial Adenomatous Polyposis Patients. *Cancer Research*, *56*, 2213–2218.

Ireland, H., Kemp, R., Houghton, C., Howard, L., Clarke, A. R., Sansom, O. J., & Winton, D. J. (2004). Inducible Cre-Mediated Control of Gene Expression in the Murine Gastrointestinal Tract: Effet of Loss of B-Catenin. *Gastroenterology*, *126*, 1236–1246. https://doi.org/10.1053/j.gastro.2004.03.020

Isotani, S., Hara, K., Tokunaga, C., Inoue, H., Avruch, J., & Yonezawa, K. (1999). Immunopurified Mammalian Target of Rapamycin Phosphorylates and Activates p70 S6 Kinase a in Vitro. *The Journal of Biological Chemistry*, *274*(48), 34493–34498.

Itzkovitz, S., Lyubimova, A., Blat, I. C., Maynard, M., van Es, J., Lees, J., … van Oudenaarden, A. (2011). Single-molecule transcript counting of stem-cell markers in the mouse intestine. *Nature Cell Biology*, *14*(1), 106–114. https://doi.org/10.1038/ncb2384

Jaeger, E., Leedham, S., Lewis, A., Segditsas, S., Becker, M., Cuadrado, P. R., … Tomlinson, I. (2012). Hereditary mixed polyposis syndrome is caused by a 40-kb upstream duplication that leads to increased and ectopic expression of the BMP antagonist GREM1. *Nature Genetics*, *44*(6), 699–703. https://doi.org/10.1038/ng.2263

Janssen, K. P., Alberici, P., Fsihi, H., Gaspar, C., Breukel, C. O. R., Franken, P., … Robine, S. (2006). APC and Oncogenic KRAS Are Synergistic in Enhancing Wnt Signaling in Intestinal Tumor Formation and Progression. *Gastroenterology*, *131*, 1096–1109. https://doi.org/10.1053/j.gastro.2006.08.011

Jiang, J., & Struhl, G. (1998). Regulation of the Hedgehog and Wingless signalling pathways by the F-box/ WD40-repeat protein Slimb. *Nature*, *391*(January), 493–496.

Jiang, Y. P., Ballou, L. M., & Lin, R. Z. (2001). Rapamycin-insensitive Regulation of 4E-BP1 in Regenerating Rat Liver. *Journal of Biological Chemistry*, *276*(14), 10943–10951. https://doi.org/10.1074/jbc.M007758200

Johnson, C. H., Ivanisevic, J., & Siuzdak, G. (2016). Metabolomics: beyond biomarkers and towards mechanisms. *Nature Reviews Molecular Cell Biology*, *17*(July), 451–459.

Kadowaki, T., Wilder, E., Klingensmith, J., Zachary, K., & Perrimon, N. (1996). The segment polarity gene porcupine encodes a putative multitransmembrane protein involved in Wingless processing. *Genes & Development*, *10*, 3116–3128.

Kamata, S., Yamamoto, J., Kamijo, K., Ochiai, T., Morita, T., Yoshitomi, Y., … Ishii, I. (2014). Dietary deprivation of each essential amino acid induces. *Molecular Nutrion & Food Research*, 1309–1321. https://doi.org/10.1002/mnfr.201300758

Kamphorst, J. J., Cross, J. R., Fan, J., Stanchina, E. De, Mathew, R., & White, E. P. (2013). Hypoxic and Ras-transformed cells support growth by scavenging unsaturated fatty acids from lysophospholipids. *Proceedings of the National Academy of Sciences of the United States of America*, *110*(22). https://doi.org/10.1073/pnas.1307237110

Khwaja, A., Rodriguez-Viciana, P., Wennstrom, S., Warne, P. H., & Downward, J. (1997). Matrix adhesion and Ras transformation both activate a phosphoinositide 3-OH kinase and protein kinase B / Akt cellular survival pathway. *The EMBO Journal*, *16*(10), 2783–2793.

Kim, D., Pertea, G., Trapnell, C., Pimentel, H., Kelley, R., & Salzberg, S. L. (2013). TopHat2 : accurate alignment of transcriptomes in the presence of insertions , deletions and gene fusions, 1–13.

Kim, K., Kakitani, M., Zhao, J., Oshima, T., Tang, T., Binnerts, M., … Tomizuka,

K. (2005). Mitogenic Influence of Human R-Spondin1 on the Intestinal Epithelium. *Science*, *309*(August), 1256–1260.

Kim, T., Escudero, S., & Shivdasani, R. A. (2012). Intact function of Lgr5 receptor-expressing intestinal stem cells in the absence of Paneth cells. *Proceedings of the National Academy of Sciences of the United States of America*, *109*(10), 1–6. https://doi.org/10.1073/pnas.1113890109

Kinzler, K. W., Nilbert, M. C., Su, L. K., Vogelstein, B., Bryan, T. M., Levy, D. B., … McKechnie, D. (1991). Identification of FAP locus genes from chromosome 5q21. *Science (New York, N.Y.)*, *253*(5020), 661–5. Retrieved from http://www.ncbi.nlm.nih.gov/pubmed/1651562

Kishida, S., Koyama, S., Matsubara, K., Kishida, M., & Matsuura, Y. (1997). Colocalization of Ras and Ral on the membrane is required for Ras-dependent Ral activation through Ral GDP dissociation stimulator. *Oncogene*, *15*, 2899–2907.

Klingensmith, J., Nusse, R., & I, N. P. (1994). The Drosophila segment polarity . gene dishevelled encodes a novel protein required for response to the wingless signal. *Genes & Development*, *8*, 118–130.

Komatsu, M., Waguri, S., Ueno, T., Iwata, J., Murata, S., Tanida, I., … Chiba, T. (2005). Impairment of starvation-induced and constitutive autophagy in Atg7-deficient mice. *The Journal of Cell Biology*, *169*(3), 425–34. https://doi.org/10.1083/jcb.200412022

Koo, B., Spit, M., Jordens, I., Low, T. Y., Stange, D. E., van de Wetering, M., … Clevers, H. (2012). Tumour suprressor RNF43 is a stem-cell E3 ligase that induces endocytosis of Wnt receptors. *Nature*, *488*(7413), 665–669. https://doi.org/10.1038/nature11308

Korinek, V., Barker, N., Moerer, P., Donselaar, E. Van, Huls, G., Peters, P. J., & Clevers, H. (1998). Depletion of epithelial stem-cell compartments in the small intestine of mice lacking Tcf-4. *Nature Genetics*, *19*(august), 379–383.

Kramps, T., Peter, O., Brunner, E., Nellen, D., Froesch, B., Chatterjee, S., … Basler, K. (2002). Wnt/wingless signaling requires BCL9/legless-mediated recruitment of pygopus to the nuclear beta-catenin-TCF complex. *Cell*, *109*(1), 47–60. Retrieved from http://www.ncbi.nlm.nih.gov/pubmed/11955446

Krishnamoorthy, T., & Pavitt, G. (2001). Tight binding of the phosphorylated α subunit of initiation factor 2 (eIF2α) to the regulatory subunits of guanine nucleotide exchange factor eIF2B is required for inhibition of translation. *Molecular & Cellular Biology*, *21*(15), 5018–5030. https://doi.org/10.1128/MCB.21.15.5018

Kuorokowa, M., Lynch, K., & Podolskyt, D. (1987). EFFECTS OF GROWTH FACTORS ON AN INTESTINAL. *Biochemical and Biophysical Research Communications*, *142*(3), 775–782.

Lambert, J. M., Lambert, Q. T., Reuther, G. W., Malliri, A., Siderovski, D. P., Sondek, J., … Der, C. J. (2002). Tiam1 mediates Ras activation of Rac by a PI(3)K-independent mechanism. *Nature Cell Biology*, (3), 621–625.

https://doi.org/10.1038/ncb833

Lamlum, H., Ilyas, M., Rowan, A., Clark, S., Johnson, V., Bell, J., … Tomlinson, I. (1999). The type of somatic mutation at APC in familial adenomatous polyposis is determined by the site of the germline mutation : a new facet to Knudson ' s " two-hit " hypothesis. *Nature Medicine*, *5*(9), 1071–1075.

Langmead, B., & Salzberg, S. L. (2012). Fast gapped-read alignment with Bowtie 2, *9*(4), 357–360. https://doi.org/10.1038/nmeth.1923

Lau, T., Chan, E., Callow, M., Waaler, J., Boggs, J., Blake, R. A., … Costa, M. (2013). A Novel Tankyrase Small-Molecule Inhibitor Suppresses APC Mutation – Driven Colorectal Tumor Growth, *73*(10), 3132–3145. https://doi.org/10.1158/0008-5472.CAN-12-4562

Lau, W. De, Peng, W. C., Gros, P., & Clevers, H. (2014). The R-spondin / Lgr5 / Rnf43 module : regulator of Wnt signal strength The R-spondin / Lgr5 / Rnf43 module : regulator of Wnt signal strength. *Genes & Development*, *28*, 305–316. https://doi.org/10.1101/gad.235473.113

Leary, R. J., Lin, J. C., Cummins, J., Boca, S., Wood, L. D., Parsons, D. W., … Velculescu, V. E. (2008). Integrated analysis of homozygous deletions , focal amplifications , and sequence alterations in breast and colorectal cancers. *Proceedings of the National Academy of Sciences of the United States of America*, *105*(42), 16224–16229.

Lee, A., Iwakoshi, N. N., & Glimcher, L. H. (2003). XBP-1 Regulates a Subset of Endoplasmic Reticulum Resident Chaperone Genes in the Unfolded Protein Response, *23*(21), 7448–7459. https://doi.org/10.1128/MCB.23.21.7448

Leedham, S. J., Rodenas-cuadrado, P., Howarth, K., Lewis, A., Mallappa, S., Segditsas, S., … Tomlinson, I. P. M. (2011). A basal gradient of Wnt and stem-cell number influences regional tumour distribution in human and mouse intestinal tracts. *Gut*, *62*, 83–94. https://doi.org/10.1136/gutjnl-2011-301601

Leevers, S., Paterson, H., & Marshall, C. (1994). Requirement for Ras in Raf activation is overcome by targeting Raf to the plasma membrane. *Nature*, *369*, 411–414.

Leppert, M., Dobbs, P., Scambler, P., O'Connell, P., Nakamura, P., Stauffer, D., … Gardner, E. (1987). The Gene for Familial Polyposis Coli Maps. *Science*, *238*, 1411–1413.

Leprivier, G., Remke, M., Rotblat, B., Dubuc, A., Mateo, A. R. F., Kool, M., … Sorensen, P. H. (2013). The eEF2 kinase confers resistance to nutrient deprivation by blocking translation elongation. *Cell*, *153*(5). https://doi.org/10.1016/j.cell.2013.04.055

Lévy, J., Cacheux, W., Bara, M. A., L'Hermitte, A., Lepage, P., Fraudeau, M., … Romagnolo, B. (2015). Intestinal inhibition of Atg7 prevents tumour initiation through a microbiome-influenced immune response and suppresses tumour growth. *Nature Cell Biology*, *17*(8). https://doi.org/10.1038/ncb3206

Lewis, A., Segditsas, S., Deheragoda, M., Pollard, P., Jeffery, R., Nye, E., … Tomlinson, I. (2010). Severe polyposis in Apc 1322T mice is associated with submaximal Wnt signalling and increased expression of the stem cell marker Lgr5. *Gut*, *59*, 1680–1686. https://doi.org/10.1136/gut.2009.193680

Li, B. D. L., Liu, L., Dawson, M., & De Benedetti, A. (1997). Overexpression of Eukaryotic Initiation Factor 4E (eIF4E) in Breast Carcinoma. *Amercian Cancer Society*, *79*, 2385–2390.

Li, V. S. W., Ng, S. S., Boersema, P. J., Low, T. Y., Karthaus, W. R., Gerlach, J. P., … Clevers, H. (2012). Wnt signaling through inhibition of β-catenin degradation in an intact Axin1 complex. *Cell*, *149*(6), 1245–56. https://doi.org/10.1016/j.cell.2012.05.002

Liu, J., Pan, S., Hsieh, M. H., Ng, N., Sun, F., Wang, T., … Harris, J. L. (2013). Targeting Wnt-driven cancer through the inhibition of Porcupine by LGK974, *110*(50), 20224–20229. https://doi.org/10.1073/pnas.1314239110

Liu, J., Xu, Y., Stoleru, D., & Salic, A. (2012). Imaging protein synthesis in cells and tissues with an alkyne analog of puromycin. *Proceedings of the National Academy of Sciences of the United States of America*, *109*(2), 413–418. https://doi.org/10.1073/pnas.1111561108

Lopez-Garcia, C., Klein, A. M., Simons, B. D., & Winton, D. J. (2010). Intestinal Stem Cell Replacement Follows a Pattern of Neutral Drift. *Science*, *330*(November), 822–825.

López-García, C., Sansregret, L., Domingo, E., McGranahan, N., Hobor, S., Birkbak, N. J., … Swanton, C. (2017). BCL9L Dysfunction Impairs Caspase-2 Expression Permitting Aneuploidy Tolerance in Colorectal Cancer. *Cancer Cell*, *31*(1), 79–93. https://doi.org/10.1016/j.ccell.2016.11.001

Love, M. I., Huber, W., & Anders, S. (2014). Moderated estimation of fold change and dispersion for RNA-seq data with DESeq2, 1–21. https://doi.org/10.1186/s13059-014-0550-8

Maddocks, O. D. K., Athineos, D., Cheung, E. C., Lee, P., Zhang, T., Broek, N. J. F. Van Den, … Vousden, K. H. (2017). Modulating the therapeutic response of tumours to dietary serine and glycine starvation. *Nature*, *544*(7650), 372–376. https://doi.org/10.1038/nature22056

Major, M., Camp, N., Berndt, J., Yi, X., Goldenberg, S., Hubbert, C., … Moon, R. (2007). Wilms Tumor Suppressor WTX Negatively Regulates WNT/B-catenin Signaling. *Science*, *316*(May), 1043–1047.

Mani, M., Carrasco, D. E., Zhang, Y., Takada, K., Gatt, M. E., Dutta-Simmons, J., … Carrasco, D. R. (2009). BCL9 promotes tumor progression by conferring enhanced proliferative, metastatic, and angiogenic properties to cancer cells. *Cancer Research*, *69*(19), 7577–86. https://doi.org/10.1158/0008-5472.CAN-09-0773

Marikawa, Y., & Elinson, R. P. (1998). B -TrCP is a negative regulator of the Wnt /B-catenin signaling pathway and dorsal axis formation in Xenopus embryos. *Mechanisms of Development*, *77*, 75–80.

Marshman, E., Booth, C., & Potten, C. S. (2002). The intestinal epithelial stem cell. *BioEssays*, *24*(1), 91–8. https://doi.org/10.1002/bies.10028

Matano, M., Date, S., Shimokawa, M., Takano, A., Fujii, M., Ohta, Y., … Sato, T. (2015). Modeling colorectal cancer using CRISPR-Cas9–mediated engineering of human intestinal organoids. *Nature Medicine*, (February). https://doi.org/10.1038/nm.3802

Mccrea, P. D., Turck, C. W., & Gumbiner, B. (1991). A Homolog of the armadillo Protein in Drosophila (Plakoglobin) Associated with E-Cadherin. *Science*, *254*(781), 1359–1362.

Metcalfe, C., Kljavin, N. M., Ybarra, R., & de Sauvage, F. J. (2014). Lgr5 + Stem Cells Are Indispensable for Radiation-Induced Intestinal Regeneration. *Stem Cell*, *14*(2), 149–159. https://doi.org/10.1016/j.stem.2013.11.008

Molenaar, M., Wetering, M. Van De, Oosterwegel, M., Peterson-maduro, J., Godsave, S., Korinek, V., … Clevers, H. (1996). XTcf-3 Transcription Factor Mediates ^{N_L} -Catenin-Induced Axis Formation in Xenopus Embryos. *Cell*, *86*, 391–399.

Montgomery, R. K., Carlone, D. L., Richmond, C. A., Farilla, L., Fogli, L. K., Algra, S., & Breault, D. T. (2010). Mouse telomerase reverse transcriptase (mTert) expression marks slowly cycling intestinal stem cells. *Proceedings of the National Academy of Sciences of the United States of America*, *108*(1), 2–7. https://doi.org/10.1073/pnas.1013004108

Moor, A. E., Anderle, P., Cantù, C., Rodriguez, P., Wiedemann, N., Baruthio, F., … Aguet, M. (2015). BCL9/9L-β-catenin Signaling is Associated With Poor Outcome in Colorectal Cancer. *EBioMedicine*, *2*(12), 1932–43. https://doi.org/10.1016/j.ebiom.2015.10.030

Moreno, J. A., Halliday, M., Molloy, C., Radford, H., Verity, N., Axten, J. M., … Mallucci, G. R. (2013). Oral Treatment Targeting the Unfolded Protein Response Prevents Neurodegeneration and Clinical Disease in Prion-Infected Mice, *5*(206).

Moser, A. M. Y. R., Pitot, H. C., Dove, W. F., & Clo, D. (1990). A Dominant Mutation That Predisposes Intestinal Neoplasia in the Mouse. *Science*, *247*, 4–6.

Munemitsu, S., Albert, I., Souza, B., Rubinfeld, B., & Polakis, P. (1995). Regulation of intracellular (B-catenin levels by the adenomatous polyposis coli (APC) tumor-suppressor protein. *Proceedings of the National Academy of Sciences of the United States of America*, *92*(March), 3046–3050.

Muñoz, J., Stange, D. E., Schepers, A. G., van de Wetering, M., Koo, B.-K., Itzkovitz, S., … Clevers, H. (2012). The Lgr5 intestinal stem cell signature: robust expression of proposed quiescent “+4” cell markers. *The EMBO Journal*, *31*(14), 3079–91. https://doi.org/10.1038/emboj.2012.166

Munzy, M, Bainbridge, M, Chang, K. (2012). Comprehensive molecular characterization of human colon and rectal cancer. *Nature*, *487*(7407), 330–337. https://doi.org/10.1038/nature11252

Myant, K. B., Cammareri, P., Hodder, M. C., Wills, J., Kriegsheim, A. Von, Rashid, M., … Sansom, O. J. (2017). HUWE 1 is a critical colonic tumour suppressor gene that prevents MYC signalling , DNA damage accumulation and tumour initiation. *EMBO Molecular Medicine*, *9*(2), 181–197. https://doi.org/10.15252/emmm.201606684

Nagase, H and Nakamura, Y. (1993). Mutations of the APC (Adenomatous Polyposis Coli) Gene. *Human Mutation*, *2*, 425–434.

Neel, N. F., Martin, T. D., Stratford, J. K., Zand, T. P., Reiner, D. J., & Der, C. J. (2011). The RalGEF-Ral Effector Signaling Network : The Road Less Traveled for Anti-Ras Drug Discovery. *Genes and Cancer*, *2*(3), 275–287. https://doi.org/10.1177/1947601911407329

Niida, A., Hiroko, T., Kasai, M., Furukawa, Y., Nakamura, Y., Suzuki, Y., … Akiyama, T. (2004). DKK1 , a negative regulator of Wnt signaling , is a target of the B-catenin / TCF pathway. *Oncogene*, *23*, 8520–8526. https://doi.org/10.1038/sj.onc.1207892

Noordermeer, J., Klingensmith, J., Perrimon, N., & Nusse, R. (1994). dishevelled and armadillo act in the Wingless signalling pathway in Drosophila. *Nature*, *367*, 80–83.

Nusse, R., & Varmus, H. E. (1982). Many Tumors Induced by the Mouse Mammary Tumor Virus Contain a Provirus Integrated in the Same Region of the Host Genome. *Cell*, *31*(November), 99–109.

Nusslein-Volhard, C., & Wieschaus, E. (1980). Mutations affecting sgement number and polarity in Drosophila. *Nature*, 795–801.

O'Farrell, P. (1975). High Resolution Two-Dimensional Electrophoresis of Proteins. *The Journal of Biological Chemistry*, *250*(10), 4007–4021.

Ong, S.-E., Blagoev, B., Kratchmarova, I., Kristensen, D. B., Steen, H., Pandey, A., & Mann, M. (2002). Stable Isotope Labeling by Amino Acids in Cell Culture, SILAC, as a Simple and Accurate Approach to Expression Proteomics. *Molecular & Cellular Proteomics*, *1*(5), 376–386. https://doi.org/10.1074/mcp.M200025-MCP200

Ong, S.-E., & Mann, M. (2006). A practical recipe for stable isotope labeling by amino acids in cell culture (SILAC). *Nature Protocols*, *1*(6), 2650–60. https://doi.org/10.1038/nprot.2006.427

Ouellette, A. J., Darmoul, D., Tran, D. A. T., Huttner, K. M., Yuan, J. U. N., & Selsted, M. E. (1999). Peptide Localization and Gene Structure of Cryptdin 4 , a Differentially Expressed Mouse Paneth Cell a-Defensin. *Infection and Immunity*, *67*(12), 6643–6651.

Ozawa, M., Baribault, H., & Kemler, R. (1989). The cytoplasmic domain of the cell adhesion molecule uvomorulin associates with three independent proteins structurally related in different species. *The EMBO Journal*, *8*(6), 1711–1717.

Palam, L. R., Gore, J., Craven, K. E., Wilson, J. L., & Korc, M. (2015). Integrated stress response is critical for gemcitabine resistance in pancreatic ductal

adenocarcinoma. *Cell Death & Disease*, *6*(10), 1–13. https://doi.org/10.1038/cddis.2015.264

Park, Y., Reyna-neyra, A., Philippe, L., Thoreen, C. C., Park, Y., Reyna-neyra, A., … Thoreen, C. C. (2017). mTORC1 Balances Cellular Amino Acid Supply with Demand for Protein Synthesis through Post- transcriptional Control of ATF4 Report mTORC1 Balances Cellular Amino Acid Supply with Demand for Protein Synthesis through Post-transcriptional Control of ATF4. *CellReports*, *19*(6), 1083–1090. https://doi.org/10.1016/j.celrep.2017.04.042

Patra, K. C., & Hay, N. (2014). The pentose phosphate pathway and cancer. *Trends in Biochemical Sciences*, *39*(8), 347–354. https://doi.org/10.1016/j.tibs.2014.06.005

Patra, K. C., Wang, Q., Bhaskar, P. T., Miller, L., Wang, Z., Chandel, N., … Robey, B. (2014). Hexokinase 2 is requried for tumor initiation and maintenance in mouse models of cancer. *Cancer Cell*, *24*(2), 213–228. https://doi.org/10.1016/j.ccr.2013.06.014.Hexokinase

Pause, A., Méthot, N., Svitkin, Y., Merrick, W. C., & Sonenberg, N. (1994). Dominant negative mutants of mammalian translation initiation factor elF-4A define a critical role for elF-4F in cap-dependent and cap-independent initiation of translation. *EMBO Journal*, *13*(5).

Pavlova, N. N., & Thompson, C. B. (2016). Perspective The Emerging Hallmarks of Cancer Metabolism. *Cell Metabolism*, *23*(1), 27–47. https://doi.org/10.1016/j.cmet.2015.12.006

Peifer, M., Pai, L., & Casey, M. (1994). Phosphorylation of the Drosophila Adherens Junction Protein Armadillo: Roles for Wingless Signal and Zeste-white 3 Kinase. *Developmental Biology*, *166*, 543–556.

Peifer, M., Sweeton, D., Casey, M., & Wieschaus, E. (1994). wingless signal and Zeste-white 3 kinase trigger opposing changes in the intracellular distribution of Armadillo, *380*, 369–380.

Peters, J., Mckay, R., Mckay, J., & Graff, J. (1999). Casein kinase I transduces Wnt signals. *Nature*, *401*(September).

Pinto, D., Gregorieff, A., Begthel, H., & Clevers, H. (2003). Canonical Wnt signals are essential for homeostasis of the intestinal epithelium. *Genes & Development*, *17*, 1709–1713. https://doi.org/10.1101/gad.267103.GENES

Pollard, P., Deheragoda, M., Segditsas, S., Lewis, A., Rowan, A., Howarth, K., … Tomlinson, I. (2009). The Apc 1322T mouse develops severe polyposis associated with submaximal nuclear beta-catenin expression. *Gastroenterology*, *136*(7), 2204-2213–13. https://doi.org/10.1053/j.gastro.2009.02.058

Porter, E. M., Bevins, C. L., Ghosh, D., & Ganz, T. (2002). The multifaceted Paneth cell. *Cellular and Molecular Life Sciences : CMLS*, *59*, 156–170.

Potten, C. S., Kovacs, L., & Hamliton, E. (1974). Continuous labelling studies on mouse skin and intestine. *Cell Tissue Kinetics*, *7*, 271–283.

Potten, C. S., Owen, G., Hewitt, D., Chadwick, C. A., Hendry, H., Lord, B. I., & Woolford, L. B. (1995). Stimulation and inhibition of proliferation in the small intestinal crypts of the mouse after in vivo administration of growth factors. *Gut*, *36*, 864–873.

Preston, S. L., Wong, W., Chan, A. O., Poulsom, R., Jeffery, R., Goodlad, R. A., … Wright, N. A. (2003). Bottom-up Histogenesis of Colorectal Adenomas : Origin in the Monocryptal Adenoma and Initial Expansion by Crypt Fission. *Cancer Rsearch*, *63*, 3819–3825.

Reddy, P., Reynolds, R., Santos, E., & Barbacid, M. (1982). A point mutation is responsible for the acquisition of transforming properties by the T24 human bladder carcinoma oncogene. *Nature*, *300*, 149–152.

Riggleman, B., Schedl, P., & Wieschaus, E. (1990). Spatial Expression of the Drosophila Segment Polarity Gene armadillo Is Posttranscriptionally Regulated by wingless. *Cell*, *63*, 549–560.

Rijsewijk, F., Schuermann, M., Wagenaar, E., Parren, L., Weigel, D., & Nusse, R. (1987). The Drosophila Homolog of the Mouse Mammary Oncogene int-1 Is Identical to the Segment Polarity Gene wingless. *Cell*, *50*, 649–657.

Rodriguez-Viciana, P., Warne, P., Dhand, R., Vanhaesebroeck, B., Gout, I., Fry, M., … Downward, J. (1994). Phosphatidylinositol-3-OH kinae as a direct target of Ras. *Nature*, *370*, 527–532.

Roose, J., Hurenkamp, J., Brantjes, H., Moerer, P., van de Wetering, M., Destree, O., & Clevers, H. (1998). Wnt effector XTcf-3 interacts with Groucho-related transcriptional repressors. *Nature*, *395*(October), 608–612.

Rosenwald, I. B., Chen, J. J., Wang, S., Savas, L., London, I. M., & Pullman, J. (1999). Upregulation of protein synthesis initiation factor eIF-4E is an early event during colon carcinogenesis. *Oncogene*, *18*(15), 2507–2517. https://doi.org/10.1038/sj.onc.1202563

Rosenwald, I. B., Kaspar, R., Rousseau, D., Gehrke, L., Leboulch, P., Chen, J. J., … London, I. M. (1995). Eukaryotic translation initiation factor 4E regulates expression of cyclin D1 at transcriptional and post-transcriptional levels. *J.Biol Chem*, *270*(36), 21176–21180.

Rosty, C., Young, J. P., Walsh, M. D., Clendenning, M., Walters, R. J., Pearson, S., … Buchanan, D. D. (2013). Colorectal carcinomas with KRAS mutation are associated with distinctive morphological and molecular features. *Modern Pathology*, *26*(6), 825–834. https://doi.org/10.1038/modpathol.2012.240

Rottman, F., Shatkin, A. J., & Perry, R. P. (1974). Sequences containing methylated nucleotides at the 5′ termini of messenger RNAs: Possible implications for processing. *Cell*, *3*(3), 197–199. https://doi.org/10.1016/0092-8674(74)90131-7

Rubinfeld, B., Albert, I., Porfiri, E., Munemitsu, S., & Polakis, P. (1997). Loss of / B-Catenin Regulation by the APC Tumor Suppressor Protein Correlates with Loss of Structure Due to Common Somatic Mutations of the Gene. *Cancer Research*, *57*, 4624–4630.

Rubinfeld, B., Souza, B., Albert, I., Muller, O., Chamberlain, S. H., Masiarz, F. R., … Polakis, P. (1993). Association of the APC Gene Product with B-Catenin. *Science*, *262*(December), 1731–1734.

Ryazanov, A. G., Shestakova, E. A. & Natapov, P. G. (1988). Phosphorylation of elongation factor 2 by EF-2 kinase affects rate of translation. *Nature*, *334*, 170–173.

Safer, Brian, W., Anderson, W. F., & Merrick, William, C. (1975). Purification and characterization of homogeneous protein synthesis initiation factor M1 from rabbit reticulocytes. *Journal of Biological Chemistry*, *250*(4).

Sakamaki, J. ichi, Wilkinson, S., Hahn, M., Tasdemir, N., O'Prey, J., Clark, W., … Ryan, K. M. (2017). Bromodomain Protein BRD4 Is a Transcriptional Repressor of Autophagy and Lysosomal Function. *Molecular Cell*, *66*(4), 517–532.e9. https://doi.org/10.1016/j.molcel.2017.04.027

Sakamoto, I., Ohwada, S., Toya, H., Togo, N., Kashiwabara, K., Oyama, T., … Akiyama, T. (2007). Up-regulation of a BCL9-related β-catenin-binding protein, B9L, in different stages of sporadic colorectal adenoma, *98*(1), 83–87. https://doi.org/10.1111/j.1349-7006.2007.00363.x

Salgado, M. C., Metón, I., Anemaet, I. G., & Baanante, I. V. (2014). Activating transcription factor 4 mediates up-regulation of alanine aminotransferase 2 gene expression under metabolic stress. *Biochimica et Biophysica Acta*, *1839*(4), 288–96. https://doi.org/10.1016/j.bbagrm.2014.01.005

Sangiorgi, E., & Capecchi, M. R. (2008). Bmi1 is expressed in vivo in intestinal stem cells. *Nature Genetics*, *40*(7), 915–920. https://doi.org/10.1038/ng.165

Sansom, O. J., Meniel, V. S., Muncan, V., Phesse, T. J., Wilkins, J. a, Reed, K. R., … Clarke, A. R. (2007). Myc deletion rescues Apc deficiency in the small intestine. *Nature*, *446*(7136), 676–9. https://doi.org/10.1038/nature05674

Sansom, O. J., Meniel, V., Wilkins, J. A., Cole, A. M., Oien, K. A., Marsh, V., … Clarke, A. R. (2006). Loss of Apc allows phenotypic manifestation of the transforming properties of an endogenous K-ras oncogene in vivo. *Proceedings of the National Academy of Sciences of the United States of America*, *103*(38).

Sansom, O. J., Reed, K. R., Hayes, A. J., Ireland, H., Brinkmann, H., Newton, I. P., … Winton, D. J. (2004). Loss of Apc in vivo immediately perturbs Wnt signaling, differentiation, and migration. *Genes & Development*, *18*(12), 1385–90. https://doi.org/10.1101/gad.287404

Sasaki, T., Giltay, R., Talts, U., Timpl, R., & Talts, J. F. (2002). Expression and Distribution of Laminin a1 and a2 Chains in Embryonic and Adult Mouse Tissues : An Immunochemical Approach. *Experimental Cell Research*, *275*, 185–199. https://doi.org/10.1006/excr.2002.5499

Sato, T., Es, J. H. Van, Snippert, H. J., Stange, D. E., Vries, R. G., Born, M. Van Den, … Clevers, H. (2011). Paneth cells constitute the niche for Lgr5 stem cells in intestinal crypts. *Nature*, *469*(7330), 415–418. https://doi.org/10.1038/nature09637

Sato, T., Stange, D. E., Ferrante, M., Vries, R. G. J., & Es, J. H. V. A. N. (2011). Long-term Expansion of Epithelial Organoids From Human Colon, Adenoma, Adenocarcinoma, and Barrett's Epithelium. *Gastroenterology*, *141*(5), 1762–1772. https://doi.org/10.1053/j.gastro.2011.07.050

Sato, T., Vries, R. G., Snippert, H. J., van de Wetering, M., Barker, N., Stange, D. E., … Clevers, H. (2009). Single Lgr5 stem cells build crypt-villus structures in vitro without a mesenchymal niche. *Nature*, *459*(7244), 262–5. https://doi.org/10.1038/nature07935

Sauer, L. A., Webster, J., Iii, S., & Dauchy, R. T. (1982). Amino Acid , Glucose , and Lactic Acid Utilization in Vivo by Rat Tumors1. *Cancer Research*, *42*(October), 4090–4097.

Scheper, G. C., & Proud, C. G. (2002). Does phosphorylation of the cap-binding protein eIF4E play a role in translation initiation? *European Journal of Biochemistry*, *269*(22), 5350–5359. https://doi.org/10.1046/j.1432-1033.2002.03291.x

Schneider-Poetsch, T., Ju, J., Eyler, D. E., Dang, Y., Bhat, S., Merrick, W. C., … Liu, J. O. (2010). Inhibition of eukaryotic elongation by cycloheximide and lactimidomycin. *Nature Chemical Biology*, *6*(3), 209–217. https://doi.org/10.1038/nchembio.304

Schneikert, J., & Fodde, R. (2006). Truncated APC is required for cell proliferation and DNA replication. *International Journal of Cancer*, *119*, 74–79. https://doi.org/10.1002/ijc.21826

Schwitalla, S., Fingerle, A. a, Cammareri, P., Nebelsiek, T., Göktuna, S. I., Ziegler, P. K., … Greten, F. R. (2013). Intestinal tumorigenesis initiated by dedifferentiation and acquisition of stem-cell-like properties. *Cell*, *152*(1–2), 25–38. https://doi.org/10.1016/j.cell.2012.12.012

Segditsas, S., & Tomlinson, I. (2006). Colorectal cancer and genetic alterations in the Wnt pathway. *Oncogene*, *25*, 7531–7537. https://doi.org/10.1038/sj.onc.1210059

Sendoel, A., Dunn, J. G., Rodriguez, E. H., Naik, S., Gomez, N. C., Hurwitz, B., … Fuchs, E. (2017). Translation from unconventional 5' start sites drives tumour initiation. *Nature*. https://doi.org/10.1038/nature21036

Seshagiri, S., Stawiski, E. W., Durinck, S., Modrusan, Z., Storm, E. E., Conboy, C. B., … De Sauvage, F. J. (2012). Recurrent R-spondin fusions in colon cancer. *Nature*, *488*(7413), 660–664. https://doi.org/10.1038/nature11282

Shen, J., Chen, X., Hendershot, L., & Prywes, R. (2002). ER Stress Regulation of ATF6 Localization by Dissociation of BiP / GRP78 Binding and Unmasking of Golgi Localization Signals. *Developmental Cell*, *3*(3), 99–111.

Shevchenko, A., Chernushevich, I., Ens, W., Standing, K. G., Thomson, B., Wilm, M., & Mann, M. (1997). Rapid " de Novo " Peptide Sequencing by a Combination of Nanoelectrospray , Isotopic Labeling and a Quadrupole/Time-of-flight Mass Spectrometer. *Rapid Communications in Mass Spectrometry*, *11*, 1015–1024.

Shibata, H., Shibata, H., Toyama, K., Shioya, H., Ito, M., Hirota, M., … Noda, T. (1997). Rapid Colorectal Adenoma Formation Initiated by Conditional Targeting of the Apc Gene Rapid Colorectal Adenoma Formation Initiated by Conditional Targeting of the Apc Gene. *Science*, *278*, 120–123. https://doi.org/10.1126/science.278.5335.120

Shih, I., Wang, T., Traverso, G., Romans, K., Hamilton, S. R., Ben-sasson, S., … Vogelstein, B. (2001). Top-down morphogenesis of colorectal tumors. *Proceedings of the National Academy of Sciences of the United States of America*, *98*(5), 2640–2645.

Shyer, A. E., Huycke, T. R., Lee, C., Mahadevan, L., & Tabin, C. J. (2015). Bending Gradients: How the Intestinal Stem Cell Gets Its Home. *Cell*, *161*, 1–12. https://doi.org/10.1016/j.cell.2015.03.041

Sidrauski, C., Acosta-Alvear, D., Khoutorsky, A., Vedantham, P., Hearn, B. R., Li, H., … Walter, P. (2013). Pharmacological brake-release of mRNA translation enhances cognitive memory. *eLife*, *2*, e00498. https://doi.org/10.7554/eLife.00498

Sidrauski, C., Tsai, J. C., Kampmann, M., Hearn, B. R., Vedantham, P., Jaishankar, P., … Walter, P. (2015). Pharmacological dimerization and activation of the exchange factor eIF2B antagonizes the integrated stress response. *eLife*, *4*, e07314. https://doi.org/10.7554/eLife.07314

Siegfried, E., Chou, T., & Perrimon, N. (1992). wingless Signaling Acts through zeste . white 3 , the Drosophila Homolog of glycogen synthase kinase-3 , to Regulate engrafted and Establish Cell Fate. *Cell*, *71*, 1167–1179.

Sinclair, L. V, Rolf, J., Emslie, E., Shi, Y., & Taylor, P. M. (2013). Antigen receptor control of amino acid transport coordinates the metabolic re-programming that is essential for T cell differentiation. *Nature Immunology*, *14*(5), 500–508. https://doi.org/10.1038/ni.2556.Antigen

Sjöblom, T., Jones, S., Wood, L. D., Parsons, D. W., Lin, J., Barber, T. D., … Velculescu, V. E. (2006). The consensus coding sequences of human breast and colorectal cancers. *Science (New York, N.Y.)*, *314*(5797), 268–74. https://doi.org/10.1126/science.1133427

Skrzypczak, M., Goryca, K., Rubel, T., Paziewska, A., Mikula, M., Jarosz, D., … Ostrowsk, J. (2010). Modeling oncogenic signaling in colon tumors by multidirectional analyses of microarray data directed for maximization of analytical reliability. *PLoS ONE*, *5*(10). https://doi.org/10.1371/journal.pone.0013091

Smith, B., Schafer, X. L., Ambeskovic, A., Spencer, C. M., Land, H., Munger, J., … Munger, J. (2016). Addiction to Coupling of the Warburg Effect with Glutamine Catabolism in Cancer Cells Article Addiction to Coupling of the Warburg Effect with Glutamine Catabolism in Cancer Cells. *CellReports*, *17*(3), 821–836. https://doi.org/10.1016/j.celrep.2016.09.045

Snippert, H. J., Flier, L. G. Van Der, Sato, T., Es, J. H. Van, Born, M. Van Den, Kroon-veenboer, C., … Clevers, H. (2010). Intestinal Crypt Homeostasis Results from Neutral Competition between Symmetrically Dividing Lgr5 Stem Cells. *Cell*, *143*(1), 134–144. https://doi.org/10.1016/j.cell.2010.09.016

Sokabe, M., Fraser, C. S., & Hershey, J. W. B. (2012). The human translation initiation multi-factor complex promotes methionyl-tRNA i binding to the 40S ribosomal subunit. *Nucleic Acids Research*, *40*(2), 905–913. https://doi.org/10.1093/nar/gkr772

Som, P., Atkins, H. L., Bandoypadhyay, D., Fowler, J. S., Macgregor, A. R., Matsui, K., … Sacker, D. F. (1980). A Fluorinated Glucose Analog , 2-fluoro-2-deoxy-D-glucose (F-18): Nontoxic Tracer for RapidTumor Detection ofacute orchronic. *The Journal of Nuclear Medicine*, *21*(7), 670–675.

Son, J., Lyssiotis, C. A., Ying, H., Wang, X., Hua, S., Kang, Y., … Asara, J. M. (2013). Glutamine supports pancreatic cancer growth through a Kras-regulated metabolic pathway. *Nature*, *496*(7443), 101–105. https://doi.org/10.1038/nature12040.Glutamine

Songster, C. L., Barrows, H., Jarrett, D. D., & Ascps, M. T. (1980). Immunochemical Detection of Fecal Occult Blood - The Fecal Smear Punch-Disc Test: A New Non-Invasive Screening Test for Colorectal Cancer. *Cancer*, *45*, 1099–1102.

Sousa, C. M., Biancur, D. E., Wang, X., Halbrook, C. J., Sherman, M. H., Zhang, L., … Kimmelman, A. C. (2016). Pancreatic stellate cells support tumour metabolism through autophagic alanine secretion. *Nature*, *536*(7617), 479–83. https://doi.org/10.1038/nature19084

Spriggs, K. A., Bushell, M., & Willis, A. E. (2010). Translational Regulation of Gene Expression during Conditions of Cell Stress. *Molecular Cell*, *40*(2), 228–237. https://doi.org/10.1016/j.molcel.2010.09.028

Su, L., Kinzler, K. W., Vogelstein, B., Preisinger, A. C., Moser, A. R., Luongo, C., … Dove, W. F. (1992). Multiple Intestinal Neoplasia Caused by a Mutation in the Murine Homolog of the APC Gene. *Science*, *256*(May), 668–671.

Su, L., Vogelstein, B., & Kinzler, K. W. (1993). Association of the APC Tumor Suppressor Protein with Catenins. *Science*, *262*(December), 1734–1738.

Takada, K., Zhu, D., Bird, G. H., Sukhdeo, K., Zhao, J.-J., Mani, M., … Carrasco, D. R. (2012). Targeted disruption of the BCL9/ß-catenin complex inhibits oncogenic Wnt signaling. *Science Translational Medicine*, *4*(148), 148ra117. https://doi.org/10.1126/scitranslmed.3003808

Takada, R., Satomi, Y., Kurata, T., Ueno, N., Norioka, S., Kondoh, H., & Takao, T. (2006). Monounsaturated Fatty Acid Modification of Wnt Protein : Its Role in Wnt Secretion. *Developmental Cell*, 791–801. https://doi.org/10.1016/j.devcel.2006.10.003

Takeda, N., Jain, R., LeBeouf, M., Wang, Q., Lu, M., & Epstein, J. (2011). Interconversion Between Intestinal Stem Cell Populations in Distinct Niches. *Science*, (December), 1420–1425.

Thibodeau, S. N., Bren, G., & Schaid, D. (1993). Microsatellite Instability in Cancer of the Proximal Colon. *Science*, *260*(May), 816–819.

Tian, H., Biehs, B., Warming, S., Leong, K. G., Rangell, L., Klein, O. D., & de Sauvage, F. J. (2012). A reserve stem cell population in small intestine

renders Lgr5-positive cells dispensable. *Nature*, *478*(7368), 255–259. https://doi.org/10.1038/nature10408

Tienen, L. M. Van, Mieszczanek, J., Fiedler, M., Rutherford, T. J., & Bienz, M. (2017). Constitutive scaffolding of multiple Wnt enhanceosome components by Legless /. *eLife*, 1–23. https://doi.org/10.7554/eLife.20882

Timosenko, E., Ghadbane, H., Silk, J. D., Shepherd, D., Gileadi, U., Howson, L. J., … Cerundolo, V. (2016). Nutritional Stress Induced by Tryptophan-Degrading Enzymes Results in ATF4-Dependent Reprogramming of the Amino Acid Transporter Pro fi le in Tumor Cells. *Cancer Research*, 6193–6205. https://doi.org/10.1158/0008-5472.CAN-15-3502

Torrance, C. J., Jackson, P. E., Montgomery, E. M., Kinzler, K. W., Voggelstein, B., Wissner, A., … Discafani, C. M. (2000). Combinatorial chemoprevention of intestinal neoplasia. *Nature Medicine*, *6*(8), 1024–1028.

Troughton, W. D., & Trier, J. S. (1969). Paneth and Goblet cell renewal in mouse duodenal crypts. *The Journal of Cell Biology*, *41*, 251–268.

Van Cutsem, E., Nordlinger, B., & Cervantes, A. (2010). Advanced colorectal cancer : ESMO Clinical Practice Guidelines for treatment. *Annals of Oncology : Official Journal of the European Society for Medical Oncology / ESMO*, *21*(Supplement 5), 93–97. https://doi.org/10.1093/annonc/mdq222

van de Wetering, M., Sancho, E., Verweij, C., Lau, W. De, Oving, I., Hurlstone, A., … Clevers, H. (2002). The B-Catenin / TCF-4 Complex Imposes a Crypt Progenitor Phenotype on Colorectal Cancer Cells. *Cell*, *111*, 241–250.

van der Flier, L. G., van Gijn, M. E., Hatzis, P., Kujala, P., Haegebarth, A., Stange, D. E., … Clevers, H. (2009). Transcription Factor Achaete Scute-Like 2 Controls Intestinal Stem Cell Fate. *Cell*, *136*(5), 903–912. https://doi.org/10.1016/j.cell.2009.01.031

van Es, J. H., Sato, T., van de Wetering, M., Lyubimova, A., Ng, A., Nee, Y., … Clevers, H. (2012). Dll1 + secretory progenitor cells revert to stem cells upon crypt damage. *Nature Cell Biology*, *14*(10), 1099–1104. https://doi.org/10.1038/ncb2581

van Es, J. H., van Gijn, M. E., Riccio, O., van den Born, M., Vooijs, M., Begthel, H., … Clevers, H. (2005). Notch /γ-secretase inhibition turns proliferative cells in intestinal crypts and adenomas into goblet cells. *Nature*, *435*(June), 959–963. https://doi.org/10.1038/nature03659

van Leeuwen, F., Harryman Samos, C., & Nusse, R. (1994). Biological activity of soluble wingless protein in cultured Drosophila imaginal disc cells. *Nature*, *368*, 342–344.

van Lidth de Jeude, J. F., Meijer, B. J., Wielenga, M. C. B., Spaan, C. N., Baan, B., Rosekrans, S. L., … Heijmans, J. (2016). Induction of endoplasmic reticulum stress by deletion of Grp78 depletes Apc mutant intestinal epithelial stem cells. *Oncogene*, (February), 1–9. https://doi.org/10.1038/onc.2016.326

Vasseur, S., Hoffmeister, A., Garcia-montero, A., Mallo, G. V., Feil, R., Ku, S., …

Iovanna, J. L. (2002). p8-decient fibroblasts grow more rapidly and are more resistant to adriamycin-induced apoptosis. https://doi.org/10.1038/sj/onc/1205222

Vermeulen, L., Morrissey, E., Heijden, M. Van Der, Nicholson, A. M., Sottoriva, A., Buczacki, S., … Winton, D. J. (2013). Defining Stem Cell Dynamics in Models of Intestinal Tumor Initiation. *Science*, *267*(November), 263–267.

Vilar, E., & Gruber, S. B. (2012). Microsatellite instability in colorectal cancer - the stable evidence. *Nature Reviews Clinical Oncology*, *7*(3), 153–162. https://doi.org/10.1038/nrclinonc.2009.237.Microsatellite

Vogelstein, B, Fearon, E, Hamilton, S, Kern, S, Preisinger A, Leppert, M, Smits, A, Bos, J. (1988). Genetic Alterations during Colorectal-Tumor Development. *New England Journal of Medicine*, *319*(1988), 525–532. https://doi.org/10.1056/NEJM198809013190901

Waaler, J., Machon, O., Tumova, L., Dinh, H., Korinek, V., Wilson, S. R., … Krauss, S. (2012). A Novel Tankyrase Inhibitor Decreases Canonical Wnt Signaling in Colon Carcinoma Cells and Reduces Tumor Growth in Conditional APC Mutant Mice, *72*(12), 2822–2833. https://doi.org/10.1158/0008-5472.CAN-11-3336

Walter, P., & Ron, D. (2011). The Unfolded Protein Response : From Stress Pathway to Homeostatic Regulation, *334*(November), 1081–1087.

Wang, X., Li, W., Williams, M., Terada, N., Alessi, D. R., & Proud, C. G. (2001). Regulation of elongation factor 2 kinase by p90 RSK1 and p70 S6 kinase. *The EMBO Journal*, *20*(16), 4370–4379.

Warburg, B. Y. O., & Wind, F. (1927). The metabolism of tumours in the body. *The Journal of General Physiology*, *8*, 519–530.

Wehrli, M., Dougan, S. T., Caldwell, K., & Keefe, L. O. (2000). arrow encodes an LDL-receptor- related protein essential for Wingless signalling. *Nature*, *407*, 527–530.

Weisenberger, D. J., Siegmund, K. D., Campan, M., Young, J., Long, T. I., Faasse, M. A., … Laird, P. W. (2006). CpG island methylator phenotype underlies sporadic microsatellite instability and is tightly associated with BRAF mutation in colorectal cancer. *Nature Genetics*, *38*(7), 2006. https://doi.org/10.1038/ng1834

Westphalen, C. B., Asfaha, S., Hayakawa, Y., Takemoto, Y., Lukin, D. J., Nuber, A. H., … Wang, T. C. (2014). Long-lived intestinal tuft cells serve as colon cancer – initiating cells. *The Journal of Clinical Investigation*, *124*(3), 1283–1295. https://doi.org/10.1172/JCI73434DS1

Wiegering, A., Uthe, F. W., Jamieson, T., Ruoss, Y., Hüttenrauch, M., Küspert, M., … Eilers, M. (2015). Targeting Translation Initiation Bypasses Signaling Crosstalk Mechanisms That Maintain High MYC Levels in Colorectal Cancer. *Cancer Discovery*, *5*(7), 768–81. https://doi.org/10.1158/2159-8290.CD-14-1040

Wielenga, M. C. B., Colak, S., Heijmans, J., van Lidth de Jeude, J. F.,

Rodermond, H. M., Paton, J. C., … van den Brink, G. R. (2015). ER-Stress-Induced Differentiation Sensitizes Colon Cancer Stem Cells to Chemotherapy. *Cell Reports*, 1–6. https://doi.org/10.1016/j.celrep.2015.09.016

Wieschaus, E., & Riggleman, R. (1987). Autonomous Requirements for the Segment Polarity Gene armadillo during Drosophila Embryogenesis. *Cell*, *49*, 177–184.

Wise, D. R., & Thompson, C. B. (2010). Glutamine addiction : a new therapeutic target in cancer. *Trends in Biochemical Sciences*, *35*(8), 427–433. https://doi.org/10.1016/j.tibs.2010.05.003

Wittinghofer, A., Scheffzek, K., & Ahmadian, M. R. (1997). The interaction of Ras with GTPase-activating proteins. *FEBS Letters*, *410*(1), 63–67. https://doi.org/10.1016/S0014-5793(97)00321-9

Wolfe, A. L., Singh, K., Zhong, Y., Drewe, P., Rajasekhar, V. K., Sanghvi, V. R., … Wendel, H.-G. (2014). RNA G-quadruplexes cause eIF4A-dependent oncogene translation in cancer. *Nature*, *513*(7516), 65–70. https://doi.org/10.1038/nature13485

Wong, H., Bourdelas, A., Krauss, A., Lee, H., Shao, Y., Wu, D., … Zheng, J. (2003). Direct Binding of the PDZ Domain of Dishevelled to a Conserved Internal Sequence in the C-Terminal Region of Frizzled. *Molecular Cell*, *12*, 1251–1260.

Wong, V. W. Y., Stange, D. E., Page, M. E., Buczacki, S., Wabik, A., Itami, S., … Jensen, K. B. (2012). Lrig1 controls intestinal stem-cell homeostasis by negative regulation of ErbB signalling. *Nature Cell Biology*, *14*(4), 401–408. https://doi.org/10.1038/ncb2464

Wood, L. D., Parsons, D. W., Jones, S., Lin, J., Sjöblom, T., Leary, R. J., … Vogelstein, B. (2007). The Genomic Landscapes of Human Breat and Colorectal Cancers. *Science*, *318*(November), 1108–1114.

Xie, X., Koh, J. Y., Price, S., White, E., & Mehnert, J. M. (2015). Atg7 overcomes senescence and promotes growth of BRAFV600E-driven melanoma. *Cancer Discovery*. https://doi.org/10.1158/2159-8290.CD-14-1473

Yan, K. S., Gevaert, O., Zheng, G. X. Y., Henning, S. J., Wong, M. H., Kuo, C. J., … Cynn, E. (2017). Intestinal Enteroendocrine Lineage Cells Possess Article Intestinal Enteroendocrine Lineage Cells Possess Homeostatic and Injury-Inducible Stem Cell Activity. *Cell Stem Cell*, *21*, 78–90. https://doi.org/10.1016/j.stem.2017.06.014

Yan, K. S., Janda, C. Y., Chang, J., Zheng, G. X. Y., Larkin, K. A., Luca, V. C., … Kuo, C. J. (2017). Non-equivalence of Wnt and R-spondin ligands during Lgr5 + intestinal stem-cell self-renewal. *Nature*, *545*(7653), 238–242. https://doi.org/10.1038/nature22313

Yanagawa, S., Matsuda, Y., Lee, J., & Matsubayashi, H. (2002). Casein kinase I phosphorylates the Armadillo protein and induces its degradation in Drosophila. *The EMBO Journal*, *21*(7), 1733–1742.

Ye, J., Kumanova, M., Hart, L. S., Sloane, K., Zhang, H., De Panis, D. N., … Koumenis, C. (2010). The GCN2-ATF4 pathway is critical for tumour cell survival and proliferation in response to nutrient deprivation. *The EMBO Journal*, *29*(12), 2082–96. https://doi.org/10.1038/emboj.2010.81

Ying, H., Kimmelman, A. C., Lyssiotis, C. A., Hua, S., Chu, G. C., Fletcher-sananikone, E., … Cantley, L. C. (2010). Oncogenic Kras Maintains Pancreatic Tumors through Regulation of Anabolic Glucose Metabolism. *Cell*, *149*(3), 656–670. https://doi.org/10.1016/j.cell.2012.01.058

Yuksekkaya, H., Yucel, A., Gumus, M., Esen, H., & Toy, H. (2016). Familial Adenomatous Polyposis; Succesful Use of Sirolimus. *American Journal of Gastroenterology*, *111*(July), 1040´-1041. https://doi.org/10.1038/ajg.2016.159

Yuneva, M. O., Fan, T. W. M., Allen, T. D., Higashi, R. M., Ferraris, D. V, Tsukamoto, T., … Bishop, J. M. (2012). The metabolic profile of tumors depends on both the responsible genetic lesion and tissue type. *Cell Metabolism*, *15*(2), 157–70. https://doi.org/10.1016/j.cmet.2011.12.015

Yuneva, M., Zamboni, N., Oefner, P., Sachidanandam, R., & Lazebnik, Y. (2007). Defi ciency in glutamine but not glucose induces MYC-dependent apoptosis in human cells, *178*(1), 93–105. https://doi.org/10.1083/jcb.200703099

Zamboni, N., Saghatelian, A., & Patti, G. J. (2015). Defining the Metabolome: Size, Flux, and Regulation. *Molecular Cell*, *58*(4), 699–706. https://doi.org/10.1016/j.molcel.2015.04.021

Zanivan, S., Maione, F., Hein, M. Y., Hernández-Fernaud, J. R., Ostasiewicz, P., Giraudo, E., & Mann, M. (2013). SILAC-based proteomics of human primary endothelial cell morphogenesis unveils tumor angiogenic markers. *Molecular & Cellular Proteomics*, *12*, 3599–3611. https://doi.org/10.1074/mcp.M113.031344

Zeng, L., Zhang, T., Hsu, W., Vasicek, T. J., Iii, W. L. P., Lee, J. J., … Costantini, F. (1997). The Mouse Fused Locus Encodes Axin , an Inhibitor of the Wnt Signaling Pathway That Regulates Embryonic Axis Formation. *Cell*, *90*, 181–192.

Zhang, J., Fan, J., Venneti, S., Cross, J. R., Takagi, T., Bhinder, B., … Thompson, C. B. (2014). Asparagine Plays a Critical Role in Regulating Cellular Adaptation to Glutamine Depletion. *Molecular Cell*, *56*(2), 205–218. https://doi.org/10.1016/j.molcel.2014.08.018

Zhou, G., Li, H., Decamp, D., Chen, S., Shu, H., Gong, Y., … Zhao, Y. (2002). 2D Differential In-gel Electrophoresis for the Identification of Esophageal Scans Cell Cancer-specific Protein Markers *. *Molecular & Cellular Proteomics*, *1*, 117–123. https://doi.org/10.1074/mcp.M100015-MCP200

Zoncu, R., Efeyan, A., & Sabatini, D. M. (2010). mTOR: from growth signal integration to cancer, diabetes and ageing. *Nature Publishing Group*, *12*(1), 21–35. https://doi.org/10.1038/nrm3025

Zong, W., Li, C., Hatzivassiliou, G., Lindsten, T., Yu, Q., Yuan, J., & Thompson, C. B. (2000). Bax and Bak can localize to the endoplasmic reticulum to

initiate apoptosis. *The Journal of Cell Biology*, *162*(1), 59–69. https://doi.org/10.1083/jcb.200302084